PhD Thesis

Employment of Synthetic Ion Transporters to Disrupt Ionic Homeostasis in LUVs and Cells

A dissertation submitted to the
Indian Institute of Technology Guwahati
as partial fulfilment for the Degree of
Doctor of Philosophy in Chemistry

By
Ms. Oindrila Biswas

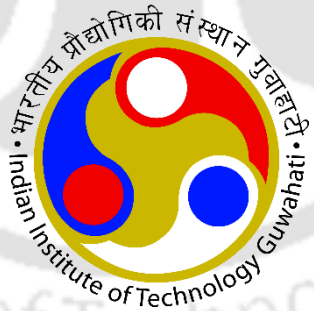

Department of Chemistry
Indian Institute of Technology Guwahati
Guwahati 781039, Assam, India

To

My Loving Mother and Sister

Declaration

6th October, 2022

I hereby declare that the thesis entitled "**Employment of Synthetic Ion Transporters to Disrupt Ionic Homeostasis in LUVs and Cells**" is the outcome of the research findings executed by me under the guidance of Prof. Debasis Manna, Department of Chemistry, Indian Institute of Technology Guwahati. The thesis has been submitted by me in the Department of Chemistry, Indian Institute of Technology Guwahati, for granting the degree of Doctor of Philosophy. In case of collaborations where the reported work has been done in association with other researchers, due credit has been given. I further declare that this work has not been submitted anywhere else for any degree, diploma, associateship or membership etc. of any Institute or University to the best of my knowledge.

Oindrila Biswas

(***Ms. Oindrila Biswas***)

भारतीय प्रौद्योगिकी संस्थान गुवाहाटी
Indian Institute of Technology Guwahati
Prof. Debasis Manna
Department of Chemistry
Phone: +91-0361-258-2325
Fax: +91-0361-258-2349
E-mail: dmanna@iitg.ac.in

To whom it may concern

6th October, 2022

This is to certify that the thesis titled "***Employment of Synthetic Ion Transporters to Disrupt Ionic Homeostasis in LUVs and Cells***" is being submitted by Ms. Oindrila Biswas (Roll No. 176122033) for the award of PhD degree in Chemistry, Indian Institute of Technology Guwahati, is genuinely her own research executed by her. The data and findings were carried out by her under strictly following my laboratory guidelines. This thesis or any part of the thesis has not been submitted elsewhere for award of any degree/diploma before.

Debasis Manna

(***Prof. Debasis Manna***)

Contents

Chapter 2

Chloride Ion Transport by PITENINs Across the Phospholipid Bilayers of Vesicles and Cells

Chapter 4

Targeted Delivery of Pro-anionophore: Photo-induced transport of Cl^- ion Across the Lipid Bilayer

Acknowledgements

This thesis is the outcome of the constant sacrifices made by my family, endless encouragement provided by supervisor, colleagues and friends.

First and foremost, I would like to thank the Almighty for providing me the constant zeal and strength to complete the task.

Next, I would like to thank my supervisor Prof. Debasis Manna, through whom I have been introduced to this fascinating world. By setting an example of punctuality, persistant-hardwork and continuous quest for novelty, he has influenced me throughout my research career. He has always extended his helpful hand towards me whenever I hit a hurdle in the road. He has enriched my experience of working in a scientific laboratory by his trustworthy recommendations and ceaseless suggestions. I really consider myself truly privileged to have been able to be part of his group. He has been my guide and mentor throughout my research work in his laboratory which has left a lasting impression in my personality.

I want to extend my heartfelt gratitude towards my collaborators Dr. Sachin Kumar (Dept. of BSBE, IIT Guwahati, India) and Dr. Niladri Patra IIT (ISM) Dhanbad for true guidance throughout the period of my research work. I want to specially mention my doctoral committee members Prof. Kalyanasis Sahu, Dr. Dipankar Srimani and Dr. Rajkumar P. Thummer for their constant scientific inputs and rigorous evaluation of my research work. Their encouragement has provided me with immense confidence about my work. I want to offer my sincere thanks to all he faculty members and office staff members of the Department of Chemistry, IIT Guwahati for their consistent assistance in all ways possible. I am immensely indebted to Central Instruments Facility (IIT Guwahati) and the Department of Chemistry for allowing me free access to all the instruments required or experimental purpose.

I would also like to aprreciate all my past and present lab members including Dr. Saurav Paul, Dr. Sreeparna Das, Dr. Subhankar Panda, Dr. Ashalata Roy, Dr. Abhishek Saha, Mr. Dipjoyti Talukdar, Dr. Nirmalya Pradhan, Dr. Nasim Akhtar, Mr. Subhasis Dey, Mr. Sribash Das, Ms. Anjali Patel, Ms. Priyanka Mazumder, Mr. Gunanka Hazarika, Mr. Biswa Mohan Prusty, Ms. Soumya Srimayee, Ms. Nikumoni Das and Mr. Mohit Kumar for maintaining a positive and thriving atmosphere in the lab.

Lastly but not the least I want to express my deepest appreciation to my mother Ms. Munni Biswas and my loving sister Ms. Anindita Biswas. My mother has been my pillar of strength since childhood and she has constantly shielded me from the other worldly problems so that I could solely focus on my research work. My sister on the other hand, though younger to me in age, has taken many responsibilities so that I can give my undivided attention in lab. Without the two of them it would have been almost impossible for me to finish my thesis work.

Thank you all for making this journey a memorable experience of my life.

Ms. Oindrila Biswas

Abstract

The thesis entitled "***Employment of Synthetic Ion Transporters to Disrupt Ionic Homeostasis in LUVs and Cells***" exemplifies the biological implications of a variety of synthetic anionophores. This thesis covers the recognition of the ions, transmembrane transport properties and possible therapeutic applications. The thesis has been divided into five chapters based on the experimental results gathered during the entire research period.

Chapter 1 instantiates the importance of the anionophores in carrying vital functions in cells. It also illustrates the therapeutic implementations of the anionophore in treating channelopathies like cystic fibrosis, triggering cancer cell death and also its use as antibacterial agents.

Chapter 2 accounts the efficient transmembrane Cl^- ion transport activity of the PITENIN derivatives. Different experiments suggest the binding of Cl^- ion with the PITENINs. Separate cellular activity studies suggest the disruption of Cl^- ion homeostasis by the PITENIN derivatives.

Chapter 3 elucidates the use of light as a competent stimulus to generate the active Cl^-/phosphate guadinium macrocycles (anionophore) from its inactive proanionophore. A concise study regarding the ion recognition, transport studies and regeneration of the active anionophore from the active anionophore under UV irradiation has been studied in LUVs and cellular conditions have been demonstrated in this chapter.

Chapter 4 summarizes the use of light as a stimulus to trigger the release of the active anionophore from its inactive proanionophore generating ROS in the process. The proanionophore group contains a CAIX inhibitor that can directly target the cancer cells having CAIX protein. A conclusive study has been shown in this chapter showing the ion recognition property, transport behaviour, regeneration of the anionophore in the presence of UV irradiation and formation of ROS in the process

List of Abbreviation

AZ	Acetazolamide
ATP	Adenosine triphosphate
ADP	Apoptotic protease activating factor-1
Apaf-1	Apoptotic protease activating factor-1
AVD	Apoptotic volume decrease
CA-IX	Carbonic anhydrase-IX
FCCP	Carbonyl cyanide *p*-trifluoromethoxyphenylhydrazone
CCCP	Carbonyl cyanide 3-chlorophenylhydrazone
CS_2	Carbon disulfide
CHOL	Cholesterol
CM	Coumarin
CF	Cystic fibrosis
CFTR	Cystic fibrosis transmembrane conductance regulator
DFT	Density functional theory
DNA	Deoxyribonucleic acid
DMF	Dimethylformamide
DPPC	Dipalmitoylphosphatidylcholine
DPPS	Dipalmitoylphosphatidylserine
DMSO	Dimethyl sulfoxide
DMEM	Dulbecco's Modified Eagle Medium
EE	Efflux efficiencies
FBS	Fetal bovine serum
FI	Fluorescent intensities
Gaff	Generalized Amber Force Field
Grp1	General Receptor for Phosphoinositides-1
GUVs	Giant Unilamellar Vesicles
GSH	Glutathione
GST	Glutathione S-transferase
EC_{50}	Half maximal effective concentration
HRMS	High-resolution mass spectra
HRP	Horseradish peroxidase

HEK	Human embryonic kidney
P_i	Inorganic phosphate
ISE	Ion selective Electrode
LUVs	Large Unilamellar Vesicles
LED	Light-emitting diode
EYPC	*L*-α-phosphatidylcholine
$HgCl_2$	Mercury (II) chloride
HgS	Mercury(II) sulfide
MMP	Mitochondrial membrane potential
MD	Molecular simulation
NMR	Nuclear Magnetic Resonance
OA	Oleic acid
ONB	*o*-nitrobenzyl
PME	Particle-mesh Ewald
*p*H	Potential of hydrogen
PARP	Poly adenosine diphosphate-ribose polymerase
PEG-400	Polyethylene glycol 400
PI	Propidium iodide
PBS	Phosphate-buffered saline
PDT	Photodynamic therapy
PI3K	Phosphatidylinositol-3 kinase
PIP_3	Phosphatidylinositol-3,4,5-trisphosphate
PH	Pleckstrin homology
RU	Response unit
rt	Room temperature
RPM	Rotation per minute
SDS-PAGE	Sodium dodecyl-sulfate polyacrylamide gel electrophoresis
SLC20A1	Solute carrier family 20 member 1
SLC34A2	Solute carrier family 34 member 2
SA	Squaric acid
SPR	Surface plasmon resonance
TBACl	Tetrabutylammonium chloride
$TBAH_2PO_4$	Tetrabutylammonium dihydrogen phosphate

$TBANO_3$	Tetrabutylammonium nitrate
THF	Tetrahydrofuran
TMS	Tetramethylsilane
Et_3N	Triethyl amine
TME	Tumor microenvironment
TLC	Thin-layer chromatography
UV	Ultraviolet
UV–Vis	Ultraviolet-visible
VRACs	Volume -regulated anion channels
YFP	Yellow fluorescent protein
POPC	1-Palmitoyl-2-oleoyl-sn-glycero-3-phosphocholine
H_2DCFDA	2', 7'-dichlorodihydrofluorescein
DCF	2',7'-dichlorofluorescein
PDK1	3-Phosphoinositide-dependent kinase 1
MTT	3-(4,5-dimethylthiazol-2-yl)-2,5-diphenyl tetrazolium bromide
HEPES	4-(2-hydroxyethyl)-1-piperazineethanesulfonic acid
HPTS	8-Hydroxypyrene-1,3,6-trisulfonic acid trisodium salt
BHK	21- Baby hamster kidney cell
AZ	Acetazolamide
ATP	Adenosine triphosphate
ADP	Apoptotic protease activating factor-1
Apaf-1	Apoptotic protease activating factor-1
AVD	Apoptotic volume decrease
CA-IX	Carbonic anhydrase-IX
FCCP	Carbonyl cyanide *p*-trifluoromethoxyphenylhydrazone
CCCP	Carbonyl cyanide 3-chlorophenylhydrazone
CS_2	Carbon disulfide
CHOL	Cholesterol
CM	Coumarin
CF	Cystic fibrosis
CFTR	Cystic fibrosis transmembrane conductance regulator
DFT	Density functional theory
DNA	Deoxyribonucleic acid

DMF	Dimethylformamide
DPPC	Dipalmitoylphosphatidylcholine
DPPS	Dipalmitoylphosphatidylserine
DMSO	Dimethyl sulfoxide
DMEM	Dulbecco's Modified Eagle Medium
EE	Efflux efficiencies
FBS	Fetal bovine serum
FI	Fluorescent intensities
Gaff	Generalized Amber Force Field
Grp1	General Receptor for Phosphoinositides-1
GUVs	Giant Unilamellar Vesicles
GSH	Glutathione
GST	Glutathione S-transferase
EC_{50}	Half maximal effective concentration
HRMS	High-resolution mass spectra
HRP	Horseradish peroxidase
HEK	Human embryonic kidney
P_i	Inorganic phosphate
ISE	Ion selective Electrode
LUVs	Large Unilamellar Vesicles
LED	Light-emitting diode
EYPC	*L*-α-phosphatidylcholine
$HgCl_2$	Mercury (II) chloride
HgS	Mercury(II) sulfide
MMP	Mitochondrial membrane potential
MD	Molecular simulation
NMR	Nuclear Magnetic Resonance
OA	Oleic acid
ONB	*o*-nitrobenzyl
PME	Particle-mesh Ewald
*p*H	Potential of hydrogen
PARP	Poly adenosine diphosphate-ribose polymerase
PEG-400	Polyethylene glycol 400

PI	Propidium iodide
PBS	Phosphate-buffered saline
PDT	Photodynamic therapy
PI3K	Phosphatidylinositol-3 kinase
PIP_3	Phosphatidylinositol-3,4,5-trisphosphate
PH	Pleckstrin homology
RU	Response unit
rt	Room temperature
RPM	Rotation per minute
SDS-PAGE	Sodium dodecyl-sulfate polyacrylamide gel electrophoresis
SLC20A1	Solute carrier family 20 member 1
SLC34A2	Solute carrier family 34 member 2
SA	Squaric acid
SPR	Surface plasmon resonance
TBACl	Tetrabutylammonium chloride
$TBAH_2PO_4$	Tetrabutylammonium dihydrogen phosphate
$TBANO_3$	Tetrabutylammonium nitrate
THF	Tetrahydrofuran
TMS	Tetramethylsilane
Et_3N	Triethyl amine
TME	Tumor microenvironment
TLC	Thin-layer chromatography
UV	Ultraviolet
UV–Vis	Ultraviolet-visible
VRACs	Volume -regulated anion channels
YFP	Yellow fluorescent protein
POPC	1-Palmitoyl-2-oleoyl-sn-glycero-3-phosphocholine
H_2DCFDA	2', 7'-dichlorodihydrofluorescein
DCF	2',7'-dichlorofluorescein
PDK1	3-Phosphoinositide-dependent kinase 1

For symbols/units

α	Alpha
Å	Angstrom
atm	Atmosphere
β	Beta
C	Celsius
J	Coupling constant
°	Degree
δ	Delta
Hz	Hertz
K	Kelvin
MHz	Megahertz
m	Meta
µg	Micro gram
µM	Micro mole
mL	Millilitre
mV	Mili Volt
min	Minute
nM	Nano mole
o	Ortho
p	Para
ppm	parts per million
%	Percent
π	Pi
ps	Pico second
s	Second

Chapter 1

1. Introduction

Preservation of the accurate ionic balance across the lipid bilayer of the cell is a very crucial function which regulates several vital events in cells like signal transduction, blood pressure regulation, hormone secretion, triggering of dell death among others. [1] Transmembrane proteins maintain the osmolality between the extra- and the intravesicular system by allowing certain substances to pass through the cellular membrane. However, impaired channel function can lead to several disease condition known as channelopathies like short QT syndrome, long QT syndrome, Bartter's syndrome and the most common being cystic fibrosis. [2]

Chloride is a very abundant ion found in the biological system. In several literature studies it has been found that in cancer cells the outside concentration of the chloride ion is higher (120 mM) w.r.t the inside concentration (5-15 mM) It was found that hindering the volume regulatory Cl^- and K^+ channels pause the cells to show classic apoptotic attributes like caspase activation, cytochrome c release and DNA laddering thus saving the cells from cell death. In line with this, increasing substantiation also shows that disrupted chloride transport in cancer cells can result in efflux of Cl^- which is considered

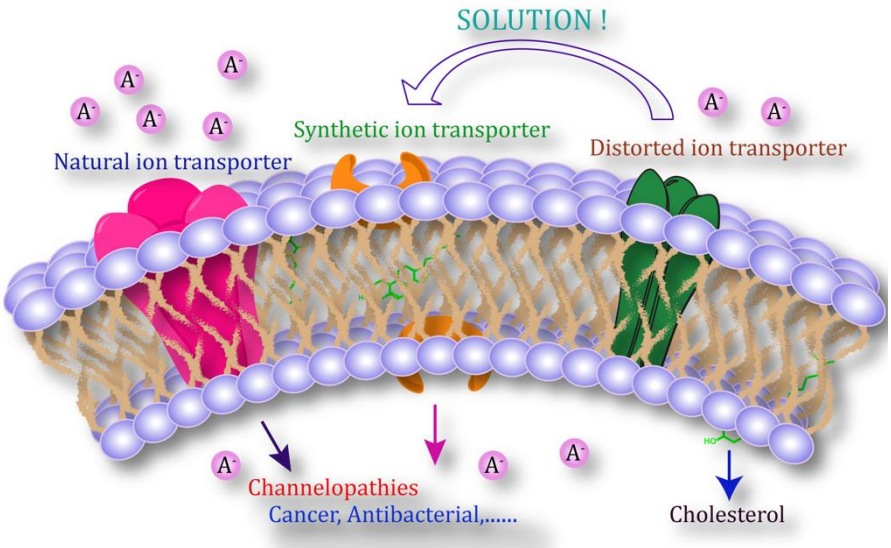

Figure 1.1. Schematic representation of numerous prospects of anionophores.

as the reason to suppress apoptosis in cancer cells. [3] Inorganic phosphate is also an essential nutrient for sustaining a cell. [4] It is a very important component of DNA,

RNA and also a part of energy rich molecules like ATP. It is also a fundamental part of cellular signalling events. In cells P_i mainly enters via Na dependent P_i transporters primarily constituting two family of inorganic phosphate transporters namely SLC20 and SLC34. [5] Furthermore, many studies propose that in tumors these P_i transporters are upregulated hence maintaining a higher concentration inside them.

The transport of the ions across the cell bilayer manages cell proliferation and apoptotic pathways. Additionally, the disruption of the ionic homeostasis in the cancer cells and destruction of the ionic gradient can trigger cancer cell death. So rather than targeting specific proteins of the cancer cells using the synthetic anionophores to aid in ion transport across the cells can be used as an excellent strategy to remove detrimental cells from our body. This novel approach of 'ion therapy' can be used to also deacidify the acidic microenvironment and thereby has massive potential to overcome the multidrug resistance of the cancer cells devised to evade cell death.

Cystic fibrosis is a deadly autosomal recessive genetic disease that occurs mainly because of the defective functionality of the CFTR (CF transmembrane conductance regulator protein). [6] Small synthetic ion transporters can be used in place of the faulty biological anion transporters because the synthetic anionophores don't target any particular protein or enzyme and are not interrupted by the different genetic mutations in the CFTR. [7] Hence the use of non-toxic synthetic anionophores along with the clinically approved drugs like lumacaftor and ivacaftor can provide a potential therapeutic strategy to restore ion transport in the CFTR cells. [8]

Recent studies revealed that small molecules which can mediate ion transport across the lipid bilayer also have *in-vitro* antibacterial effects. The antibacterial resistance is one of the foremost problems jeopardizing the effectiveness of the antibiotics. Several bacteria have been enlisted by the Centre for Disease Control (CDC) as potentially harmful threat to the mankind. The finding that several naturally occurring cationophores like valinomycin can act as antibiotics has led to the emergence of the idea that synthetic ion transporters can also have the same effect. Though a direct correlation between the ion transport activity and the antibacterial property can't be clearly drawn while a general trend can be seen. Anionophores having good Cl^- ion mediated transport efficiencies have successfully been used against clinically relevant bacterial strains. [9, 10] The membrane localization property

of the anionophores makes it very much tough for the bacteria to cultivate resistance against the anionophores. However, the used synthetic ionophores should have low toxicity towards the normal cell lines. Therefore, in the thesis diverse potential ion transporting molecules were designed and synthesised and their ion transport properties were explored through various biophysical assays. Their biological implications particularly towards cancer were also studied through a set of known *in vitro* experiments. The complete thesis has been divided into five chapters as explained below, in each chapter inspecting a divergent class of synthetic anionophores, their ion transport studies and their possible therapeutic effects.

Chapter 1 mainly argues the importance of the transmembrane transporters in the biological system and the disease conditions which can pose due to stunted transport by the natural systems. **Chapter 2** involves the exploration of the PITENIN-based transporters, their moderately good H^+/Cl^- transportation proficiency, pH stimulated increased transport efficiency and apoptosis instigating behaviour in cancer cells. **Chapter 3** emphasizes the use of light to induce the generation of the active anionophore which transports Cl^-/ across LUVs to improve the selectivity of the towards the cancer cells. **Chapter 4** embodies the use of photocleavable targeted-proanionophore to better target the cancer cells and reduce toxicity in the normal cells. The PDT activity of the photo product has also been investigated here.

Chapter 2

2. Chloride Ion Transport by PITENINs Across the Phospholipid Bilayers of Vesicles and Cells

To achieve the synthetic mimic of the natural transporter systems, PITENIN derivatives (**2.1**-**2.7**) were synthesized by condensation of the benzoyl isothiocyanates and substituted corresponding amines. [11, 12] Discerning their membrane localization property, presence of acyl thiourea group and phenolic OH, their good ion transport capability was hypothesised. To recognize the role of lipophilicity of the transporters **2.3** and **2.5 (DM-PIT-1)** were synthesized and to better analyse the necessity of the acylthiourea group benzanilide **2.6** was synthesized. Transporters **2.1**, **2.2 (PIT-1)**, **2.4**, and **2.7** were synthesized to assess the importance of the phenolic OH moiety in anion transport properties. The ^{1}H NMR

and UV-titration experiments done using transporters **2.2 (PIT-1)** and **2.5 (DM-PIT-1)** with TBACl depicted Cl^- ion recognition of the transporters.

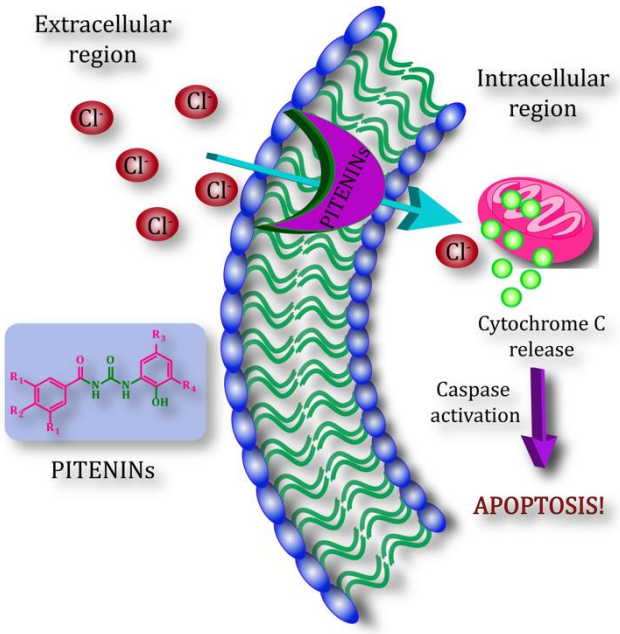

Figure 2.1. Anticancer activities of the PITENIN derivatives.

These results encouraged us to examine the Cl^- transport behaviour of these derivatives across the bilayer of EYPC/CHOL-LUVs⊃HPTS by employing a pH gradient (pH_{in} = 7.2, pH_{out} = 7.8) in the extravesicular solution. The preliminary screening data shows that **2.2 (PIT-1)** is the most efficient Cl^- ion transporter and follows the order of **2.2 (PIT-1)** ≈ **2.3** > **2.5 (DM-PIT-1)** > **2.1** > **2.6** > **2.7** > **2.4**. Among all the transporters **2.2 (PIT-1)** and **2.5 (DM-PIT-1)** were chosen to carry further experiments. Anion and cation selectivity studies across the LUVs indicated high selectivity for Cl^- ion and no significant change on changing the metals outside suggesting the metals are not involved in the mechanistic pathway. Considering the pKa of **2.5 (DM-PIT-1)** (6.43), it was found that **2.5 (DM-PIT-1)** has 20-fold superior Cl^- ion transport ability in slightly acidic condition (pH 5.5) than under physiological conditions. Hence, **2.5 (DM-PIT-1)** can be used as a switch ON Cl^- ion transporter upon the alternation of pH within a narrow window of the physiological pH. The ion transport properties of the **2.2 (PIT-1)** and **2.5 (DM-PIT-1)** in presence of FCCP and valinomycin exhibited that the synthetic transporters are involved in H^+/Cl^- transport. The U-Tube experiment and the cholesterol dependency assay authenticates the carrier mediated transport behaviour of the transporters. The MTT

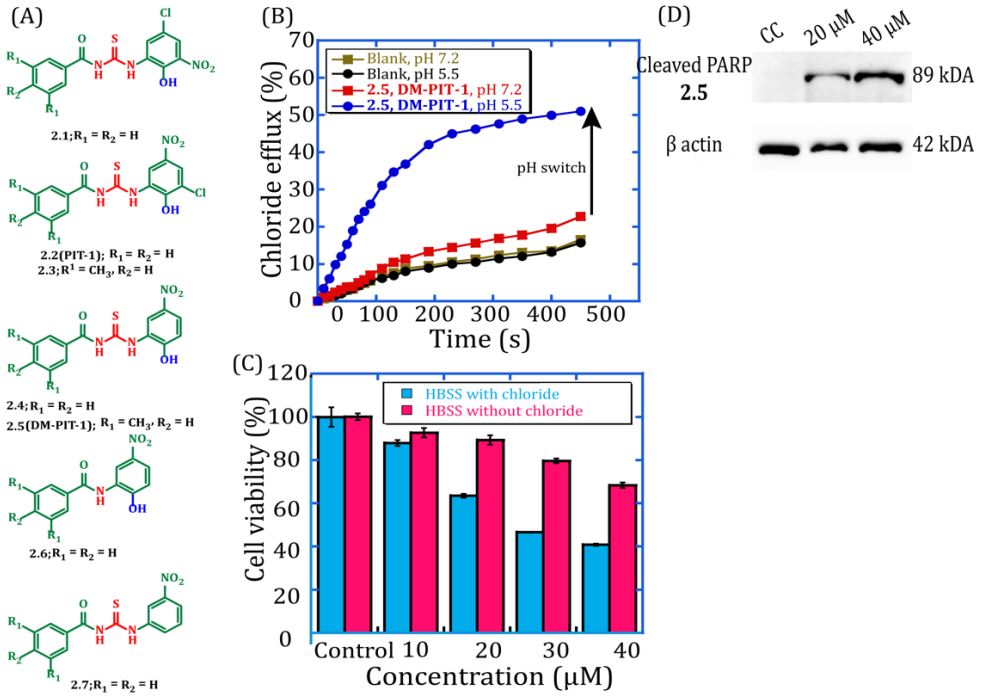

Figure 2.2. Structure of the PITENIN compounds (A). Comparisons of ion transport activity of **2.5** across EYPC/CHOL-LUVs at pH 5.5 and pH 7.2 (B). Chloride ion efflux capability of **2.5 (DM-PIT-1)** across EYPC/CHOL-LUVs (C)**.** Cell viability of in HeLacell line in presence of **2.5 (DM-PIT-1)** Cell viability of **2.5 (DM-PIT-1)** in HeLa in HBSS buffer with and without Cl^- ion at different concentrations (C) and Western Blot analysis of HeLa cells in presence of **2.5 (DM-PIT-1)** (D).

assay showed that, in the presence of **2.5 (DM-PIT-1)** and **2.2 (PIT-1)**, the viability of cancer (HeLa, human breast cancer; MDA-MB-231) and healthy (baby hamster kidney; BHK-21) cells decreases in a dose-dependent manner. To further probe into the reason of low cell viability of HeLa cells we have done the MTT experiment in HBSS (Hank's balanced salt solution), having two different salt compositions (one with a Cl^- ion and the other without a Cl^- ion). Lower viability was noticed for cells in the Cl^- ion-containing buffer as compared to the one in which there was no Cl^- ion validating the fact that the decrease in cell viability is due to Cl^- transport by the anionophores. The JC-1 dye experiment, western blot experiment and FACs analysis corroborated the apoptotic cell death of the cancer cells. Overall, this investigation revealed the anticancer activities of **2.2 (PIT-1)** and **2.5 (DM-PIT-1)**, not only because of its capability to inhibit the interaction between PIP_3 and AKT-PH domain but also for its transmembrane Cl^- ion transport activity.

Chapter 3

3. Photoinduced Generation of the Active Chloride/Phosphate Anionophore from its Inactive Proanionophore

Ion transport-promoted unwanted death of normal cells remains a major concern for ion therapy. So, to minimize the apoptosis of the normal cells and selectively target the cancer cells, in this work photo-triggered ion transporters has been used which can give site-selective precise control over the functioning of the ion transporters. Herein, a C2 symmetric guanidinium-based macrocycle was synthesised. [13] The ion binding scaffold and the hydrophobic domain impart lipophilicity to transport the ions. To further explore the concept of a photocleavable proanionophore, the o-nitrobenzyl (ONB) group with the guanidinium-N moiety was attached. [14]

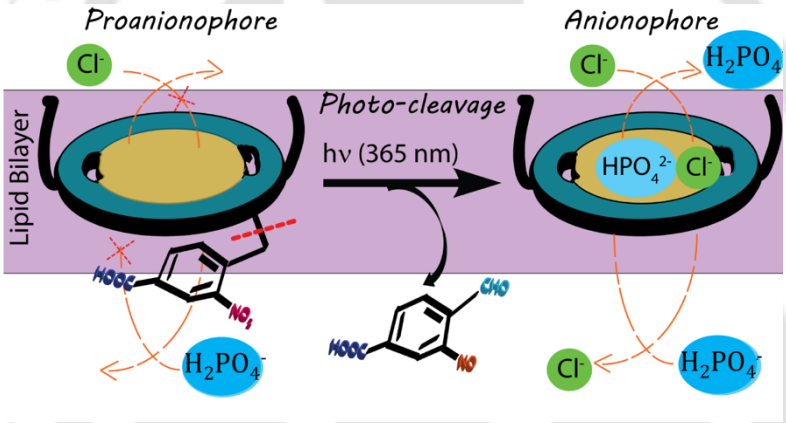

Figure 3.1. Schematic representation of the photomediated generation of ionophore from ONB-linked proanionophore.

Initially, thiourea-based macrocyclic intermediate was synthesized, and then desulfurization of thiourea moiety with alkyl amines resulted in the expected guanidinium-based macrocyclic compounds. To investigate the importance of hydrophobicity in ion transportation, alkyl amines of different chain lengths (n = 4, 8, and 10) were used. Compound **3.2** showed better binding with phosphate ion and Cl^- rather than NO_3^-. Eventually the ion transport properties of the anionophores (**3.1-3.2**) were explored in EYPC/CHOL⊃lucigenin using the fluorescence-based assay. The phosphate transport efficacy of compound **3.2** was higher than the compounds **3.1, 3.3**, and **3.4**. The higher transport proficiency of compound **3.2**

could be attributed to its subtle balance of hydrophilicity and membrane residence aptitude. The anion selectivity of compound **3.2** was performed by lucigenin assay dispersing the LUVs in an aqueous of 225 mM Na_xA_y salt (where Na_xA_y = NaH_2PO_4, Na_2SO_4, NaOAc, $NaClO_4$, and $NaNO_3$). The selectivity studies revealed that compound **3.2** is more selective towards phosphate ions than the other tested oxyanions. To comprehend the mechanistic pathway, the cation selectivity of compound **3.2** was checked in the presence of Na^+ and K^+ ions. The Cl-ISE-based assay showed compound **3.2** mediated transport of phosphate/Cl^- ions across the lipid bilayers. Additionally, when Na_2SO_4 was kept outside, no change in fluorescence intensity was observed due to inability of the anionophore to facilitate the SO_4^{2-}/phosphate antiport process as the selectivity for SO_4^{2-} is too low for compound **3.2**. This result also supports the independent nature of the transport mechanism with respect to the cations. The non-involvement of H^+ in the mechanistic pathway could be assured from the enhancement of the HPTS fluorescence intensity when FCCP was added along with the transporter. The only persisting pathway is the phosphate/Cl^- antiport mechanism. Moreover, the U-tube assay also propounds a similar result. Gradually with progression of time, NaCl and NaH_2PO_4 steadily increases in the opposite arms of the U-Tube. This result also indicates carrier mediated pathway followed by the transporters. This outcome was moreover concluded with the help of temperature-dependent DPPC assay. The transport activities across the Tb(III)-complex-based fluorescent chemosensor (of phosphate ion) LUVs also demonstrated the phosphate transport activities of compound **3.2**. The transmembrane transport of phosphate ions in the presence of compound **3.2** using giant unilamellar vesicles (GUVs) was deployed. Furthermore, ^{31}P NMR experiments were done to provide undeniable proof of the phosphate/Cl^- antiport process carried by compound **3.2.** After incubation with compound **3.2**, the ^{31}P peak decreased which can only be feasible after the phosphate transport, mediated by the transporter **3.2**. The molecular dynamics (MD) simulation studies with compound **3.2** and phosphate ion embedded inside a preequilibrated dipalmitoyl phosphocholine (DPPC)/water lipid bilayer system studies revealed the retention of the compound within the bilayer and expulsion of phosphate ion from the complex suggesting the successful transport of the phosphate ion by the compound. To assess the photo-triggered cleavage of proanionophore **3.4** and in-situ generation of anionophore **3.2** the ^1H NMR-based

study was performed. After photo irradiation with an LED lamp (365 nm), a new peak was seen at δ = 10.25 ppm, which implies the formation of 4-formyl-3-nitrosobenzoic acid, a plausible result of the photocleavage of the proanionophore **3.4**. The successful generation of the anionophore was also studied in the membrane environment. The ion transport activities of proanionophore **3.4** were recorded before and after photo irradiation. It was perceived that the transport efficacy increased by 60%. Consequently, by both the NMR and fluorescence-based methods, the resurgence of the anionophore **3.2** from proanionophore **3.4** was be affirmed.

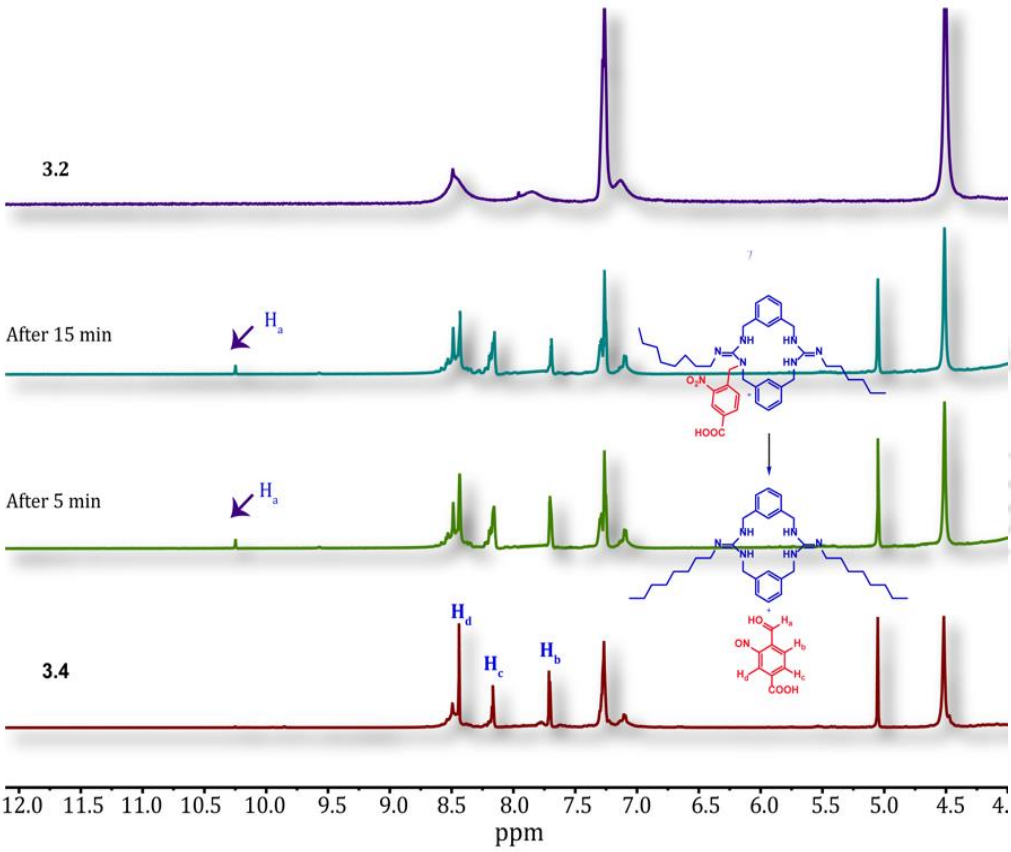

Figure 3.2. Photoinduced release of anionophore **3.2** from proanionophore **3.4** was monitored by ^{1}H NMR titration experiment in DMSO-d_6 solvent.

The perturbation of chloride-phosphate ion homeostasis in the cancer cells could induce apoptosis or other cell death pathways. The MTT-based cell viability assay revealed that compound **3.2** induced moderate toxicity (IC_{50} = 20 μM) to the HeLa cells. However, the proanionophore **3.4** showed negligible toxicity even after treatment with 60 μM concentration. Interestingly, photo irradiation (UV 365 nm, 5 min) of proanionophore **3.4** promoted moderate toxicity to the HeLa cells (IC_{50} = 36

μM). Whereas only photo irradiation (UV 365 nm, 5 min) without the treatment of proanionophore **3.4** did not significantly alter the viability of the HeLa cells. Hence, the lower viability after the photo irradiation could be due to cleavage of proanionophore **3.4** and in-situ generation of active anionophore **3.2** under the cellular environment. Overall, these results successfully established that photoinduced disruption of chloride-phosphate ions homeostasis induces cancer cell death.

Chapter 4

4. Targeted Delivery of Pro-anionophore: Photo-induced transport of Cl^- ion Across the Lipid Bilayer

Photocleavable proanionophores have attracted interest due to their controlled biological activities. In this work, the "photocleavable targeted-proanionophore" strategy was incorporated into the domain of artificial ion transporters and a cancer cell targeting proanionophore that undergoes photo-controlled release of an active anionophore to promote Cl^- ion transport-mediated cell death developed. photocleavable targeted-proanionophore fusings with three important bits. [15] The first is the macrocycle, the primary ion recognition scaffold, the cholic amine, the hydrophobic domain accountable for membrane insertion. The last is the acetazolamide grafted photoactivable moiety, which could be inserted selectively into the targetted cancer cells, and then photo- release would generate the active anionophore. Acetazolamide is a known carbonic anhydrase IX (CA-IX) inhibitor that is overexpressed in certain types of cancers. CA-IX is directly associated with the hallmarks of cancer like invasion, angiogenesis, proliferation, and adaptation to microenvironmental stresses (acidosis, hypoxia, deprivation of nutrients). Various studies demonstrated that CA-IX inhibitor diminishes tumor cell proliferation and induces apoptosis. However, only the solitary use of CA-IX inhibitor may not be effectual, and its use along with the apoptosis-inducing anionophore may have an operative therapeutic effect.

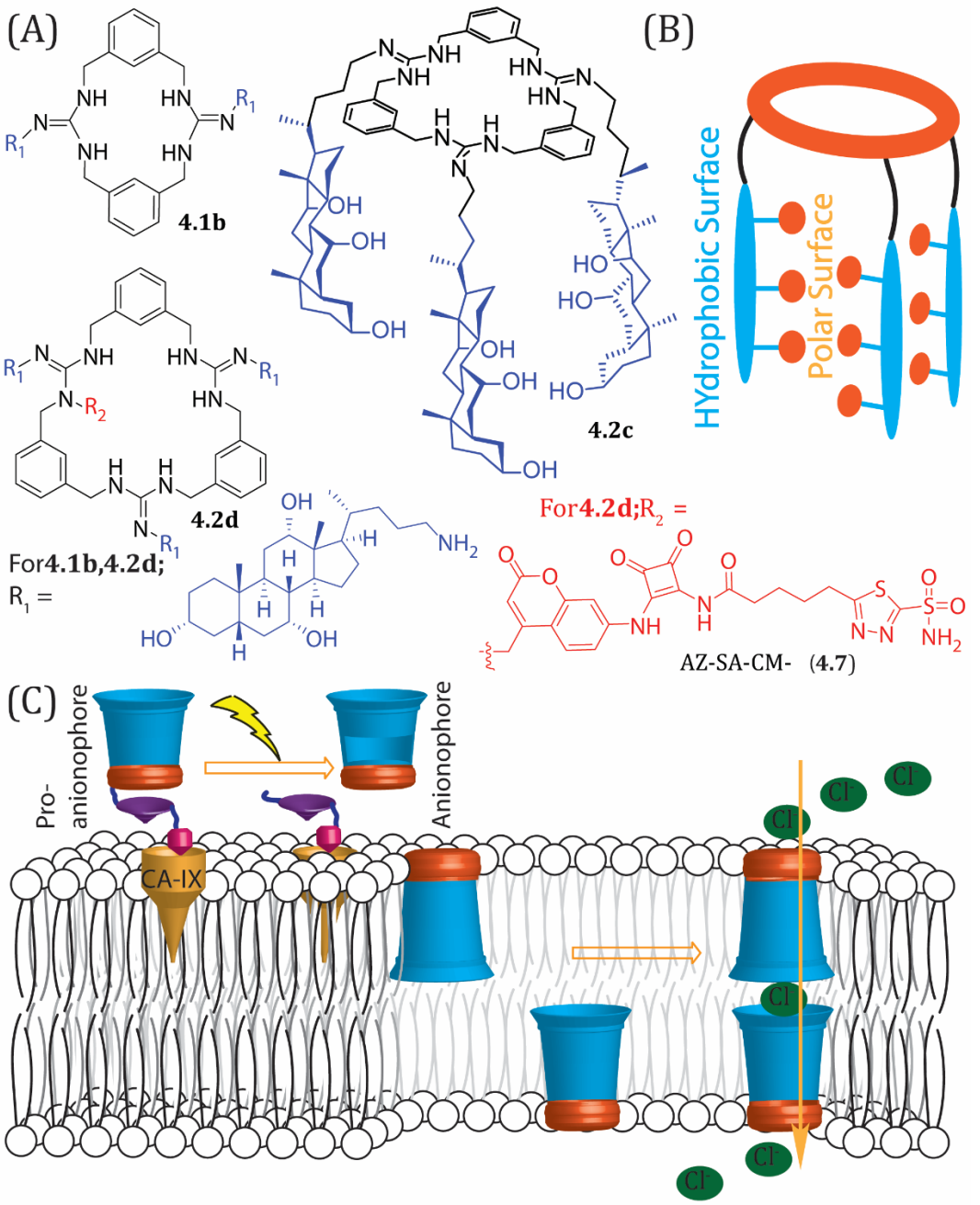

Figure 4.1. Transport of the guadinium-based macrocycle anionophores across LUVs.

The desired guanidine-based macrocyclic compounds were synthesized from thiourea-based macromolecules following reported protocols. The cancer cell targeting photolabile moiety, AZ-SA-CM-Br **(4.7)** was affixed to the macrocyclic compound **4.2c** to achieve the photocleavable targeted-proanionophore **4.2d**. Initially, the anion recognition properties of the compounds were investigated using UV-titration with Cl^- ions. The binding of the compounds with Cl^- follows a 2:1 host/guest stoichiometry as obtained from the BindFit analysis, suggesting that two anionophores are necessitated in the binding event. Next the ion transport

properties of the macrocyclic anionophores were evaluated using EYPC/CHOL-LUVs⊃Lucigenin. Compound **4.2c** showed the highest Cl^- ion transport properties among the tested ones. Compound **4.2d**, on the contrary, showed limited Cl^- ion transporting ability, which could be due to its structural properties. Meanwhile, it was disclosed from the dose-dependent experiment that 'n', known as the 'Hill coefficient' and referring to the number of species involved in the transport process showed a value of 2.0, implying the assembly of two molecules of anionophore **5.2c** (host/guest = 2:1) is the active structure for the Cl^- ion transport process. The anionophore showed highest anion selectivity for Cl^- among the Na_2SO_4, $NaHCO_3$, NaOAc, $NaClO_4$, and NaCl salts. The transport efficiency was kept unaltered when the external cations were varied (M^+ = Li^+, Na^+, K^+, Rb^+ and Cs^+) eliminating the prospect of M^+ transport along with Cl^- ions. The result of Cl^- ion transport efficiency mediated by the anionophore in presence of FCCP evinces that the potent anionophore was unable to carry H^+ across the lipid bilayer. The enhancement of the Cl^- transport in presence of valinomycin and **4.2c** as seen in EYPC/CHOL⊃lucigenin validates the antiport transport mechanism followed by **4.2c**. To delve into the mode of transport adopted by the anionophore, a temperature-dependent anionophore activity was investigated using the model lipid bilayers of DPPC which showed no significant change in the Cl^- ion transport rate at 25 °C and 45 °C suggesting that the transport properties of anionophore **4.2c** might not be via carrier pathway but via pore formation across the lipid bilayer.[16] In addition, the CHOL dependent anionophore activity measurements revealed that the rate of Cl^- transportation by anionophore **4.2c** was not significantly affected by the concentration of CHOL within the lipid bilayers, which also suggested the bi-molecular pore formation could be the operating pathway for the transport of Cl^- ion for anionophore **4.2c**. Photo-induced regeneration of anionophore **4.2c** from AZ-SA-CM-linked proanionophore **4.2d** (405 nm, 2 W cm^{-2}) was investigated following the increase in fluorescence intensity of the photoproduct which is fluorescent for different time intervals (0-30 min). Concurrently, the Cl^- ion transport activity of the regenerated active anionophore **4.2c** was scrutinized by the Cl-ISE-based assay. The increase in Cl^- ion efflux efficiency suggests the in-situ generation of active anionophore. Similar results were obtained with the help of fluorescence-based experiment using EYPC/CHOL⊃HPTS.

Now to check the therapeutic potency of the anionophore **4.2c**, the cell viability was checked in HeLa, T47D and HEK 293 cells. After UV irradiation the cell viability was seen lowest in the HeLa cells as the photoproduct contains the acetazolamide derivative which synergistically brings about cancer cell death along with the anionophoric activity of the anionophore **4.2c.** Due to presence of 7-amino coumarin group in the photoproduct, ROS generation in the cancer cells also increased as measured using ROS-sensitive DCFDA dye.

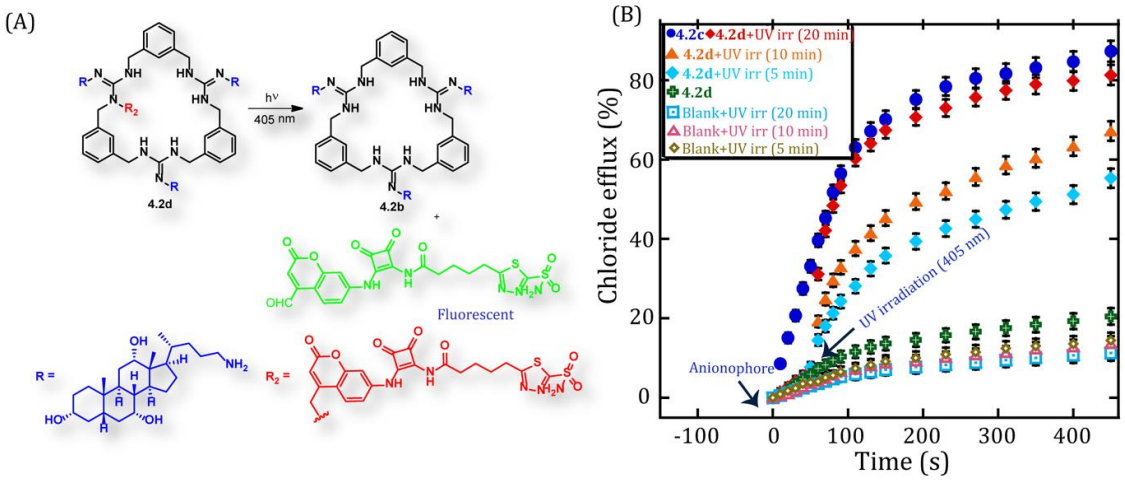

Figure 4.2. Proposed regeneration pathway for the active anionophore from the proanionophore under UV irradiation (405 nm) (A). Cl^- ion transport activity of the proanionophore under UV irradiation (405 nm) using the HPTS-based fluorescence assay (C).

5. Conclusion

Accordingly in this thesis four different scaffolds were designed and synthesised and their curative properties were investigated thoroughly. In **Chapter 1** the importance of several anionophores and their several therapeutic applications were discussed in detail. Subsequently in **Chapter 2** a new class of anionophore was developed, their Cl^- ion ability was studied and their anticancer properties were investigated. To further achieve selectivity over the cancer cells, light as a stimulus was used in **Chapter 3** and the generation of the active anionophore from the inactive anionophore was studied along with the Cl^- ion arbitrated phosphate ion transport ability of the anionophore. **Chapter 4** demonstrated the construction of photocleavable targeted proanionophore to better target the cancer cells and induce

cancer cell death due to enhanced production of ROS upon UV irradiation on the proanionophores. Overall, in the thesis anionophoric properties of a number of synthetic transporters were investigated with the help of well-known experiments and their biological applications were examined.

6. References

(1) Akhtar, N.; Biswas, O.; Manna, D. J. C. C. Biological applications of synthetic anion transporters. *Chem. Commun.* **2020**, *56* (91), 14137-14153.

(2) Davis, J. T.; Gale, P. A.; Quesada, R. J. C. S. R. Advances in anion transport and supramolecular medicinal chemistry. *Chem. Soc. Rev.* **2020**, *49* (16), 6056-6086.

(3) Saha, T.; Hossain, M. S.; Saha, D.; Lahiri, M.; Talukdar, P. J. J. o. t. A. C. S. Chloride-mediated apoptosis-inducing activity of bis (sulfonamide) anionophores. *J. Am. Chem. Soc.* **2016**, *138* (24), 7558-7567.

(4) Lacerda-Abreu, M. A.; Russo-Abrahão, T.; de Queiroz Monteiro, R.; Rumjanek, F. D.; Meyer-Fernandes, J. R. J. B. e. B. A.-R. o. C. Inorganic phosphate transporters in cancer: Functions, molecular mechanisms and possible clinical applications. **2018**, *1870* (2), 291-298.

(5) Song, W.; Li, D.; Tao, L.; Luo, Q.; Chen, L. J. A. P. S. B. Solute carrier transporters: the metabolic gatekeepers of immune cells. *Acta Pharmacologica Sinica* **2020**, *10* (1), 61-78.

(6) Edelman, A.; Saussereau, E. J. A. d. P. O. O. d. l. S. F. d. P. Cystic fibrosis and other channelopathies. *Archives de Pediatrie* **2012**, *19*, S13-16.

(7) Li, H.; Valkenier, H.; Thorne, A. G.; Dias, C. M.; Cooper, J. A.; Kieffer, M.; Busschaert, N.; Gale, P. A.; Sheppard, D. N.; Davis, A. P. J. C. s. Anion carriers as potential treatments for cystic fibrosis: transport in cystic fibrosis cells, and additivity to channel-targeting drugs. *Chem. Sci.* **2019**, *10* (42), 9663-9672.

(8) Sheppard, D. N.; Davis, A. P. Pore-forming small molecules offer a promising way to tackle cystic fibrosis. Nature Publishing Group: 2019.

(9) Carreira-Barral, I.; Rumbo, C.; Mielczarek, M.; Alonso-Carrillo, D.; Herran, E.; Pastor, M.; Del Pozo, A.; García-Valverde, M.; Quesada, R. J. C. C. Small molecule anion transporters display in vitro antimicrobial activity against clinically relevant bacterial strains. *Chem. Commun.* **2019**, *55* (68), 10080-10083.

(10) Elie, C. R.; David, G.; Schmitzer, A. R. J. J. o. M. C. Strong antibacterial properties of anion transporters: a result of depolarization and weakening of the bacterial membrane. *J. Med. Chem.* **2015**, *58* (5), 2358-2366.

(11) Haynes, C. J.; Busschaert, N.; Kirby, I. L.; Herniman, J.; Light, M. E.; Wells, N. J.; Marques, I.; Félix, V.; Gale, P. A. J. O.; chemistry, b. Acylthioureas as anion transporters: the effect of intramolecular hydrogen bonding. *Org. Biomol. Chem.* **2014**, *12* (1), 62-72.

(12) Biswas, O.; Akhtar, N.; Vashi, Y.; Saha, A.; Kumar, V.; Pal, S.; Kumar, S.; Manna, D. J. A. A. B. M. Chloride ion transport by PITENINs across the phospholipid bilayers of vesicles and cells. *ACS Appl. Bio Mater.* **2020**, *3* (2), 935-944.

(13) Biswas, O.; Mazumder, P.; Naskar, A.; Srimayee, S.; Kumar, S.; Patra, N.; Manna, D. Photoinduced generation of the active chloride-phosphate anionophore from its inactive proanionophore. *ChemRxiv.* **2022**.

(14) Salunke, S. B.; Malla, J. A.; Talukdar, P. J. A. C. I. E. Phototriggered Release of a Transmembrane Chloride Carrier from an o-Nitrobenzyl-Linked Procarrier. *Angew. Chem.* **2019**, *58* (16), 5354-5358.

(15) Mora, N. L.; Bahreman, A.; Valkenier, H.; Li, H.; Sharp, T. H.; Sheppard, D. N.; Davis, A. P.; Kros, A. J. C. s. Targeted anion transporter delivery by coiled-coil driven membrane fusion. *Chem. Sci.* **2016**, *7* (3), 1768-1772.

(16) Behera, H.; Madhavan, N. Anion-Selective Cholesterol Decorated Macrocyclic Transmembrane Ion Carriers. *J Am Chem Soc* **2017**, *139* (37), 12919-12922. DOI: 10.1021/jacs.7b07479.

Chapter 1

Synthetic Anion Transporters and their Potential Biological Applications

1.1. Introduction

The interchange of materials across cells is a very crucial phenomenon. This happening ensures to maintain the optimum osmotic balance across the cells which is crucial in maintaining many cellular activities of the cells [1, 2, 3]. However due to the semi-permeable nature of the plasma membrane, ionic substances (solutes) can't pass through the membrane. Nevertheless, neutral substances like water and carbon dioxide easily traverses through the lipid bilayer [4, 5]. Therefore, in case of solutes, aid of the membrane spanning proteins in carrying the ions through the hydrophobic bilayer or to provide a hydrophilic passage for the ion transport is very much necessary. In case of ion channels numerous non-covalent interactions with the ions, assist in the movement of ions through them. Anions, specially play a pivotal role in maintaining cell volume, pH, osmotic pressure and they also help in cell signalling processes. Hence any mutation of the genes encoding the transmembrane proteins or any structural rearrangement can result in stunted ion transport across the lipid bilayer which gives rise to a number of diseases like QT syndrome, cystic fibrosis, Isaac's syndrome, Bartter's syndrome among others and are collectively known as 'Channelopathies'.

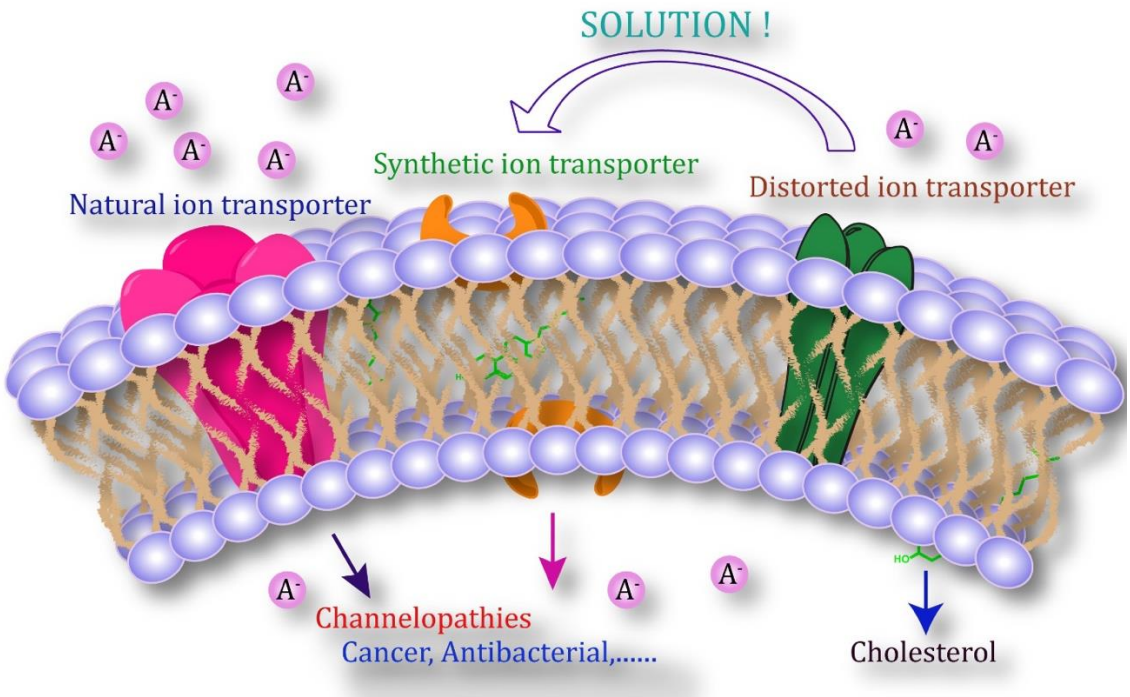

Figure 1.1. Therapeutic prospects of anionophores.

During the last two decades anion receptor chemistry received the much-revered attention. Several potent anion recognising scaffolds were recognized and

later similar moieties also exhibited ion transport properties. With the help of several biophysical experiments their ion transport behaviour across model membranes were explored which gave very promising results. Hence the concept of using the anion receptor like molecules which can mimick the natural transmembrane proteins came. In some of the cases the transporters were used in channelopathy related conditions like cystic fibrosis.

1.2. Different modes of transport of the ion transporters

The much-coveted ion transport by the synthetic transporters can transpire either by the carrier-mediated pathway or by forming channels. In carrier mediated pathway, the lipophilic natural transporters commute ions across the hydrophobic lipid bilayer. While in case of channels, the transporters self-assemble due to the presence of non-covalent interactions and form an immobile membrane spanning hydrophilic system assisting in the movement of the polar ion across them. Carriers usually transport more selectively than the channel transporters. Additionally, the transport activity of the natural carrier molecules found in the biological system is not gated whereas the activity of the channel systems is gated like in response to ligands or mechanical stress or change in membrane potential.

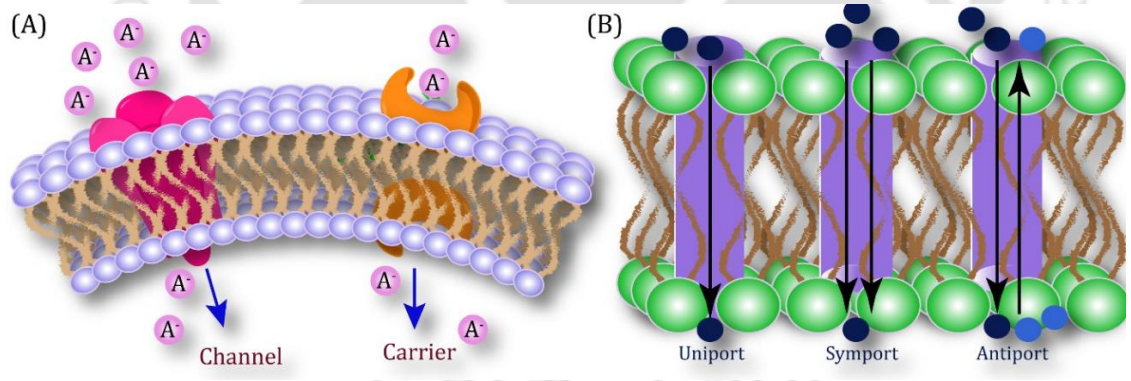

Figure 1.2. Different modes of ion transport.

The transporters based on their direction of transport and the number of ions involved can be classified into uniport, symport and antiport transporters. If there is an involvement of a single molecule then they are termed as uniport transporters. When two ions are being transported in the same direction, they are known as symporters while the transport of two ions in the reverse directions are known as antiport transporters. Symport and antiport transporters maybe collectively called

co-transporters. Uniport transporters result in the accumulation of transmembrane potential due to the one-sided movement of the ion. Whereas symport and antiport transport leads to electroneutral transport where no net build of charge takes place due to the coequal movement of ions across the bilayer. Moreover, the transport of the ions across the cells can occur by passive transport or active transport. In passive transport, movement of the ions follows the electrochemical gradient (from high concentration towards low concentration) while in active transport, the transport happens opposite the concentration gradient from high concentration towards low concentration which requires energy expenditure in the form of ATP hydrolysis for primary active transport. Now to transport the ions across the biological membrane binding them is a prerequisite. This binding process occurs with the help of many non-covalent interactions like electrostatic interactions including the charge-charge, charge-dipole, dipole-dipole and hydrogen bonding interactions.

1.3. Therapeutic applications of ion transport

Therefore, the synthetic ion transporters have been used for many therapeutic targets. In cancer cell several of the ion channels and ion pumps are upregulated which help in cell migration, cell adhesion, cell proliferation and also in aberrant tumor growth.[6, 7, 8] Cancer cells have a high concentration of Cl^- ions inside (~120 mM) and the outside concentration is quite low (5-15 mM).[9, 10] Due to the abnormal ionic gradient in the cancer cells, it evades the apoptosis process. Apoptosis is a strictly monitored cell death process which removes the detrimental cells from our body. Hence the disruption of this carefully maintained ionic gradient in the tumor cells with the help of synthetic transporters can trigger cancer cell death. Besides due to the slightly acidic tumor cell extracellular composition, the uptake efficiency of the weak base chemotherapeutic drugs alleviates and the cancer cell develop drug resistance against the chemotherapeutic drugs. Synthetic ionophores have been shown to deacidify several cell organelles along with the tumour microenvironment owing to which the multidrug resistance of the cancer cells can be curbed.

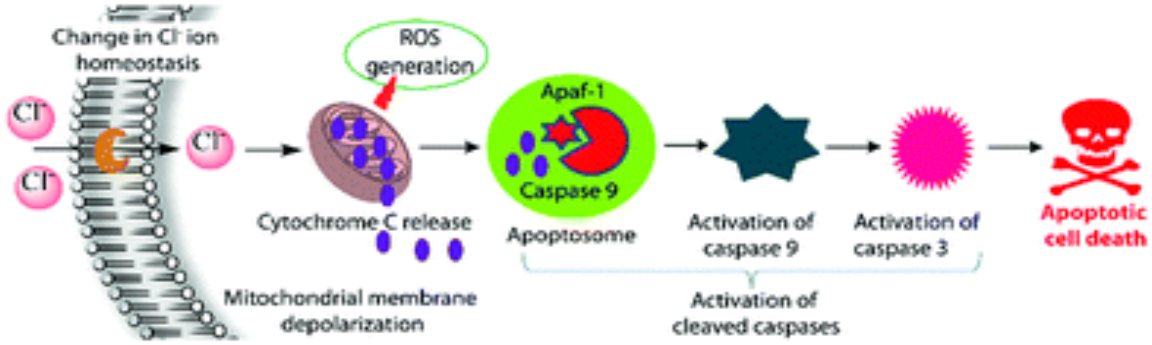

Figure 1.3. Schematic representation of the anionophore mediated intrinsic pathway of apoptosis

In addition, the synthetic anionophores have been also used in channelopathy conditions like cystic fibrosis.[11] Selective transport of Cl^- and HCO_3^- across the epithelial cells through CFTR. Any mutation in the gene encoding CFTR can lead to disrupted transport of the ions causing the genetic disease of cystic fibrosis. Though there are some medicinally approved drugs for treating CF like lumacaftor and ivacaftor, however due to the large number of mutations possible in CF, the efficiency of the drugs greatly diminishes.[12] As synthetic anionophores don't target a particular gene, enzyme or protein and solely depend on the selective transport of the anions, they can be effectively used either independently or in combination with drugs that target CF.[13] However low cytotoxicity towards the normal cells is the main prerequisite of the synthetic transporters to be used in the disease condition.

Though preliminarily the undivided attention of using the synthetic anionophore has been given to trigger cancer cell death and to be used in CF condition, later it has been found that potent Cl^- ion transporters can also show excellent antibacterial properties.[14, 15, 16, 17] Antibacterial resistance is one of the leading problems in the world today which greatly restricts the use of antibiotics. After investigating the mechanism of action in most of the cases it has been established that the anion transporters work by membrane depolarisation method and as a consequence making it hard for the bacteria to develop resistance against them. Hence, by the same the same argument the synthetic anionophores should show activity against the drug resistant bacteria also. The synthetic transporters used for these purposes should be very less toxic towards the human cell lines. Though a direct correlation couldn't be obtained in several cases, in many cases potent anionophores have shown very good antibacterial properties.

1.4. Ion transport and cell death

The concentration of the various ion in the cells is precisely maintained with the assistance of natural ion channels ion pumps. Specifically, the concentration of chloride, phosphate, calcium, sodium and potassium is very much crucial for normal cell functioning. The alteration in the concentration of these ions can be responsible for the inception of apoptosis.[18]

Calcium predominantly acts as a messenger and plays a vital role in many cellular functions like cell differentiation, cell proliferation, cell death among others.[19, 20] Escalation in the cytosolic calcium concentration can help in the further advancement of apoptosis across all stages. For example, elevated cytosolic calcium concentration can result in excess mitochondrial calcium uptake which in turn can stimulate the intrinsic pathway of apoptosis. Modification of the calcium concentration in the endoplasmic reticulum can induce mitochondria independent apoptotic pathway. Oxygen and glucose deficiency triggers calcium dependent caspase 12 activation and cleavage which is the main reason for the cell death in such cases. Surge in cytosolic calcium concentration in turn also activates several endonucleases which are DNA degrading. The calcium concentration in the cytosol, endoplasmic reticulum and mitochondrial are maintained by different calcium permeable ion channels located in the plasma membranes or in the membrane of the cell organelles. These channels' expression and normal functioning contribute to the changed calcium concentration by tuning Ca^{+2} influx rate, Ca^{+2} uptake and release from cellular organelles and affect various processes like apoptosis.

K^+ ion is present in high abundance in the cells and is one of the principal ions involved in maintaining cell volume. Decrease in cytoplasmic K^+ concentration initiates the activation of nucleases and caspases, activating apoptosis.[21, 22] Whereas excessive K^+ concentration in the extracellular medium impedes both the intrinsic and extrinsic pathway of apoptosis. As K^+ has been identified as the pro-apoptotic factor, the K^+ ion channels effluxing the ion outside the cell has proved to be good therapeutic targets to modulate apoptosis.

Apart from K^+, other monovalent ions like Cl^- and Na^+ play a very determining role both in maintaining cell volume and apoptosis. Rise in the intracellular Na^+ levels happen in early apoptotic events.[23] Besides it has been seen that the concentration of sodium inside the cells, directs K^+ efflux in the event of apoptosis. Na^+ ions are

transported into the cells with the help of integral membrane proteins selective to Na^+ ions. During hypoxemia conditions the voltage dependent sodium channels gets activated which in turn initiates the caspase-3-dependent apoptosis process. This activation has been proved by using a sodium channel blocker tetrodoxin which diminishes this caspase-3 mediated activation of apoptosis. While a sodium channel modulator (veratridine) promotes the neuronal apoptotic pathway. A sodium channel blocker named saxitoxin averts apoptosis in Jurkat-T-cells by blocking sodium influx. In various cancers of lung, breast, prostate, colon, skin and others abnormal expression of sodium channels were found.

Apoptotic volume decrease (AVD) is one of the hall marks of apoptosis and apart from potassium ions, chloride ions are also responsible for AVD.[24, 25] In addition to the K^+ ions, Cl^- ions also leave the cell during AVD. The Cl^- ions efflux rates increase in reception of apoptotic stimuli. Checking this efflux of Cl^- ions have shown to control AVD and in turn apoptosis. The chloride transport across the biological membrane is mainly carried with the help of chloride selective ion channels. They help to maintain the cell volume, cell cycle, help in acidification of cell organelles and apoptosis. The Cl^- ion channels are however not solely selective towards the Cl^- ions, hence the final effects of the transport is not the singular transport of the Cl^- ions. However, considering the fact that Cl^- ion is the most abundant anion found in the biological system, it can be assumed that it is the most prevalent ion passing through the ion channel. Volume -regulated anion channels (VRACs) are the most explored Cl^- ion channel for their involvement in AVD. Cellular swelling alerts VRACs which initiates K^+ and Cl^- efflux from the cell accompanying osmotically directed H_2O efflux from the cell, thereby managing the cell swelling. With regards to various apoptotic stimuli, the VRACs gets activated.

Phosphorous is a very important element found in the biological system. Mammals acquire inorganic phosphate (P_i) through diet with the help of absorption in the small intestine. P_i is a constituent of high energy molecules like ATP, ADP, GMP among others and also an elemental component of various phospholipids and RNA and DNA.[26] This P_i is very much associated with vital cell processes like energy metabolism with the help ATP by carrying energy, in the kinase signalling event, etc. It is also linked to various important phosphorylation and dephosphorylation processes of the body. The P_i concentration is maintained in the body of a healthy

mammal within the range of 0.8 to 1.5 mM conditional to fasting, gender, age, diet, etc. Very low concentration of P_i (<2.5 mg/dL) gives rise of hypophosphatemia and high concentrations of P_i (normally 7–9 mg/dL) gives rise to hyperphosphatemia resulting in consequential health risks.[27] However, P_i is prevalent in the body mainly in its anionic form which doesn't get transported across the semi-permeable membrane normally. Hence the transmembrane proteins are needed to assist the transport the P_i across the lipid bilayer of the cells. Specially in mammals the phosphate transporting proteins can be vividly categorized into three families namely NaPi-I, NaPi-II (subfamilies-NaPi-IIa (SLC34A1), NaPi-IIb (SLC34A2), and NaPi-IIc (SLC34A3)) and NaPi-III (subfamilies-PiT-1 (SLC20A1) and PiT-2 (SLC20A2). According to the recently proposed "growth rate hypothesis" tumour cells show higher concentration of phosphorous.[28] This higher concentration of phosphorous is necessary to meet the escalated energy demands of the tumor cells due to the necessity of larger number of ribosomes to generate proteins to sustain the fastened proliferation rates of the tumor cells. This higher concentration of phosphorous is not seen in the normal cells.

Lately it has been shown that higher concentration of inorganic phosphate in the tumor microenvironment (TME) is a newly established hallmark of tumor progression.[29] Surge in the P_i in TME can be increased ATP hydrolysis in the tumor cells due to hypoxia condition. The microenvironment P_i in the tumor cells can also increase in concentration because of high dietary P_i intake and absorption, increasing the level generation of free P_i in the microenvironment with the help of ectoenzymes and processes like necrosis, upregulating the expression of P_i transporters like Slc34a2 and Slc20a1. The concentration of interstitial P_i is a vital signalling molecule stimulating cell transformation by means of molecular mechanisms like stimulation of angiogenesis. Hence in such a situation influencing P_i concentration in cells (active regulator of cellular conduct) can be used as an unorthodox strategy to check aberrant cell growth of the tumor cells lacking damaging cellular effects. The P_i levels can be checked at many levels-lowered P_i in the diet, suppression of P_i absorption in intestine, controlling the production of P_i in the tumor microenvironment, aiming the P_i transporters in the malignant cells, targeting the P_i stimulated paracrine factors that give rise to more P_i. Surprisingly it has been found that limiting the P_i consumption through diet attenuates the probability of tumor commencement and

in a number of instances it has been seen, lower P_i uptake slows tumor advancement. In addition to controlling the dietary intake of P_i, its absorption in the intestine should also be controlled to slow the tumor growth. Hence, using phosphate binders in this case is a good option as explicitly targeting Pi transporters is particularly challenging. Keeping the events of generation of the free P_i (ectoenzyme activity and necrosis of the neighbouring cells of tumor) in check can also be a novel therapeutic trategy to manage P_i in the tumor microenvironment. Slc34a2 and Slc20a1 are actively linked with tumor cell proliferation and angiogenesis. Their overexpression has been associated to various types of cancer. Consequently, targeting these P_i transporters in the cancer cells has proven to be effectual in many cases. Clinically approved inhibitor of P_i, Foscavir (a pyrophosphate analog) has shown promising results in some cases.

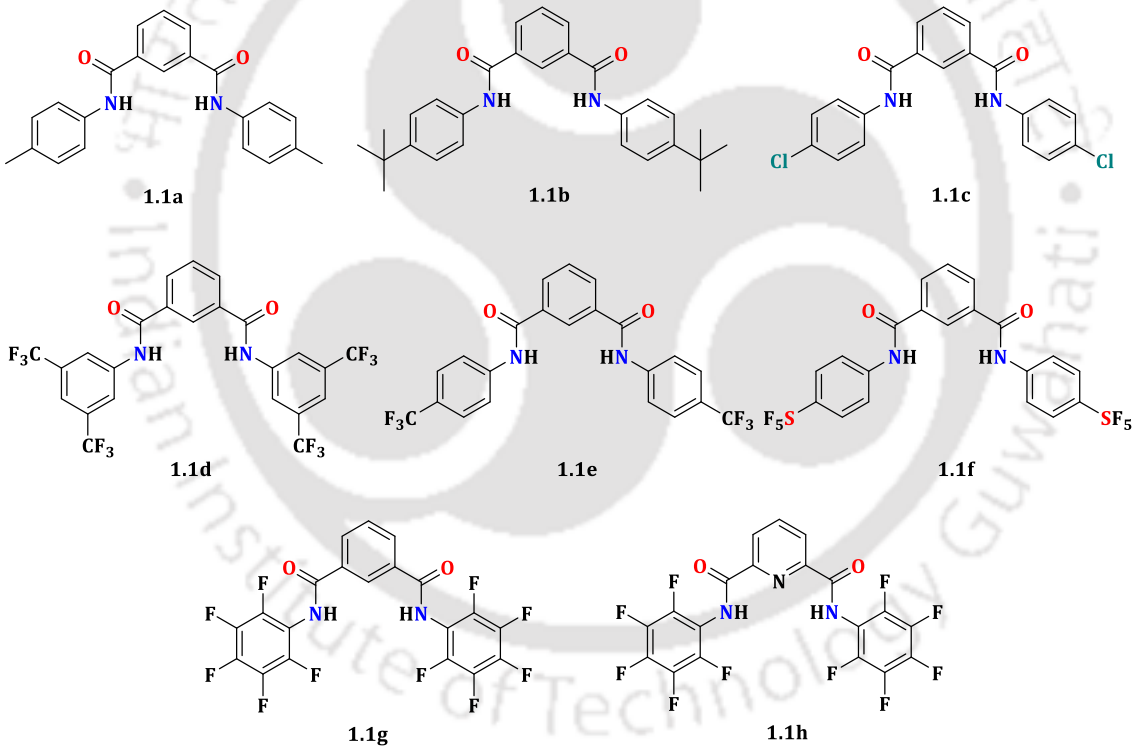

Figure 1.4. Diarylisophthalamide-based anionophores.

1.5. Artificial anionophores

1.5.1. Diarylisophthalamide-based anionophores

Many simple compounds were designed in the last two decades to explore the ion transport properties of small molecules across the biological layer. Caltagirone, Quesada and co-workers have presented derivatives of diarylisophthalamide and a

N,N′-diaryldipicolineamide derivative (**1.1a-1.1h**) and explored the effect of substitution pattern of these derivatives on their ion binding and corresponding transport across the biological membrane.[3, 30]

The anionophores showed modest ion binding behaviour for Cl^- as obtained through ^1H NMR titration DMSO-d_6. The anionophores also exhibited moderate Cl^-/NO_3^- and Cl^-/HCO_3^- transport across the POPC composed liposomes. Introducing electron withdrawing substitutents improved the ion transport property of the anionophores (**1.1c-1.1f**). The ability of pH discharge of the anionophores, as observed using the HPTS-fluorescence were in good accord with their previously observed values of Cl^- and NO_3^- transport.

1.5.2. Diamidocarbazole-based anionophores

Chmielewski and co-workers described the structure, synthesis, anion binding properties and anion transport capabilities of the 1,8-Diamidocarbazole derivatives.[31] The simple compounds showed outstanding binding selectivity for $H_2PO_4^-$ and AcO^- w.r.t Cl^- in DMSO + 0.5% H_2O. The fluorescent emission properties of **1.2e** and **1.2f** containing two *t*-BuCH_2-groups were studied. Pronounced enhancement in fluorescent intensity was observed on addition of $H_2PO_4^-$ and AcO^{--}. Whereas on addition of 100 equiv. of Cl^- no significant changes in fluorescent intensity were seen. Compound **16** exhibited almost 15-fold surge in fluorescent intensity upon addition of $H_2PO_4^-$ and $PhCOO^-$. Hence these two anionophores showed fluorescent turn-ON behaviour for $H_2PO_4^-$ and AcO^-. The Cl^- efflux properties of the anionophores were also investigated using ion selective electrode (ISE). Anionophores **1.2a**-**1.2d** were found to be putative Cl^- ion transporters. Simple substituent tuning showed dependency of ion transport potency on the substitution pattern.

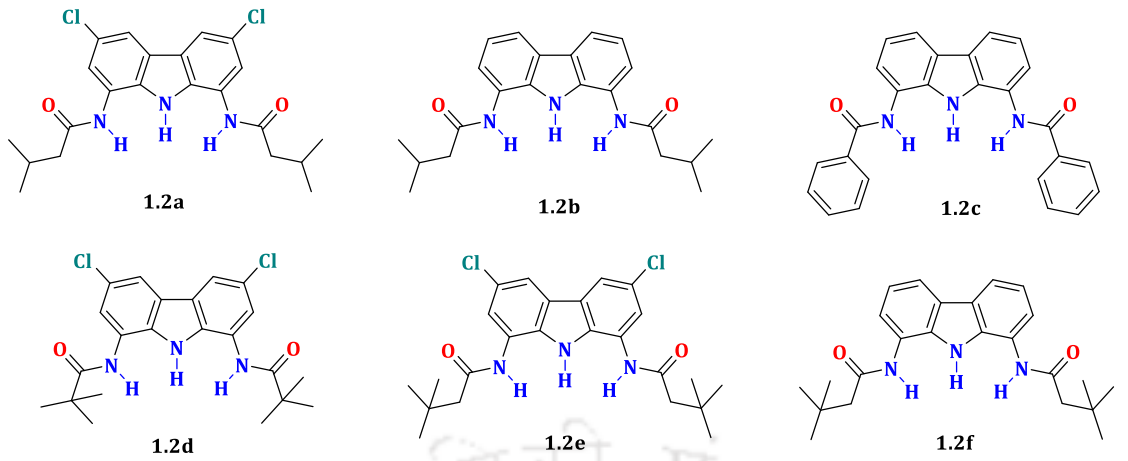

Figure 1.5. 1,8-Diamidocarbazole-based anionophores.

1.5.3. ortho-phenylenediamine-based anionophores

Gale and co-workers exhibited the excellent transport properties of highly simple and putative ortho-phenylenediamine-based bisureas (**1.3a–1.3h**) which perform even at 1:1 000 000 (receptor to lipid ratio) and compared their properties with the monoureas (**1.3j-1.3k**) [32] They have showed excellent H^+/Cl^- symport, Cl^-/NO_3^- and Cl^-/HCO_3^- antiport properties with the help of fluorescent-based assays and ion-selective electrode.

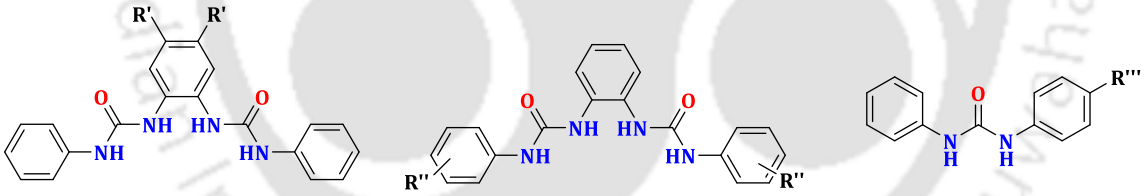

Figure 1.6. *o*-phenylenediamine-based bisurea anionophores.

1.5.4. trans-decalin-based anionophores

Gale and co-workers efficiently used the preorganised structure of trans-decalin tethered with flexible bis-urea arms to circumscribe the Cl^- ion with 8 H-bonds, which aids in ion transport across the lipid bilayer.[33] Marek, Rissanena and Davis co-workers also investigated through computation and theoretical experiments the wide range of potent ion binding behaviour of diureidodecalin **1.4**.[34] It is a potent non-toxic ion transporter with probable fascinating biological

applications. The studies confer that during the ion binding event the previously occurring H-bonding don't occur, giving rise to high binding efficiencies with a large spectrum of ions.

1.5.5. Anthracene 1,8-bisureas -based anionophores

Valkenier and Davis co-workers inspected the powerful anthracene 1,8-bisureas which are very impressive in ferrying ions across the LUVs.[35] Specially the bis-nitrophenyl derivative which was synthesised in two easy steps, offered great deliverability and excellent transferability across the vesicles. There was no need to preincorporate it in the vesicles beforehand and worked in an exceptional way when added after vesicles formation at very low concentration. Hence scaffolds like this can be used in future against cystic fibrosis condition.

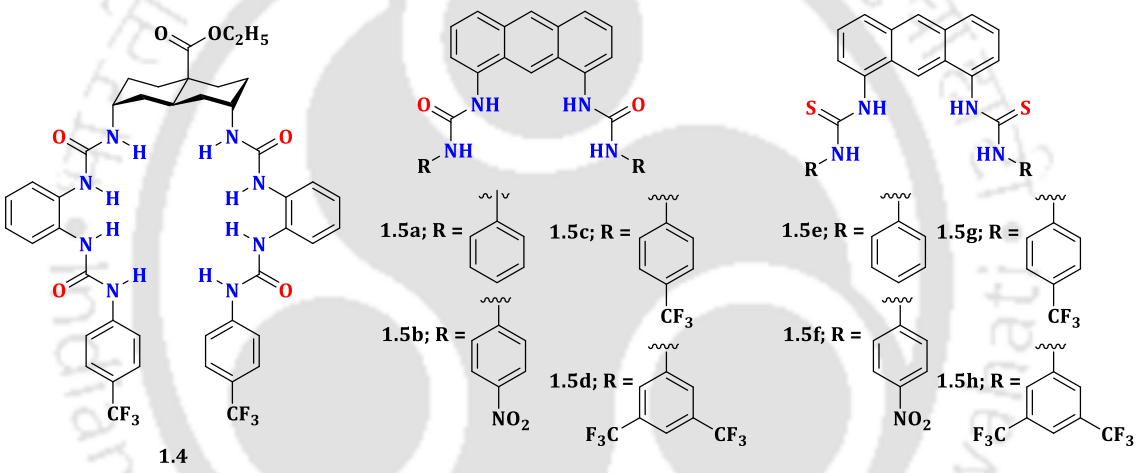

Figure 1.7. *trans*-decalin -based and anthracene 1,8-bisurea-based anionophores.

1.5.6. Valinomycin-like carriers

Electrogenic H^+/OH^- transport by synthetic ion transporters can lead to pH dissipation and finally toxicity in the cells. Two new scaffolds were designed which successfully mediated electrogenic Cl^- transport without being involved in H^+ or OH^- transport, i.e., without dispersing the pH thereby imitating the natural K^+ transporter, valinomycin.[36] The tripodal receptors offer two special advantage to permit $Cl^- > H^+/OH^-$ selectivity-Cl^- is entrapped better due to the presence of the preorganised cage-like structure of the tripodal transporters and thereby aiding in anion desolvation, also the chelating effect of the tripodal synthetic transporters help in better Cl^- ion binding than the monopodal transporters. Wu and Gale in 2016 surveyed the use of synthetic ion transporters which can function as mimics of

natural uncoupling proteins.[36] The synthetic transporters (**1.6a-1.6d**, having H-bonding and **1.6e**, possessing halogen bonding) displayed fatty acid activated H^+/OH^- transfer across the vesicles. The most potent transporter found was **1.6a**, which evinced considerable folds of higher H^+/OH^- potency in presence of oleic acid (OA). For all the transporters except for **1.6d**, the binding to AcO^- were stronger as compared to Cl^- due to more charge density in AcO^-. Here AcO^- has been used as a model to represent fatty acid anions. The strength of anion binding nature complies the sequence **1.6a**>**1.6c**>**1.6b**>**1.6d** which coincides with the H-bonding capability and the acidity of the synthetic transporters. Here the synthetic ion transporters act as flippase towards fatty acid ions. It was also observed that methylation in the binding site of the anion leads to reduced ion binding and hence loss in activity of transport.

1.5.7. Tren-based urea and thiourea derivatives

Gale and co-workers previously investigated the tren-based urea and thiourea containing synthetic transporters and their ion transport efficacy.[37] With the help of ion selective electrode, they studied the mechanism of chloride transport of the transporters through various routes like Cl^-/H^+, Cl^-/NO_3^-, Cl^-/HCO_3^- and the exciting Cl^-/SO_4^{2-}. On increasing the lipophilicity of the tripodal synthetic transporters with addition of fluoride the efficacy of the transport increases at low receptor to lipid ratios of 1:250000. The most potent receptor **1.7e** was tested to show cell cytotoxicity in the cancer cell line with the help of *in vitro* experiments. The mechanistic details of the transporters were revisited and reanalysed years later with the help with new assays.[38] The binding studies revealed the presence of 1:2 species as the dominant one. The previously found effective compound **1.7e** was shown to be the strongest uniporter of Cl^-. After addition of fatty acids also the mono- and non-fluorinated compounds showed some selectivity of Cl^- ion transport. Also, the nitrate transport potency of the

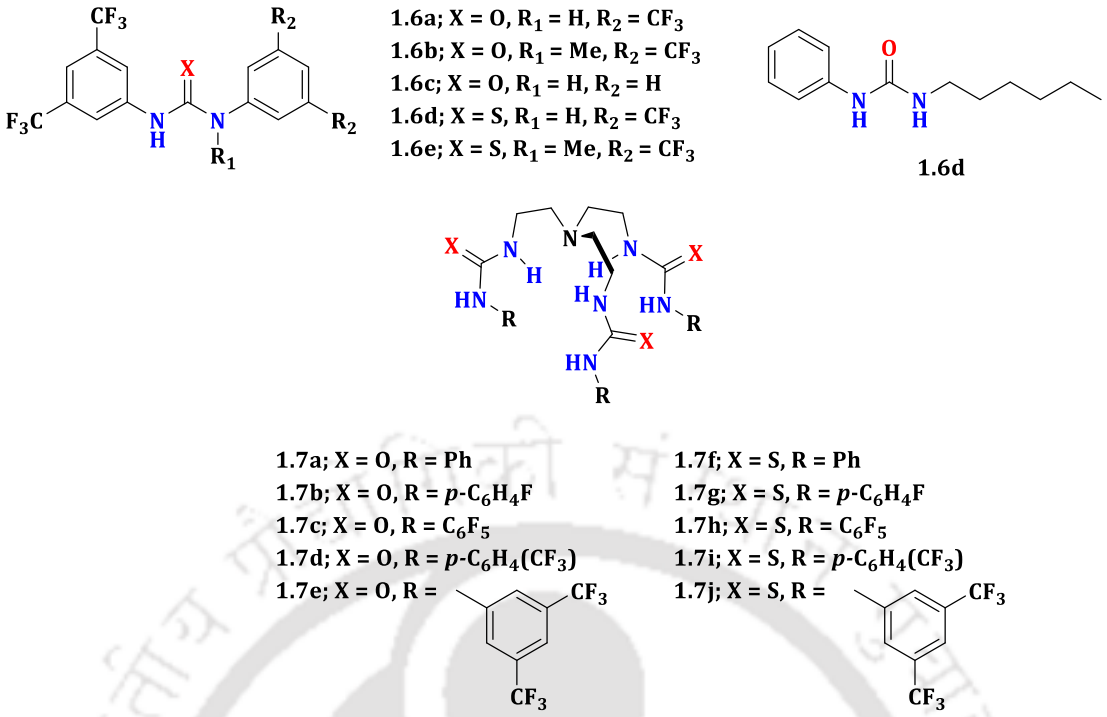

Figure 1.8. Structure of valinomycin-like carriers and tren-based urea and thiourea carriers.

anionophores evaluated and selectivity for Cl^- ion transport even in presence of NO_3^- ion was observed. A novel method was developed for analysing and quantifying sulfate transport and the EC_{50} values were determined. Additionally, the bicarbonate transport of the anionophores was also scrutinized.

1.5.8. Calixarene-based ion transporters

Valkenier, Jabin, Bartik and co-workers has in detail scrutinized the ion transporting behaviour of the cavity possessing calix[6]arenetris(thio)ureas (**1.8a-1.8d**).[39] The calixarenes were competent in transporting the ion pairs (organic) $PrNH_3Cl$ and *t*$BuNH_3Cl$ across the vesicles. The cotransport ability of the previously synthesised tripodal receptors were also investigated using similar assays. The assays depicted that the tripodal receptors were also able to transfer $PrNH_3Cl$ and *t*$BuNH_3Cl$ across the vesicles. This conveys that though presence of cavity shows a positive effect on the transport efficacy of the ion pairs, in absence of the cavity also the transport takes place. Here thulium complex was employed as the shift reagent to show undeniably that $PrNH_3^+$ is being transported across the vesicles with the help of ^1H NMR studies. This informative study can be used further to design complicated

cavity containing ion transporters to successfully transport biologically important ammonium ions.

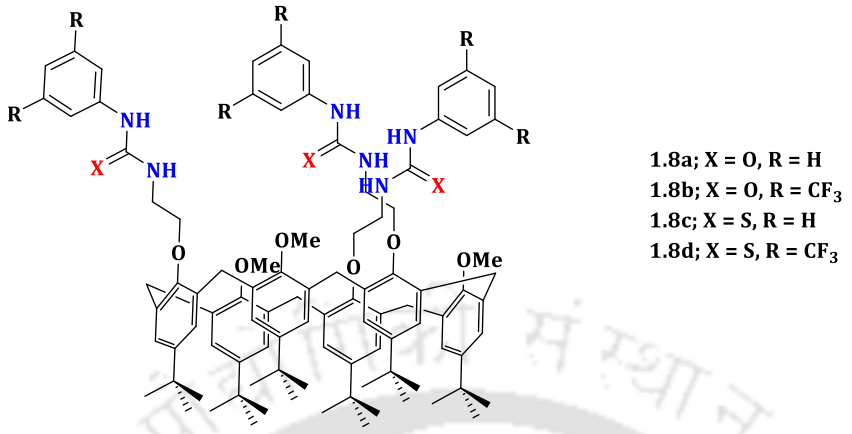

Figure 1.9. Structure of calixarenes.

1.5.9. Bispidine-based transporters

Shinde and Talukdar explored the H^+/Cl^- ion transport efficiency of the bispidine bicyclic transporter having H-bond donor sites (presence of two butyl amino group). [40] With the help of X-Ray crystallographic study, it was established that 2 H^+ and 2 Cl^- ions are involved with two consecutive melamine scaffold giving rise to the bispidine.$(HCl)_2$ complex. By varying the extravesicular salts and with the help of U-tube experiment, measuring Cl^- ion transport efficacy across EYPC-LUVs in presence and absence of FCCP and valinomycin along with the transporter proves that bispidine is efficient in transporting H^+/Cl^- across the lipid bilayer. At higher (8) or lower pH (5.8) transport efficiency is reduced and shows utmost efficiency at pH 7.

1.5.10. Cyclic peptide-based transporters

Amorin and Granja co-workers developed α, γ-cyclic peptide dimers where each cyclic peptide is tethered with three perpendicular pyridine rings.[41] Here the pyridine rings serve as the recognising moiety. The *ortho cyclic peptide transports superior Cl^- than the meta one. Here the same identification motif recognises both anions and cations with great efficacy. Behera and Madhavan also developed a classic triamide macrocycle decorated with hydrophobic appendages (*cholic acid, cholesterol chains, alkyl and oligoether) (**1.10c-1.10f**). [42] *The macrocycle with the hydrophobic*

cholesterol attached showed the lowest EC_{50} of 0.44 μM across the EYPC composed LUVs due to the superior membrane permeability of the cholesterol appendage.

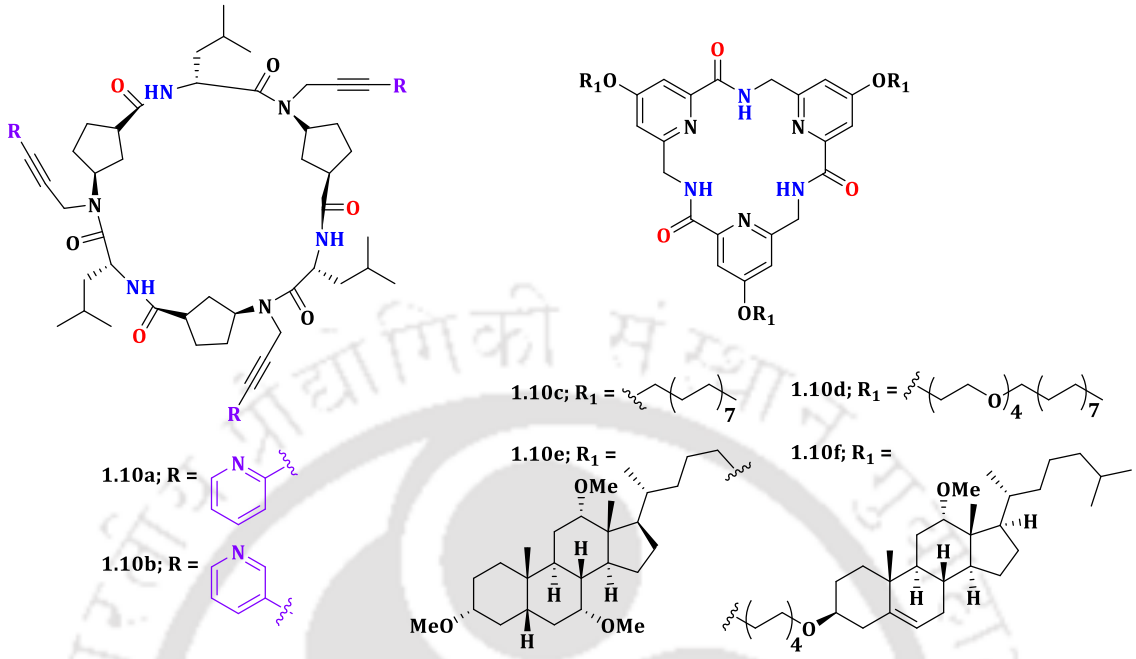

Figure 1.10. Macrocycle-based synthetic ion transporters.

1.5.11. Bis-amido imidazole derivatives

Shinde and Talukdar prepared a group of bis(amido) imidazoles (**1.11a-1.11f**).in the protonated state of the imidazole ring binded Cl^- ion studied with the help of ^1H NMR studies.[43] With the help of various biophysical assays, it was established that **1.11a** was the most efficient transporter of H^+/Cl^- via the mobile carrier pathway across the EYPC vesicles.

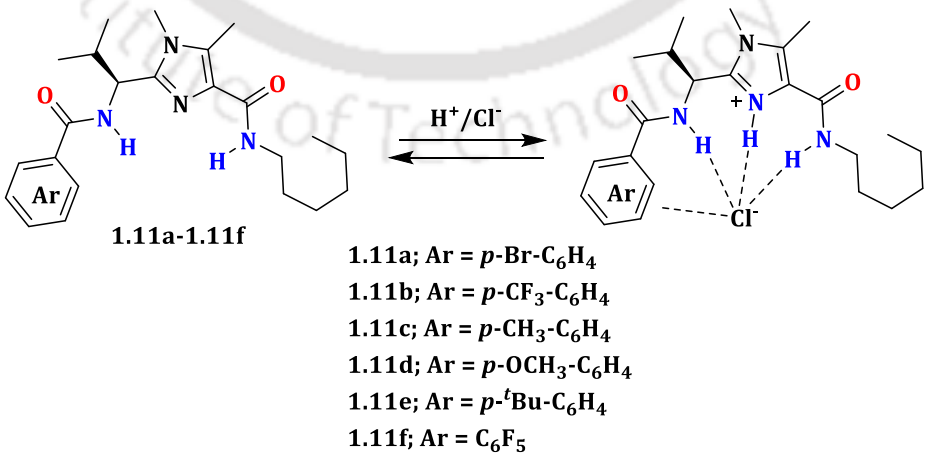

Figure 1.11. Structure of potent bis(amido) imidazole-based synthetic ion transporters.

1.5.12. Sulfonamide-based ion transporters

Shinde and Talukdar also developed o- phenylenediamine moieties linked to different phenyl substitutents through sulfonamide linkage.[44] The pK_a of the N-H of sulfonamide groups for some of the derivatives lies in the physiological range. Transporter **1.12d** is the most potent ion transporter, mediating H^+/Cl^- transport. With the help of X-Ray crystallography experiment it was seen two Cl^- was binded by two synthetic ion transporter molecules. By performing various fluorescence-based experiments the U-Tube experiment, it was established that the sulfonamide derivatives mediated H^+/Cl^- transport across the LUVs.

1.5.13. Triazine-based ion transporters

Talukdar and co-workers also explored prearranged synthetic anionophores based on triazine core moiety having a cavity.[45] The triazine core was appended with 3,7-diazabicyclo[3.3.1]nonane arms to obtain the preorganised structure with cavity. The functionalisation of the arms helped in controlling the lipophilicity and protonation site which aided in bonding of the ion and its transport. Compound **1.13a** was found as the most efficient transporter with the help of the dose-dependent experiment with an EC_{50} of 0.25 μM, n = 1.09. Receptors **1.13a** and **1.13b** specifically showed selective Cl^- transport behaviour in an antiport fashion across the LUVs. The chloride efflux potency of the two receptors **1.13a** and **1.13b** were checked at 5 different pH (5.3, 6.0, 7.0, 8.0, 8.8). Receptor **1.13a** showed the highest Cl^- transport at pH 7.0 which can be explained based on its pKa value as obtained from both Jaguar module and MarvinSketch program.

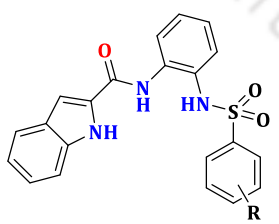

1.12a; R = 2,3,4,5,6-Pentafluoro
1.12b; R = *p*-Br
1.12c; R = *p*-NO_2
1.12d; R = *p*-Me

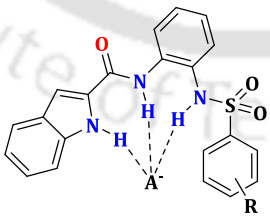

1.12e; R = *p*-CF_3
1.12f; R = *p*-OMe
1.12g; R = 2,4,6-Trifluoro

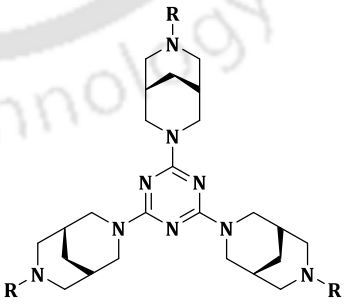

1.13a; R = -$CH_2C_6H_5$, 1.13b; R = -$CH_2C_6F_5$, 1.13b; R = -H

Figure 1.12. Sulfonamide-based and triazine-based tripodal receptors.

1.5.14. Phosphazene-based ion transporters

For many years, ion binding and sensing have been operated almost solely by organic receptor molecules owing to their easy synthesis. In this regard Wright and co-workers have been investigated the anion binding and transport properties of a small series of phosphazanes having H-bonding network to bind the Cl^- ion.[46] With the help of NMR titration studies, it was observed that the binding affinity follows the order **1.14c**>**1.14b**>**1.14a**. In the ion transport experiment transporter containing electron

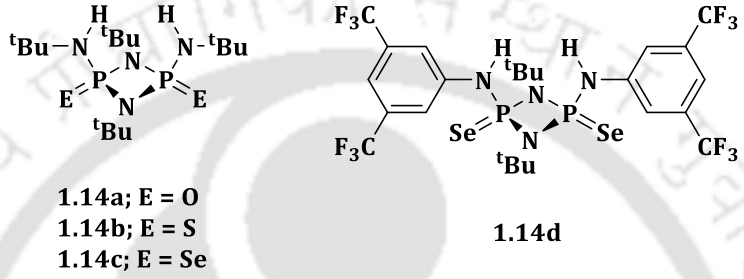

Figure 1.13. Structure of phosphazane anion receptors receptors.

withdrawing groups was found to be a better transporter than **1.14c** having electron donating groups following the Cl^- ion binding values. Matile et al. have reported several ion transporters showing chalcogen bonding, halogen bonding and pnictogen bonding. [57, 58, 59] The heavier chalcogen congeners were found to be better transporter of the Cl^- ion across the LUVs using both lucigenin and HPTS dye, due to increased hydrophobicity and better anion affinity. Thus, using this work as the base platform, main group elements can be incorporated to design highly potent anion transporters.

1.5.15. Tetraurea macrocycle-based ion transporter

Gale and co-workers reported a preorganised tetraurea macrocycle that recorded a high H^+/Cl^- transport across the vesicles.[47] With the help of HPTS entrapped LUVs, the anion selectivity was checked by comparing the EC_{50} values of H^+/X^- (X^- = Cl^-, Br^-, I^-, $NO_3^-$and ClO_4^-). The anion selectivity was found to follow the order $Cl^- > Br^- > I^- > NO_3^- > ClO_4^-$. Besides the H^+/Cl^-, the macrocycle **1.15a** was found to also mediate antiport process across the vesicles. Due to lack of uniport transport activity of **1.15a**, the ion channel formation tendency of potent macrocycle can be negated. This result along with the observation of high binding affinity of **1.15a** with

$H_2PO_4^-$ led to the hypothesis that the macrocycle is involved in binding the lipid headgroup in the vesicles. Hence the H^+/Cl^- transport activity of the macrocycle **1.15a** and prodigiosin was investigated using the voltage-dependent experiment. In the macrocycle **1.15a** and not prodigiosin displayed voltage switchable ion transport behaviour. Among the five series of compounds, the voltage switchable behaviour was observed for the transporter with the strongest binding affinity for $H_2PO_4^-$ and not for the most potent transporter of Cl^- ion. This unusual study and the results can be used for the use of highly potent synthetic ion transporters and as a therapeutic target to treat the cancer cells by targeting their unusual membrane potential.

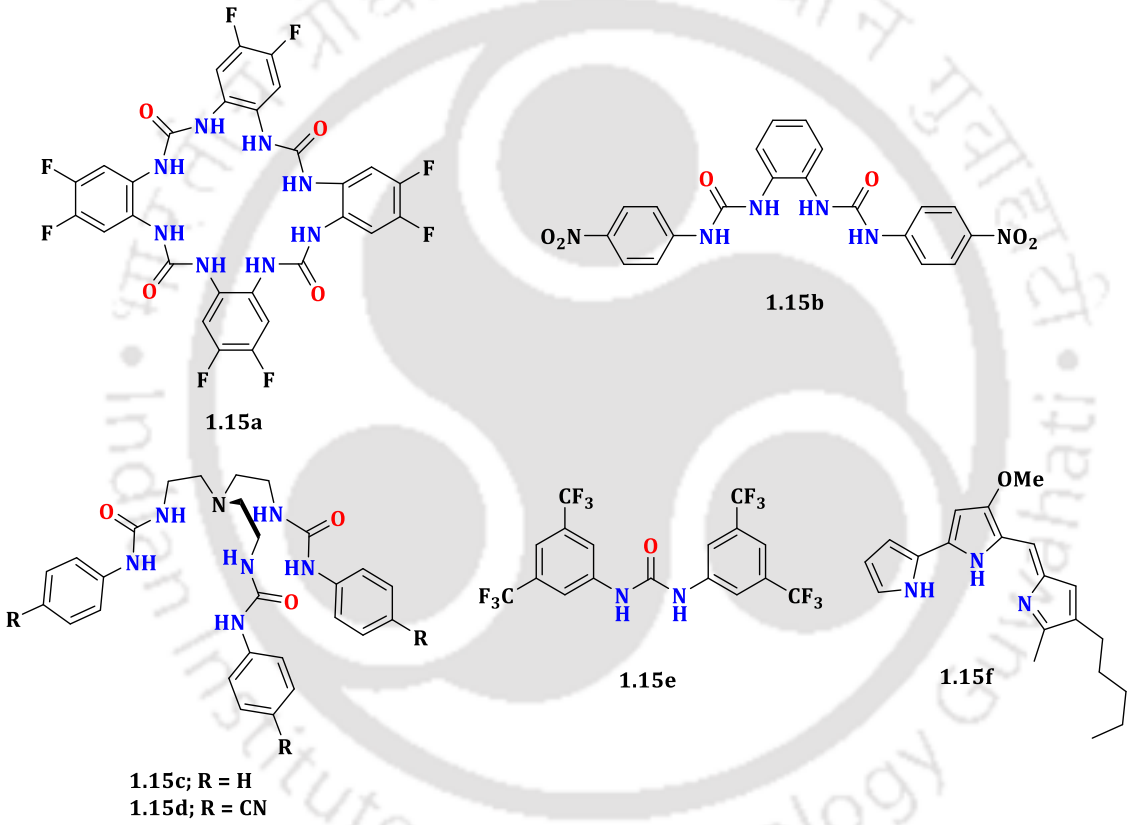

Figure 1.14. Structure of voltage switchable ion receptors receptors.

1.5.16. Fatty acid-based ion transporters

Gale and co-workers explored the novel concept of fatty acid injection to create a pH gradient across the lipid bilayer ($pH_{in} < pH_{out}$) which triggers enormous H+/Cl- transport mediated by synthetic transporters across the vesicles.[48] The synthetic transporters (**1.16a**-**1.16c**) used here was also previously studied in detail regarding Cl^- transport. Using the HPTS-based fluorescence assay, the pH dissipation property of the transporters **1.16a**-**1.16c** were studied and it was found that on addition of

the transporters to the previously added oleic acid (OA) vesicles, efflux of H^+ happens along with Cl^- ion. To demonstrate, that H^+ efflux must be accompanied with Cl^- efflux from the vesicles, CCCP (a protonophore) was used in place of the transporters. However no significant change in pH was observed showing results similar to when DMSO was added thereby confirming pH efflux alone is not possible to maintain charge balance. In another experiment 0.01 mol% of the transporter **1.16a** was used followed by subsequent addition of OA (2.5 μM) to decrease the inner pH to fuel H^+/Cl^- transport mediated by the transporters. After each addition of OA, the pH gradient restabilises, while the presence of **1.16a** ensured again H+/Cl- efflux. However, after 5 cycles of OA addition, the pH dissipation capacity of the transporter **1.16a** decreases due to build-up of Cl^- ion gradient outside the vesicles. Similar results of OA fuelled H^+/Cl^- transport across the vesicles mediated by the transporters were obtained from lucigenin entrapped LUVs. Hence it was predicted that most synthetic transporters can be used as such thereby having wide application in bioenergetics.

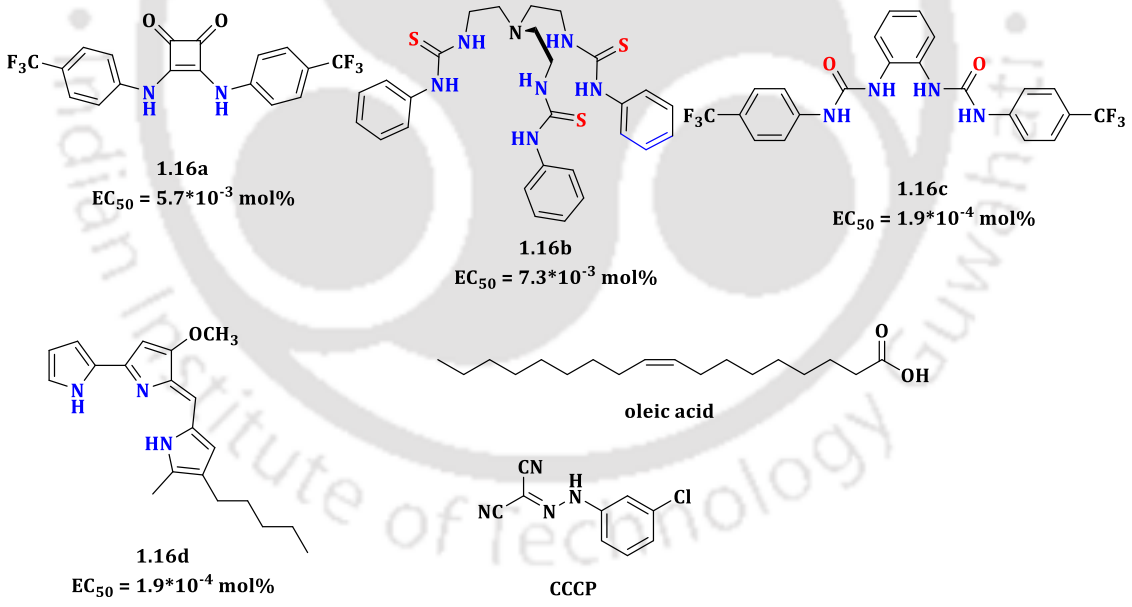

Figure 1.15. Ion transporters showing FA fueled ion transport.

1.5.17. Organic cage-based ion transporter

Row, Kim and co-workers have developed an 3D organic cage **1.17**, taking motivation from their previous work.[49, 50] The organic cage is substantial internal cavity to allow the ions to pass through it and also the size of the cage is 3.64 nm which seems to allow the organic cage to wholly span across the lipid bilayer.

Additionally, the cage is also easily synthesizable in one pot with high yield using DCC approach. With the help of lucigenin-based fluorescence assay the dose-dependent

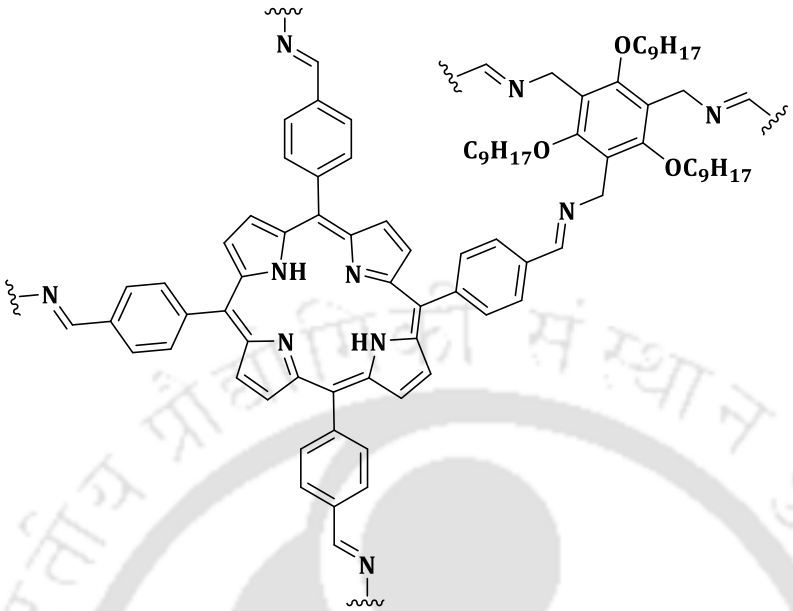

1.17

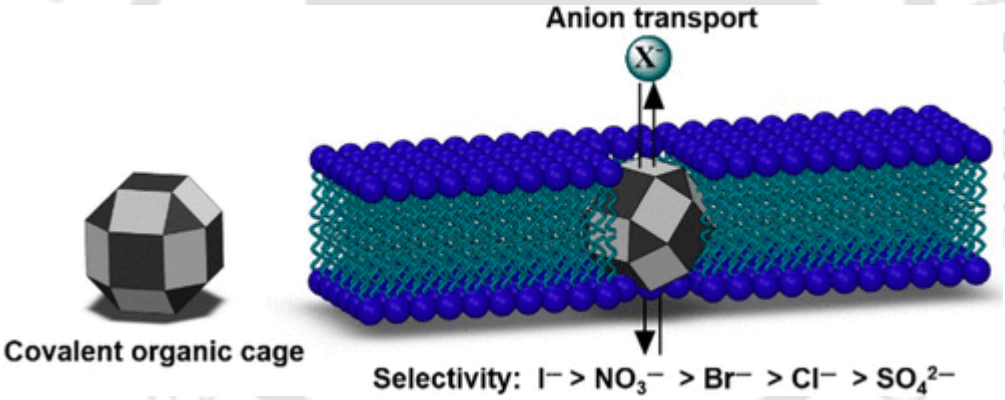

Figure 1.16. Structure of 3D organic cage

Cl^- ion transport was investigated and the linear increment relationship in the transport rate with concentration of the organic cage corroborates the Cl^- transport mediated by **1.17.** It was also seen that for **1.17**, the antiport transport of Cl^-/NO_3^- is more preferable than the symport transport of Na^+/Cl^-. With the help of HPTS-based fluorescence experiment, the anion selectivity was checked by applying NaX gradient in which **1.17** showed highest selectivity for I^-. This trend greatly indicates that dehydration of the concerned anion is absolutely necessary in its transport mediated by **1.17**. The voltage clamp experiments suggest that **1.17** acts as a dynamic ion channel. The potency of **1.17** to mediate iodide transport across HEK-293T cells

were explored with the help of iodide sensitive yellow fluorescent protein (YFP-H148Q/I152L) gene. After addition of **1.17** consequent quenching of fluorescent intensity suggested iodide ion influx. Hence using the structural framework of the organic cage further potent transporters can be developed in future which can be used for iodide deficiency related ailments.

1.5.18. Metal-organic synthetic ion transporters

Kemp and Schmitzer synthesised two 2,4,7-triphenyl-benzimidazole functionalised and used their self-assembled structure in the phospholipid bilayer to successfully transport ion across the vesicles.[51] The in-situ formation of MOST in the lipid environment was efficiently studied with the help of fluorescence. After addition of $PdCl_2$ in EYPC liposomes containing 2 or 3, a quenching of fluorescence intensity was observed which directly points at the possibility of self-assembling of ligands 2 and 3. Due to the self-assembling process the spatial distance between two ligands decreases which ensued in photon transfer between them and consequently decrease in fluorescence intensity. With the help of UV/Vis titration experiment of

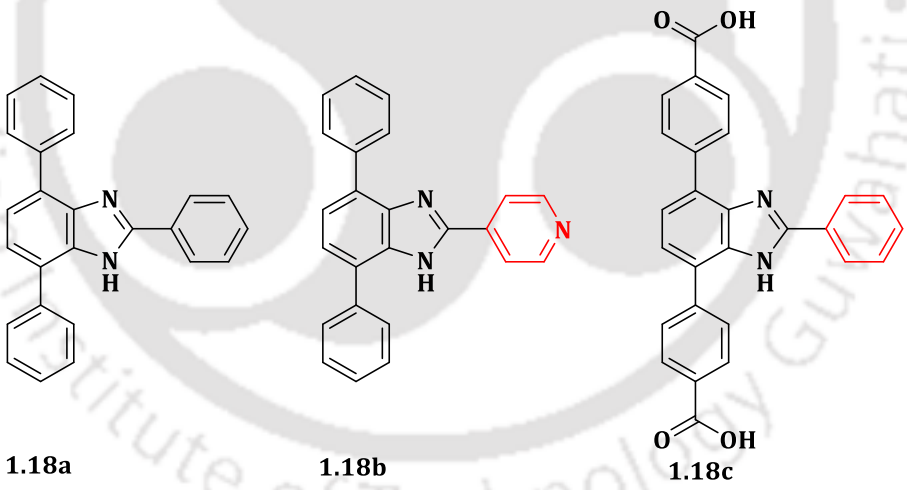

Figure 1.17. Triphenyl-benzimidazole functionalised ligands.

the ligands (**1.18a-1.18c**) with $PdCl_2$, the metal ligand binding and their stoichiometries were determined. In case of ligand **1.18a** and **1.18c**, 1:1 complex was recognised with $PdCl_2$ and with ligand **1.18b** 2:1 complex formed with $PdCl_2$. The anionophoric capability of **1.18a** was investigated previously in a different work.[52] In this work after addition of Pd^{+2} and Ru^{3+}, the Cl^- transport efficiency of **1.18b** and **1.18c** surged enormously. However, such results were not obtained after addition of

$HAuCl_4$ and $AgBF_4$. With the assistance of various biophysical experiments, in case of Pd^{2+}(**1.18b**) MOST, the symport (Cl^-/cation$^+$) and antiport (Cl^-/anion$^-$), both the processes were found to be equally probable. But in case of Pd^{2+}(**1.18c**) MOST, the symport mechanism was found to be the presiding one. Being encouraged with the results of ion transport across LUVs and by analysing the porous nature of the MOST, their effect on gram-positive bacteria. After addition of $PdCl_2$ on previously incubated gram-positive bacteria, bacterial cell death was observed, hence creating the platform for using this kind of MOSTs against resistant bacterial strains.

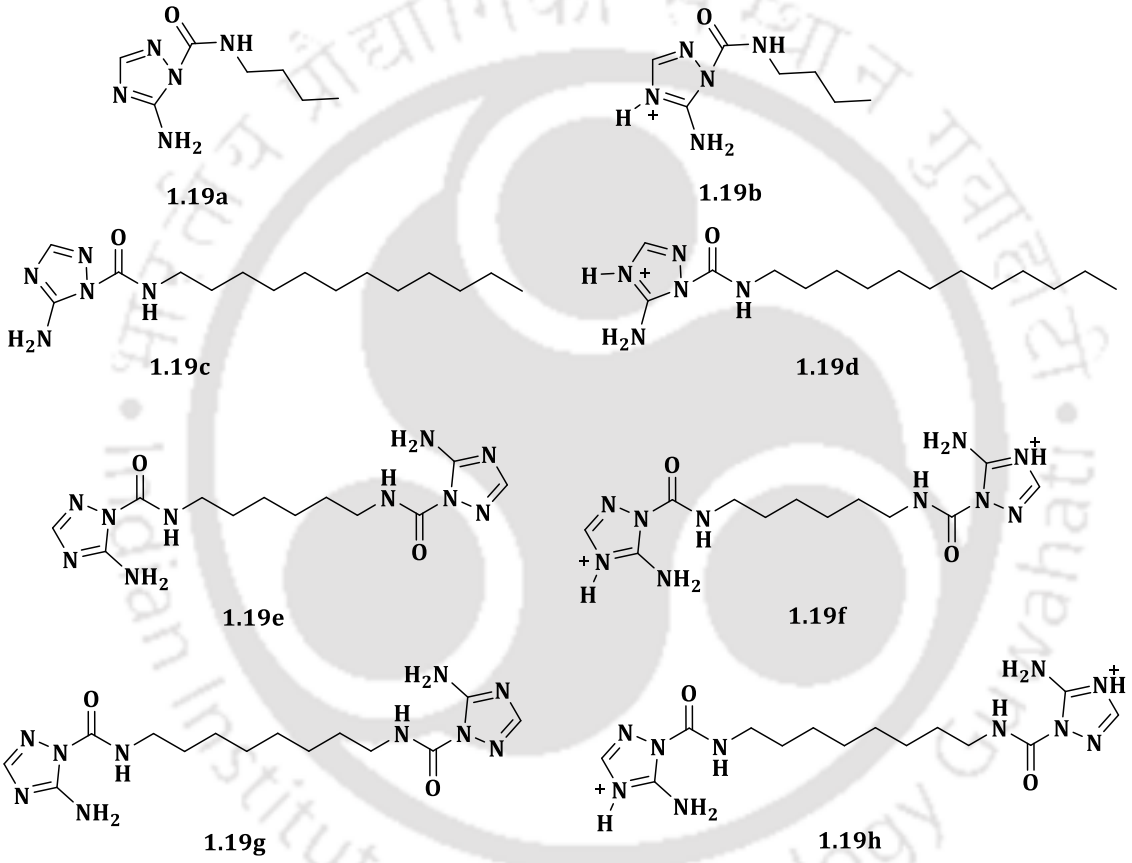

Figure 1.18. Structure of amino-triazole cation amphiphile.

1.5.19. Triazole quartet-based anion channel

Barboiu and co-workers wonderfully developed amino-triazole (TH^+) cation amphiphile which self assembles in the lipid bilayer and is stabilised with the help of various favourable interactions of the anion channel with the anions (H-bonding, electrostatic interaction and anion-Π interactions).[53] The presence of the triazole quartets removes the water molecules of a hydrated anion similar to that in natural

ion channels. The study also showed that by simply tuning the alkyl chains from short to long, the transport efficiencies of the anions can be varied.

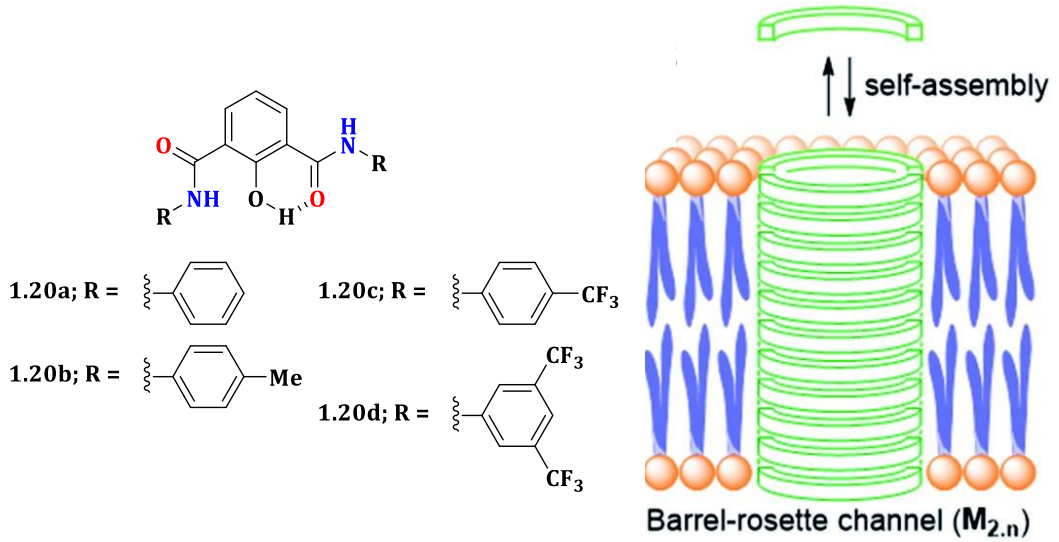

Figure 1.19. Structure of diarylisophthalamide derivatives.

1.5.20. Diarylisophthalamide-based ion channels

Talukdar and co-workers developed diarylisophthalamide based ion channels which are fluorescent.[54] With the help of EYPC-LUVs⊃HPTS, the ion transport efficiency follows the order **1.20d>>1.20c>1.20b>1.20a**, clearly correlating with the pK_a value of the amide proton of the synthetic transporters rather than the logp value of the transporters. Transporter **1.20d** bearing two 3,5-bis(trifluoromethyl)phenyl appendages was the potent ion transporter with an EC_{50} value of 0.48 μM (0.58 mol% w.r.t lipid). With the help of dose-dependent Cl^- transport activity data of **1.20d**, it was found that n = 2 which means that a dimeric active structure of the transporter forming the ion channel is responsible in transporting Cl^- across the vesicles. On checking the anion selectivity, **1.20d** showed highest selectivity for Cl^- among the other anions being tested. Among the alkali metals, **1.20d** was most selective for both K^+ and Rb^+. With the help of various biophysical experiments, it was established that the transporters mediated M^+/Cl^- transport. By measuring the ionic conductance across the lipid bilayer, it was established that **1.20d** forms ion channels. Utilizing the inherent fluorescent property of **1.20d**, the time taken by it to get inside the cells was evaluating by

incubating **1.20d** in MCF7 cell line. It was observed that within few seconds of incubation **1.20d** was able to enter the cells and within just few minutes AVD could be observed in the cells which is a well-known hallmark of early apoptosis. Encouraged with the results, the dose dependent cell viability was checked of MCF7 cells in presence of **1.20d**, and the IC_{50} of approximately 5 μM was calculated. With the help of HBSS experiment, it was established that the cell death is because of M^+/Cl^- transport. Next with the help of JC-1 dye experiment, ROS measuring experiment, western blotting and with PI staining experiment, the triggering of the apoptotic pathway by **1.20d** was proved.

1.5.21. Non-toxic anionophores

Other than targeting cancer, many anionophores were designed to cure other channelopathies like cystic fibrosis.[55] Due to the large number of mutations possible, only the medically approved drugs are not that much effective to treat cancer. As the anionophores don't target a particular gene, protein or enzyme in CFTR, they can be used as additives along with medically approved drugs. They tested a total set of 22 anionophores in real time with the help of fluorophore YFP-H148Q/I152L which is halide sensitive in the FRT cells. When the YFP-FRT cells are treated with anionophores, I^- is being transported inside due to which a quenching of YFP fluorescence was observed. In the control experiment (DMSO was added in place of the anionophore), no significant fluorescence quenching was noticed which proves that iodide by itself can't enter the YFP-FRT cells. Also, cystic fibrosis occurs in the epithelial cells, hence it is very much important for the anionophores to show transport activity in the epithelial cell lines especially of the respiratory airways. Anionophores **1.21a**, **1.21b**, **1.21c** and **1.21d**. Next to investigate whether the transport activity of the anionophores have some supplementary effect to CFTR, the anionophores were treated to FRT cells expressing both CFTR and YFP. For the anionophores **1.21a**, **1.21b**, **1.21c** and **1.21d**, the fluorescence intensity profiles were in addition to forskolin (10 μM) and the CFTR inhibitor 10 μM and in their absence. To be able to use the anionophore as additives to CF approved drugs, the cytotoxicity to the normal cell line shall be minimum. Hence the cytotoxicity of the anionophores were evaluated in YFP-CFBE cells. Anionophore **1.21a** showed minimal cytotoxicity in all concentrations, however anionophores **1.21b**, **1.21c** and **1.21d** showed some cell death. Hence this extensive study initiates the use of

potential anionophores alone or in combination with approved drugs to treat channelopathies like cystic fibrosis.

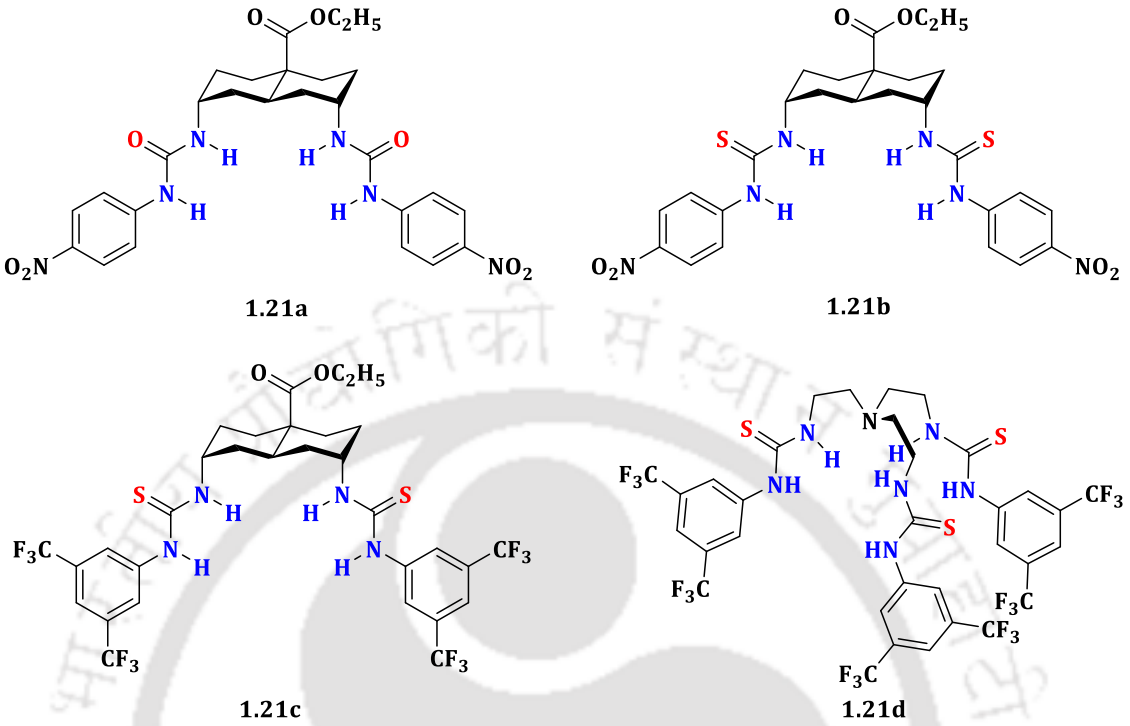

Figure 1.20. Structure of non-toxic anionophores.

1.5.22. Anionophores transporting other ions

In the last two decades, the emphasis of ion transport has been only to less hydrophilic anions like Cl^-, HCO_3^- and only in two instances SO_4^{2-}. The transport of highly hydrophilic oxoanions like $H_2PO_4^-$, HPO_4^{2-}, SO_4^{2-}, which are also found in high abundance in the biological medium and are also physiologically very important have been sidelined over decades. Their transport is extremely tough due to their very high hydration energies, geometrically complex structures and also because of absence of a direct method to measure their transport activity. In this regard Kros, Chmielewski and co-workers used simple bis(thioamido)carbazole-based derivative **1.22** and with the help of lucigenin-based fluorescent experiment, they demonstrated the transport of organic phosphates as well as anti-inflammatory drugs like aspirin across LUVs and GUVs [56]. The fluorescence intensity of lucigenin quenches in presence many biologically important anions like, chloride, phosphates, organic phosphates. Transporter **1.22** was found to efficiently transport chloride, carboxylate, benzoate and aspirin across the GUVs. In presence of **1.22**, the

movement of diphenyl phosphate across the lipid bilayers is quickened. With the help of lucigenin experiment, the half live values of the decay curves of the various anions were obtained and they follow the selectivity order aspirin>$(PhO)_2PO_2^-$>$PhCOO^-$ >Cl^-. Hence taking cues from the promising oxoanion transport candidate, future anionophores can be designed which will be able to more efficiently transport the important oxoanions across the vesicles.

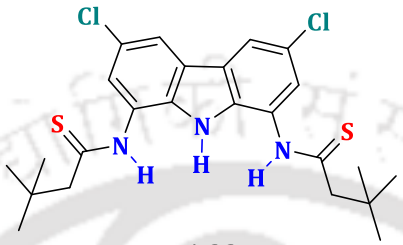

1.22

Figure 1.21. Structure of bis(thioamido)carbazole-based derivative.

1.6. Summary

During the last two decades the ion transport mediated by small synthetic ion transporters has garnered a lot of efforts from the supramolecular chemists and also attention for their therapeutic values specially in case of cancer and cystic fibrosis (a common channelopathy). There are some biologically important ions which are found in the biological medium in high abundance. Hence such ions like Cl^-, HCO_3^- have been targeted and their transport has been facilitated with the help of synthetic ion transporters. The synthetic ion transporters showing toxicity in the cancer cells were used against the cancer cells and impressive results were obtained. Nevertheless, the selectivity issue (cancer cells over the normal cells) remains a daunting task to achieve. The anionophores which showed very less toxicity towards the normal cell lines were used to treat channelopathies like cystic fibrosis and also showed very promising results. Also, in the future this 'ion therapy' has huge prospects to be used for therapeutic purposes for other channelopathies.

1.9. Objective of research work

The thesis has primarily divided into five chapters. **Chapter 1** mainly argues the importance of the transmembrane transporters in the biological system and the disease conditions which can pose due to stunted transport by the natural systems. **Chapter 2** involves the exploration of the PITENIN-based transporters, their

moderately good H^+/Cl^- transportation proficiency, pH stimulated increased transport efficiency, and apoptosis instigating behaviour in cancer cells. **Chapter 3** emphasizes the use of light to induce the generation of the active anionophore, which transports Cl^-/ across LUVs to improve the selectivity of the cancer cells. **Chapter 4** embodies the use of photocleavable targeted-proanionophore to target the cancer cells better and reduce toxicity in the normal cells. The PDT activity of the photo product has also been investigated here.

1.8. References

(1) Prevarskaya, N.; Skryma, R.; Shuba, Y. J. P. r. Ion channels in cancer: are cancer hallmarks oncochannelopathies? **2018**, *98* (2), 559-621.

(2) Gokel, G. W.; Carasel, I. A. J. C. S. R. Biologically active, synthetic ion transporters. *Chem. Soc. Rev.* **2007**, *36* (2), 378-389.

(3) Davis, J. T.; Gale, P. A.; Quesada, R. J. C. S. R. Advances in anion transport and supramolecular medicinal chemistry. *Chem. Soc. Rev.* **2020**, *49* (16), 6056-6086.

(4) Saha, T.; Hossain, M. S.; Saha, D.; Lahiri, M.; Talukdar, P. J. J. o. t. A. C. S. Chloride-mediated apoptosis-inducing activity of bis (sulfonamide) anionophores. *J. Am. Chem. Soc.* **2016**, *138* (24), 7558-7567.

(5) Saha, T.; Gautam, A.; Mukherjee, A.; Lahiri, M.; Talukdar, P. J. J. o. t. A. C. S. Chloride transport through supramolecular barrel-rosette ion channels: lipophilic control and apoptosis-inducing activity. *J. Am. Chem. Soc.* **2016**, *138* (50), 16443-16451.

(6) Litan, A.; Langhans, S. A. J. F. i. c. n. Cancer as a channelopathy: ion channels and pumps in tumor development and progression. *Front. Cell. Neurosci.* **2015**, *9*, 86.

(7) Lang, F.; Stournaras, C. J. P. T. o. t. R. S. B. B. S. Ion channels in cancer: future perspectives and clinical potential. *Philos. Trans. R. Soc. B* **2014**, *369* (1638), 20130108.

(8) Repke, K. R. The role of the Na+/K+ pump in normal and cancer cell proliferation. In *Biomembranes*, Springer, 1988; pp 160-176.

(9) Park, S.-H.; Park, S.-H.; Howe, E. N.; Hyun, J. Y.; Chen, L.-J.; Hwang, I.; Vargas-Zuñiga, G.; Busschaert, N.; Gale, P. A.; Sessler, J. L. J. C. Determinants of ion-transporter cancer cell death. *Chem* **2019**, *5* (8), 2079-2098.

(10) Andersen, A. P.; Moreira, J. M.; Pedersen, S. F. J. P. T. o. t. R. S. B. B. S. Interactions of ion transporters and channels with cancer cell metabolism and the tumour microenvironment. *Philos. Trans. R. Soc. B* **2014**, *369* (1638), 20130098.

(11) Fiorotto, R.; Strazzabosco, M. J. C.; Gastroenterology, M.; Hepatology. Pathophysiology of cystic fibrosis liver disease: a channelopathy leading to alterations in innate immunity and in microbiota. *CMGH Cellular and Molecular Gastroenterology and Hepatology* **2019**, *8* (2), 197-207.

(12) Connett, G. J. D. D., Development; Therapy. Lumacaftor-ivacaftor in the treatment of cystic fibrosis: Design, development and place in therapy. *Drug Des Devel Ther* **2019**, *13*, 2405.

(13) Pier, G.; Prince, A.; Cantin, A. J. N. M. Cystic fibrosis: an-ion transport issue? *Nat. Med.* **2011**, *17*, 166-167.

(14) Xin, P.; Zhao, L.; Mao, L.; Xu, L.; Hou, S.; Kong, H.; Fang, H.; Zhu, H.; Jiang, T.; Chen, C.-P. J. C. C. Effect of charge status on the ion transport and antimicrobial activity of synthetic channels. *Chem. Commun.* **2020**, *56* (89), 13796-13799.

(15) Elie, C. R.; David, G.; Schmitzer, A. R. J. J. o. M. C. Strong antibacterial properties of anion transporters: a result of depolarization and weakening of the bacterial membrane. *J. Med. Chem.* **2015**, *58* (5), 2358-2366.

(16) Carreira-Barral, I.; Rumbo, C.; Mielczarek, M.; Alonso-Carrillo, D.; Herran, E.; Pastor, M.; Del Pozo, A.; García-Valverde, M.; Quesada, R. J. C. C. Small molecule anion transporters display in vitro antimicrobial activity against clinically relevant bacterial strains. *Chem. Commun.* **2019**, *55* (68), 10080-10083.

(17) Gürbüz, M. U.; Aghatabay, N. M.; Karabulut, H. R. F. J. J. o. H. C. Synthesis, Structural Aspects, Antimicrobial Activity, and Ion Transport Investigations of Four New [1+ 1] Condensed 12-Membered Cyclophane Amides. *J. Heterocycl. Chem.* **2017**, *54* (2), 952-958.

(18) Kondratskyi, A.; Kondratska, K.; Skryma, R.; Prevarskaya, N. J. B. e. B. A.-B. Ion channels in the regulation of apoptosis. *Biochim. Biophys. Acta* **2015**, *1848* (10), 2532-2546.

(19) Patergnani, S.; Danese, A.; Bouhamida, E.; Aguiari, G.; Previati, M.; Pinton, P.; Giorgi, C. J. I. J. o. M. S. Various aspects of calcium signaling in the regulation of apoptosis, autophagy, cell proliferation, and cancer. *Int. J. Biol. Sci.* **2020**, *21* (21), 8323.

(20) Bruce, J. I. J. W. J. o. B. C. Plasma membrane calcium pump regulation by metabolic stress. *World J Biol Chem* **2010**, *1* (7), 221.

(21) Felippe Gonçalves-de-Albuquerque, C.; Ribeiro Silva, A.; Ignácio da Silva, C.; Caire Castro-Faria-Neto, H.; Burth, P. J. M. Na/K pump and beyond: Na/K-ATPase as a modulator of apoptosis and autophagy. *Molecules* **2017**, *22* (4), 578.

(22) Chen, D.; Song, M.; Mohamad, O.; Yu, S. P. J. B. c. Inhibition of Na+/K+-ATPase induces hybrid cell death and enhanced sensitivity to chemotherapy in human glioblastoma cells. *BMC Cancer* **2014**, *14* (1), 1-15.

(23) Yurinskaya, V. E.; Vereninov, I. A.; Vereninov, A. A. J. F. i. c.; biology, d. Balance of Na+, K+, and Cl–Unidirectional Fluxes in Normal and Apoptotic U937 Cells Computed with All Main Types of Cotransporters. *Front Cell Dev Biol* **2020**, *8*, 591872.

(24) Bortner, C. D.; Cidlowski, J. A. J. C. d.; differentiation. Apoptotic volume decrease and the incredible shrinking cell. *Cell Death Differ.* **2002**, *9* (12), 1307.

(25) Maeno, E.; Tsubata, T.; Okada, Y. J. C. Apoptotic volume decrease (AVD) is independent of mitochondrial dysfunction and initiator caspase activation. *Cell* **2012**, *1* (4), 1156-1167.

(26) Russo-Abrahão, T.; Lacerda-Abreu, M. A.; Gomes, T.; Cosentino-Gomes, D.; Carvalho-de-Araújo, A. D.; Rodrigues, M. F.; Oliveira, A. C. L. d.; Rumjanek, F. D.; Monteiro, R. d. Q.; Meyer-Fernandes, J. R. J. P. o. Characterization of inorganic phosphate transport in the triple-negative breast cancer cell line, MDA-MB-231. *PLOS ONE* **2018**, *13* (2), e0191270.

(27) Tinawi, M. J. A. o. C.; Research, B. Disorders of Phosphate Metabolism: Hypophosphatemia and Hyperphosphatemia. *Arch. clin. biomed. res.* **2021**, *5*, 538-555.

(28) Bobko, A. A.; Eubank, T. D.; Driesschaert, B.; Dhimitruka, I.; Evans, J.; Mohammad, R.; Tchekneva, E. E.; Dikov, M. M.; Khramtsov, V. V. J. S. r. Interstitial inorganic phosphate as a tumor microenvironment marker for tumor progression. *Sci. Rep.* **2017**, *7* (1), 1-12.

(29) Arnst, J. L.; Beck Jr, G. R. J. B. P. Modulating phosphate consumption, a novel therapeutic approach for the control of cancer cell proliferation and tumorigenesis. *Biochem. Pharmacol.* **2021**, *183*, 114305.

(30) Picci, G.; Carreira-Barral, I.; Alonso-Carrillo, D.; Sanz-González, D.; Fernández-López, P.; García-Valverde, M.; Caltagirone, C.; Quesada, R. J. S. C. Simple isophthalamides/dipicolineamides as active transmembrane anion transporters. *Supramol Chem* **2020**, *32* (2), 112-118.

(31) Bąk, K. M.; Chabuda, K.; Montes, H.; Quesada, R.; Chmielewski, M. J. J. O.; Chemistry, B. 1, 8-Diamidocarbazoles: an easily tuneable family of fluorescent anion sensors and transporters. *Org. Biomol. Chem.* **2018**, *16* (28), 5188-5196.

(32) Moore, S. J.; Haynes, C. J.; González, J.; Sutton, J. L.; Brooks, S. J.; Light, M. E.; Herniman, J.; Langley, G. J.; Soto-Cerrato, V.; Pérez-Tomás, R. J. C. S. Chloride, carboxylate and carbonate transport by ortho-phenylenediamine-based bisureas. *Chem. Sci.* **2013**, *4* (1), 103-117.

(33) Valkenier, H.; Dias, C. M.; Butts, C. P.; Davis, A. P. J. T. A folding decalin tetra-urea for transmembrane anion transport. *Tetrahedron* **2017**, *73* (33), 4955-4962.

(34) Jurček, O.; Valkenier, H.; Puttreddy, R.; Novák, M.; Sparkes, H. A.; Marek, R.; Rissanen, K.; Davis, A. P. J. C. A. E. J. Anion Recognition by a Bioactive Diureidodecalin Anionophore: Solid-State, Solution, and Computational Studies. *Chemistry* **2018**, *24* (32), 8178-8185.

(35) Dias, C. M.; Valkenier, H.; Davis, A. P. J. C. A. E. J. Anthracene bisureas as powerful and accessible anion carriers. *Chem. Eur. J.* **2018**, *24* (23), 6262-6268.

(36) Wu, X.; Judd, L. W.; Howe, E. N.; Withecombe, A. M.; Soto-Cerrato, V.; Li, H.; Busschaert, N.; Valkenier, H.; Pérez-Tomás, R.; Sheppard, D. N. J. C. Nonprotonophoric electrogenic Cl− transport mediated by valinomycin-like carriers. *Chem* **2016**, *1* (1), 127-146.

(37) Busschaert, N.; Wenzel, M.; Light, M. E.; Iglesias-Hernández, P.; Pérez-Tomás, R.; Gale, P. A. J. J. o. t. A. C. S. Structure–activity relationships in tripodal transmembrane anion transporters: the effect of fluorination. *J. Am. Chem. Soc.* **2011**, *133* (35), 14136-14148.

(38) Jowett, L. A.; Howe, E. N.; Wu, X.; Busschaert, N.; Gale, P. A. J. C. A. E. J. New insights into the anion transport selectivity and mechanism of tren-based tris-(thio) ureas. *Chem. Eur. J.* **2018**, *24* (41), 10475-10487.

(39) Grauwels, G.; Valkenier, H.; Davis, A.; Jabin, I.; Bartik, K. Repositioning Chloride Transmembrane Transporters: Transport of Organic Ion Pairs. Angewandte Chemie, 131 (21), 6995-6999. *Angew. Chem.*

(40) Shinde, S. V.; Talukdar, P. J. A. C. I. E. A Dimeric Bis (melamine)-Substituted Bispidine for Efficient Transmembrane H+/Cl− Cotransport. *Angew. Chem.* **2017**, *56* (15), 4238-4242.

(41) Fuertes, A.; Amorín, M.; Granja, J. R. J. C. C. Versatile symport transporters based on cyclic peptide dimers. *Chem. Commun.* **2020**, *56* (1), 46-49.

(42) Behera, H.; Madhavan, N. J. J. o. t. A. C. S. Anion-selective cholesterol decorated macrocyclic transmembrane ion carriers. *J. Am. Chem. Soc.* **2017**, *139* (37), 12919-12922.

(43) Shinde, S. V.; Talukdar, P. J. O.; Chemistry, B. Transmembrane H+/Cl– cotransport activity of bis (amido) imidazole receptors. *Org. Biomol. Chem.* **2019**, *17* (18), 4483-4490.

(44) Shinde, S. V.; Talukdar, P. J. C. C. An anion receptor that facilitates transmembrane proton–anion symport by deprotonating its sulfonamide N–H proton. *Chem. Commun.* **2018**, *54* (73), 10351-10354.

(45) Roy, A.; Saha, D.; Mandal, P. S.; Mukherjee, A.; Talukdar, P. J. C. A. E. J. pH-Gated Chloride Transport by a Triazine-Based Tripodal Semicage. *Chem. Eur. J.* **2017**, *23* (6), 1241-1247.

(46) Plajer, A. J.; Zhu, J.; Proehm, P.; Bond, A. D.; Keyser, U. F.; Wright, D. S. J. J. o. t. A. C. S. Tailoring the binding properties of phosphazane anion receptors and transporters. *J. Am. Chem. Soc.* **2019**, *141* (22), 8807-8815.

(47) Wu, X.; Small, J. R.; Cataldo, A.; Withecombe, A. M.; Turner, P.; Gale, P. A. J. A. C. I. E. Voltage-switchable HCl transport enabled by lipid headgroup–transporter interactions. *Angew. Chem.* **2019**, *58* (42), 15142-15147.

(48) Howe, E. N.; Gale, P. A. J. J. o. t. A. C. S. Fatty acid fueled transmembrane chloride transport. *J. Am. Chem. Soc.* **2019**, *141* (27), 10654-10660.

(49) Jung, M.; Kim, H.; Baek, K.; Kim, K. J. A. C. I. E. Synthetic ion channel based on metal–organic polyhedra. *Angew. Chem.* **2008**, *47* (31), 5755-5757.

(50) Benke, B. P.; Aich, P.; Kim, Y.; Kim, K. L.; Rohman, M. R.; Hong, S.; Hwang, I.-C.; Lee, E. H.; Roh, J. H.; Kim, K. J. J. o. t. A. C. S. Iodide-selective synthetic ion channels based on shape-persistent organic cages. *J. Am. Chem. Soc.* **2017**, *139* (22), 7432-7435.

(51) Kempf, J.; Schmitzer, A. R. J. C. A. E. J. Metal–Organic Synthetic Transporters (MOST): Efficient Chloride and Antibiotic Transmembrane Transporters. *Chem. Eur. J.* **2017**, *23* (26), 6441-6451.

(52) Kempf, J.; Noujeim, N.; Schmitzer, A. J. R. A. 2, 4, 7-Triphenylbenzimidazole: the monomeric unit of supramolecular helical rod-like transmembrane transporters. *RSC Adv.* **2014**, *4* (80), 42293-42298.

(53) Zheng, S. P.; Li, Y. H.; Jiang, J. J.; van der Lee, A.; Dumitrescu, D.; Barboiu, M. J. A. C. Self-Assembled Columnar Triazole Quartets: An Example of Synergistic Hydrogen-Bonding/Anion–π Interactions. *Angew. Chem.* **2019**, *131* (35), 12165-12170.

(54) Malla, J. A.; Umesh, R. M.; Vijay, A.; Mukherjee, A.; Lahiri, M.; Talukdar, P. J. C. s. Apoptosis-inducing activity of a fluorescent barrel-rosette M+/Cl− channel. *Chem. Sci.* **2020**, *11* (9), 2420-2428.

(55) Li, H.; Valkenier, H.; Thorne, A. G.; Dias, C. M.; Cooper, J. A.; Kieffer, M.; Busschaert, N.; Gale, P. A.; Sheppard, D. N.; Davis, A. P. J. C. s. Anion carriers as potential treatments for cystic fibrosis: transport in cystic fibrosis cells, and additivity to channel-targeting drugs. *Chem. Sci.* **2019**, *10* (42), 9663-9672.

(56) Bąk, K. M.; van Kolck, B.; Maslowska-Jarzyna, K.; Papadopoulou, P.; Kros, A.; Chmielewski, M. J. J. C. C. Oxyanion transport across lipid bilayers: direct measurements in large and giant unilamellar vesicles. *Chem. Commun.* **2020**, *56* (36), 4910-4913.

(57) Lee, M. L.; Tsemperouli, M.; Bahamonde, I. A.; Benz, S.; Sakai, N.; Sugihara, K.; Matile, S. Anion Transport with Pnictogen Bonds in Direct Comparison with Chalcogen and Halogen Bonds. *J. Am. Chem. Soc.* **2019**, *141* (2) 810–814.

(58) Benz, S.; Macchione, M.; Verolet, Q.; Mareda, J.; Sakai, N.; Matile, S. Anion Transport with Chalcogen Bonds. *J. Am. Chem. Soc.* **2016**, *138* (29) 9093–9096.

(59) Jentzsch, V. A.; Hennig, A.; Mareda, J.; Matile, S. Synthetic Ion Transporters that Work with Anion–π Interactions, Halogen Bonds, and Anion–Macrodipole Interactions. *Acc. Chem. Res.* **2013**, 46 (12) 2791–2800.

Chapter 2

Chloride Ion Transport by PITENINs Across the Phospholipid Bilayers of Vesicles and Cells

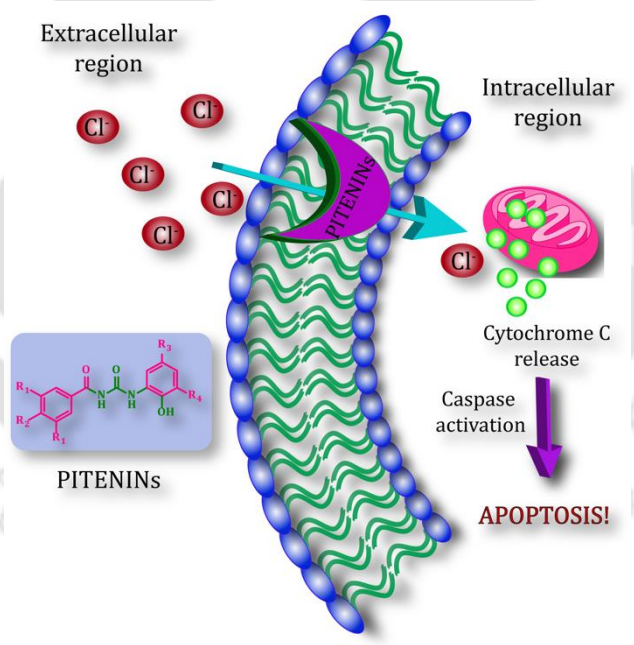

2.1. Background and objective of present work

The literature reviewed in chapter 1 concluded that dysregulation of the cellular Cl^- ion transport system is related to several diseases (i.e., channelopathies) such as myotonia, epilepsy, kidney disorders, cystic fibrosis, and others [1, 2, 3]. Hence there is a growing need of the synthetic mimic of the natural transporter systems that has the potential to replace the defective natural transport system for the clinical management of channelopathies by overcoming the interrupted activities of the natural transporters. Also, latest studies revealed that the unnatural ionophores are capable of inducing apoptosis in various model cancer cells, indicating their potential use as anticancer agents [4,5,6,7,8,9,10].

However, most of these synthetic ion transporters failed to differentiate healthy cells from the cancer cells which are detrimental to the body. To increase the selectivity of the synthetic ion transporters towards the cancer cells, pH as a stimulus can be used for the discrimination purpose. Cancer cells have a slightly acidic pH (6.1-6.8) as a mechanism of defence to develop drug resistance w.r.t the normal cells which are slightly basic in nature. Hence proanionophores which are inactive in its initial state, and becomes highly proficient ion transporter ferrying ions across the cell on coming in contact of an acidic environment is highly viable to be efficiently used against the cancer cells producing less toxicity in the cancer cells.

Hence with the intention of using pH as a stimulus, here in this work acylthiourea moiety has been adopted to mediate the ion across the lipid bilayer. The natural product prodigiosin and small synthetic molecules like perenosins and bis(sulfonamide) showed anticancer activities due to their spontaneous Cl^- ion transport activities [11, 12]. These small hydrophobic molecules contain a Cl^- ion binding motif, including urea, thiourea, amide, squaramide, sulphonamide, and benzimidazole. A thorough structural analysis of these synthetic anion transporters revealed that the lipophilicity of the compounds plays a crucial role in their Cl^- ion transport activities. However, the hydrogen-bond acidity and molecular size have smaller contributions for their anion transport behavior. Suitable lipophilicity of a bioactive molecule increases its membrane permeability, leading to its better absorption and distribution. Using these concepts, acylthiourea-based lipophilic anion transporters were developed by Gale and co-workers [13]. The acylthiourea

moiety is also present in several bioactive molecules and shows hedgehog inhibition, antiviral, nematicidal, anticancer, and other activities [14, 15, 16, 17].

Recently, acylthiourea-based phosphatidylinositol-3,4,5-trisphosphate (PIP_3) inhibitors (PITENINs) were reported [17]. These PITENINs inhibit the phosphatidylinositol-3 kinase (PI3K)-dependent membrane localization of the pleckstrin homology (PH) domain comprising host proteins like Akt, PDK1, Grp1, and ARNO. The PIP_3 lipid is one of the second messengers, and it regulates numerous cellular processes, including cell metabolism, survival, and apoptosis. The dysregulation of the PI3K-PDK1-AKT pathway is associated with several diseases. In particular, the up-regulation of the PI3K signaling pathway plays a crucial role in tumorigenesis [18, 19]. This PITENINs-dependent suppression of the PI3K-PDK1-AKT signaling pathway has significant antitumor activity, including stimulation of apoptosis and reduction of the tumor growth rate [17, 20]. Additional activity studies revealed that the PITENINs prevent the growth factor promoted actin remodeling, cell migration, lamellipodia formation, invasion, and others. However, it is not clear from these studies whether the PITENINs bind to the PH domain of the host protein at the cytoplasm or membrane environment. The pH domains of Akt and PDK1 and other peripheral proteins are known to bind PIP_3 lipids and penetrate the membrane bilayer to fully activate the host proteins [21, 22].

Consequently, encouraged with the therapeutic prospects of the acylthiourea derivatives, new acylthiourea derivatives were designed and synthesised. The initial investigations revealed that the potent PITENINs, including **2.2** (**PIT-1**) and **2.5** (**DM-PIT-1**), have moderate membrane permeability (cLogP values within 3.85–4.27), which suggests that these compounds are primarily localized at the plasma membrane and interact with PH domain-containing proteins. The presence of acylthiourea and phenolic OH moieties and the membrane localization prospect of PITENINs allows us to hypothesize that the PITENINs can also transport anions [23]. We also envisage that the anticancer activities of the PITENINs could be due to both deregulation of PI3K-PDK1-AKT-dependent signaling pathways and anion transport abilities. In this study, we investigated the role of PITENINs as a Cl^- ion transporter. The study provided a detailed understanding of the relationship between structure, lipophilicity, anion recognition, and transport activities of these synthesized compounds. The **2.2** (**PIT-1**), **2.5** (**DM-PIT-1**), and other PITENINs were synthesized

to investigate the significance of acylthiourea and phenolic OH moieties in the transport of Cl^- ions. The Cl^- ion transport efficacies of compounds **2.2** (**PIT-1**), **2.3**, and **2.5** (**DM-PIT-1**) were markedly higher among the synthesized compounds. The surface plasmon resonance (SPR) analysis reconfirmed the PH domain binding abilities of these compounds. The *in vitro* cellular activity studies showed that these PITENINs also induce apoptosis of the cancer cells.

2.2. Results and discussions

2.2.1. Design and synthesis of the acylthiourea derivatives

A small series of PITENINs, including **2.2** (**PIT-1**), **2.5** (**DM-PIT-1**), and their analogues were synthesized following the reported methods [17, 24]. First, the benzoyl isothiocyanates were synthesized from the corresponding benzoyl chloride and potassium thiocyanate in the presence of a phase transfer catalyst (PEG-400). Then, condensation of substituted aminophenol with these benzoyl isothiocyanates produced the targeted PITENINs in a good yield under the mild reaction conditions. Substituents at the acyl and 2-aminophenol moieties were altered to synthesize the compounds (**2.1**–**2.7**) with desired

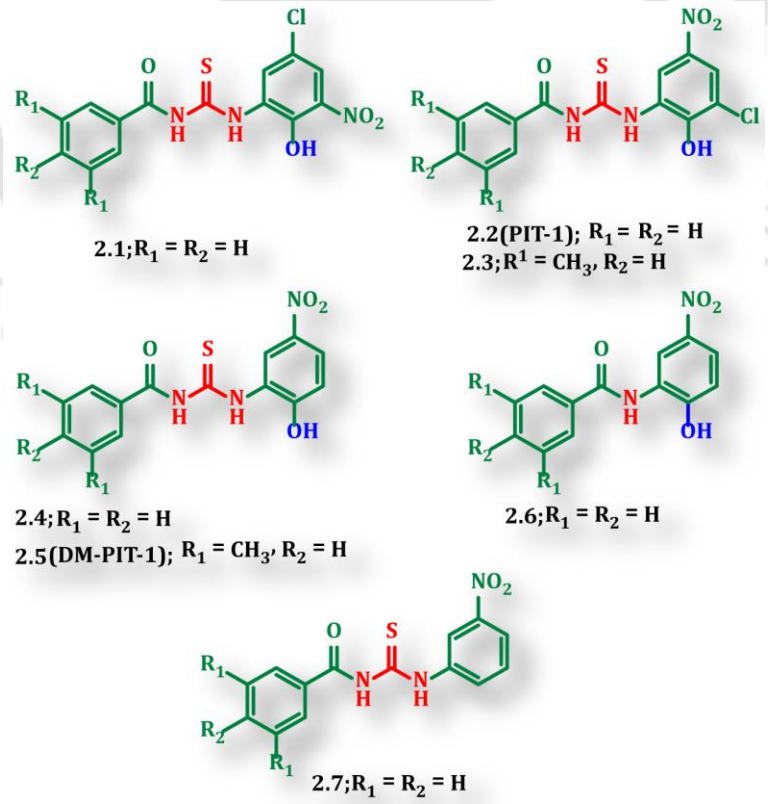

Figure 2.1. Synthesized acylthiourea derivatives.

lipophilicity (cLogP) and N–H and/or O–H proton acidity (pK_a), which is essential in accomplishing the improved lipid-bilayer permeability and Cl^- ion transport proficiency. To understand the role of lipophilicity, the compounds **2.3** and **2.5** (**DM-PIT-1**) were synthesized. The benzanilide **2.6** was synthesized to examine the significance of the acylthiourea group. Compounds **2.1**, **2.2** (**PIT-1**), **2.4**, and **2.7** were synthesized to evaluate the importance of the phenolic OH moiety in anion transport properties. The stability of the compounds in aqueous buffered solution (pH 5.5 and 7.2) was tested by HPLC analysis. The cLogP and pK_a values of the compounds, with the help of the MarvinSketch program (Fig. 2.1, Table 2.1).

Table 2.1. Chemical properties of the compounds.

Compound	clogp[a]	pK_a (N-H$_a$) [a]	pK_a (O-H$_a$) [a]	EC$_{50}$ (μM); (n[b])
2.1	3.85	9.90	5.40	5.10 ± 0.86 (0.97)
2.2 (**PIT-1**)	3.85	9.90	5.02	1.34 ± 0.49 (0.85)
2.3	4.88	9.90	5.02	1.25 ± 0.25 (0.88)
2.4	3.25	10.02	6.43	
2.5 (**DM-PIT-1**)	4.27	10.02	6.43	3.26 ± 1.15 (1.14)
2.6	2.70	15.10	6.33	
2.7	3.55	10.01		

[a]cLogP and pK_a values of the PITENINs were computed using the MarvinSketch program.
[b]EC$_{50}$ values were calculated using the HPTS-based fluorescence assay, *n* = Hill coefficient.

2.2.2. Anion binding studies of the acylthiourea derivatives

At first, the Cl^- ion recognition capabilities of the PITENINs were investigated by ^{1}H NMR titration experiments. The spectral analysis revealed that both acylthiourea and phenolic OH moieties interact with the Cl^- ion (Fig. S2.1-S2.4). The chemical shifts (Δδ) for N–H$_b$ and C–H$_d$ protons, respectively, were monitored to measure the association constants (*K*) for the complexation of compound **2.2** (**PIT-1**) and **2.5** (**DM-PIT-1**) with the Cl^- ion. The Δδ values of N–H$_b$ or O–H$_c$ of the **2.5** (**DM-PIT-1**) compound were not monitored due to lower changes of Δδ values or insufficient data. The *K* value was computed by the BindFit v0.5 program using a 1:1 binding model [25, 26]. The Cl^- ion binding studies of **2.2** (**PIT-1**) and **2.5** (**DM-PIT-1**)

provided the *K* values within the range of 21.784 ± 1.671 and 23.436 ± 3.725 M^{-1}, respectively, signifying their moderate Cl^- ion binding abilities in the solution phase.

To obtain structural insights into the geometry of Cl^- ion bound compounds, the density functional theory (DFT) calculations were performed using B3LYP/6-31+G(d) and B3LYP/6-31++G (d,p) methods [27, 28]. The optimized structure of the compounds showed that the phenolic O–H proton and the N–H protons of the compounds are mainly accountable for their interactions with the Cl^- ion (Table 2.1-2.2). The DFT analysis also demonstrated that the distance for the interactions of **2.5** (**DM-PIT-1**) with a Cl^- ion is within the range of hydrogen bonding (2.070–2.349 Å). The interaction energy of the Cl^- ion with the **2.2** (**PIT-1**) (92.431 kcal/mol) is higher than the **2.5** (**DM-PIT-1**) (89.925 kcal/mol). These theoretical results are in accordance with the *K* values from the ^1H NMR titrations. The UV–vis spectroscopic titrations also suggest the interaction of Cl^- ions with**2.5** (**DM-PIT-1**) in the solution phase. The binding affinities of the potent compounds were measured by both ^{1}HNMR titration and UV–vis spectroscopic titration. However, the binding constants of the same compound were quite different, which could be due to the difference in sensitivity and experimental conditions of NMR and UV–vis techniques.

2.2.3. Chloride ion transport activities of the acylthiourea derivatives

Theoretical lipophilicity values (clogP = 3.85–4.27) showed that these PITENINs possess a higher affinity for the lipophilic environment, while the test for leaching established that the compounds preferentially localize within the membrane bilayer. This membrane residence property and Cl^- ion binding aptitude encouraged us to examine the Cl^- ion transport properties across the bilayers of large unilamellar vesicles (LUVs). The 8-hydroxypyrene-1,3,6-trisulfonate (HPTS) dye encapsulated LUVs were prepared using phosphatidylcholine (EYPC) and cholesterol lipids (6:4 molar ratio) in 20 mM HEPES buffer at pH 7.2, containing 100 mM NaCl. The transport of Cl^- ions across the bilayer of EYPC/CHOL-LUVs⊃HPTS in the absence and presence of PITENINs was examined by employing a pH gradient (pH_{in} = 7.2, pH_{out} = 7.8) in the extravesicular solution. The changes in the HPTS fluorescence signal (λ_{ex} = 450 nm and λ_{em} = 510 nm) in the absence and presence of PITENINs (6.70 μM) was monitored to estimate their Cl^- ion transport activity (Fig. 2.2). The plot shows that **2.2** (**PIT-1**) is the most efficient Cl^- ion transporter and

follows the order of **2.2** (**PIT-1**) ≈ **2.3** > **2.5** (**DM-PIT-1**) > **2.1** > **2.6** > **2.7** > **2.4**. Concentration-dependent HPTS analysis showed that the EC_{50} values of **2.1**, **2.2** (**PIT-1**), **2.3**, and **2.5** (**DM-PIT-1**) are within 1.25–5.10 μM (Fig. S2.5). The superior Cl^- ion transport properties of **2.2** (**PIT-1**), **2.3**, and **2.5** (**DM-PIT-1**) could be because of the lower pK_a values of N–H or O–H proton and membrane permeability. The lower Cl^- ion transport efficacies of compounds **2.1**, **2.4**, **2.6**, and **2.7** suggest that both acylthiourea and phenolic OH moieties play important roles in the recognition and transport of Cl^- ions.

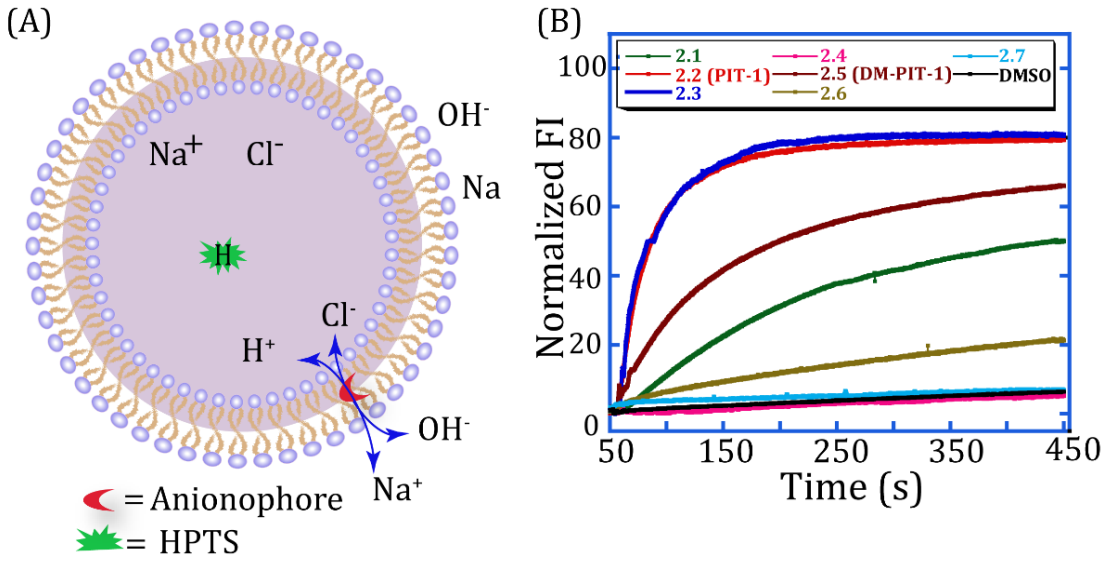

Figure 2.2. Schematic representation of fluorescence-based ion transport activity assay using EYPC/CHOL-LUVs⊃HPTS (A) Comparisons of ion transport activity of **2.1**-**2.7** across EYPC/CHOL-LUVs⊃HPTS (B)

2.2.4. Relative cation and anion selectivity studies of the acylthiourea derivatives

The PITENINs, **2.2** (**PIT-1**) and/or **2.5** (**DM-PIT-1**) were selected to explore the ion selectivity, ion transport mechanism, and other biophysical or biochemical studies. These PITENINs showed strong Cl^- ion transport activity and also had anticancer activities. To investigate the consequence of extravesicular anions or cations on the Cl^- ion transport activity of the compounds, the HPTS assay was performed by applying a pH gradient (pH_{in} = 7.2, pH_{out} = 7.8). The use of different NaX salts (Cl^-, I^-, Br^-, NO_3^-, and ClO_4^-) in the extravesicular solution and iso-osmotic buffer solution of NaCl in the intravesicular solution at pH 7.2 showed considerable

differences in the anion transport activities for **2.2** (**PIT-1**) and **2.5** (**DM-PIT-1**) (Fig. 2.3A, 2.3B). The observed data revealed that the compounds **2.2** (**PIT-1**) and **2.5** (**DM-PIT-1**) have Cl^- ion selectivity over the other tested anions.

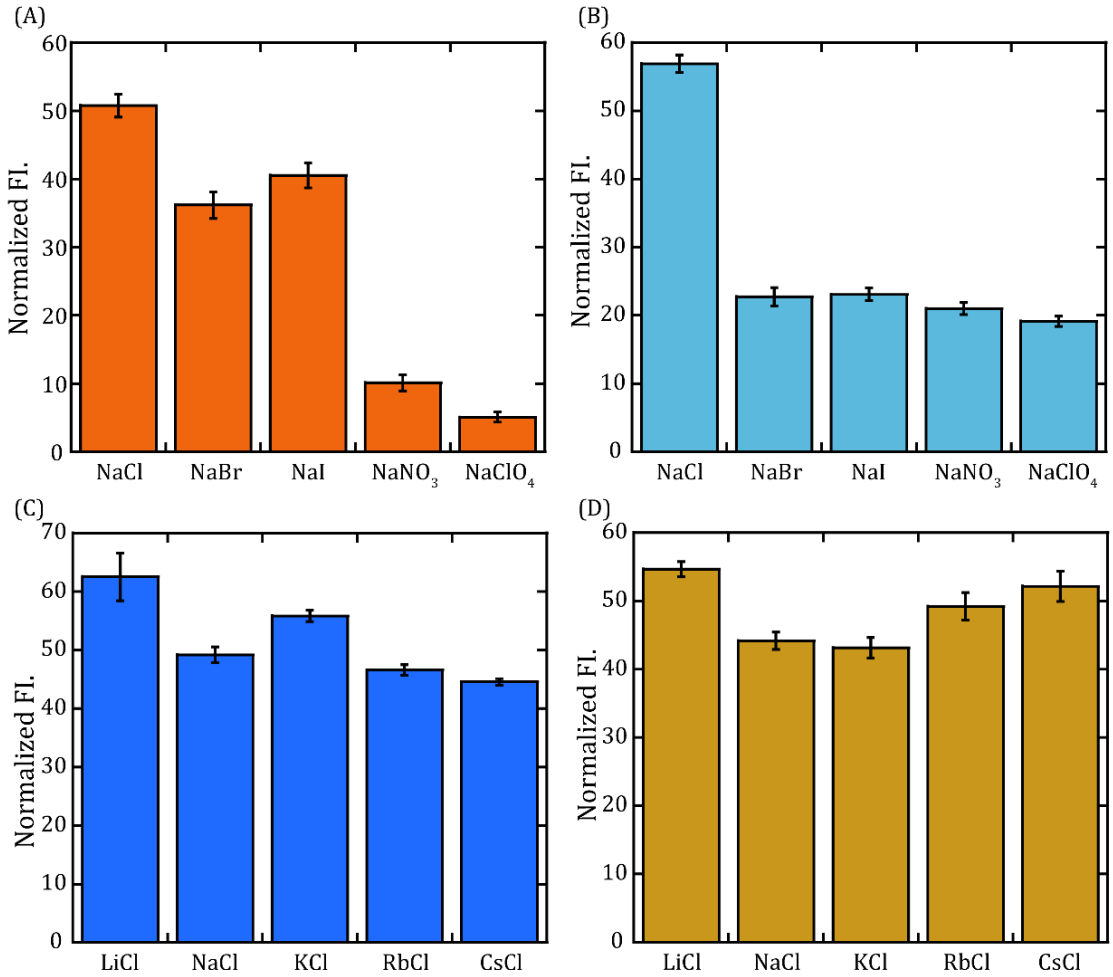

Figure 2.3. Anion (A) and cation transport (B) selectivity of **2.5** (**DM-PIT-1**) (A), and **2.2** (**PIT-1**) (C) and (D) across EYPC/CHOL-LUVs⊃HPTS.

However, in this anion selectivity assay, NaCl was used in the intravesicular solution, and different anions were used in the extravesicular solution, which may generate a membrane potential and affect the true anion selectivity. To resolve this indistinctness, a competitive transport assay was implemented without applying any pH gradient ($pH_{in} = pH_{out} = 7.2$) [29]. In the competitive transport assay, different anions in the intravesicular and extravesicular solutions were used to produce a pH gradient only based on the different transport rates of anions. Interestingly, this competitive assay also exhibited a higher Cl^- ion transport selectivity in comparison with the

other anions, which is in good agreement with the HPTS assay in the presence of base pulse (Fig. S2.8-S2.11). The variation of different chloride salts (M^+ = Li^+, K^+, Na^+, Rb^+, and Cs^+) in the extravesicular solution and iso-osmotic buffer solution of NaCl in the intravesicular solution at pH 7.2 showed very small differences in the Cl^- ion transport activity for the **2.2** (**PIT-1**) and **2.5** (**DM-PIT-1**) (Fig. 2.3C, 2.3D). The results indicate that the transport of Cl^- ions is impervious toward the cations, which could be due to their nonspecific interaction with the compounds. However, the Cl^- ion selectivity of these compounds could be due to the stronger binding of the Cl^- ion within the pocket of the aminophenol-containing PITENINs. The pK_a values of the PITENINs and the presence of the phenolic OH moieties incited us to hypothesize that the Cl^- ion transport activity of **2.2** (**PIT-1**) and **2.5** (**DM-PIT-1**) could be due to the pH of the environment. In this regard, we performed a concentration-dependent ion-selective electrode (ISE)-based assay of these potent PITENINs at pH 5.5 and 7.2 (Fig. S2.6-S2.7).[30,31] For this ISE-based assay, the intravesicular solution of the vesicles contains 5 mM phosphate buffer, pH 7.2 (containing 100 mM NaCl), and the-

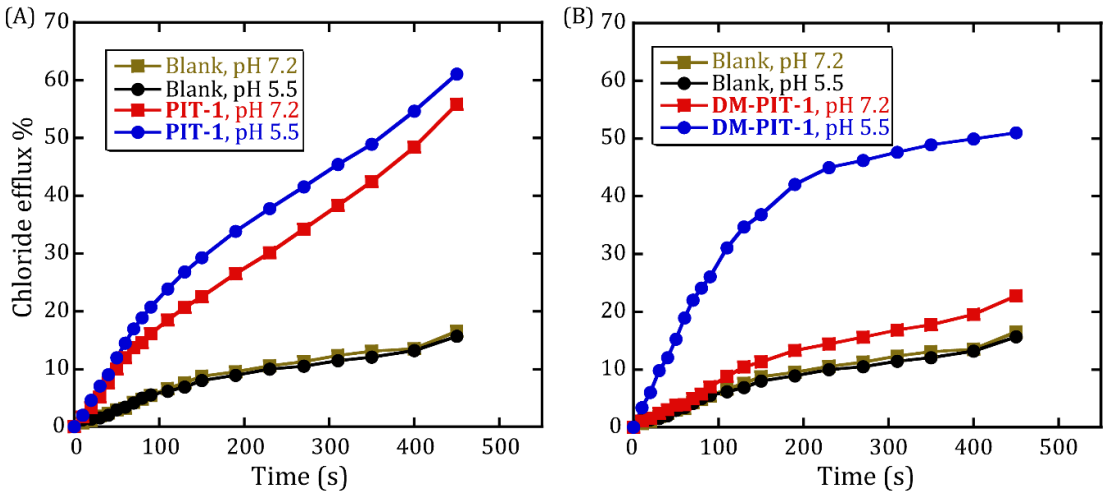

Figure 2.4. Chloride ion transport capability of compound **2.2** (**PIT-1**) (A)and **2.5** (**DM-PIT-1**) (B) (0.098 μM) at pH 5.5 and 7.2.

extravesicular solution contains an isotonic $NaNO_3$ solution (100 mM) buffered to pH 7.2. The assay was performed without applying any pH gradient, and the results revealed that **2.5** (**DM-PIT-1**) has around a 20-fold stronger Cl^- ion transport ability in the slightly acidic medium (pH 5.5) than under physiological conditions. The EC'_{50} values of **2.5** (**DM-PIT-1**) were 0.65 and 0.031 μM at pH 7.2 and 5.5, respectively, suggesting that the **2.5** (**DM-PIT-1**) can be used as a switched ON Cl^- ion transporter

upon the alternation of pH within a narrow window of the physiological pH (Fig. 2.4) The superior Cl^- ion transport selectivity of **2.5** (**DM-PIT-1**) could be due to the collective effect of hydrophobicity and the acidity of the phenolic OH (pK_a = 6.43). However, compound **2.2** (**PIT-1**) did not show any significant difference in its Cl^- ion transport properties at pH 5.5 and 7.2, which could be due to its pK_a value phenolic OH (5.02).

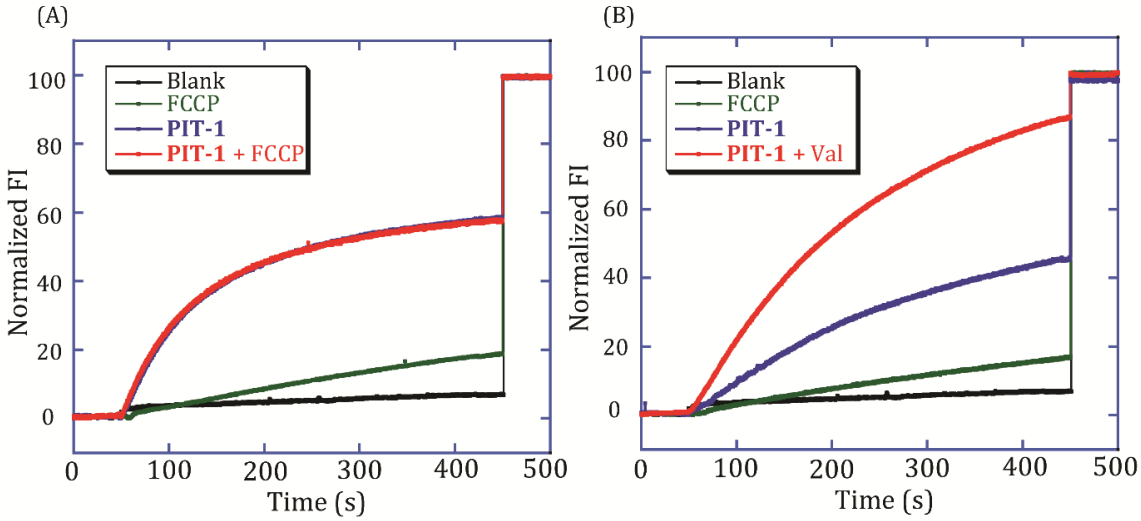

Figure 2.5. Cl^- ion transport behavior of **2.2** (**PIT-1**) (1.34 μM) in the presence and absence of FCCP, both at 7.2 (A). Comparison of the ion transport activity of compound **2.2** (**PIT-1**) (1.34 μM) in the presence and absence of valinomycin (Val), both at 7.2 (B).

2.2.5. Mechanism of chloride ion transport activities of the acylthiourea derivatives

The transport of Cl^- ions create a charge imbalance across the lipid bilayer, which can be compensated by either the transport of other anions in the opposite direction (antiport) or transport of any cation in the same direction (symport). The antiport pathway could be due to H^+/M^+ and OH^-/A^- transportation. The symport pathway may follow the H^+/A^- and M^+/OH^- transport mechanism. The ion transport properties of **2.2** (**PIT-1**) and **2.5** (**DM-PIT-1**) were also analyzed by 4-(trifluoromethoxy)phenylhydrazone (FCCP; a protonophore), and valinomycin (potassium ionophore) assays. The FCCP assay showed no substantial alternation in the transport rates of Cl^- ions for both the compounds, suggesting no complaisant effect between the **2.2** (**PIT-1**)/**2.5** (**DM-PIT-1**) and FCCP. Hence, there is a

possibility of H^+ efflux by these compounds at pH 7.2 (Fig. 2.5-2.6). The low pK_a value of the compounds also suggests the probability of H^+ transport by deprotonation of the phenolic OH group. Besides, we performed the conventional U-tube experiment to get direct confirmation of Cl^- ion transport activities of **2.2** (**PIT-1**) and **2.5** (**DM-PIT-1**) [32]. The changes in pH and Cl^- ion concentration in the right arm of the U-tube were monitored by using pH and chloride ion-selective electrodes. A decrease in the pH and an increase in Cl^- ion concentration directly confirmed the transport of H^+/Cl^- .

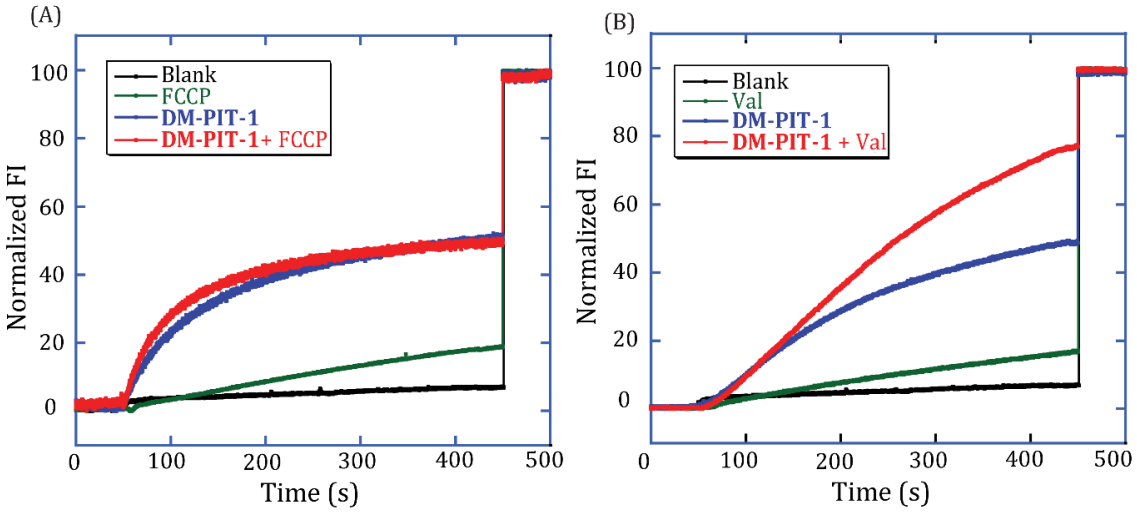

Figure 2.6. Cl^- ion transport behavior of **2.5** (**DM-PIT-1**) (3.26 μM) in the presence and absence of FCCP, both at 7.2 (A). Comparison of the ion transport activity of compound **2.5** (**DM-PIT-1**) (3.26 μM) in the presence and absence of valinomycin (Val), both at 7.2 (B).

The cation selectivity assay excludes any considerable role of the cations on the Cl^- ion transport activity of **2.2** (**PIT-1**) / **2.5** (**DM-PIT-1**), which eliminates the probability of the M^+/OH^- cotransport mechanism. We also performed a valinomycin assay and assumed that the influx of K^+ ions by valinomycin would induce the concurrent OH^- influx and/or Cl^- ion efflux to withstand the charge neutrality of the solution. However, the enhancement of Cl^- ion transport rates for **2.2** (**PIT-1**) and **2.5** (**DM-PIT-1**) in the presence of valinomycin specifies the possibility of the OH^-/Cl^- antiport mechanism with superior transport of OH^- over the Cl^- ion (Fig. 2.5-2.6).

The cholesterol concentration-dependency assay was performed to explore whether the Cl^- ion transport activity of **2.2** (**PIT-1**) and **2.5** (**DM-PIT-1**) follows the

carrier or channel mechanism under the liposomal environment [33]. The results revealed that, with the increase in cholesterol concentration within the lipid bilayer, the Cl^- ion transport efficiency got reduced, suggesting the carrier pathway for compounds **2.2** (**PIT-1**) and **2.5** (**DM-PIT-1**), whereas the Cl^- ion transport rate remains unaffected for channel-based transport pathways. The U-tube assay also established that the compounds transport Cl^- ions through carrier pathways. The nonleaking capability of the calcein dye from the vesicles in the presence of compounds also supports the mobile carrier mechanism and dismisses the possibility of pore or channel formations in the membrane bilayer (Fig. S2.12-S2.13).

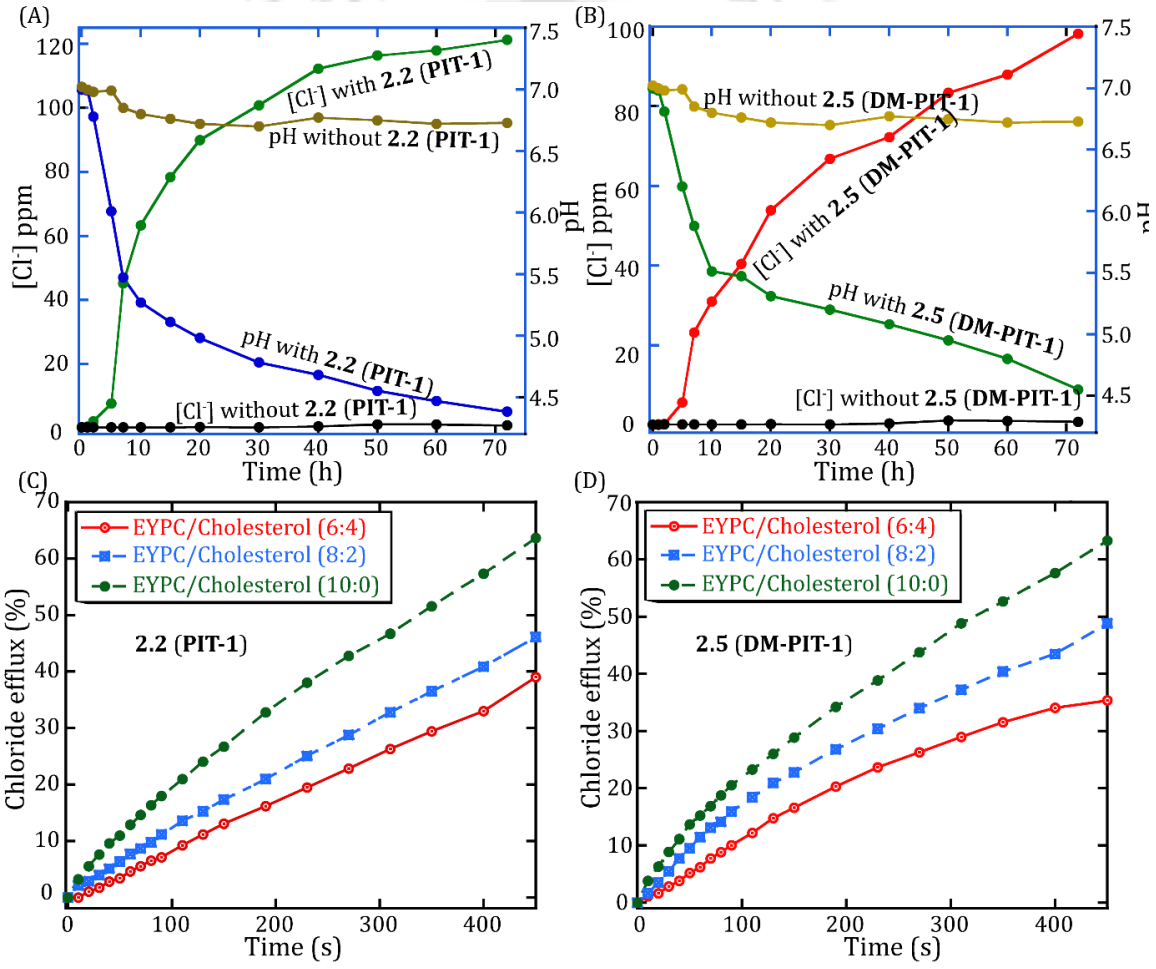

Figure 2.7. H^+/Cl^- transport efficacy of compound **2.2** (**PIT-1**) (2 mM; A) and **2.5** (**DM-PIT-1**) (2 mM; B) was measured across a U-tube by applying the HCl gradient, using a chloride ion-selective electrode and pH meter. Effect of the concentration of cholesterol (EYPC/cholesterol membrane) on the transport of Cl^- ions in the presence of compounds **2.2** (**PIT-1**) (1.34 μM; C) and **2.5** (**DM-PIT-1**) (3.26 μM; D).

2.2.6. Pleckstrin Homology Domain Binding Ability of the PITENINs

The PITENINs are a well-known binding partner of the PH domain of the AKT protein. We hypothesized that the biological activities of these PITENINs could be due to both AKT-PH domain binding capability and Cl^- ion transport activity. In this regard, we reinvestigated the binding ability of the AKT-PH domain with the **2.2** (**PIT-1**) and **2.5** (**DM-PIT-1**) compounds. The direct binding of **2.2** (**PIT-1**) and **2.5** (**DM-PIT-1**) with the AKT-PH domain was investigated by surface plasmon resonance (SPR) analysis [34,35,36]. The protein was immobilized on the CM5 sensor chip using the GST capture kit. The SPR analysis showed that both the compounds reversibly bind to the AKT-PH domain with K_d = 88–110 μM. The AKT-PH-domain binding properties of the compounds are in accordance with the reported values, suggesting that both the compounds are capable of inhibiting the PIP_3/AKT-PH domain interaction at the membrane surface. The PIP_3/PH domain binding is a universal upstream pathway in PI3K/AKT signaling; hence, the inhibition of the PIP_3/AKT-PH domain binding is considered as a powerful approach to regulating the PI3K signaling.

2.2.7. Activities of the PITENINs under Cellular Environment

The Cl^- ion transport properties encouraged us to reinvestigate the bioapplicability of the PITENINs. Recent studies described that the disruption of ionic homeostasis by the unnatural Cl^- ion transporters persuade apoptosis in cancer cells. Therefore, to investigate whether the previously reported apoptotic activities by the PITENINs are only because of the repression of the PIP_3–PH domain interactions, initially the MTT assay was performed. First, the viability of human cervical cancer HeLa cells in the absence and presence of compounds **2.1**–**2.7** was performed at 25 μM. The compounds **2.1**, **2.2** (**PIT-1**), and **2.5** (**DM-PIT-1**) showed a higher cell death rate. The MTT assay showed that, in the presence of **2.5** (**DM-PIT-1**) and **2.2** (**PIT-1**), the viability of cancer (HeLa, human breast cancer; MDA-MB-231) and healthy (baby hamster kidney; BHK-21) cells decreases in a dose-dependent manner (Fig. 2.8, S2.14-S2.15). The calculated IC_{50} values of **2.5** (**DM-PIT-1**) in HeLa, MDA-MB-231, and BHK-21 cells were 24.82 ± 3.56, 100.50 ± 5.49, and 68.69 ± 7.42 μM, respectively. Whereas the IC_{50} values of **2.2** (**PIT-1**) in HeLa, MDA-MB-231, and BHK-21 cells were 12.74 ± 3.44, 29.20 ± 4.43, and 16.27 ± 2.39 μM, respectively. The IC_{50} values of compound **2.1** in HeLa and BHK-21 cells were 11.38 ± 1.75 and

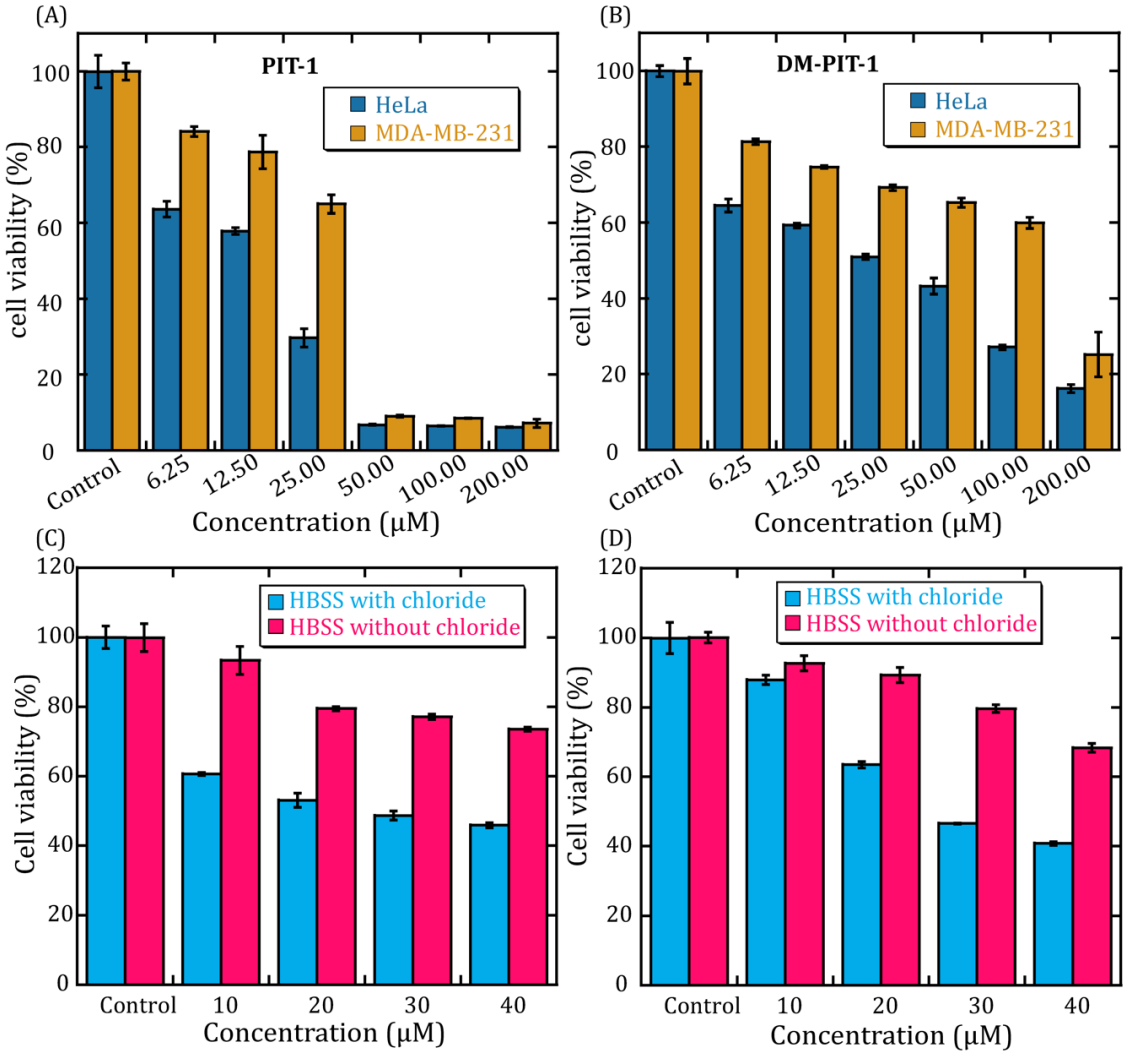

Figure 2.8. Viability of **2.2** (**PIT-1**) (A) and **2.5** (**DM-PIT-1**) (B) measured in HeLa and MDA-MB-231 cells after incubation for 48 h. All MTT assays were performed in triplicates. Viability of HeLa cells was investigated by the MTT assay in the absence and presence of Cl^- ions in HBSS buffer in the presence of different concentrations of **2.2** (**PIT-1**) (C) and **2.5** (**DM-PIT-1**) (D) after 24 h of treatment. All measurements were performed in triplicates.

16.76 ± 2.47 μM, respectively (Table 2.5). However, compound **2.1** showed poor ion transport efficiency in comparison to **2.2** (**PIT-1**) and **2.5** (**DM-PIT-1**), and it also showed very similar cell viabilities as of **2.2** (**PIT-1**). Hence, compounds **2.5** (**DM-PIT-1**) and **2.2** (**PIT-1**) were selected for the further cellular activity studies for their stronger Cl^- ion transport efficiency and previously reported apoptosis triggering behavior. A slightly higher cell death rate was observed for **2.2** (**PIT-1**) than for **2.5** (**DM-PIT-1**), complying with the higher Cl^- ion transportability of **2.2** (**PIT-1**). The

outcome of the MTT assays is in accordance with the earlier reports. It is well demonstrated that the binding of both **2.5** (**DM-PIT-1**) and **2.2** (**PIT-1**) to the PH domain of AKT protein induces apoptosis through the inhibition of the PI3K-PDK-AKT pathway. Cell death in the presence of **2.2** (**PIT-1**) and **2.5** (**DM-PIT-1**) showed various apoptotic features. The treatment of **2.2** (**PIT-1**) resulted in a significant increase in subG1 DNA content both in HeLa and BHK-21 cells. An increase in subG1 and DNA content was also observed in **2.5** (**DM-PIT-1**) treated BHK-21 cells.

Now to comprehend whether the decrease in cell viability is only due to the suppression of the PI3K-PDK1-Akt pathway or transmembrane Cl^- transport by the PITENINs also has a role to play, the viability of the HeLa cells was assessed by changing the extracellular Cl^- ion concentrations. Cells were incubated separately in HBSS (Hank's balanced salt solution), having two different salt compositions (one with a Cl^- ion and the other without a Cl^- ion). Then, to compare the viabilities of HeLa cells in the different salt compositions of HBSS, cells were incubated with **2.5** (**DM-PIT-1**) and **2.2** (**PIT-1**) separately. Lower viability was detected for cells in the Cl^- ion-containing buffer as compared to the one in which there was no Cl^- ion. This observation validates that the decrease in cell viability is also due to the transport of Cl^- ions by **2.5** (**DM-PIT-1**) and **2.2** (**PIT-1**) across the cell membrane.

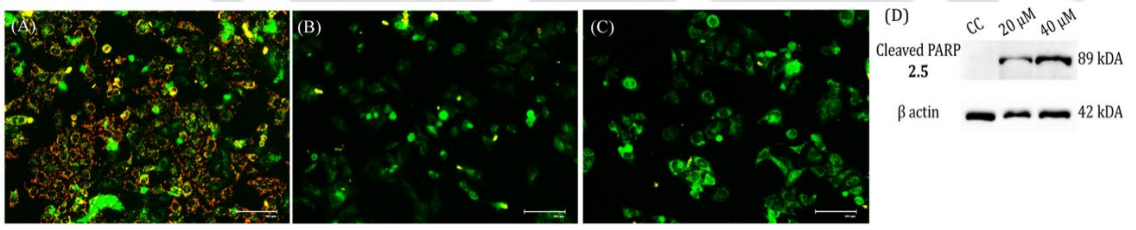

Figure 2.9. Representative images of HeLa cells in the absence and presence of **2.2** (**PIT-1**) (25 μM) and **2.5** (**DM-PIT-1**) (50 μM) after 24 h of incubation (A-C). Cells were stained with JC-1 dye. Both red and green channels were merged into each image. Western blot analysis of HeLa cells in the presence of **2.2** (**PIT-1**) and **2.5** (**DM-PIT-1**) after 24 h of treatment (D). The PARP and β-actin antibodies were used to develop the Western blot.

The difference between the cell viability in HBSS buffer in the presence and absence of a Cl^- ion is in accordance with earlier reports. However, it is incredibly challenging to prepare a complete Cl^- ion free extracellular environment because

intracellular Cl^- ions can also efflux out to balance the Cl^- ion gradient across the membrane. The excessive imbalance of the Cl^- ion gradient can lead to cell death. The interference of the mitochondrial membrane potential (MMP) also suggests the Cl^- ion transport efficacies of the compounds (Fig. 2.9). We also performed the HPTS quenching assay using giant unilamellar vesicles (GUV). The result of the HPTS quenching assay disclosed that the-presence of the compound significantly induces the influx of Cl^- ions (Fig. 2.10, S2.16).confirmed that the transport of Cl^- ions results in faster quenching of the encapsulated HPTS fluorescence. Therefore, the MTT assay in HBSS media and GUV-based HPTS quenching assays propose that the **2.5** (**DM-PIT-1**) mediated transport of the Cl^- ion enhanced the intracellular Cl^- ion concentration, and this higher intracellular Cl^- ion concentration is directly related to the viability of the HeLa cells. Other research groups and we already showed that chloride transport causes an imbalance in ionic homeostasis in cells, which in turn induces apoptotic cell death. It is well documented

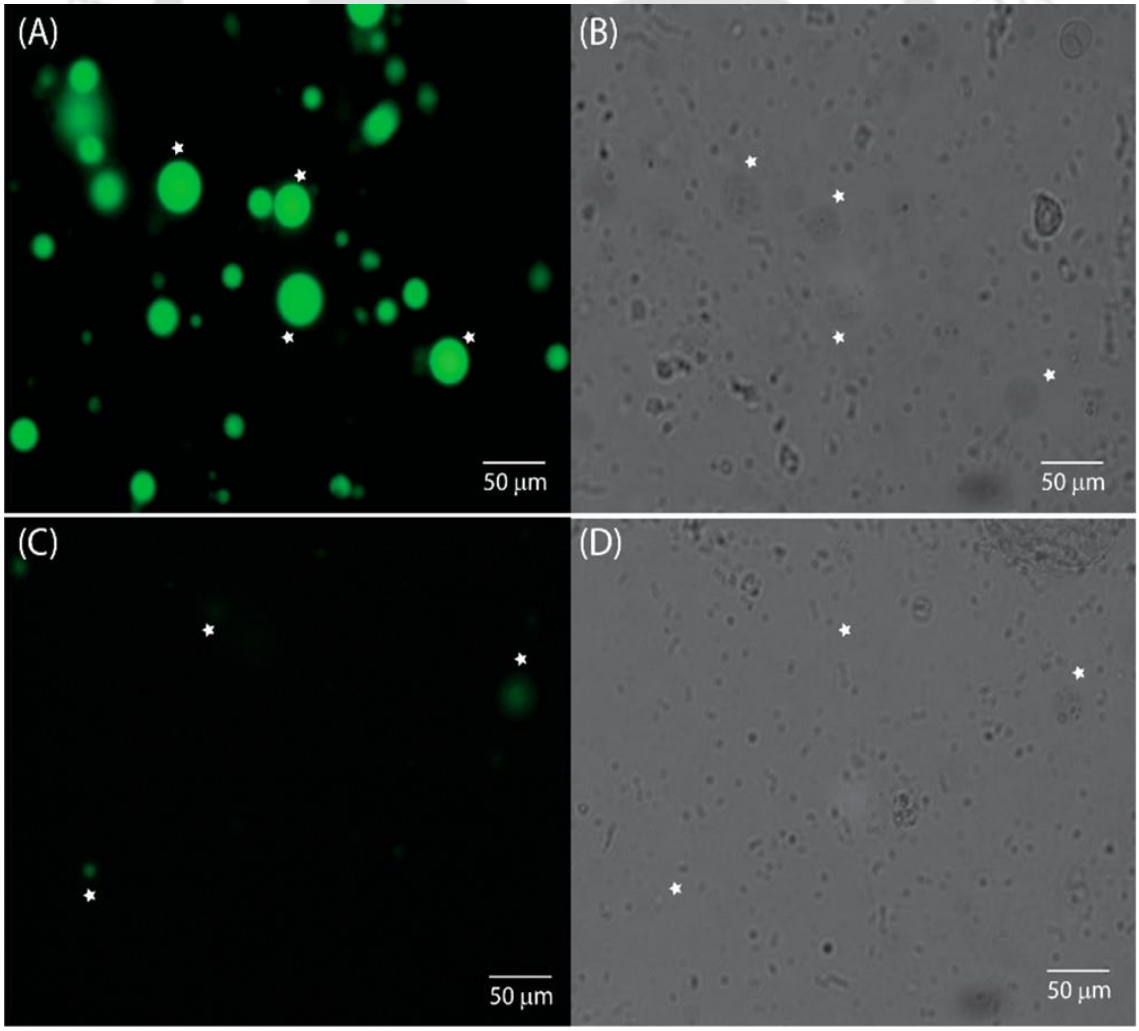

Figure 2.10. Green channel and bright-field images microscopic images of the HPTS-encapsulated GUVs before (A, C) and after 2 min of the addition of 0.1 mM of **2.5** (**DM-PIT-1**) and NaCl (B, D).

that the transport of Cl^- ion disrupts the mitochondrial membrane potential and persuades the cytochrome c release from mitochondria. The released cytochrome c forms a cytochrome c/Apaf-1 complex, which stimulates numerous caspase-9-mediated pathways to persuade cellular apoptosis. Hence, the apoptotic process can be scrutinized by investigating the change in mitochondrial membrane potential and concurrent release efficiency of cytochrome c, level of expression of caspases, and extent of nuclear fragmentation. The family of poly(ADP-ribose) polymerase (PARP) proteins is associated with several cellular functions including expression of crucial genes, DNA repair, apoptosis, and others. Meanwhile, the existence of cleaved PARP protein is regarded as a trademark of apoptosis in the presence of active caspases. The presence of cleaved PARP (Fig. 2.10) confirmed the caspase-mediated apoptotic cell death in the presence of **2.2** (**PIT-1**) and **2.5** (**DM-PIT-1**). Inhibition of the PIP_3/AKT interactions also promotes cancer cell death through an apoptotic pathway. However, it is difficult to estimate/quantitatively measure the extent of cell death caused by the inhibition of the PIP_3/AKT interaction or by transmembrane transport of Cl^- ions by the compounds, which is beyond the scope of this investigation. Overall, the results suggest the transmembrane Cl^- ion transportability of the PITENINs.

Overall, the current study describes a different approach to PITENINs-mediated regulation of cellular AKT signaling, targeting transmembrane Cl^- ion transport. Due to the different mode of actions, the PITENINs can be combined with the existing selective AKT kinase inhibitor to accomplish greater efficacy in promoting apoptosis in cancer cells. The different modes of action of PITENINs may assist in blocking PIP_3 signaling in combination with the PI3K inhibitors because of the inactivation of PIP_3 phosphatase in the breast, endometrium, colon, and other cancer cells. These dual activities of PITENINs may also represent a promising strategy to fight against PIP_3 phosphatase-deficient tumors. However, further studies are required to understand the role of PITENINs in other cancer cells. Target specific delivery of PITENINs to these PIP_3 phosphatase-deficient cancer cells could also limit side effects related to

the inhibition of the PI3K signaling pathway. Furthermore, PITENINs with such different modes of action could be an attractive class of lead compounds for anticancer drug discovery.

2.3. Summary

In summary, we demonstrated that the PITENINs could function as synthetic Cl^- ion transporters. The Cl^- ion binding aptitudes of the PITENINs were confirmed by ^1H NMR titration experiments. The DFT analysis also supported their interaction with the Cl^- ion. The pH-dependent measurements showed that the Cl^- ion transport property of the PITENINs is switched "ON" slightly below the physiological pH. The cholesterol concentration-dependent transport activity suggests that the PITENINs are the transmembrane carrier of Cl^- ions. Thorough mechanistic studies with the potent transporters, **2.2** (**PIT-1**) and **2.5** (**DM-PIT-1**), confirmed the H^+/Cl^- transport pathway. The cell viability of **2.2** (**PIT-1**) and **2.5** (**DM-PIT-1**) suggests that the IC_{50} values are contrariwise associated with Cl^- transport activities. The supplementary cell viability and GUV analysis also suggest that the transport of Cl^- ions into the intracellular/intravesicular matrix is caused by the potent compounds. Overall, this investigation revealed the anticancer activities of **2.2** (**PIT-1**) and **2.5** (**DM-PIT-1**), not only because of its capability to inhibit the interaction between PIP_3 and AKT-PH domain but also for its transmembrane Cl^- ion transport activity.

As a result, a pH sensitive anion transporter was studied with the help of various fluorescence studies. Due to the presence of pH-based stimuli a certain extent of selectivity for the cancer cells (specially for HeLa cells) was found. However, other methodologies to increase the selectivity of the anionophore towards the cancer cells should be developed to decrease the toxicity towards the normal cells. Another approach can be to target an ion which has high concentration in the cancer cells. Therefore, the disruption of the ionic imbalance due to ion transport mediated by anionophore can cause cell death which is our main target.

2.4. Experiential section

2.4.1. Synthesis of compounds

2.4.1.1. General information

All the required reagents and solvents were purchased from Sigma-Aldrich, Alfa Aesar and these were used without additional purification unless otherwise

specified. Thin-layer chromatography (TLC) was performed using silica gel 60 F254 (0.25 mm). The column chromatography was carried out using Spectrochem silica gel of 120-200 mesh. ^{1}H NMR and ^{13}C NMR measurements were carried out with Bruker NMR (ASCEND 600) instrument at 600 and 150 MHz respectively, and TMS was used as internal standard. The chemical shifts (δ) values were represented in parts per million (ppm) downfield from TMS. The coupling constant (J) values were reported in hertz and the following abbreviations were used to designate signal multiplicity: s, singlet; d, doublet; t, triplet; q, quartet; m, multiple; br, broadened. High-resolution mass spectra (HRMS) were recorded by using Agilent Q-TOF mass spectrometer with Z-spray source using built-in software for analysis of the recorded data. Egg yolk phosphatidylcholine (EYPC) and cholesterol were purchased from Sigma-Aldrich. Dipalmitoylphosphatidylcholine (DPPC) and dipalmitoylphosphatidylserine (DPPS) were purchased from Avanti Polar Lipids. HEPES buffer, HPTS, lucigenin, Triton X-100, NaOH and inorganic salts were purchased of molecular biology grade from Sigma-Aldrich. Ultrapure water (Milli-Q system, Millipore, Billerica, MA) was used for the preparation of buffers. Stock solutions of all the compounds were prepared in gas chromatographic grade DMSO solvent (Sigma-Aldrich). Stock solutions of EYPC and cholesterol were prepared in spectroscopic grade $CHCl_3$/MeOH at 8:2 ratios.

2.4.1.2. Synthetic Procedure of the Compounds

2.4.1.2.1. Synthesis of acyl isothiocyanate derivatives [17]

To a stirring solution of acid derivatives (1 equiv.) in dichloromethane solvent at 0 °C oxalyl chloride (5 equiv.) and 2-3 drops of DMF was added. The reaction mixture was then allowed to stir at room temperature for 5-8 hours under N_2 atmosphere. After that, the reaction mixture was cooled down to room temperature, and the excess oxalyl chloride was removed under reduced pressure. The oily reaction mixture (of crude acid chloride) was then directly used without further purification. In the next step, the resulting crude acid chloride mixture was added drop-wise to a suspension of powdered potassium thiocyanate (2 equiv.), and PEG-400 (30 µL) in dichloromethane solvent (25 mL) and the mixture was allowed to stir for 3-4 hours at room temperature. After completion of the reaction, the reaction

mixture was filtered and concentrated under reduced pressure. The crude acylisothiocyanate derivatives were stored at –20 °C.

2.4.1.2.2. Synthesis of acyl thiourea derivatives [17]

To a stirring solution of substituted amino phenol (1 equiv.) in dichloromethane (or acetonitrile) was added the crude isothiocyanate derivatives (≈ 1 equiv.). The reaction mixture was stirred at room temperature for 4-5 hours, and the advancement of the reaction was checked by TLC. After completion of the reaction, the mixture was allowed to settle down for 1 hour, and the precipitate was washed with diethyl ether, dichloromethane to get the solid product. The crude solid was recrystallized from appropriate solvents to get pure acylthioureas. However, the semi-solid acyl thioureas were purified by column chromatography.

2.4.1.2.3. Synthesis of benzamide derivatives [37]

To a stirring solution of acid chloride in dichloromethane at 0 °C temperature was added the aminophenol, and the stirring was continued for 10 minutes. After that, the reaction mixture was warmed up to the room temperature, and stirring was continued for additional 2-3 hours. The precipitation generated from the reaction mixture was purified by the washing with diethyl ether to get the desired colorless solid product.

2.4.1.2.4. Synthesis of *N*-((3-nitrophenyl)carbamothioyl)benzamide [38]

To a stirring solution of crude benzoyl isothiocyanate derivatives (≈ 1 equiv.) in acetonitrile was added 3-nitroaniline (1 equiv.). The reaction mixture was stirred at room temperature for 4-5 hours, and the advancement of the reaction was inspected by TLC. The precipitation generated from the target compound was purified by the washing the reaction mixture with diethyl ether to get the desired colorless solid product.

2.4.1.3. Characterization of the synthesized compounds:

2.4.1.3.1 *N-((5-chloro-2-hydroxy-3-nitrophenyl)carbamothioyl)benzamide (2.1)*

Following the general procedure as mentioned before, the reaction of the

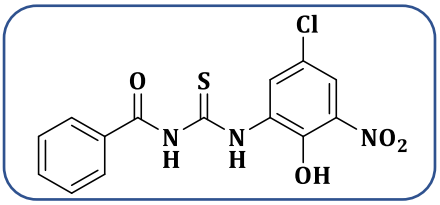

benzoyl isothiocyanate (100 mg, 0.613 mmol) with 2-amino-4-chloro-6-nitrophenol (216 mg, 0.613 mmol) resulted in *N*-((5-chloro-2-hydroxy-3-

nitrophenyl)carbamothioyl)benzamide (**2.1**) as a yellow solid compound with 70% yield. The product was confirmed by HRMS, ^{1}H NMR and ^{13}C NMR data. **M.P.**: 172-175 °C; **IR (Nujol)**: 3322, 1681, 1528, 1460, 1357, 1296, 1164, 1051cm^{-1}; **^{1}H NMR (600 MHz, $CDCl_3$)** δ 13.29 (s, 1H), 11.04 (s, 1H), 9.38 (d, *J* = 2.5 Hz, 1H), 9.10 (s, 1H), 7.91 (d, *J* = 2.5 Hz, 1H), 7.87 (d, *J* = 12.0 Hz, 2H), 7.62 (t, *J* = 7.4 Hz, 1H), 7.51 (t, *J* = 7.7 Hz, 2H); **^{13}C{1H} NMR (151 MHz, $CDCl_3$)** δ 177.5, 166.8, 145.6, 134.1, 133.2, 131.0, 129.9, 129.3, 128.7, 127.6, 124.6, 120.3; .**HRMS (ESI)** calcd. for $C_{14}H_{10}ClN_3O_4S$ $(M+H)^+$: 352.0153, found: 352.0167.

2.4.1.3.2. *N-((3-chloro-2-hydroxy-5-nitrophenyl)carbamothioyl)benzamide (2.2; PIT-1)*

Following the general procedure as mentioned before, the reaction of benzoyl isothiocyanate (100 mg, 0.613 mmol) and 2-amino-6-chloro-4-nitrophenol (216 mg, 0.613 mmol) resulted in *N*-((3-chloro-2-hydroxy-5-nitrophenyl)carbamothioyl)benzamide (**2.2; PIT-1**) as a yellow solid compound with 30% yield.[17] The product was confirmed by HRMS, ^{1}H NMR and ^{13}C NMR data. **M.P.:** 248-251 °C. **IR (Nujol):** 3332, 1691, 1538, 1450, 1337, 1286, 1174, 1061cm^{-1}. **^{1}H NMR (600 MHz, DMSO-d_6):** δ 13.38 (s, 1H), 11.21 (s, 1H), 9.93 (d, *J* = 3.0 Hz, 1H), 7.98 – 7.95 (m, 3H), 7.66 – 7.63 (m, 1H), 7.55-7.52 (m, 2H). **^{13}C{1H} NMR (151 MHz, DMSO-d_6):** δ 174.9, 167.4, 133.3, 132.8, 129.0, 128.9, 123.7, 120.5, 114.2. **HRMS (ESI):** calcd. for $C_{14}H_{10}ClN_3O_4S$ $(M+H)^+$: 352.0153, found: 352.0165.

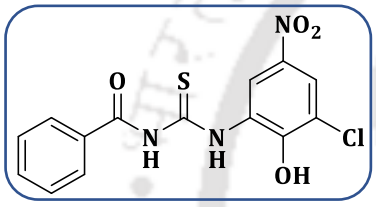

2.4.1.3..3. *N-((3-chloro-2-hydroxy-5-nitrophenyl)carbamothioyl)-3,5-dimethylbenzamide (2.3)*

Following the general procedure as mentioned before, the reaction of the 3,5-dimethylbenzoyl isothiocyanate (100 mg, 0.522 mmol) and 2-amino-6-chloro-4-nitrophenol (184 mg, 0.522 mmol) resulted in *N*-((3-chloro-2-hydroxy-5-nitrophenyl)carbamothioyl)-3,5-dimethylbenzamide (**2.3***)* as a yellow solid compound with 70% yield. The product was confirmed by HRMS, ^{1}H NMR and **^{13}C{1H}** NMR data. **M.P.:** 218-221 °C. **IR (Nujol):** 3342, 2863, 1681, 1548, 1450, 1337, 1286, 1184, 1091cm^{-1};.**^{1}H NMR (600 MHz, DMSO-d_6):** δ 13.15 (s, 1H), 11.72 (s, 1H), 8.90 (d, *J* =

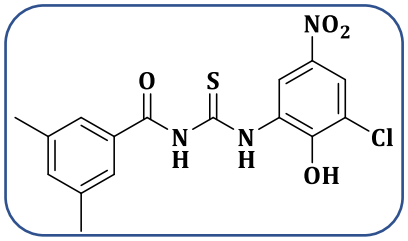

2.7 Hz, 1H), 7.91 (d, *J* = 2.7 Hz, 1H), 7.62 (s, 2H), 7.31 (s, 1H), 2.35 (s, 6H); **^{13}C NMR (151 MHz, DMSO-*d*$_6$):** δ 179.7, 168.9, 138.2, 137.5, 135.1, 132.1, 131.7, 128.7, 126.9, 121.6, 21.2; **HRMS (ESI):** calcd. for $C_{16}H_{14}ClN_3O_4S$ $(M+H)^+$: 380.0466, found: 380.0481.

2.4.1.3.4. ***N-((2-hydroxy-5-nitrophenyl)carbamothioyl)benzamide (2.4)*** – Following the general procedure as mentioned before, the reaction of benzoyl isothiocyanate (100 mg, 0.613 mmol) and 2-amino-4-nitrophenol (95 mg, 0.613 mmol) resulted in *N*-((2-hydroxy-5-nitrophenyl)carbamothioyl)benzamide (**2.4**) as a yellow solid compound with 70% yield. The product was confirmed by HRMS, ^{1}H NMR and ^{13}C NMR data. **M.P.:** 190-197 °C. **IR (Nujol):** 3342, 1681, 1548, 1450, 1337, 1286, 1184, 1091cm^{-1};.**1H NMR (600 MHz, DMSO-*d*$_6$):** δ 13.28 (s, 1H), 11.78 (s, 1H), 9.81 (d, *J* = 2.9 Hz, 1H), 8.07-8.05 (m 1H), 7.99-7.96 (m, 3H), 7.69-7.66 (m, 1H), 7.56-7.53 (m, 2H), 7.13 (d, *J* = 9.0 Hz, 1H); **^{13}C{1H} NMR (151 MHz, DMSO-*d*$_6$):** δ 178.5 , 169.0 , 155.6 , 138.9 , 133.7 , 132.4 , 129.3 , 128.9 , 126.8 , 123.0 , 118.2 , 115.3; **HRMS (ESI):** calcd. for $C_{14}H_{11}N_3O_4S$ $(M+H)^+$: 318.0543, found: 318.0555.

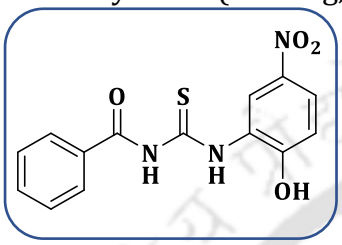

2.4.1.3.5. ***N-((2-hydroxy-5-nitrophenyl)carbamothioyl)-3,5-dimethylbenzamide (2.5; DM-PIT-1)***

Following the general procedure as mentioned before, the reaction of 3,5-dimethylbenzoyl isothiocyanate (100 mg, 0.522 mmol) and 2-amino-4-nitrophenol (81mg, 0.522 mmol) resulted in *N*-((2-hydroxy-5-nitrophenyl)carbamothioyl)-3,5- dimethyl benzamide (**2.5**; **DM-PIT-1**) as a yellow solid compound with 75% yield. The product was confirmed by HRMS, ^{1}H NMR and ^{13}C NMR data**. M.P.:** 235-237 °C; **IR (Nujol):** 3345, 2853, 1689, 1625, 1565, 1363, 1211, 1187, 103 4 cm^{-1};.**^{1}H NMR (600 MHz, DMSO-*d*$_6$):** δ 13.32 (s, 1H), 11.62 (s, 1H), 9.82 (d, *J* = 2.8 Hz, 1H), 8.06-8.04(m, 1H), 7.63 (s, 2H), 7.30 (s, 1H), 7.11 (d, *J* = 9.0 Hz, 1H), 2.35 (s, 6H); **^{13}C{1H} NMR (151 MHz, DMSO-*d*$_6$):** δ 178.4, 169.1, 138.7, 138.2, 135.0, 132.1, 126.9, 126.8, 122.9, 118.0, 115.3, 21.1; **HRMS (ESI:)** calcd. for $C_{16}H_{15}N_3O_4S$ $(M+H)^+$: 346.0856, found: 346.0869.

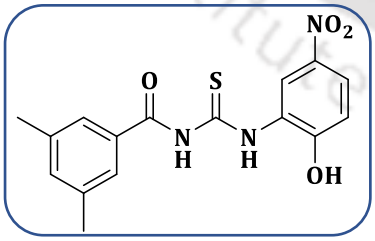

2.4.1.3.6. *N-(2-hydroxy-5-nitrophenyl) benzamide (2.6)*

Following the general procedure as mentioned before, the reaction between benzoyl chloride (83 µL, 0.711 mmol) and 2-amino-4-nitrophenol (109 mg, 0.711 mmol) resulted in *N*-(2-hydroxy-5-nitrophenyl) benzamide (**2.6**) as a yellow solid compound with 75% yield. The product was confirmed by HRMS, ^{1}H NMR and ^{13}C NMR data. **. M. P.:** 230-232 °C**; IR (Nujol):** 3425, 1740, 1567, 1374, 1233, 1144 cm^{-1}; **^{1}H NMR (400 MHz, DMSO-d$_6$):** δ 11.65 (s, 1H), 9.63 (s, 1H), 8.77 (d, J = 2.8 Hz, 1H), 8.02-7.97 (m, 3H), 7.64-7.61 (m, 1H), 7.57-7.53 (m, 2H), 7.09 (d, J = 9.0 Hz, 1H); **^{13}C{1H} NMR (101 MHz, DMSO-d$_6$):** δ 165.9, 156.2, 139.6, 134.4, 132.5, 129.1, 128.1, 126.6, 122.3, 119.5 , 115.7; **HRMS (ESI):** calcd. for $C_{13}H_{10}N_2O_4$ $(M+H)^+$: 259.0641, found: 259.0651.

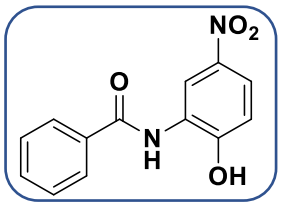

2.4.1.3.7. *N-((3-nitrophenyl)carbamothioyl)benzamide (2.7)*

Following the general procedure as mentioned before, the reaction of benzoyl isothiocyanate (100 mg, 0.613mmol) and 3-nitroaniline (85 mg, 0.613 mmol) resulted in *N*-((3-nitrophenyl)carbamothioyl)benzamide (**2.7**) as a yellow solid compound with 70% yield. The product was confirmed by the HRMS, ^{1}H NMR and ^{13}C NMR data**. M.P.:** 158-160 °C. **IR (Nujol):** 3345, 1689, 1645, 1555, 1343, 1221, 1185, 102 4 cm^{-1}.**^{1}H NMR (400 MHz, CDCl$_3$):** δ 12.83 (s, 1H), 9.17 (s, 1H), 8.69 (t, *J* = 2.2 Hz, 1H), 8.08-8.05 (m, 1H), 8.01-7.98 (m, 1H), 7.86 – 7.83 (m, 2H), 7.64 – 7.59 (m, 1H), 7.54-7.48 (m, 3H). **^{13}C{1H} NMR (101 MHz, CDCl$_3$):** δ 178.9, 167.2, 148.3, 138.7, 134.0, 131.2, 129.7, 129.6, 129.3, 127.5, 121.3, 118.9; **HRMS (ESI):** calcd. for $C_{14}H_{11}N_3O_3S$ $(M+ H)^+$: 302.0521, found: 302.0535.

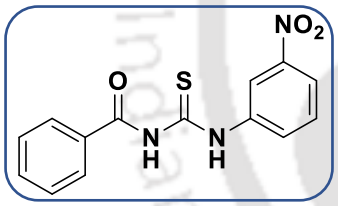

2.4.2. Solution phase anion binding studies

2.4.2.1. ^{1}H-NMR Titrations

2.4.2.1.1. Anion binding analysis by ^{1}H-NMR titration

2.2 (**PIT-1**) and **2.5** (**DM-PIT-1**) were dissolved in DMSO-*d*$_6$ and used for ^{1}H-NMR titration using 600 MHz Brucker NMR instrument (ASCEND 600). Tetrabutylammonium chloride (TBACl) was used as the source of Cl^- ion, and its concentration was sequentially increased during the titration. The chemical shift

(Δδ) of both N-H proton and the O-H proton of compounds were recorded, and the extents of shift (Δδ) of N-H as well as the O-H protons were recorded for all the tested compounds. All ^{1}H NMR spectra were stacked by using the MestReNova software. Changes in chemical shift against the concentration of Cl^{-} ion were fitted using BindFit v0.5 program [25, 26].

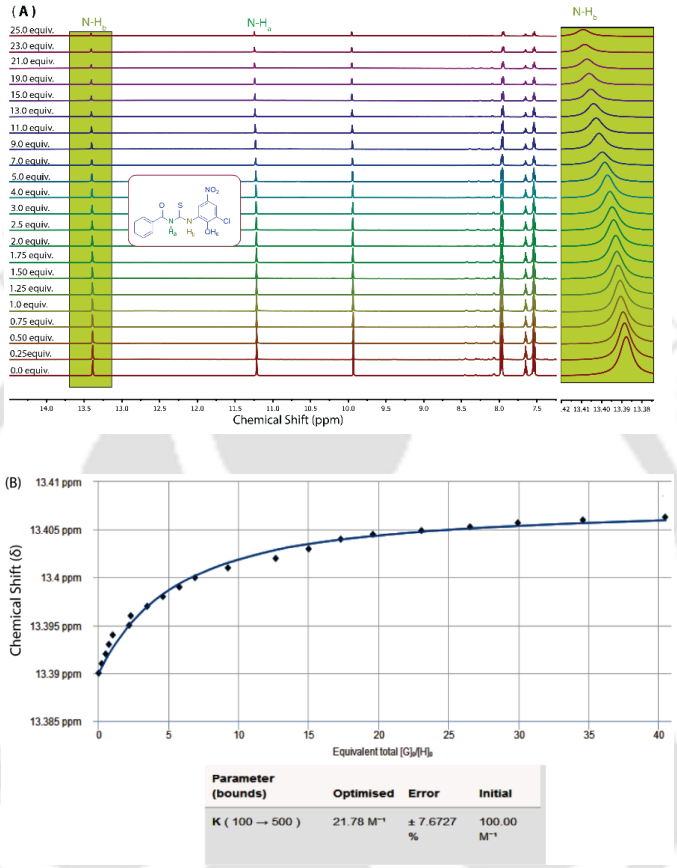

Figure S2.1. ^{1}H NMR (600MHz) titration spectra for compound **2.2** (**PIT-1**) with a sequential addition of TBACl in DMSO-d_6 solvent. (**A**). Plot of chemical shift (δ) of N-H proton *vs* equivalent total ($[G]_0/[H]_0$) added, fitted to 1:1 binding model of BindFit v0.5 program (**B**). H = host = **2.2** (**PIT-1**) and G = guest = TBACl.

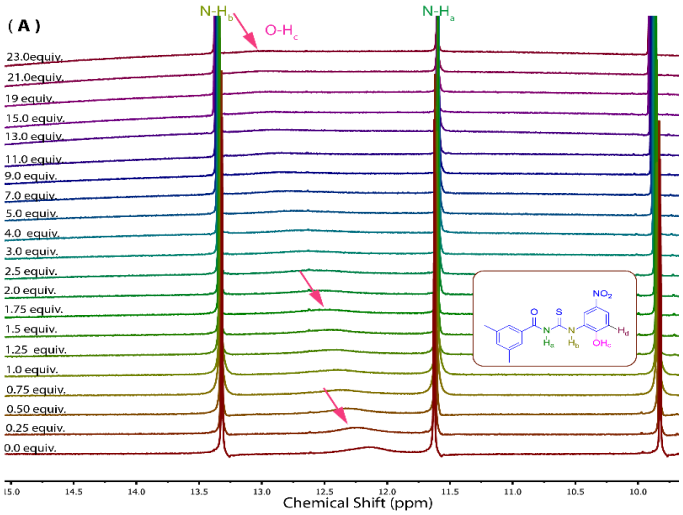

Figure S2.2. ^{1}H NMR (600MHz) titration spectra for compound **2.5** (**DM-PIT-1**) with a sequential addition of TBACl in DMSO-d_6 solvent. Plot of chemical shift (δ) of O-H proton *vs* equivalent total ($[G]_0/[H]_0$) added, could not be fitted properly using BindFit v0.5 program due to insufficient data. H = host = **2.5** (**DM-PIT-1**) and G = guest = TBACl.

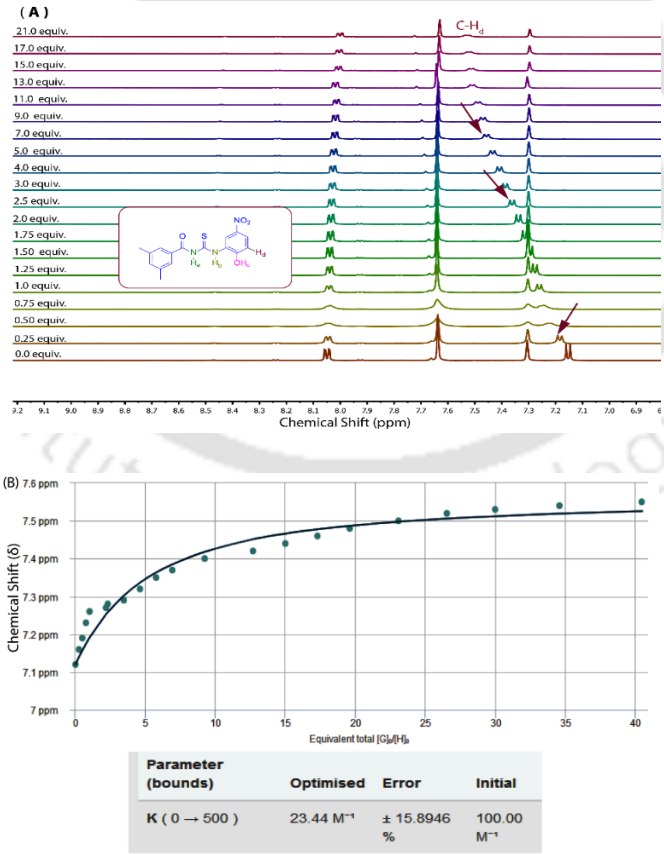

Figure S2.3. ^{1}H NMR (600MHz) titration spectra for compound **2.5** (**DM-PIT-1**) with a sequential addition of TBACl in DMSO-d_6 solvent. (**A**). Plot of chemical shift (δ) of C-

H proton *vs* equivalent total ($[G]_0/[H]_0$) added, fitted to 1:1 binding model of BindFit v0.5 program (**B**). H = host = **2.5** (**DM-PIT-1**) and G = guest = TBACl.

2.4.2.2. UV-Vis Titrations

A 50 μM stock solution of **2.5** (**DM-PIT-1**) was taken in DMSO in a quartz cuvette, and the UV-Vis absorbance spectrum at 298 K was recorded between 250 nm and 550 nm. Aliquots of the DMSO stock solution of 12.5 mM TBACl were sequentially added to the receptor solution, and the UV-Vis spectra were documented each time. Equilibrium constant (m2) of complex (1:1) was calculated using the equation, y = (m0 × m1)/ (m0 + m2), where m0 = [Cl^-], y = A - Ao (A is the absorbance at a certain concentration of anions and Ao is the absorbance without anions).

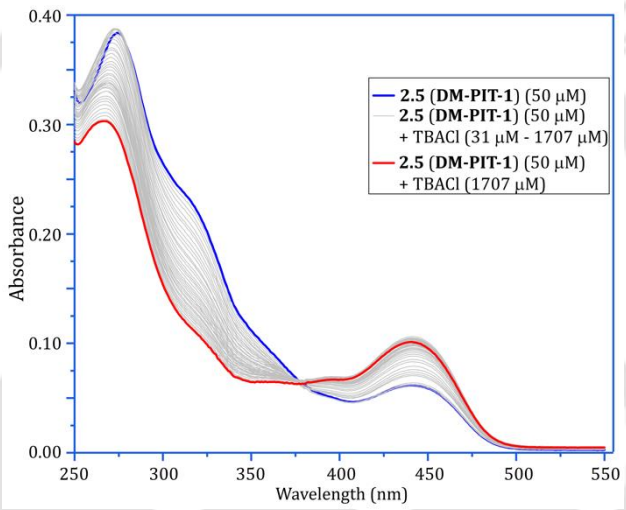

Figure S2.4. UV-Vis titration of **2.5** (**DM-PIT-1)** with TBACl (0-1396 μM).

2.4.3. The density functional theory (DFT) calculations using B3LYP/6-31+G(d) and B3LYP/6-31++G (d,p) methods

The density functional theory (DFT) is recognized as one of the most famous and successful approaches for inspecting the structural and electronic properties of molecules and also their interacting systems. For probing various non-covalent interactions like hydrogen bond and charge distribution of the molecules or atoms, it is widely used. DFT analysis (using the Gaussian 09 program) was performed to explore the stability of compound- Cl^- ion complex and interacting patterns of the compounds with the Cl^- ion where the molecule **2.2** (**PIT-1**) behaves as host and the chloride ion behaves as guest molecules in the complex system. All the considered electronic structure were fully optimized at B3LYP/6-31+G(d) and B3LYP/6-

31++G(d,p) level of theories using the Gaussian 09 program package [39, 27] . The examination showed that the Cl^- ion interacts with **2.2** (**PIT-1**). The interatomic bond distance [r (Cl^----H)] and the interaction energies were tabulated in Table S2. The interaction energies and the number of active hydrogen bonds with the Cl^- ion strongly support the ion recognition capability and transport abilities of **2.2** (**PIT-1**). These results strongly support the ion recognition and of these compounds in physiological conditions. Similarly, calculations were also done for compound **2.5** (**DM-PIT-1**), and the calculated bond distances and the interaction energy are tabulated in Table 2.2.

Table 2.2. Energy minimized structure of the compounds generated by DFT method using the hybrid density functional B3LYP with the 6-31+G (d) and 6-31++G (d,p) basis sets.

	DFT energy minimized structures	***IE* and *r* (Cl----H) Å**
B3LYP/6-31+G(d)	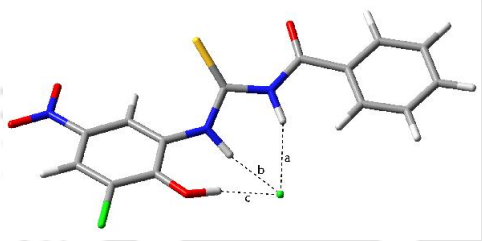 **2.2** (**PIT-1**)	*-92.228* a = 2.338 b = 2.155 c = 2.048
	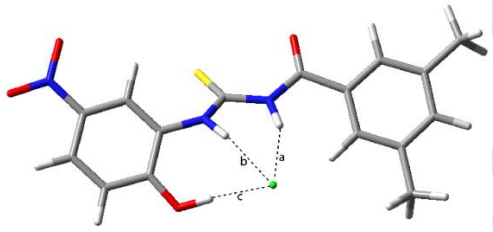 **2.5** (**DM-PIT-1**)	*-89.642* a = 2.348 b = 2.174 c = 2.070

B3LYP/6-31++G(d,p)	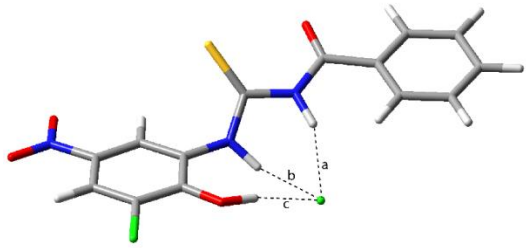 **2.2 (PIT-1)**	*-92.431* a = 2.338 b = 2.155 c = 2.048
	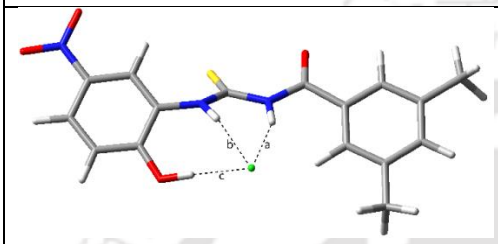 **2.5 (DM-PIT-1)**	*-89.925* a = 2.349 b = 2.173 c = 2.070

Interaction Energy, IE (Kcal/mol) given in Italics.

2.4.4. Ion Transport Activity Studies

2.4.4.1. Preparation of EYPC-LUVs⊃HPTS

In a clean and dry sample vial, egg yolk phosphatidylcholine (EYPC, 50 mg/mL in deacidified $CHCl_3$) and cholesterol (25 mg/mL in deacidified $CHCl_3$) were taken such that the molar ratio of EYPC and cholesterol is 6:4. The solution was then dried under vacuum for at least 6 hours to form a transparent thin film followed by rehydration using 0.5 mL buffer (1 mM HPTS, 20 mM HEPES and 100 mM NaCl, pH 7.2). The solution was then kept at room temperature for 1 hour and occasionally vortexed (6-7 times). Then this suspension was subjected to minimum 17-19 freeze-thaw cycles and vortexed for the next 15 minutes. Subsequently, the lipid suspension was extruded by a mini extruder with a polycarbonate membrane from Avanti Polar Lipids having 200 nm pore size for minimum 19-21 times (must be an odd number). Eventually, to remove all the unencapsulated dye from the extravesicular solution, gel filtration technique was used (Sephadex G-50) using 20 mM HEPES buffer, pH 7.2, containing 100 mM NaCl as the eluting buffer. The final lipid concentration obtained was 25 mM (assuming 100 % lipid regeneration).

2.4.4.2. Ion transport activity across EYPC/CHOL-LUV⊃HPTS

For the HPTS fluorescence assay, 2890 µL of buffer solution (20 mM HEPES and 100 mM NaCl, pH 7.2), 50 µL of EYPC/CHOL-LUV⊃HPTS and 50 µL of 0.75 M NaOH were taken in a clean and dry 3 mL fluorescence cuvette. It was placed in the fluorescence spectrophotometer (Fluoromax-4 spectrofluorometer) under the slow stirring condition for approximately 3 minutes to generate a pH gradient of around 0.6 between the extra and intra-vesicular system. The HPTS fluorescence intensity was monitored (at t = 0 s) at λ_{em} = 510 nm (λ_{ex} = 450 nm). To initiate the kinetics, 10 µL of the synthetic transporter was added to the solution at t = 50 s. The vesicles were lysed by adding 20 µL of 20% of Triton X-100 at t = 450 s, and the fluorescence intensity measurement was continued for further 50 s (total t = 500 s).

2.4.4.3. Quantitative measurement of transport activity from HPTS assay

The fluorescence emission intensities of the HPTS dye were normalized and the intensities were appearing at t = 0 and t = 500 s were taken as 0 and 100 units, respectively. The normalized fluorescent intensities (FI) at t = 450 s (prior to the addition of Triton X-100 solution) were considered to measure the transport activity of the compounds.

$$i.e.\ Transport\ activity,\ \ T_{HPTS} = \frac{F_t - F_0}{(F_\infty - F_0)} \times 100\ \%$$ Eq.-S1

Where, F_t = fluorescence intensity at t = 450 s (prior to the addition of Triton X-100 solution), F_0 = fluorescence intensity immediately before the addition of the transporter (t = 0 s) and F_∞ = fluorescence intensity after addition of Triton X-100 solution (i.e., at saturation after complete leakage at t = 500 s).

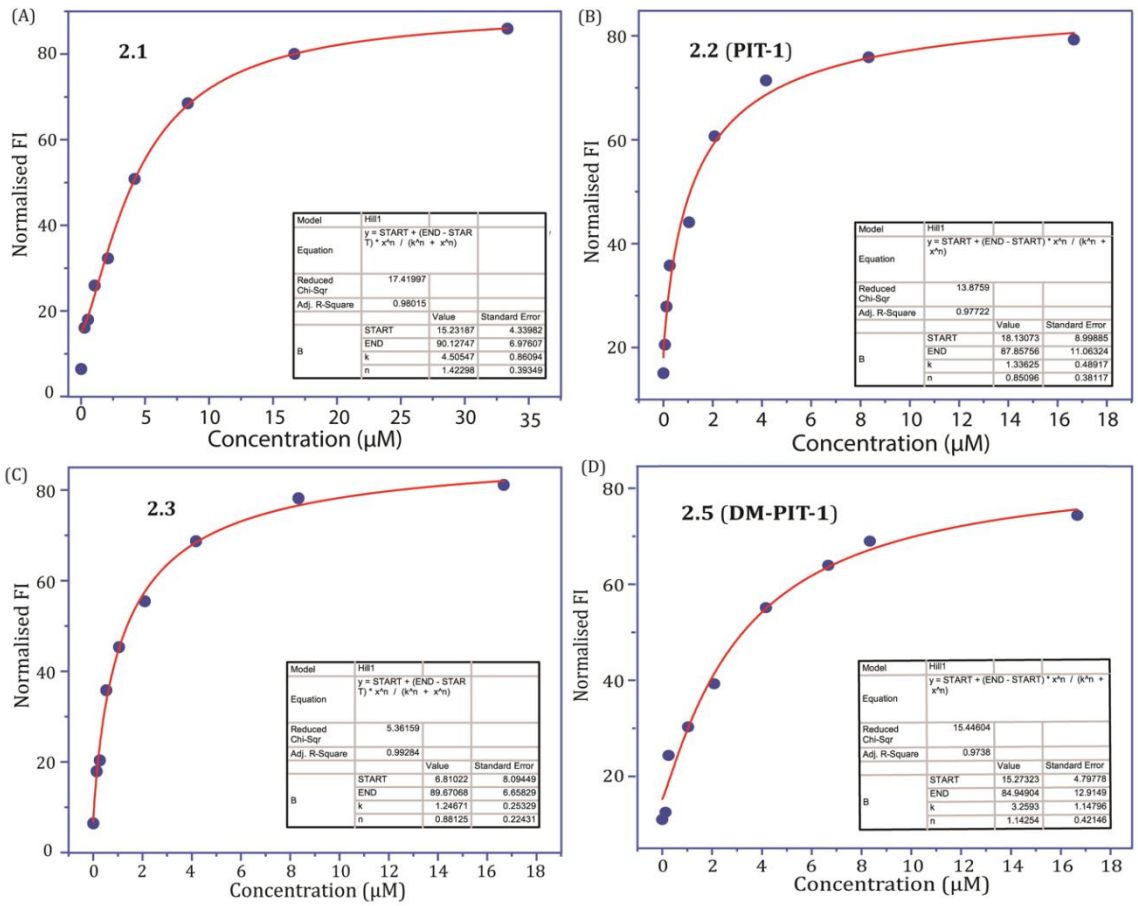

Figure S2.5. Concentration-dependent transmembrane Cl− ion transport activity of the compounds (**2.1**, **2.2** (**PIT-1**), **2.3**, **2.5** (**DM-PIT-1**)) across EYPC/CHOL-LUV⊃HPTS was measured by fluorescence assay at pH 7.2. The EC_{50} value was calculated using the Hill equation (A-D)

2.4.4.4. Ion transport activity studies using ion-selective electrode-based assay

2.4.4.4.1. Chloride ion efflux studies using chloride ion-selective electrode (chloride ISE)

Cl^- ion efflux from the EYPC/CHOL-LUV was measured using a chloride ion-selective electrode (ISE) from Thermo Scientific™ Orion™. Before each experiment, the chloride ISE was calibrated using standard aqueous solutions of NaCl (1 ppm, 10 ppm, and 100 ppm).

2.4.4.4.2. Preparation of EYPC/CHOL-LUV

Briefly, in a clean, dry sample vial, 66 μL of egg yolk phosphatidylcholine (EYPC,100 mg/mL in deacidified $CHCl_3$) was taken along with 40μL of cholesterol (25 mg/mL in deacidified $CHCl_3$) so as to maintain the molar ratio of EYPC and cholesterol as 8:2 in this case. Then the solution was dried under vacuum for at least

5 hours to form a thin film of lipid followed by rehydration of the thin film of lipid by adding 0.5 mL of buffer (20 mM HEPES buffer at pH 7.2 containing 100 mM NaCl). This suspension was kept for 1 hour and was occasionally vortexed (6-7 times) during this period of time. Then this suspension was subjected to minimum freeze-thaw cycles of 17-19 times and vortexed for the next 15 min. After 30 minutes the suspension was extruded using a mini extruder having a polycarbonate membrane with a pore size of 200 nM. The resulting unilamellar vesicles were dialyzed with 5 mM phosphate buffer at pH 7.2 containing 100 mM $NaNO_3$ (iso-osmolar with 100 mM NaCl buffer) to remove the extravesicular NaCl solution. The LUVs were then collected, and the final volume was adjusted to 800 µL using 5 mM phosphate buffer at pH 7.2 containing 100 mM NaCl.

2.4.4.4.3. Chloride efflux study across EYPC/CHOL-LUV

In a clean and dry glass vial 3940 µL of buffer solution (5 mM phosphate and 100 mM $NaNO_3$, pH 7.2) and 50 µL of the EYPC/CHOL-LUV were taken, and the glass electrode was immersed into the solution under mild stirring condition. The efflux of Cl^- was monitored using a chloride ion-sensitive electrode (t = 0 s). After 50 s, 10 µL of the respective transporter (from their respective DMSO stock solution) was added to initiate the Cl^- transport kinetics. Consequently, at t = 500 s the vesicles were lysed using 50 µL of 20% of Triton X-100 solution. Total Cl^- ion efflux reading was taken at t = 700 s. The initial reading was considered as 0% Cl^- efflux, and the final reading at t = 700 s was considered as 100% Cl^- efflux.

2.4.4.4.4. Quantitative measurement of transport activity from chloride ISE assay

The Cl^- ion efflux efficiency of the compounds was normalized and the Cl^- ion efflux efficiency appearing at t = 0 and t = 700 s were taken as 0 and 100 units, respectively. The normalized chloride efflux efficiencies (EE) at t = 500 s (just before the addition of Triton X-100 solution) were considered for the measurement of chloride transport efficiency of the compounds.

$$i.e.\ Chloride\ efflux\ efficiency,\quad EE_{Chloride} = \frac{EE_t - EE_0}{(EE_\infty - EE_0)} \times 100\ \%$$ Eq.-S2

Where, EE_t = Cl^- ion efflux efficiency at t = 500 s (just before the addition of Triton X-100 solution), EE_0 = Cl^- ion efflux efficiency immediately before the addition of the

compound (t = 0 s) and EE_∞ = Cl^- ion efflux efficiency after addition of Triton X-100 solution

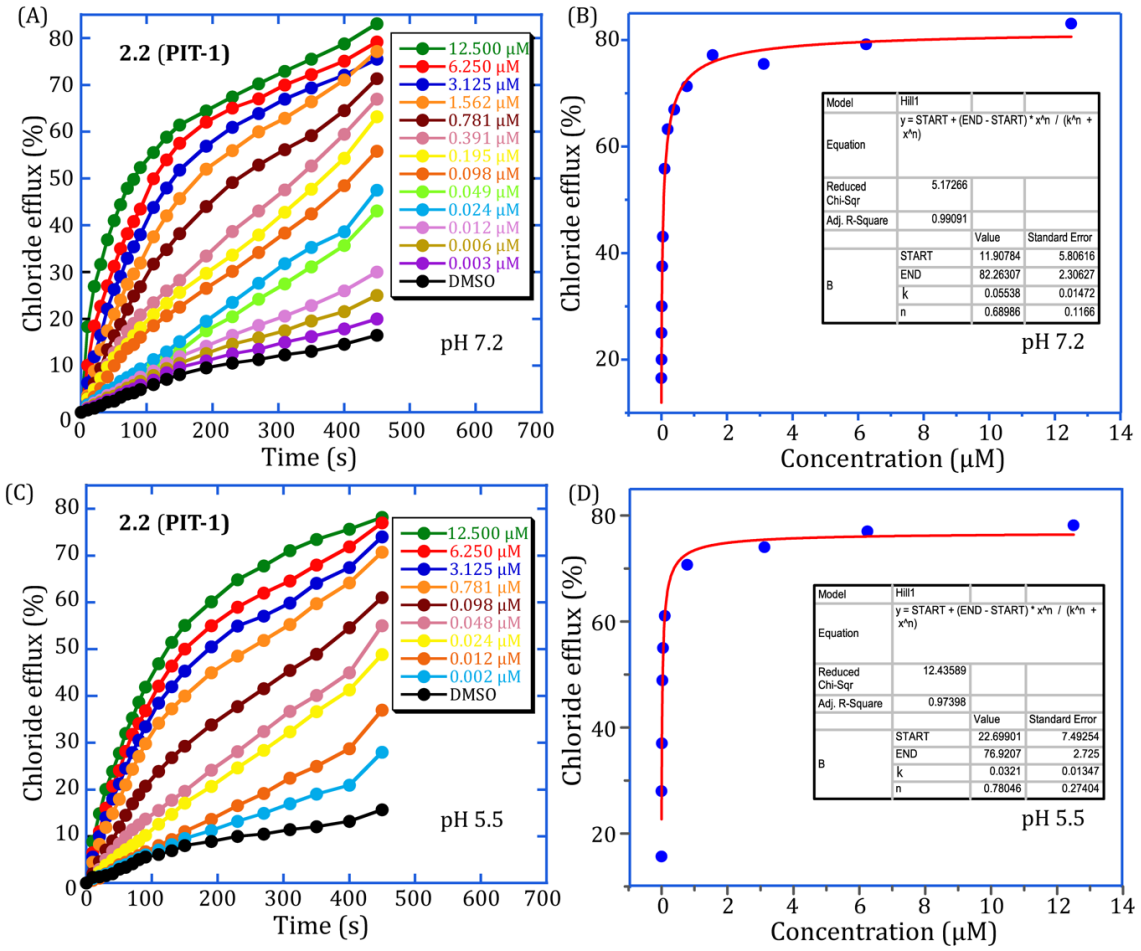

Figure S2.6. Concentration-dependent transmembrane Cl^- ion transport activity of **2.2** (**PIT-1**) across EYPC/CHOL-LUV was measured by chloride ion-selective electrode pH 7.2 (A) and pH 5.5 (C). The EC'50 values at pH 7.2 and pH 5.5 was calculated using the Hill equation (B, C).

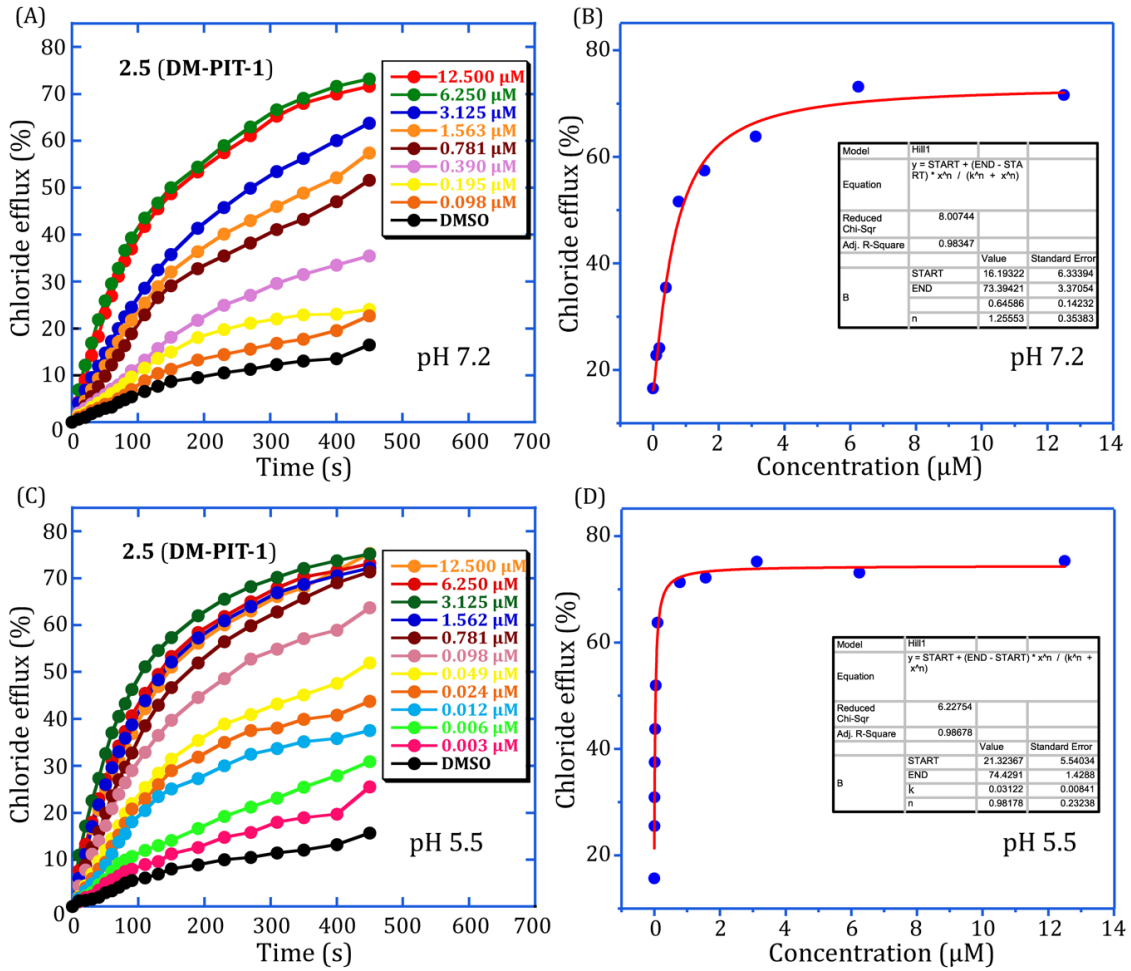

Figure S2.7. Concentration-dependent transmembrane Cl^- ion transport activity of **2.5** (**DM-PIT-1**) across EYPC/CHOL-LUV was measured by chloride ion-selective electrode at pH 7.2 (A) and pH 5.5 (C). The EC_{50} values at pH 7.2 and pH 5.5 was calculated using the Hill equation (B, D).

2.4.4.5. Ion Selectivity Studies

2.4.4.5.1. Buffer and stock solution preparation

Required amount of HEPES and MCl or Na_xA salt (LiCl, NaCl, KCl, RbCl, CsCl, NaBr, NaI, $NaNO_3$, $NaClO_4$, and NaOAc) were added and dissolved in Milli-Q water to attain a final concentration of 20 mM HEPES and 100 mM of the respective salt.

2.4.4.5.2. Cation selectivity studies

For the HPTS fluorescence assay, 2890 µL of buffer solution (20 mM HEPES containing 100 mM of the respective MCl salt, pH 7.2 where M = Li^+, Na^+, K^+, Rb^+, and Cs^+), 50 µL of EYPC/CHOL-LUV⊃HPTS and 50 µL of 0.75 M NaOH was taken in a clean and dry 3 mL fluorescence cuvette. It was placed in the fluorescence

spectrophotometer (Fluoromax-4 spectrofluorometer) under the slow stirring condition for approximately 3 minutes to allow a pH gradient of around 0.6 to be generated between the extra and intra-vesicular system. The HPTS fluorescence intensity was monitored (t = 0 s) at λ_{em} = 510 nm (λ_{ex} = 450 nm). After 50 s, 10 µL of the respective compound was added to the solution to initiate the transport kinetics. Finally, at t = 450 s, the vesicles were lysed by adding 20 µL of 20% of Triton X-100 solution, and the fluorescence measurement was continued for further 50 s (total t = 500 s).

2.4.4.5.3. Anion selectivity studies

2.4.4.5.3.1 Anion selectivity studies (in the presence of base pulse)

A similar procedure was followed for anion selectivity measurements, as mentioned in section 5.2. Here, 20 mM HEPES buffer at pH 7.2 containing 100 mM Na_xA solution was used. In each experiment, NaOH was used to generate the pH gradient.

2.4.4.5.3.2 Anion selectivity studies (without base pulse)

A competitive transport assay was performed to examine the anion selectivity in the absence of any pH-gradient (pH_{in} = pH_{out} = 7.2). In this assay different anions in the intravesicular and extravesicular solutions were used to produce a pH gradient only based on dissimilar transport rates of anions. The EYPC/CHOL-LUV⊃HPTS was prepared as mentioned in earlier sections. The LUVs were prepared in 10 mM HEPES buffer pH 7.2 containing 100 mM NaX salt. The LUVs were dispersed in 10 mM HEPES buffer pH 7.2 containing 100 mM NaY salt. The fluorescence measurements were performed as mentioned earlier. The initial basification of the intravesicular solution was induced by the compound suggests the $X^- > Y^-$ selectivity of the compound which suggest faster H^+/X^- efflux rates than H^+/Y^- influx rates. Whereas, the initial acidification of the extravesicular solution was induced by the compound suggests the $Y^- > X^-$ selectivity of the compound which suggest faster H^+/Y^- influx than H^+/X^- efflux rates than rates.

2.4.4.6. Chloride Efflux Studies at Different pH Using ISE

The ISE based studies were performed to investigate the Cl^- transport efficiency of the compounds (**2.2**, **PIT-1** and **2.5**, **DM-PIT-1**). The EYPC/CHOL-LUV was prepared according to the protocol mentioned in section 5.2.2. Here, 5 mM phosphate

buffer containing 100 mM NaCl at different pH (pH 7.2 and pH 5.5) was used for the preparation of LUVs. Dialysis was performed using 5 mM phosphate buffer containing 100 mM $NaNO_3$ at different pH (pH 7.2 and pH 5.5). The Cl^- efflux efficiency at pH 5.5 and 7.2 was measured at different compound concentrations using the method described in section 5.2.3.

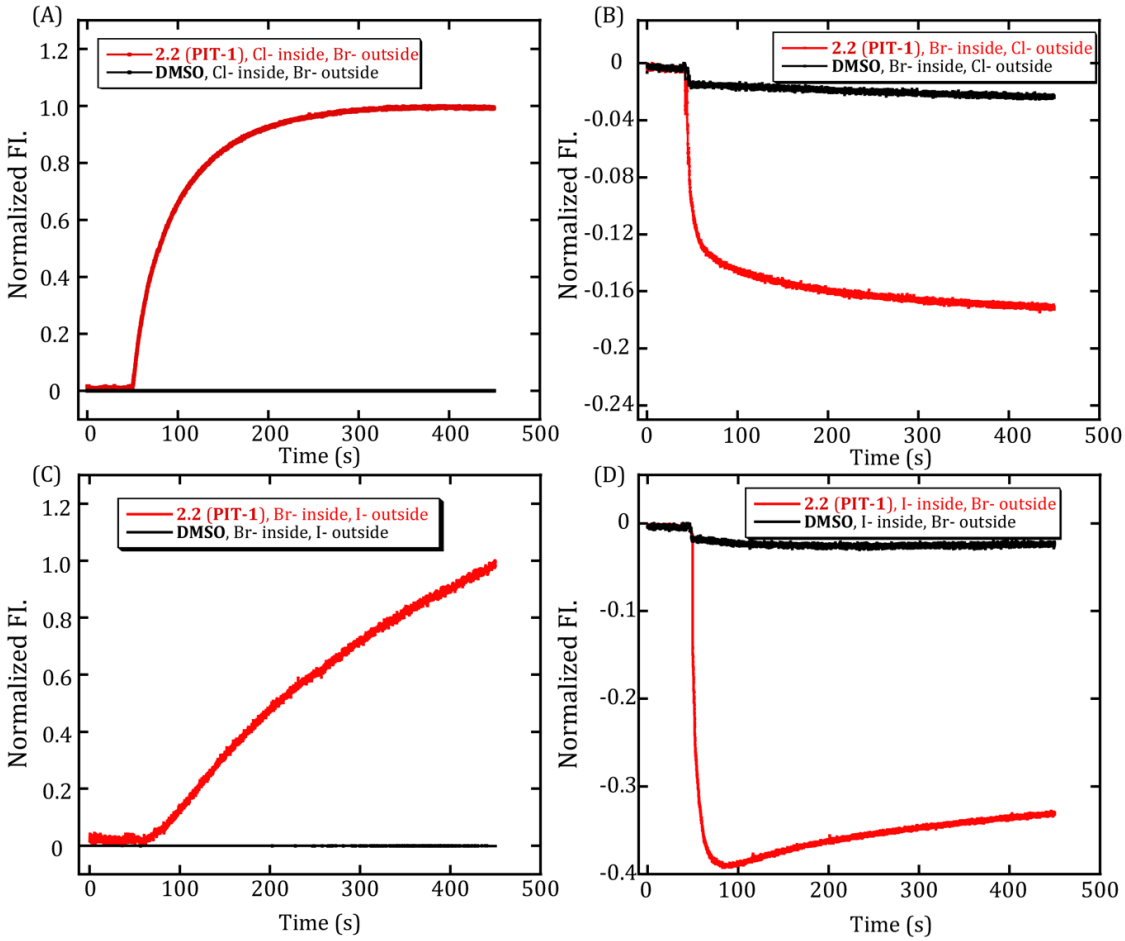

Figure S2.8. Investigation of Cl— vs. Br— (A and B) and Br— vs. I — (C and D) selectivity of compound **2.2** (**PIT-1**). The LUVs were prepared in 10 mM HEPES buffer pH 7.2 containing 100 mM NaCl (A) or NaBr (B and C) or NaI (C) salt. The LUVs were dispersed in 10 mM HEPES buffer pH 7.2 containing 100 mM NaBr (A) or NaCl (B and D) or NaI (C) salt. Compound **2.2** (**PIT-1**) (33.33 µM in DMSO) or DMSO was added to initiate the anion transport kinetics. The directions of pH gradients in the presence of compound **2.2** (**PIT-1**) (Cl— inside Br— outside and Br— inside Cl— outside) confirmed its Cl— > Br— selectivity. The directions of pH gradients in the presence of compound **2.2** (**PIT-1**) (Br— inside I— outside and I— inside Br— outside) confirmed its Br— > I— selectivity.

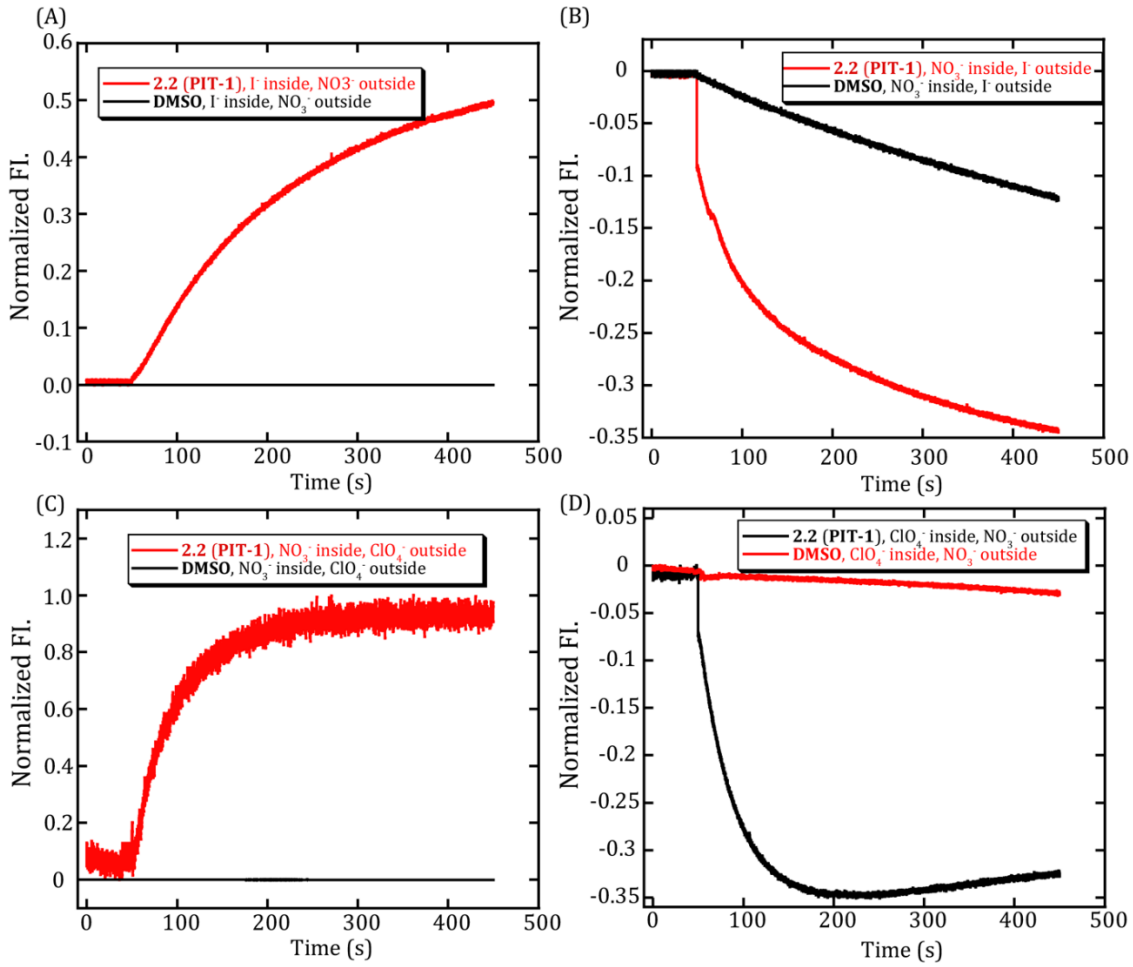

Figure S2.9. Investigation of I^- vs. NO_3^- (A and B) and NO_3^- vs. ClO_4^- (C and D) selectivity of compound **2.2** (**PIT-1**). The LUVs were prepared in 10 mM HEPES buffer pH 7.2 containing 100 mM NaI (A) or $NaNO_3$ (B and C) or $NaClO_4$ (C) salt. The LUVs were dispersed in 10 mM HEPES buffer pH 7.2 containing 100 mM $NaNO_3$ (A and D) or NaI (B) or $NaClO_4$ (C) salt. Compound **2.2** (**PIT-1**) (33.33 μM in DMSO) or DMSO was added to initiate the anion transport kinetics. The directions of pH gradients in the presence of compound **2.2** (**PIT-1**) (I^- inside NO_3^- outside and NO_3^- inside I^- outside) confirmed its $I^- > NO_3^-$ selectivity. The directions of pH gradients in the presence of compound **2.2** (**PIT-1**) (NO_3^- inside ClO_4^- outside and ClO_4^- inside NO_3^- outside) confirmed its $NO3^- > ClO4^-$ selectivity. Hence order of selectivity for compound PIT-1 was $Cl^- > Br^- > I^- > NO3^- > ClO4^-$.

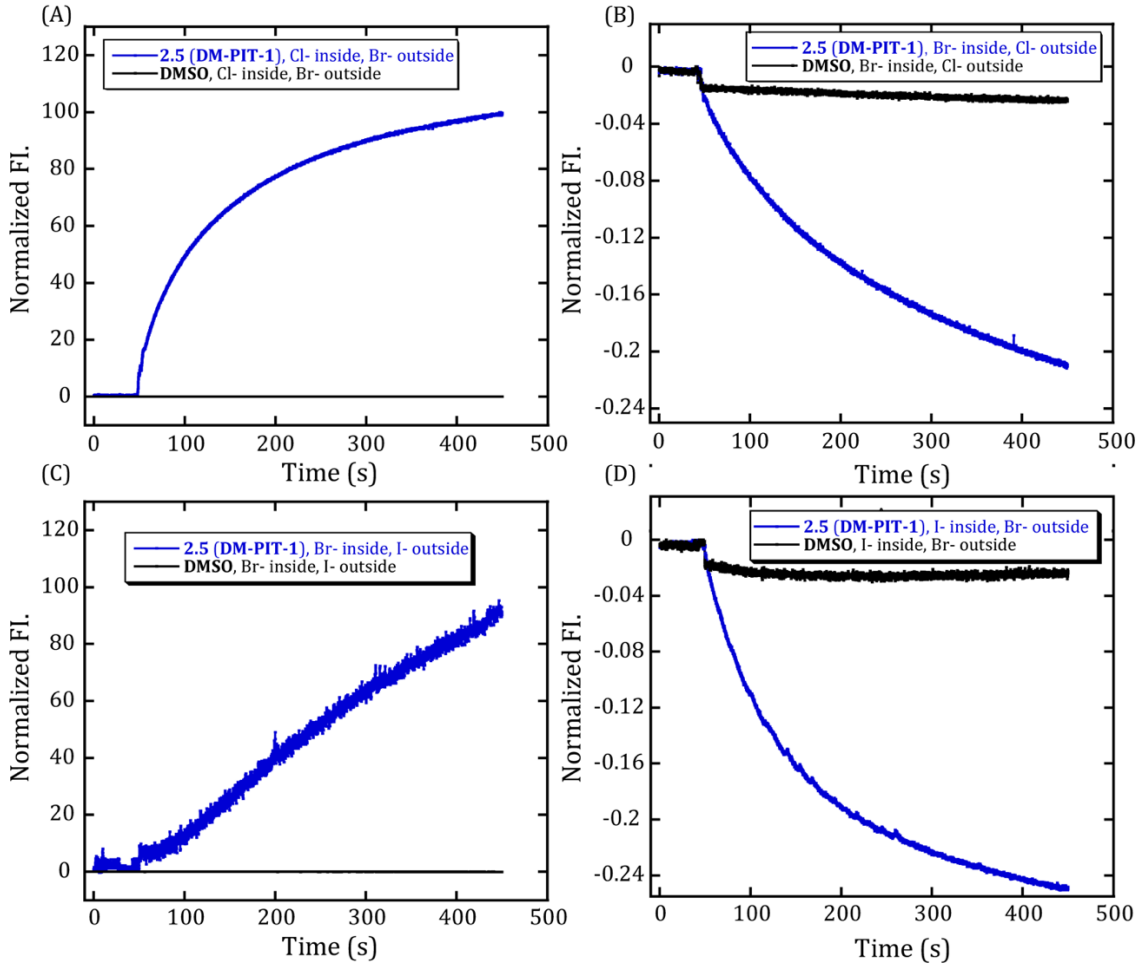

Figure S2.10. Investigation of Cl^- vs. Br^- (A and B) and Br^- vs. I^- (C and D) selectivity of compound **2.5** (**DM-PIT-1**). The LUVs were prepared in 10 mM HEPES buffer pH 7.2 containing 100 mM NaCl (A) or NaBr (B and C) or NaI (C) salt. The LUVs were dispersed in 10 mM HEPES buffer pH 7.2 containing 100 mM NaBr (A) or NaCl (B and D) or NaI (C) salt. Compound **2.5** (**DM-PIT-1**) (33.33 μM in DMSO) or DMSO was added to initiate the anion transport kinetics. The directions of pH gradients in the presence of compound **2.5** (**DM-PIT-1**) (Cl^- inside Br^- outside and Br^- inside Cl^- outside) confirmed its $Cl^- > Br^-$ selectivity. The directions of pH gradients in the presence of compound **2.5** (**DM-PIT-1**) (Br^- inside I^- outside and I^- inside Br^- outside) confirmed its $Br^- > I^-$ selectivity.

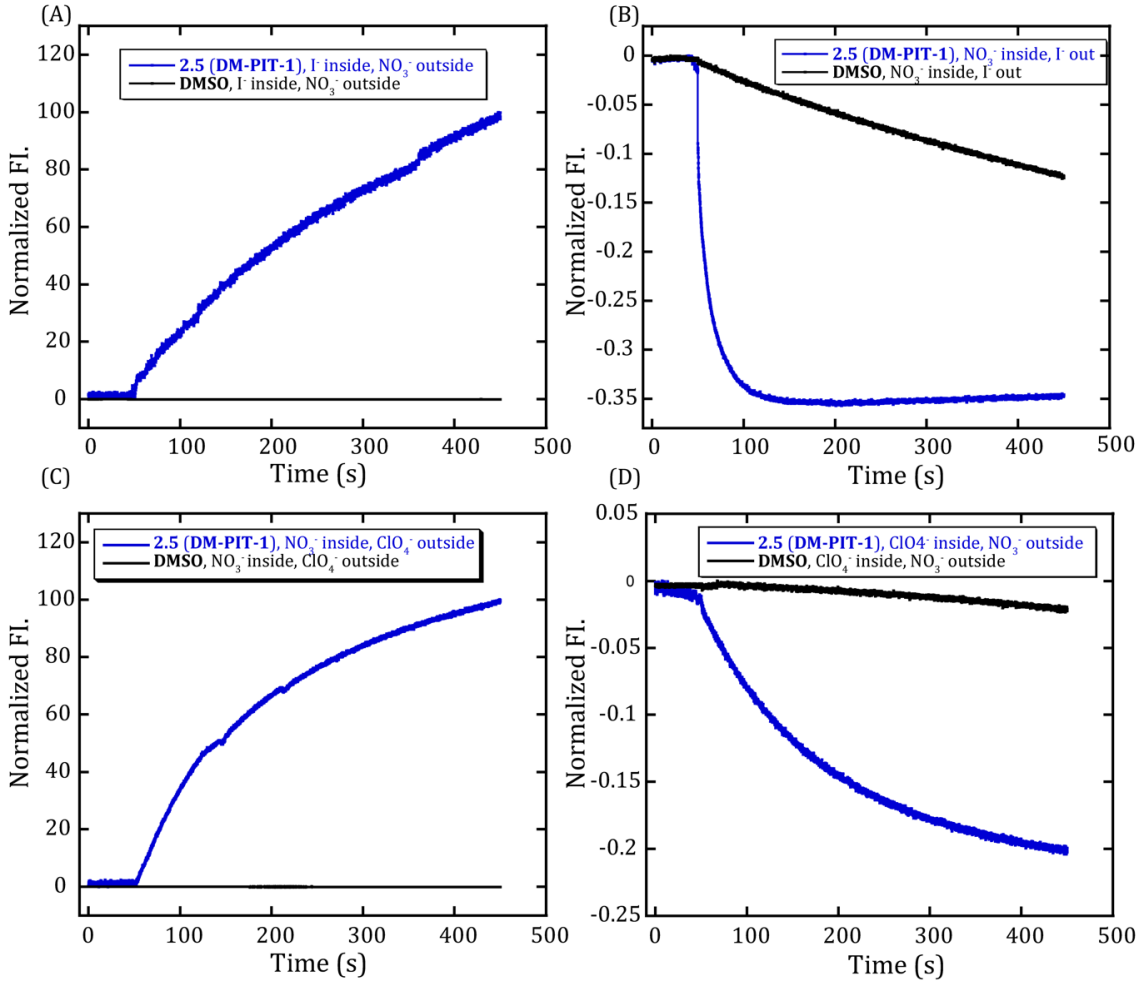

Figure S2.11. Investigation of I^- vs. NO_3^- (A and B) and NO_3^- vs. ClO_4^- (C and D) selectivity of compound **2.5** (**DM-PIT-1**). The LUVs were prepared in 10 mM HEPES buffer pH 7.2 containing 100 mM NaI (A) or $NaNO_3$ (B and C) or $NaClO_4$ (C) salt. The LUVs were dispersed in 10 mM HEPES buffer pH 7.2 containing 100 mM $NaNO_3$ (A and D) or NaI (B) or $NaClO_4$ (C) salt. Compound **2.5** (**DM-PIT-1**) (33.33 μM in DMSO) or DMSO was added to initiate the anion transport kinetics. The directions of pH gradients in the presence of compound **2.5** (**DM-PIT-1**) (I^- inside NO_3^- outside and NO_3^- inside I^- outside) confirmed its I^- > NO_3^- selectivity. The directions of pH gradients in the presence of compound **2.5** (**DM-PIT-1**) (NO_3^- inside ClO_4^- outside and ClO_4^- inside NO_3^- outside) confirmed its NO_3^- > ClO_4^- selectivity. Hence order of selectivity for compound **2.5** (**DM-PIT-1**) was Cl^- > B^- > I^-> NO_3^- > ClO_4^-.

2.4.4.6.1. Measurement of half-maximal effective concentrations (EC_{50}) of the compounds at different pH from chloride efflux studies

The Cl^- ion efflux efficiency at various concentrations of the compounds **2.2** (**PIT-1**) and **2.5** (**DM-PIT-1**) were measured at different pH (pH 7.2 and pH 5.5) to

determine the EC_{50} values (i.e., half-maximal effective concentration). The efflux efficiency (Y-axis) obtained from the chloride ISE measurements were normalized [t = 0 to t = 700 s (X-axis)]. The normalized efflux efficiency (EE) values at t = 500 s (just before the addition of Triton X-100 solution) were considered as the transport activity of the compounds. The efflux efficiency (EE) of a compound at a particular concentration was determined by using equation Eq.-S3. Effective concentration (EC_{50}) of the compound was calculated by plotting the Cl^- efflux efficiency values against concentration (μM) and fitted in the Hill equation Eq. −S3

$$T = T_\infty + \frac{T_0 - T_\infty}{\left[1 + \left(\frac{c}{EC_{50}}\right)^n\right]} \ldots\ldots\ldots\ldots\ldots\ldots\ldots\ldots \text{Eq.} -2.1$$

Here, T_0 and T_∞ correspond to the transport activity obtained in the absence and at an excess concentration of the compound, respectively. c = concentration of the respective compound. EC_{50} value corresponds to the concentration of compound required to obtain half of the maximum transport activity. The number of molecules required for the transportation of a single ion is given by 'n' also known as the Hill coefficient for the compound.

2.4.4.7. Evidence for the Mechanistic Pathway for Chloride ion Transport

2.4.4.7.1. Ion transport activity in the presence of FCCP (FCCP assay)

For this assay, first 2890 μL of buffer (20 mM HEPES and 100 mM NaCl, pH 7.2), 50 μL of EYPC/CHOL-LUV⊃HPTS and 50 μL of 0.75 M NaOH was taken in a 3 mL fluorescence cuvette and then the cuvette was placed in the fluorescence spectrophotometer (Fluoromax-4 spectrofluorometer) under slow stirring condition for approximately 3 minutes to allow a pH gradient of around 0.6 to be generated between the extra and intra-vesicular system. HPTS fluorescence intensity was monitored (t = 0 s) at 510 nm (λ_{ex} = 450 nm). To initiate the kinetics at t = 50 s, 8 μL of the compound and 2 μL of FCCP (1 nM) were added to the cuvette. After, t = 450 s the vesicles were lysed by adding 20 μL of 20% of Triton X-100 solution and the fluorescence measurement was carried out for a further 50 s (total t = 500 s). The control experiment was carried out in the absence of FCCP (2 μL of DMSO was added in place of FCCP).

2.4.4.7.2. Ion transport activity in the presence of valinomycin (valinomycin assay)

The vesicles were prepared by following a similar procedure as described in section 6.1.1. In this assay, the extravesicular solution was replaced with 20 mM HEPES and 100 mM KCl, pH 7.2 buffer. For the valinomycin assay, first 2890 µL of buffer (20 mM HEPES buffer at pH 7.2 containing 100 mM KCl), 50 µL of EYPC/CHOL-LUV⊃HPTS and 50 µL of 0.75 M NaOH was taken in a 3 mL fluorescence cuvette and then the cuvette was placed in the fluorescence spectrophotometer (Fluoromax-4 spectrofluorometer) under slow stirring condition for approximately 3 minutes to allow a pH gradient of around 0.6 to be generated between the extra and intra-vesicular system. HPTS fluorescence intensity was monitored (t = 0 s) at 510 nm (λ_{ex} = 450 nm). To initiate the kinetics at t = 50 s, 8 µL of the compound and 2 µL of valinomycin (6 7 nM) were added to the cuvette. After, t = 450 s the vesicles were lysed by adding 20 µL of 20% of Triton X-100 solution and the fluorescence measurement was carried out for a further 50 s (total t = 500 s). The control experiment was carried out in the absence of valinomycin (2 µL of DMSO was added in place of valinomycin).

2.4.4.8. Evidence for mobile carrier mechanism

2.4.4.8.1. Cholesterol dependency assay

By varying the molar ratios of EYPC and cholesterol as 6:4, 8:2 and 10:0 to inquire into the fact whether increasing the cholesterol ratio in the vesicles has any effect on the Cl^- ion transport activity of the transporters. The chloride transport activity of the transporter was measured using the HPTS assay. Cholesterol is known to increase the rigidity of the lipid bilayer, hence in case of a mobile carrier the transport activity should decrease on increasing the molar ratio of cholesterol (increasing cholesterol slows the diffusion process) while for an ion channel mechanistic pathway effectively no difference in transport activity should be there. Similar procedure was followed using three compositions of liposomes each time. No notable change was observed in the chloride ion transport activity indicating mobile carrier mechanism being followed by the **2.2** (**PIT-1)** and **2.5** (**DM-PIT-1)**.

2.4.4.8.2. U-tube experiment

To confirm the carrier mechanism for the Cl^- ion transportation by the compounds, the U-tube experiment was performed. The lipid bilayer was mimicked here by using 8 mL of chloroform as the organic layer containing the transporters (2 mM). The

source end was filled with 12 mL of 100 mM HCl at pH 1.03 and the receiver end was filled with 12 mL of 100 mM $NaNO_3$ at pH 7.0. The organic phase was stirred gently using a magnetic stirrer, and the Cl^- ion concentration and the pH of the receiver end was monitored using a chloride ion-selective electrode and a pH meter for a period of 72 hours.

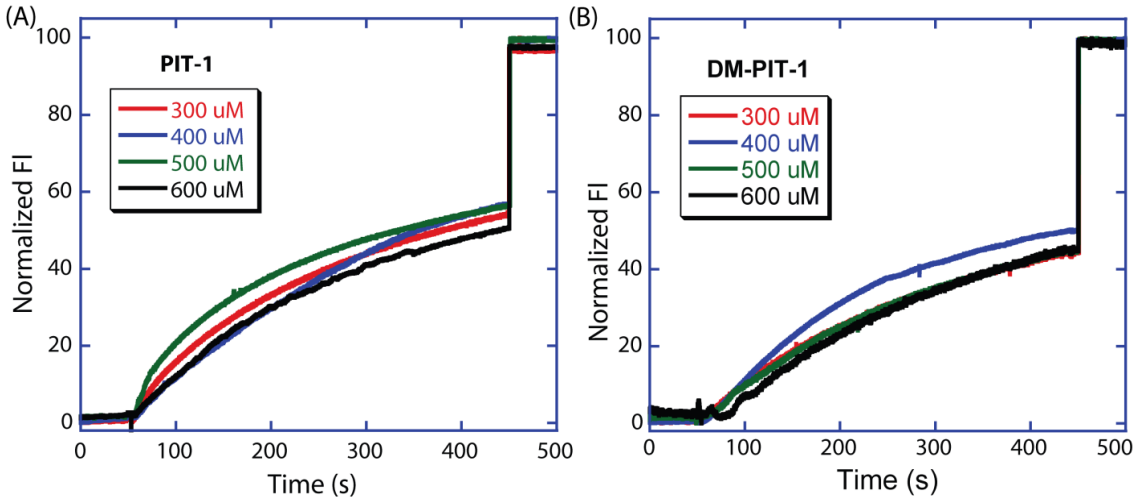

Figure S2.12. Leaching experiment for compounds **2.2** (**PIT-1**) (1.34 µM) (A) and **2.5** (**DM-PIT-1**) (3.26 µM) (B).

2.4.4.9. Test for the leaching-out of the compounds from the membrane bilayer environment

This assay was performed to investigate whether the compounds are within the EYPC/CHOL membrane of the prepared vesicles or they come out in the aqueous solution over the course of the different experiments being performed. If the compounds are in the aqueous solution, on dilution of the lipid solution the transport rate should decrease, while if the compounds are in the EYPC/CHOL membrane then with a dilution of the lipid solution the transport efficiency should remain same. For this assay, 2890 µL of buffer (20 mM HEPES and 100 mM NaCl, pH 7.2), 50 µL of various concentrations of EYPC/CHOL-LUV⊃HPTS (final concentration of the vesicles were 300 µM, 400 µM, 500 µM, and 600 µM) and 50 µL of 0.75 M NaOH were taken in a 3 mL fluorescence cuvette followed by addition of the compound (10 µL from the DMSO stock solution to maintain a fixed anionophore/lipid ratio in all cases) at t = 50 s to initiate the kinetics. After, t = 450 s, the vesicles were lysed by adding 20 µL of 20% of Triton X-100 solution and the fluorescence measurement was carried

out for a further 50 s (total t = 500 s). Four lipid concentrations were used for this assay, and the transport efficacy was found to be same in all these four cases.

2.4.4.10. Evidence of vesicle stability in the presence of the compounds

2.4.4.10.1. Calcein leakage assay

The vesicles were prepared according to the method described in section 6.1.1., except for the fact that in this assay 50 mM calcein was used for the vesicle preparation (instead of 1 mM HPTS). For this assay, 2940 µL of buffer (20 mM HEPES buffer at pH 7.2, containing and 100 mM NaCl) along with 50 µL of LUV was added in a clean and dry 3 mL fluorescence cuvette and the cuvette was placed in the fluorescence spectrophotometer at 37 °C under slow stirring condition to allow maximum incorporation of the compounds into the lipid bilayer. The calcein fluorescence intensity was monitored (t = 0 s) at 520 nm (λ_{ex} = 490 nm). After t= 50 s, 10 µL of the compound from the stock solution was added, and the change in calcein fluorescence intensities was monitored using the fluorescence spectrophotometer. After 450 s the vesicles were lysed by using 50 µL of 20% Triton-X 100 solution was added to the cuvette and the fluorescence measurement was carried out for further 50 s (t = 500 s).

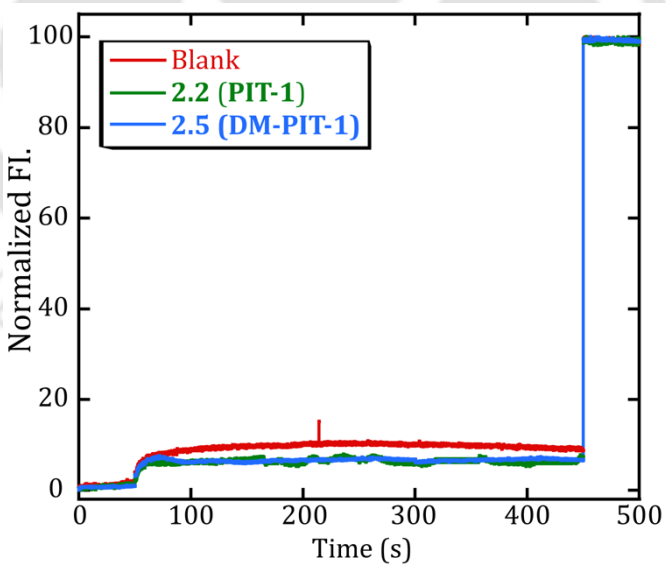

Figure S2.13. The extent of calcein leakage from the EYPC/CHOL-LUV⊃calcein with time in the presence of **2.2** (**PIT-1**) and **2.5** (**DM-PIT-1**) (6.67 µM).

2.4.4.11. Surface Plasmon Resonance (SPR) Binding Analysis

The surface plasmon resonance (SPR) analysis was carried out according to the reported procedure with minor modifications. In brief, the measurements were performed at 25 ºC on Biacore-X100 instrument using CM5 sensor chip (GE Healthcare). PBS buffer at pH 7.4 was used as running buffer. The surface of the CM5 sensor chip was first modified with Anti-GST Antibody using the amine-coupling kit at a flow rate of 30 µL/ minute, followed by AKT-PH domain protein (30 µg/mL) immobilization using GST-capture kit at a flow rate of 10 µL/minute for 2 minutes. AKT-PH domain protein capture level was 4000 response unit (RU). The binding efficacy (association constant; k_a) of the compounds was determined by measuring the change in RU of the SPR sensorgrams in the absence or presence of the compounds (0 to 50 µM).

2.4.4.12. Biological Activity Studies

2.4.4.12.1. MTT-based cytotoxicity assay

Effect of all the compounds (**2.1**-**2.7**) on the viability of HeLa and MDA-MB-231 cells were tested by using 3-[4,5-dimethylthiazol-2-yl]-2,5 diphenyl tetrazolium bromide (MTT) assay. HeLa and MDA-MB-231 cells were seeded in 96-well flat-bottom tissue culture plates, at a density of 10^5 cells/well (per 100 µL) containing 10% fetal bovine serum (FBS) in Dulbecco's Modified Eagle Medium (DMEM) and incubated at 37°C in 5% CO_2. After 16 h, media was discarded, and each well was washed with phosphate-buffered saline (PBS) followed by the addition of the compounds to each well plate with media. After 48 h treatment, 10 µl of MTT solution (5 mg/ml) was added to each well, and the plates were incubated for another 4 h. MTT containing media was removed from each well, and 100 µL of DMSO was added, dissolving the formazan crystals. The absorbance was recorded on a microplate reader (Multiskan™ GO) at the wavelength of 570 nm. All experiments were performed in triplicate, and the relative cell viability (%) was expressed as a percentage relative to the untreated cells.

2.4.4.12.2. Flow cytometry analysis

The identification of apoptotic cells was investigated by staining the cells with propidium iodide (PI) as described earlier. HeLa and BHK21 cells were seeded on a 6-well plate. Cells were treated with 40 µM of compounds **2.2** (**PIT-1**) and **2.5** (**DM-PIT-1**). After 24 hours, cells were harvested and suspended in 0.5 mL of PBS. Cells

were gently aspirated several times with pipette to obtain a mono-dispersed cell suspension, with minimal cell aggregation. Cells were fixed by adding ice-cold 70% ethanol dropwise, with constant vortexing and incubated overnight at 4 ºC. On the next day, ethanol-suspended cells were centrifuged for 10 min at 300g and ethanol was decanted thoroughly. The cell pellet was suspended in 3 ml of PBS and centrifuged at 300g for 10 min. Cells were resuspended in 200 µl of staining solution (PBS with 100 µg/mL RNase A and 50 µg/mL Propidium Iodide). The resuspended cells were incubated at 37 °C for 20 min. The samples were then transferred to the flow cytometer and cell fluorescence was measured. The samples were excited at 488 nm and emission were collected at 635/20-nm filter (FL2-A) respectively. Appropriate gating of cell populations was performed to identify and determine healthy, early apoptotic, late apoptotic and dead cells from the total population of the cells. Cells treated with serum-free medium alone were considered as control and used to draw the initial quadrant.

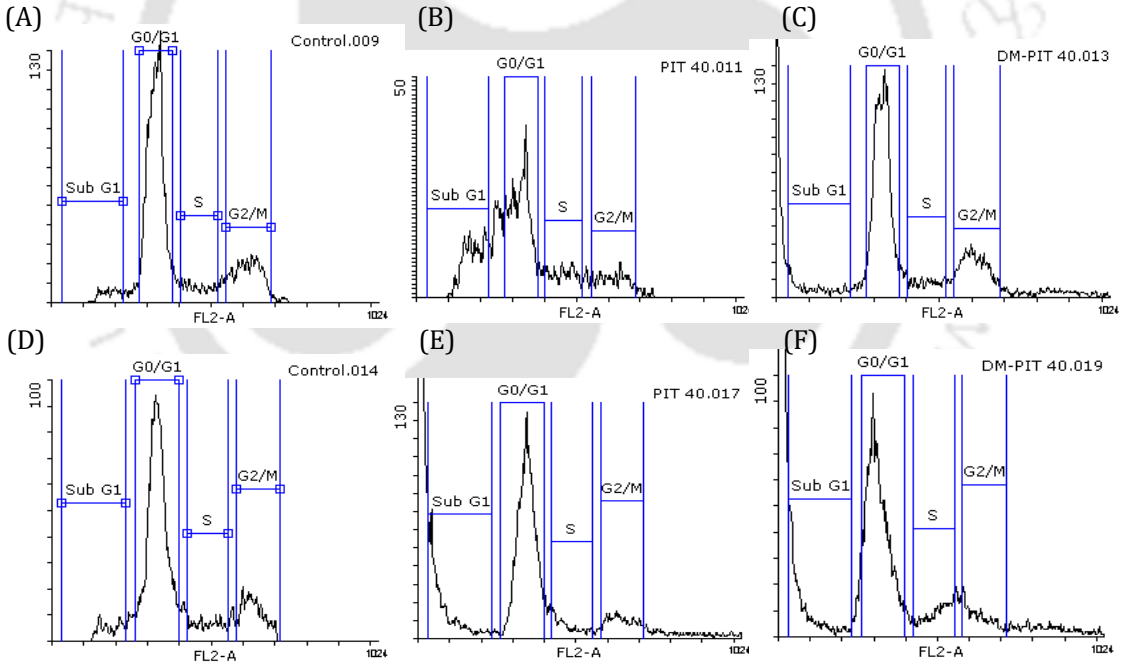

Figure S2.14. DNA content frequency histograms of HeLa and BHK-21 cells in the absence and presence of compounds (A-F). Cells were treated with 40 µM of **2.2** (**PIT-1**) and **2.5** (**DM-PIT-1**) that induce apoptosis. The cells were stained with PI, according to standard protocols, respectively. Fluorescence of the PI-stained cells was measured using CellQuest software (BD Biosciences). Histograms were plotted by the Flowing Software (Version 2.5.1). The software provided the estimate of the

percentage of cells with fractional DNA content (apoptotic cells: Sub G1) and cells in G0/G1, S, and G2/M phases of the cycle.

Table 2.5. The population of cells in the absence and presence of potent compounds.

Compound	Cell	G0/G1 (% of cells)	S (% of cells)	G2/M (% of cells)	Sub G1 (% of cells)
Control	HeLa	60.34	7.59	19.13	4.03
	BHK-21	61.48	8.87	15.30	5.91
2.2 (PIT-1)[a]	HeLa	38.27	10.74	10.45	19.3
	BHK-21	35.47	4.21	6.65	14.77
2.5 (DM-PIT-1)[a]	HeLa	35.75	4.64	12.79	4.95
	BHK-21	29.49	5.83	5.18	10.18

[a]Compound concentration = 40 μM.

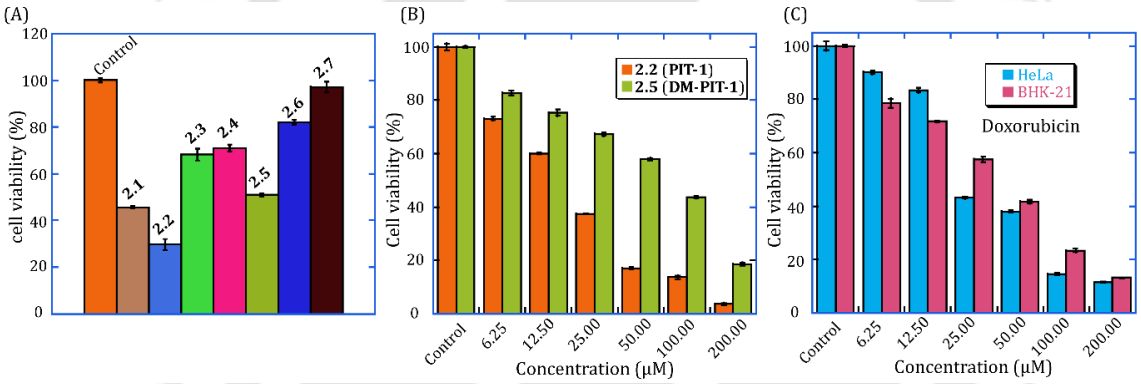

Figure S2.15. Cell viability of the compounds **2.1**–**2.7** was measured at a fixed concentration of 25 μM. Cell viability was measured in HeLa, after 48 h of compound treatment (A). Viability of **2.2** (**PIT-1**) and **2.5** (**DM-PIT-1**) was measured in BHK-21 cells after incubation for 48 hours (B). The viability of doxorubicin was measured in HeLa and BHK-21 cells after incubation for 48 hours. All MTT assays were performed in triplicates (C).

2.4.4.12.3. Chloride mediated cell death

2.4.4.12.3.1. HBSS assay

MTT assay was repeated using HBSS (Hank's balanced salt solution) buffer in presence and absence of Cl^- ion. HeLa cells were maintained and prepared according to the above-mentioned procedure. HBSS buffer (with Cl^- and without Cl^-) containing 10% FBS replaced cell culture media. The transporters **2.5** (**DM-PIT-1**) and **2.2** (**PIT-1**) were added to each well in different concentration and incubated for

48 h. MTT containing media was removed from each well, and 100 µL of DMSO was added, dissolving the formazan crystals. The absorbance was recorded on a microplate reader (Multiskan™ GO) at the wavelength of 570 nm. All experiments were performed in triplicate, and the relative cell viability (%) was expressed as a percentage relative to the untreated cells. Hank's balanced salt solution with Cl^- ion has the following composition: 136.9 mM NaCl, 5.5 mMKCl, 0.34 mM Na_2HPO_4, 0.44 mM KH_2PO_4, 0.81 mM $MgSO_4$, 1.25 mM $CaCl_2$, 5.5 mM D-glucose, 4.2 mM $NaHCO_3$ and 10 mM HEPES (pH 7.4) Hank's balanced salt solution without Cl^- ion was prepared using 136.9 mM Na-gluconate, 5.5 mM K-gluconate, 0.34 mM Na_2HPO_4, 0.44 mM KH_2PO_4, 0.81 mM $MgSO_4$, 1.25 mM Ca-gluconate, 5.5 mM D-glucose, 4.2 mM $NaHCO_3$ and 10 mM HEPES (pH 7.4).

2.4.4.12.2.2. Analysis of mitochondrial membrane potential

Analysis of mitochondrial membrane potential was done using 5,5,6,6'-tetrachloro-1,1',3,3' tetraethylbenzimidazoylcarbocyanine iodide (JC-1) dye. HeLa cells were seeded in 6 well plates at density not exceeding 10^6 cells/cm containing 10% fetal bovine serum (FBS) in Dulbecco's Modified Eagle Medium (DMEM) and incubated at 37°C in 5% CO_2. After 16 h, media was discarded and each well was washed with phosphate-buffered saline (PBS) followed by addition of **2.2** (**PIT-1**) and. **2.5** (**DM-PIT-1**) to each well at 25 µM and 50 µM concentrations respectively with HBSS buffer containing Cl^-. After 12 hours, 2 µM (final concentration) of JC-1 dye was added in each well and incubated at 37°C, 5% CO_2 for 15-30 min. Cells were then washed with PBS and observed under fluorescence microscope (FLoid Cell Imaging Station, Thermo Fischer Scientific) for progressive loss of red J-aggregate fluorescence and cytoplasmic diffusion of green monomer fluorescence.

2.4.4.12.3. Immunoblot analysis

Cultured HeLa cells were grown on 6-well plate and treated with different concentrations of **2.5** (**DM-PIT-1**) and **2.2** (**PIT-1**). After 24 h, cells were washed with PBS. 100 µl of sodium dodecyl sulfate-polyacrylamide gel electrophoresis (SDS-PAGE) loading buffer was added to each well for immediate cell lysis and increased the viscosity of the sample. The extract was transferred to a microcentrifuge tube and heated at 95°C for 10 min. Total cell protein was separated by 12% SDS-PAGE and transferred to a nitrocellulose membrane. Membranes were blocked in Phosphate-

buffered saline 5% dry milk for 2 h and incubated with primary antibody overnight at 4 ℃ with shaking. The membranes were washed several times with Phosphate-buffered saline/Tween-20 and incubated with horseradish peroxidase (HRP)-labeled secondary antibody for 1 h at room temperature with shaking. Band intensity was detected by ECL detection reagent (Biorad) with β-actin as an internal control.

2.4.4.13. Transportation of Chloride Ion across Giant Unilamellar Vesicles (GUVs)

2.4.4.13.1. Ion transport measurements using GUVs-floated in the solution

In a clean and dry glass vial EYPC, cholesterol and DPPS (from the respective stock solution) were taken in the molar ratio of 6:3.5:0.5 and dried under vacuum for 6 hours. To that lipid film, 200 µL of light liquid paraffin oil was added and sonicated for 30 minutes until the lipid film gets completely dissolved in the oil. After that, 20 µL of the upper buffer (100 mM HEPES, 200 mM sucrose, 1 mM 8-hydroxypyrene-1,3,6-trisulfonic acid (HPTS) in H_2O, pH = 7.4) was added, and the solution was mixed thoroughly to form an emulsion. The emulsion was then carefully added to 500 µL of lower buffer (100 mM HEPES, 200 mM glucose in H_2O, pH = 7.4) in a centrifuge tube and the whole mixture was pipetted up and down thoroughly to mix everything. The emulsion was centrifuged for 15 minutes at 10000 rpm to remove the oil as well as the extravehicular dye. This process was repeated for 4-5 times for maximum removal of paraffin oil from the solution. The final precipitate (GUVs) was mixed with 100 µL of lower buffer (final vesicle conc. of 15 mM). The microscopic images were collected and/ or video was recorded using this floating GUVs.

2.4.4.13.2. Ion transport measurements using GUVs coated on the glass surface

The mussel-inspired GUVs were prepared by following reported methods with minor modifications. In an acid-washed glass vial, *N*-(3,4-dihydroxyphenethyl)palmitamide and DPPS solutions were taken in the molar ratio of 1:4 and dried under vacuum for 6 hours. The mixture was dissolved in 0.1 mL of tetrahydrofuran/water (9:1 v/v) mixture, and the solution was injected to 0.9 mL 5 mM PBS buffer of pH 5.6 (final conc. of 0.2 mM). The solution was then sonicated for 5 minutes. The prepared vesicle solution was directly used for the glass coating. The vesicle solution was drop casted on the surface of a glass-bottom disk and incubated for overnight at 37 °C. Finally, the substrate was washed by HEPES buffer thoroughly.

The prepared GUV solution (100 µL) mixed with **2.5** (**DM-PIT-1**) (0.1 mM) was taken on a hydrophobic coated glass-bottom dish. The GUVs were allowed to settle down for 5 hours. After that, NaCl solution (0.1 M) was added. At this stage, the image was taken (in a Nikon ECLIPSE Ts2R fluorescence microscope) before and after the addition of NaCl in the green channel as well as in the bright field to ensure the quenching of HPTS fluorescence intensity. Here the decay of the HPTS fluorescence intensity is due to Cl^- influx and consequently OH^- efflux (as compound follow OH^-/Cl^- antiport mechanism for its chloride transport activity).

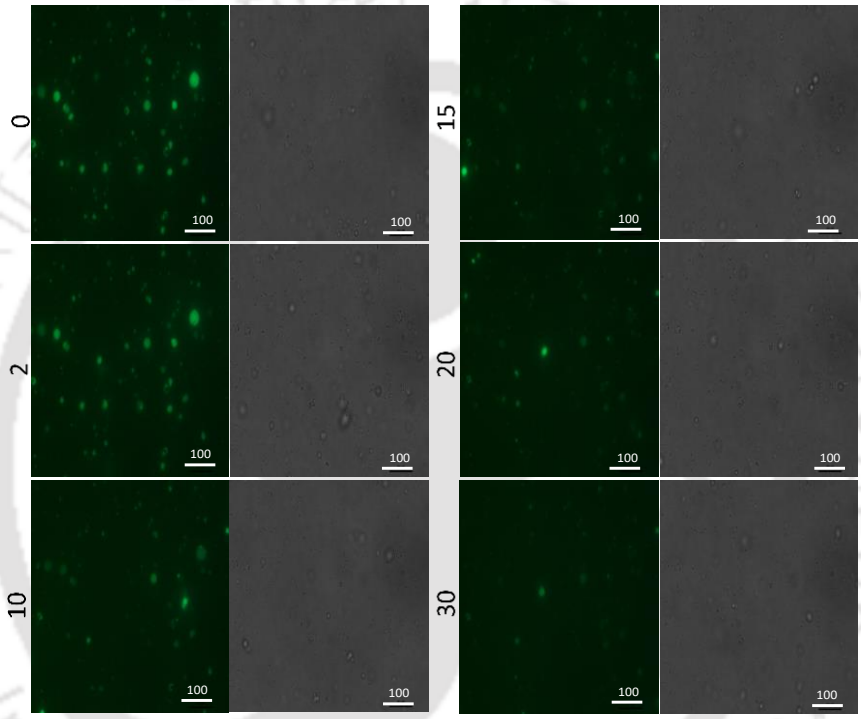

Figure S2.16. Fluorescence microscopic images of the HPTS encapsulated GUVs were generated using EYPC, cholesterol and DPPS lipids (with molar ratio of 6:3.5:0.5). Green channel (A) and bright field (B) images illustrates the images before and after the addition of 0.1 mM of **2.5** (**DM-PIT-1**) and 0.1 mM NaCl to the extravehicular region of the GUVs.

2.4.4.13.3. Fluorescence Microscope Imaging Assay

The vesicle solution (100 µL) mixed with **2.5** (**DM-PIT-1**) (0.25 mM) was taken on a hydrophobic coated glass-bottom dish. The GUVs were allowed to settle down for 30 min. Images were collected using an inverted fluorescence microscope (using Nikon ECLIPSE Ts2R fluorescence microscope). After that, 2 µL of NaCl solution (0.4 M) was added, which results in the quenching of HPTS fluorescence intensity within

a few seconds. At this stage, images were collected toensure the undamaged GUVs (i.e., quenching of HPTS fluorescence intensity was not due to the bursting of the GUVs during the experimental conditions). Hence, the decay of the HPTS fluorescence intensity was because of Cl^- influx and consequently OH^- efflux (as compound follow OH^-/Cl^- antiport mechanism for ion transport activity).

2.4.5. HPLC analysis of the compounds and stability test for the potent compounds

To check the purity and stability of the compounds, HPLC analyses using a reverse phase HPLC column were performed. The pH-dependent stability of **2.2** (**PIT-1**) and **2.5** (**DM-PIT-1**) was also checked using HPLC analysis by dissolving 50 µM of the respective compounds in 10 mM phosphate buffer at two pH (5.5 and 7.2) and the solution was incubated in 37 °C for a period of 48 h. Then the aliquot was injected (2 mL) in HPLC (UltiMate 3000) with Luna® 5 µm C18(2) 100 Å columns using a UV-Vis detector at 254 nm to monitor the stability of the compounds. Methanol/water gradient (95% methanol and 5% water) was used as the mobile phase at a flow rate of 10 mL/minute for 20 minutes run time. The HPLC traces proved that the compounds are stable in these two pH buffer solutions.

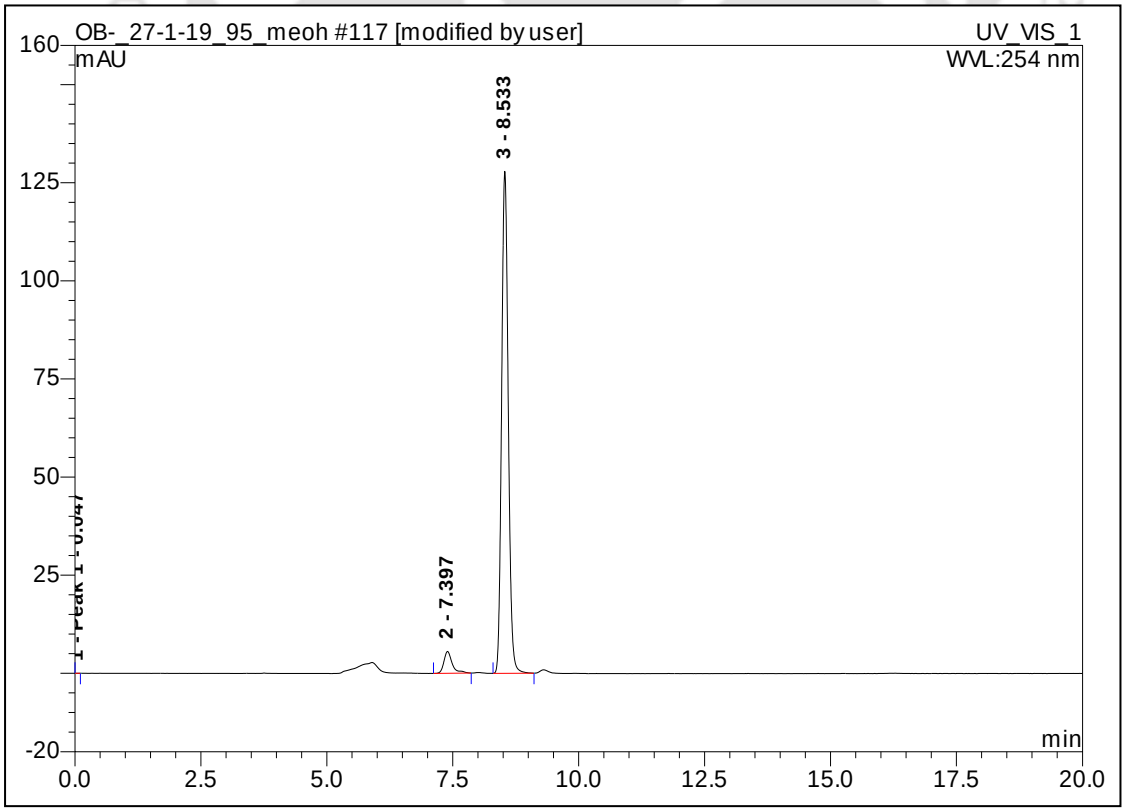

Figure S2.17. HPLC traces of compound **2.1** (pH 7.2).

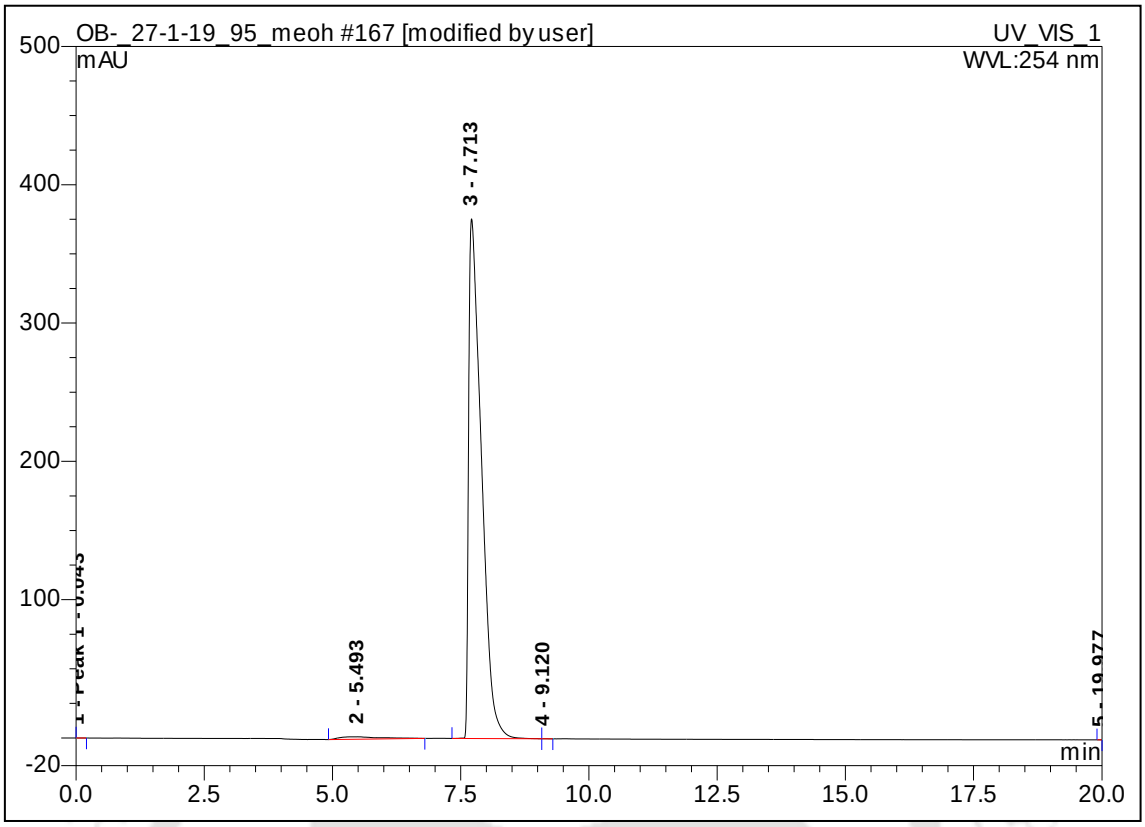

Figure S2.18. HPLC traces of compound **2.2 (PIT 1)** (pH 7.2).

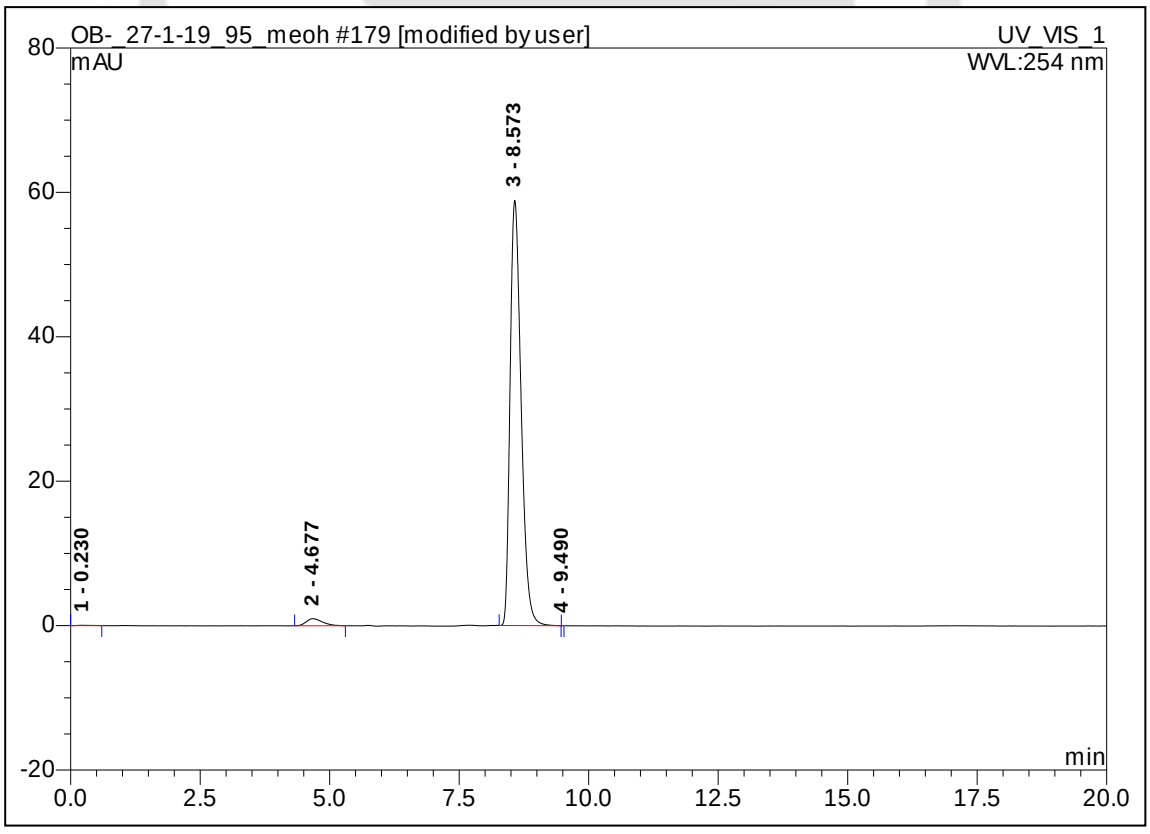

Figure S2.19. HPLC traces of compound **2.3** (pH 7.2).

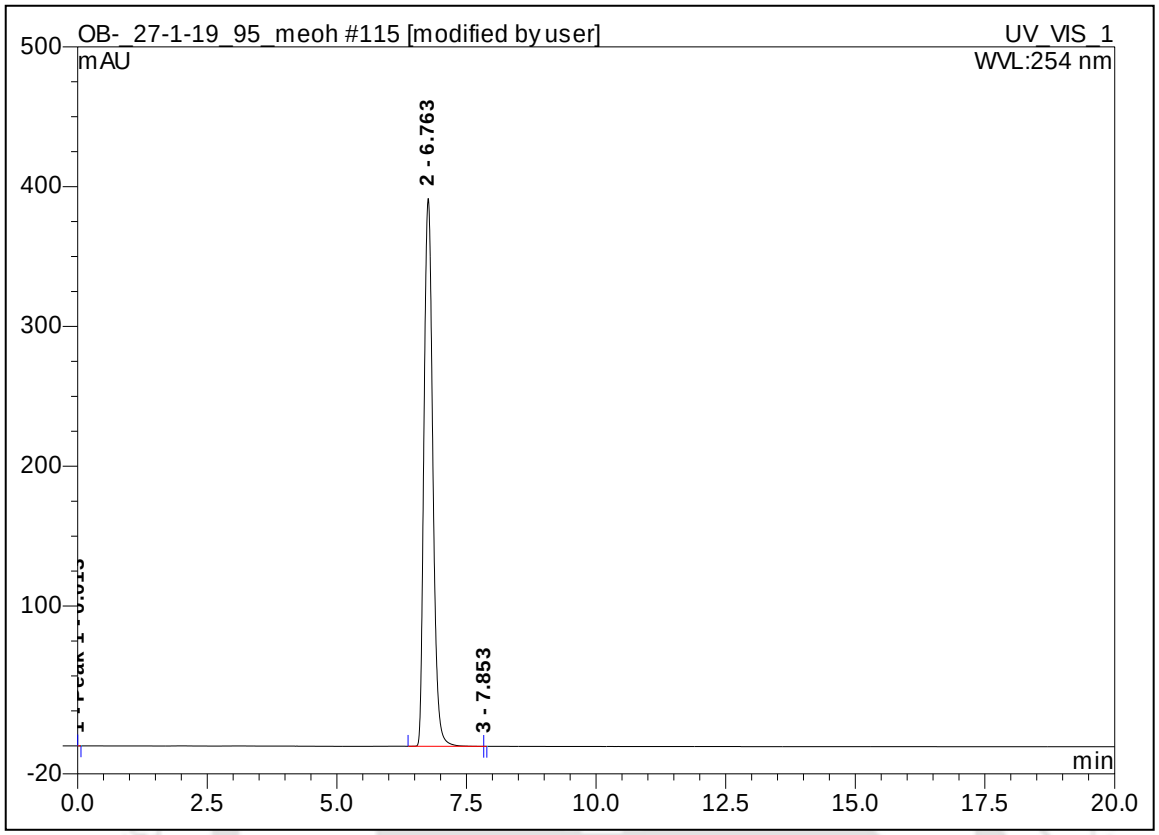

Figure S2.20. HPLC traces of compound **2.4** (pH 7.2).

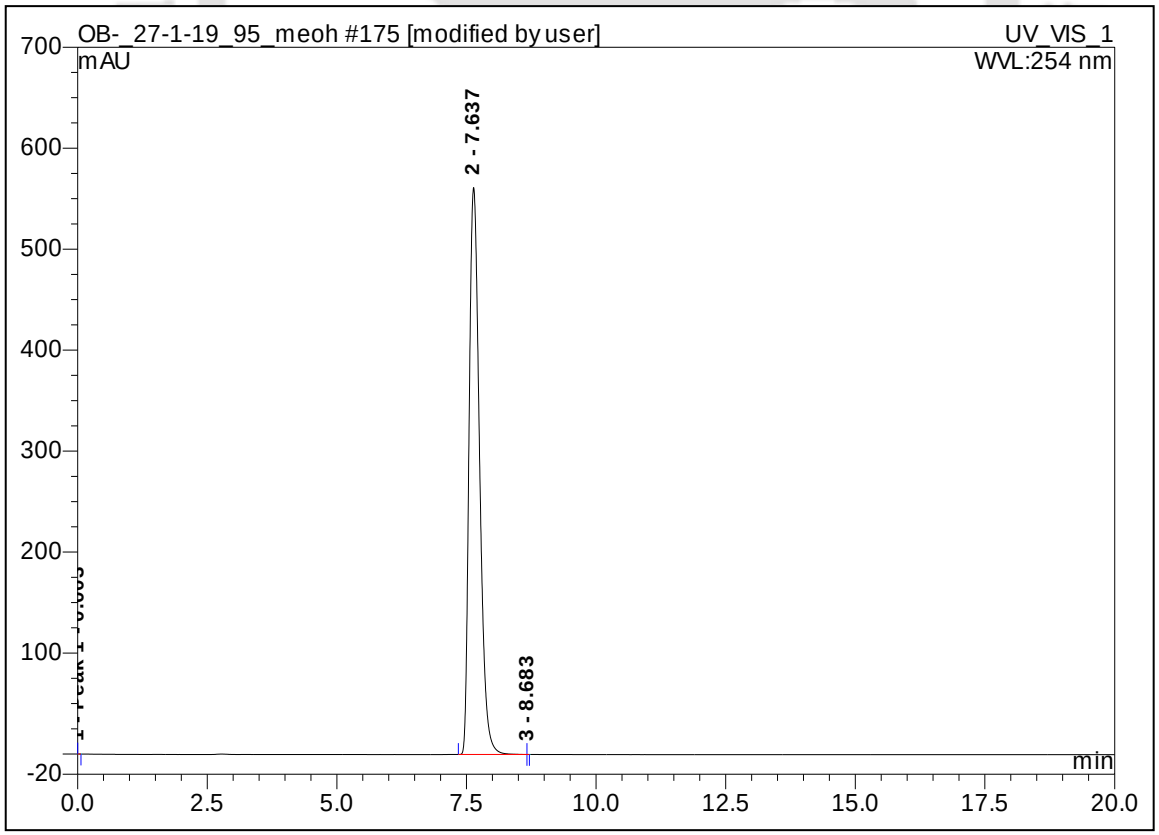

Figure S2.21. HPLC traces of compound **2.5 (DM-PIT-1)** (pH 7.2).

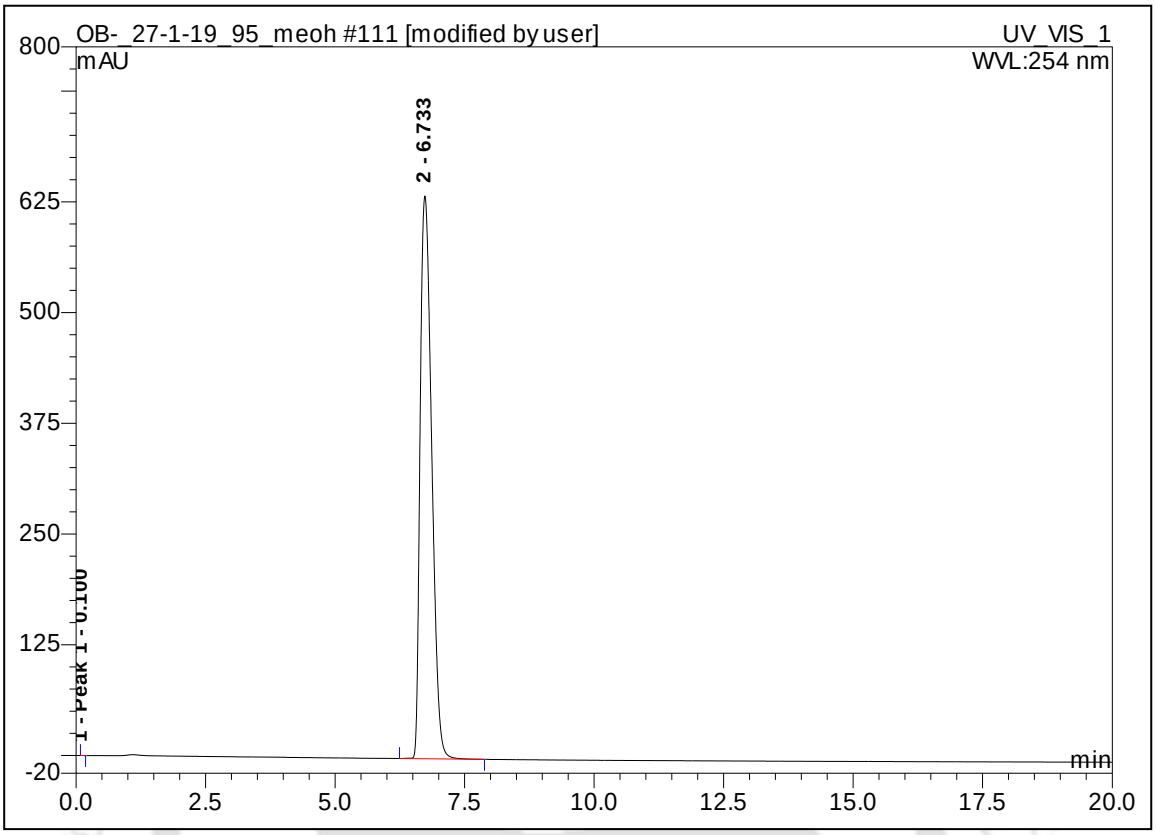

Figure S2.22. HPLC traces of compound **2.6** (pH 7.2).

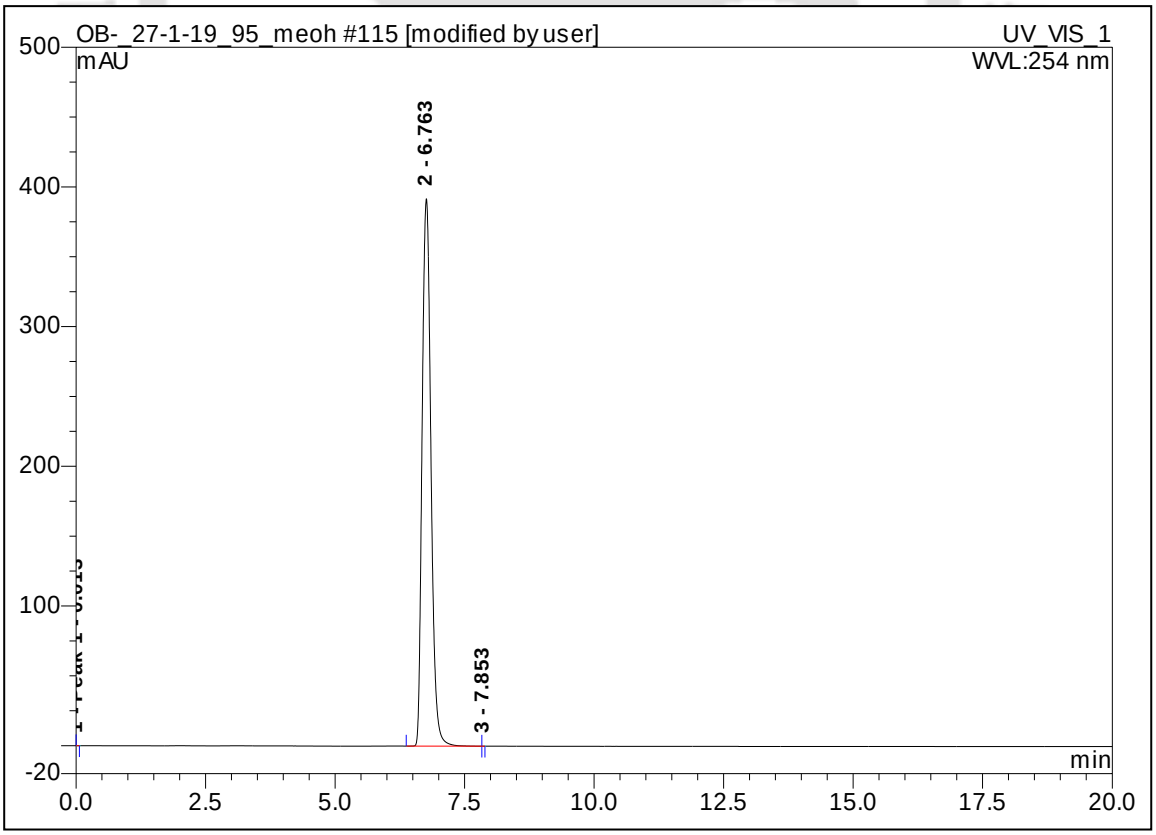

Figure S2.23. HPLC traces of compound **2.7** (pH 7.2).

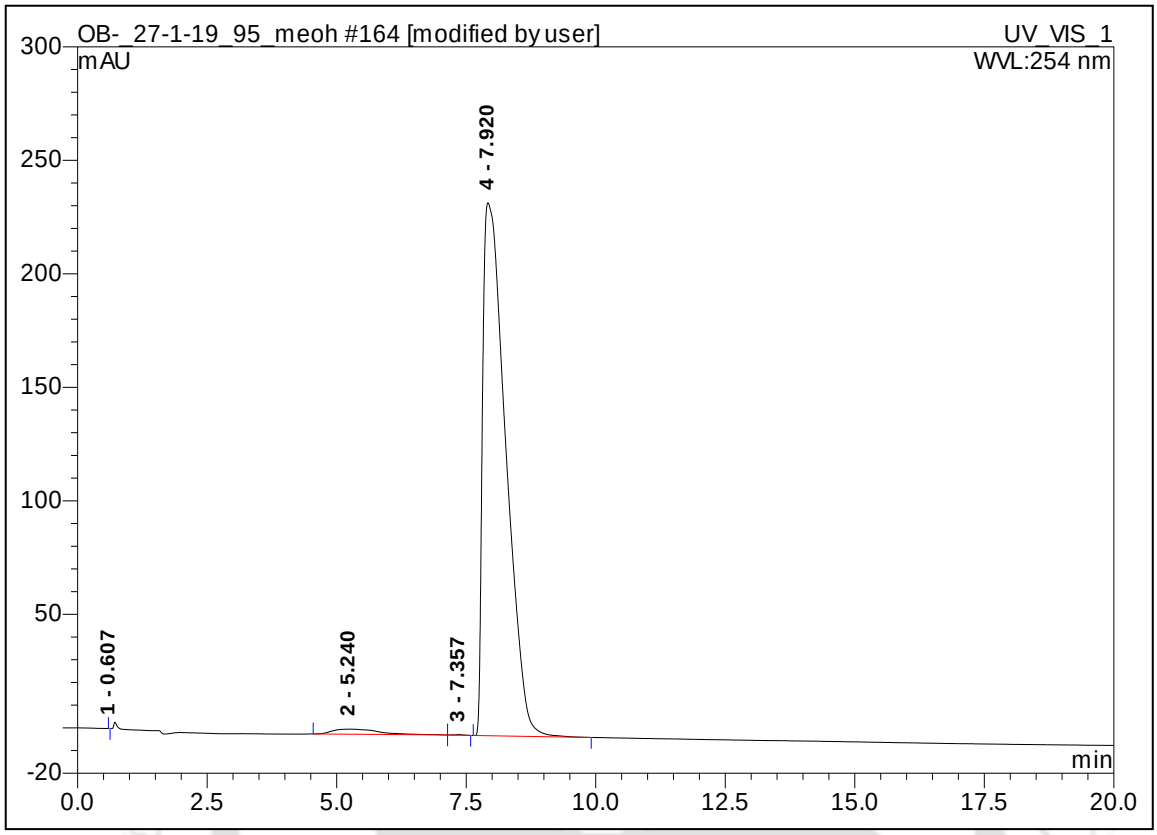

Figure S2.24. HPLC traces of compound **2.2 (PIT 1)** (pH 5.5).

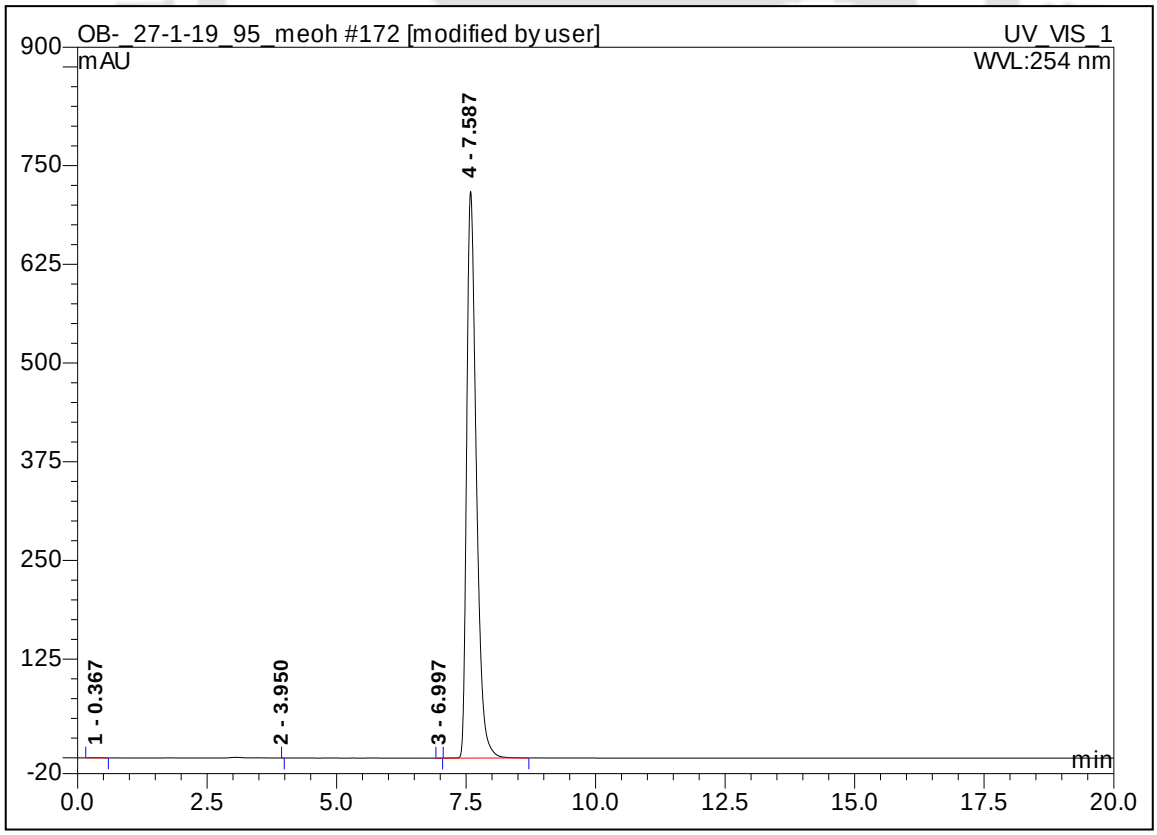

Figure S2.25. HPLC traces of compound **2.5 (DM-PIT-1)** (pH 5.5)

2.5. ^{1}H NMR and ^{13}C NMR of the compounds

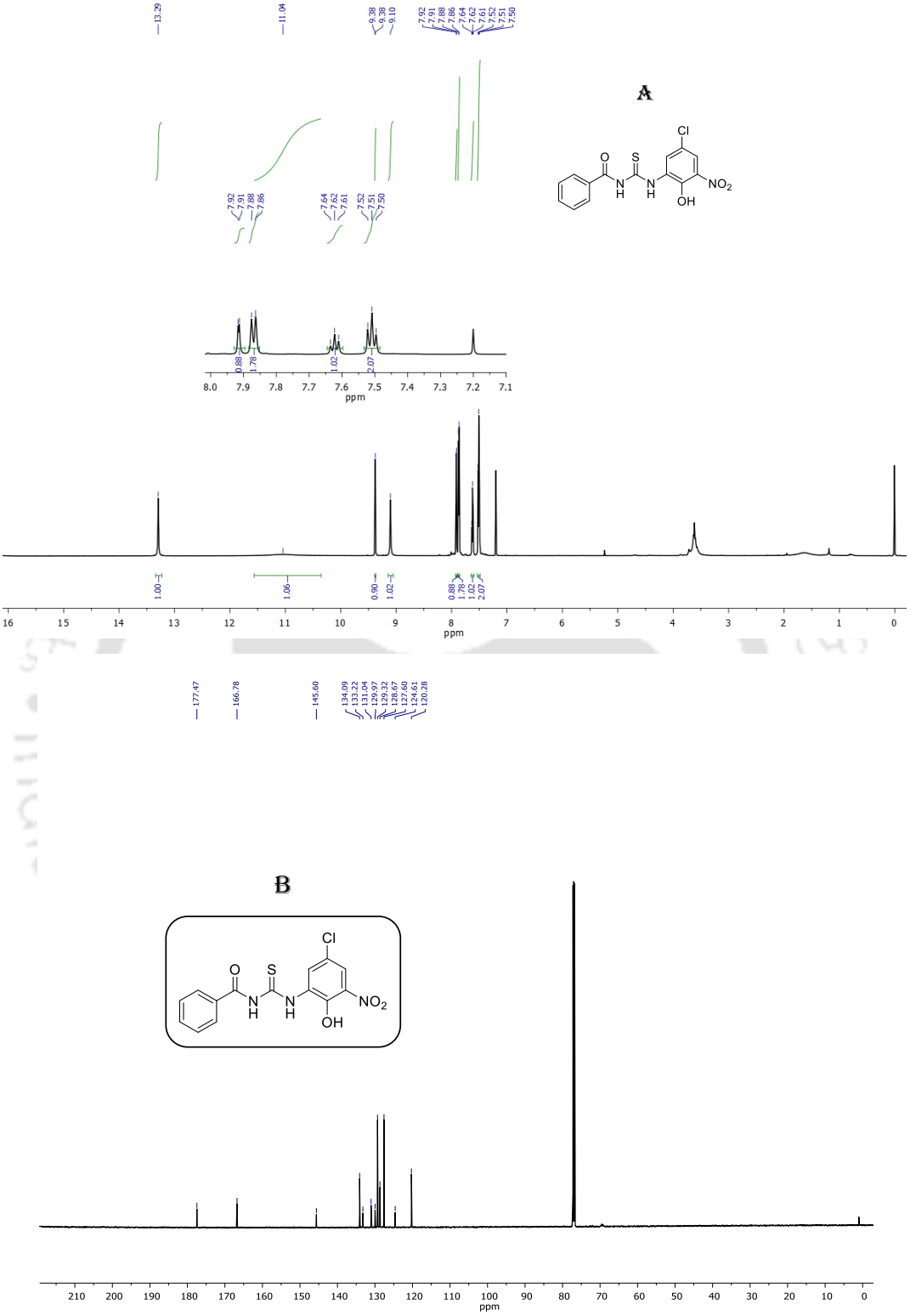

Figure S2.26. ^{1}H NMR (A) and ^{13}C{^{1}H} NMR (B) spectra of compound **2.1.**

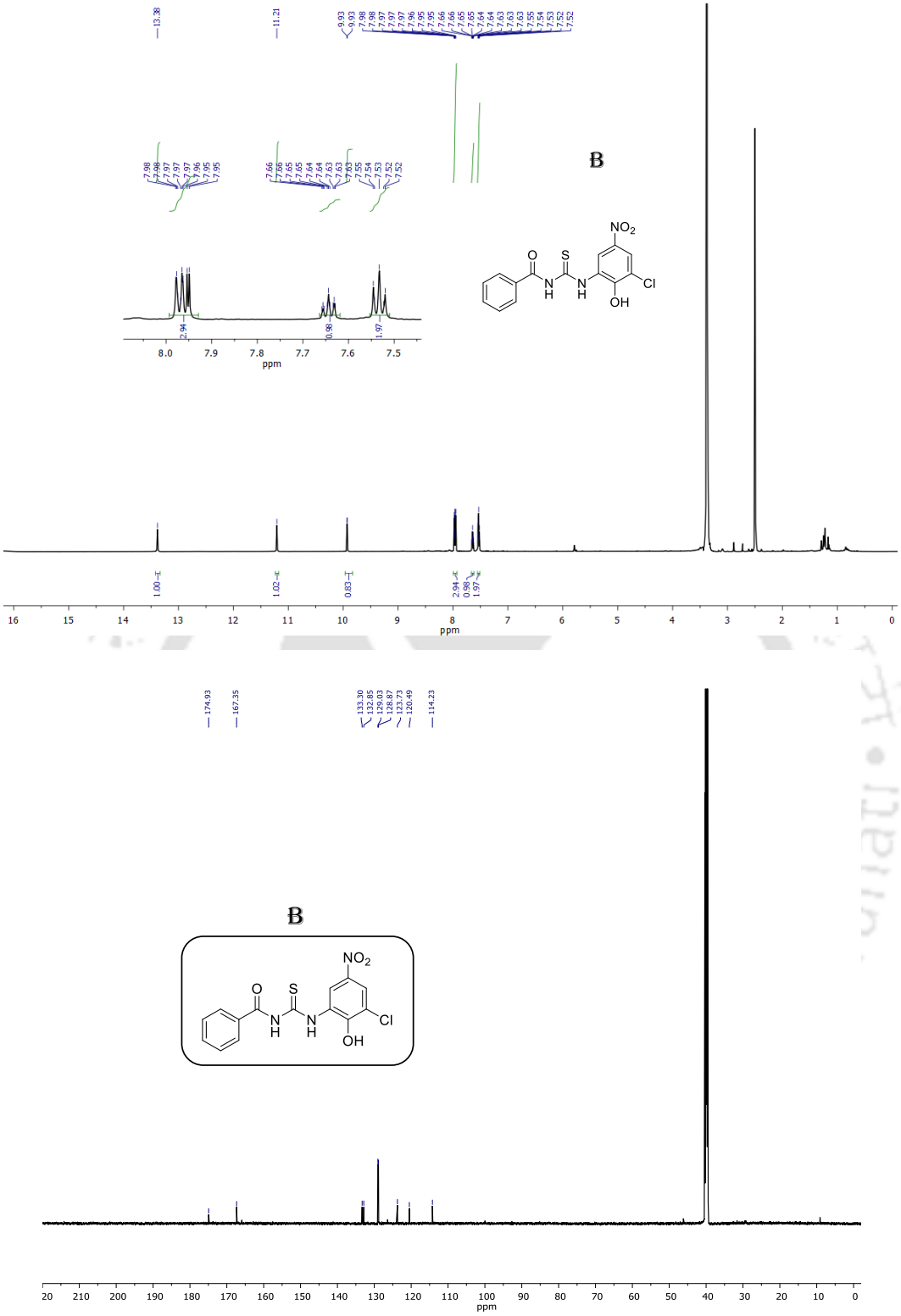

Figure S2.27. ^{1}H NMR (A) and ^{13} C{1H} NMR (B) spectra of compound **2.2.**

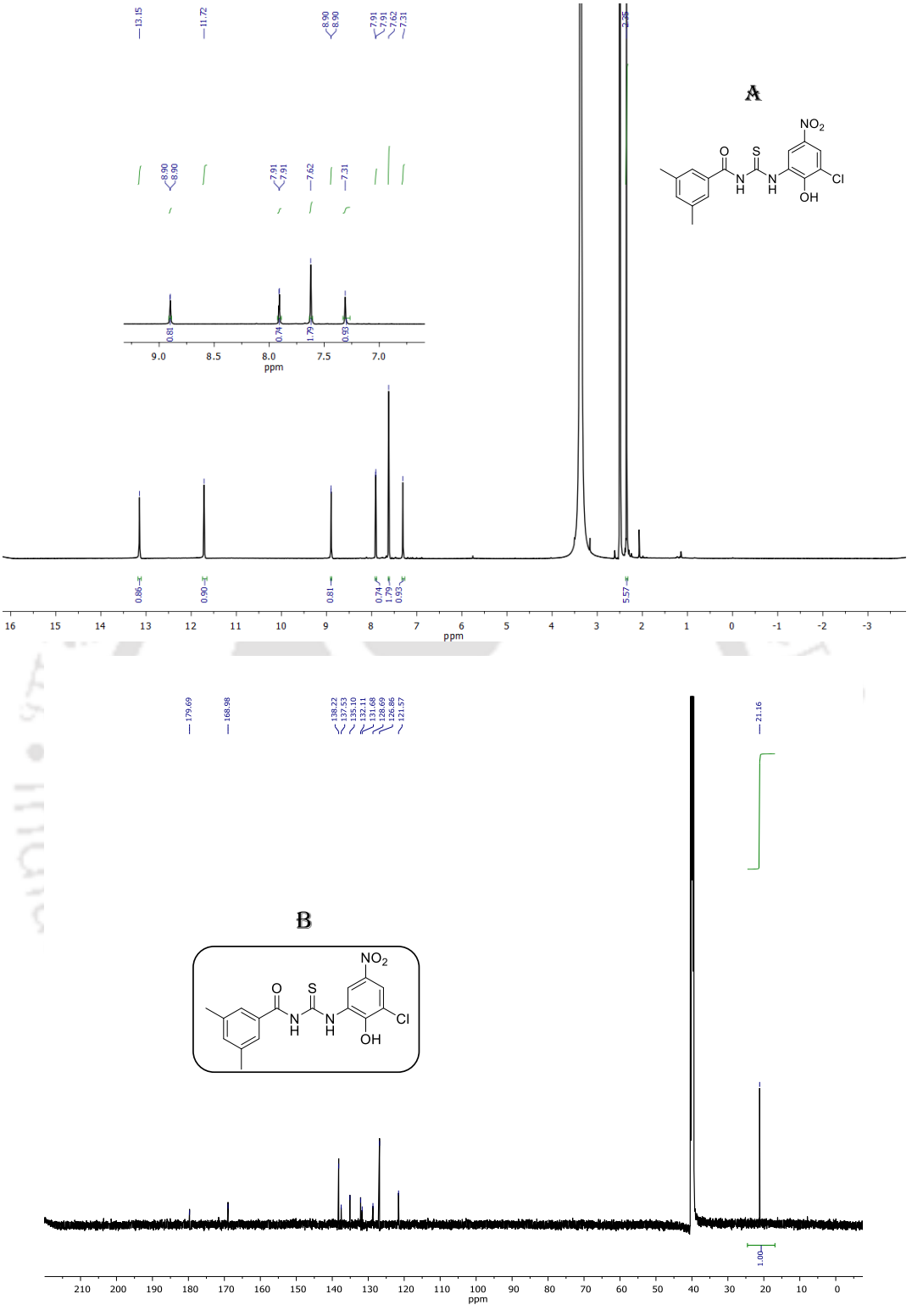

Figure S2.28. ^{1}H NMR (A) and $^{13}C\{1H\}$ NMR (B) spectra of compound **2.3.**

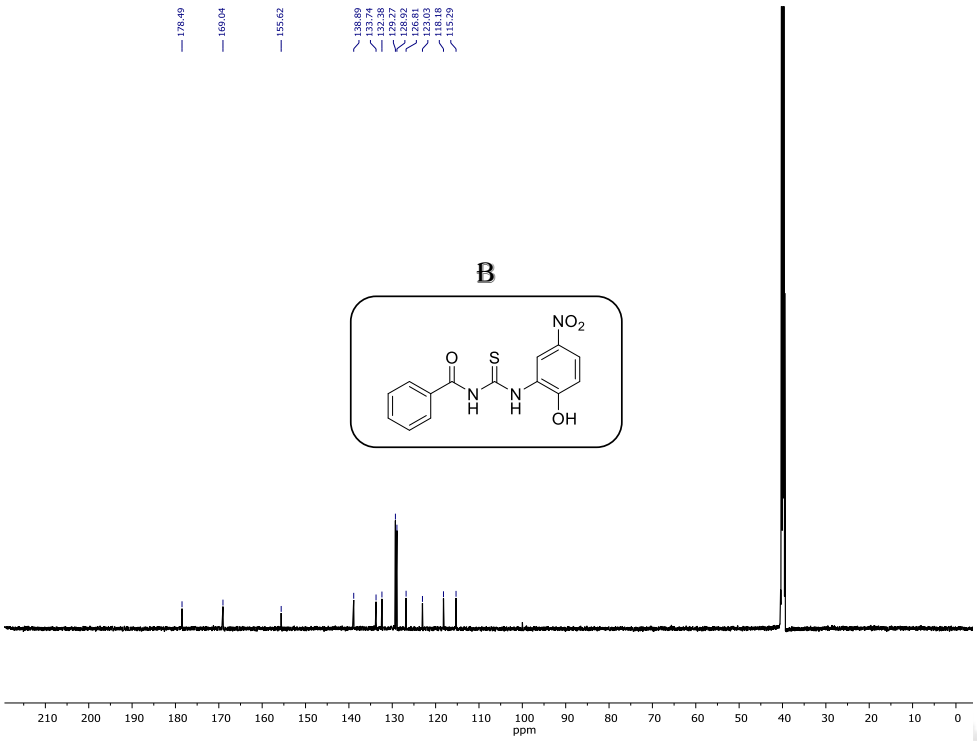

Figure S2.29. ^{1}H NMR (A) and $^{13}C\{1H\}$ NMR (B) spectra of compound **2.4.**

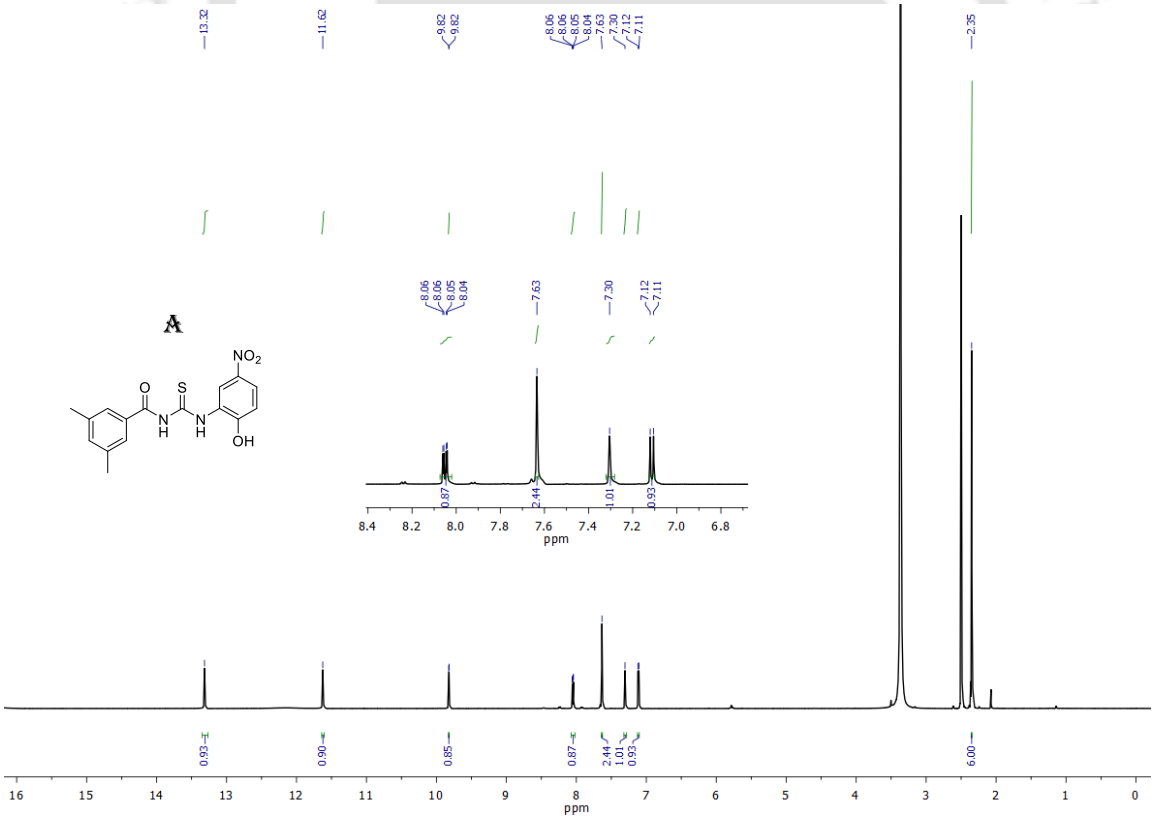

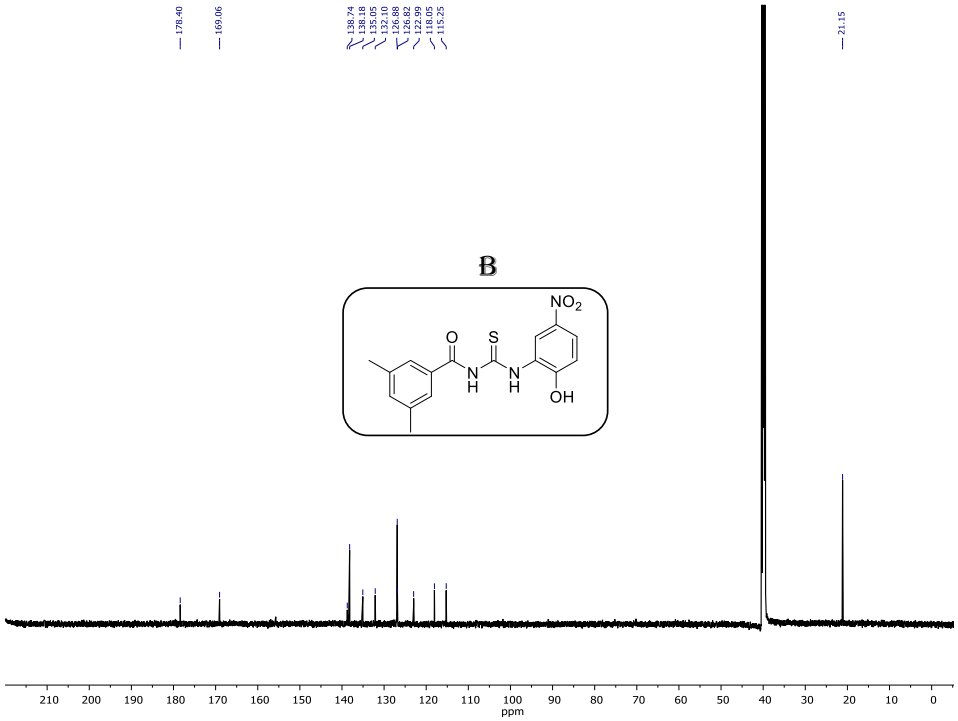

Figure S2.30. ^{1}H NMR (A) and $^{13}C\{1H\}$ NMR (B) spectra of compound **2.5.**

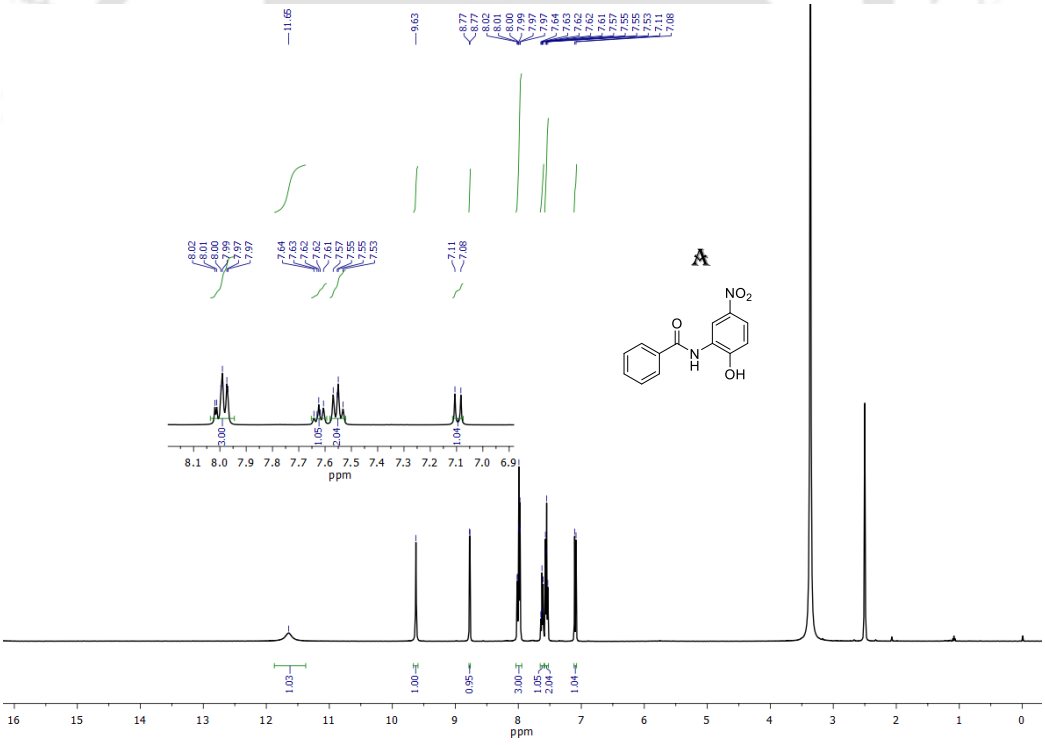

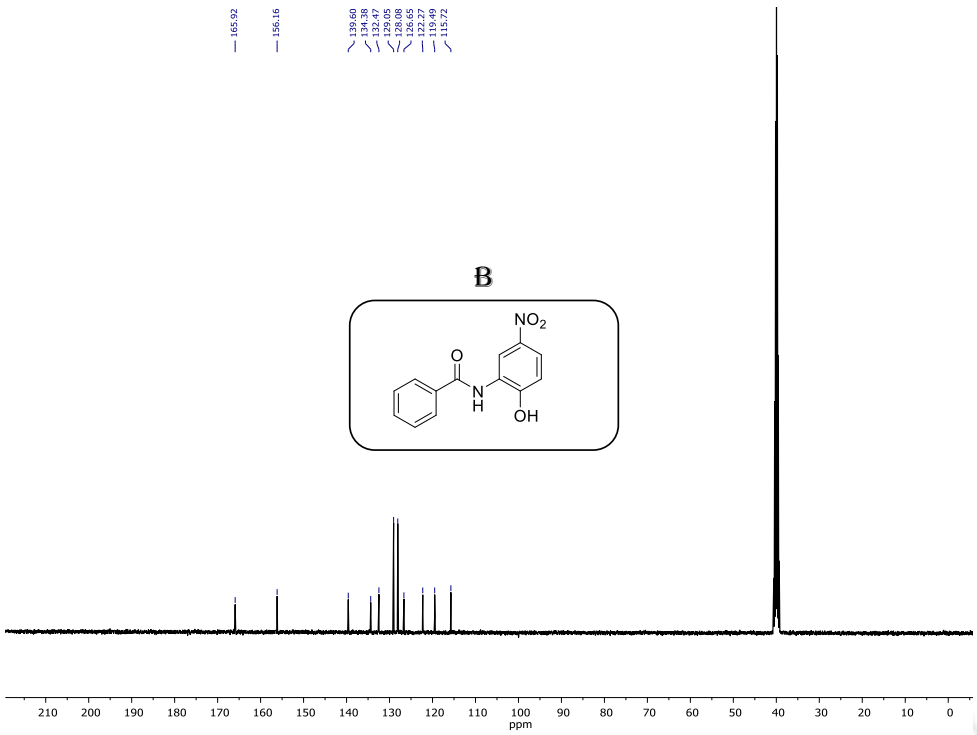

Figure S2.31. ^{1}H NMR (A) and ^{13} C{1H} NMR (B) spectra of compound **2.6.**

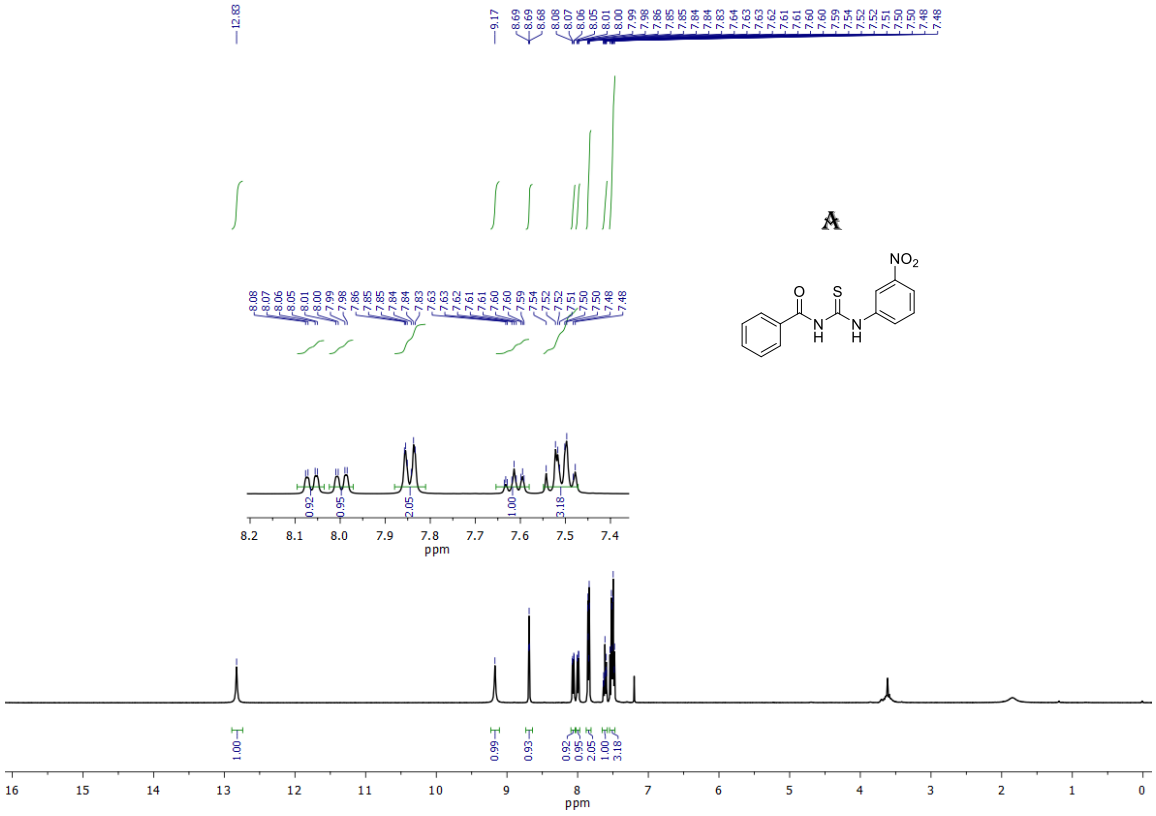

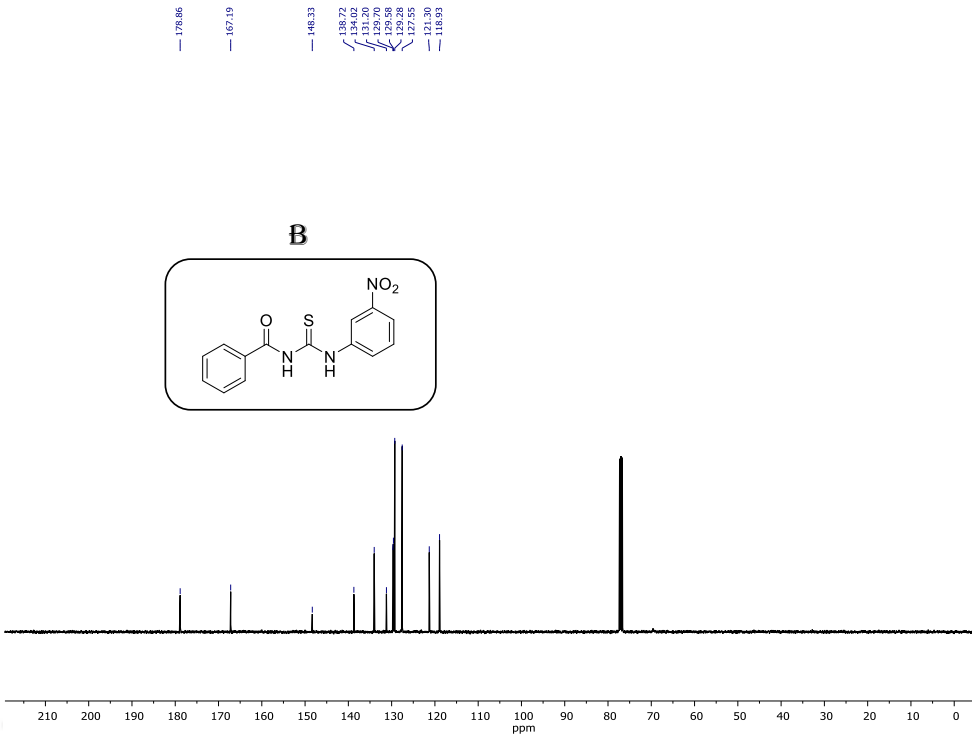

Figure S2.32. ^{1}H NMR (A) and ^{13} C{1H} NMR (B) spectra of compound **2.7.**

2.6. References

(1) Duran, C.; Thompson, C. H.; Xiao, Q.; Hartzell, C. J. A. r. o. p. Chloride channels: often enigmatic, rarely predictable. *Annu. Rev. Physiol.* **2010**, *72*, 95.

(2) Dworakowska, B.; Dołowy, K. J. A. B. P. Ion channels-related diseases. *Acta Biochim. Pol.* **2000**, *47* (3), 685-703.

(3) Akhtar, N.; Pradhan, N.; Saha, A.; Kumar, V.; Biswas, O.; Dey, S.; Shah, M.; Kumar, S.; Manna, D. J. C. C. Tuning the solubility of ionophores: glutathione-mediated transport of chloride ions across hydrophobic membranes. *Chem. Commun.* **2019**, *55* (58), 8482-8485.

(4) Gale, P. A.; Perez-Tomas, R.; Quesada, R. J. A. o. c. r. Anion transporters and biological systems. **2013**, *46* (12), 2801-2813.

(5) Saha, T.; Dasari, S.; Tewari, D.; Prathap, A.; Sureshan, K. M.; Bera, A. K.; Mukherjee, A.; Talukdar, P. J. J. o. t. A. C. S. Hopping-mediated anion transport through a mannitol-based rosette ion channel. *J. Am. Chem. Soc* **2014**, *136* (40), 14128-14135.

(6) Saha, T.; Hossain, M. S.; Saha, D.; Lahiri, M.; Talukdar, P. J. J. o. t. A. C. S. Chloride-mediated apoptosis-inducing activity of bis (sulfonamide) anionophores. *J. Am. Chem. Soc* **2016**, *138* (24), 7558-7567.

(7) Sessler, J. L.; Eller, L. R.; Cho, W. S.; Nicolaou, S.; Aguilar, A.; Lee, J. T.; Lynch, V. M.; Magda, D. J. J. A. C. I. E. Synthesis, anion-binding properties, and in vitro anticancer activity of prodigiosin analogues. **2005**, *44* (37), 5989-5992.

(8) Akhtar, N.; Saha, A.; Kumar, V.; Pradhan, N.; Panda, S.; Morla, S.; Kumar, S.; Manna, D. J. A. a. m.; interfaces. Diphenylethylenediamine-based potent anionophores: Transmembrane chloride ion transport and apoptosis inducing activities. *ACS Appl. Mater. Interfaces* **2018**, *10* (40), 33803-33813.

(9) Saha, A.; Akhtar, N.; Kumar, V.; Kumar, S.; Srivastava, H. K.; Kumar, S.; Manna, D. J. O.; Chemistry, B. pH-Regulated anion transport activities of bis (iminourea) derivatives across the cell and vesicle membrane. *Org. Biomol. Chem.* **2019**, *17* (23), 5779-5788.

(10) Saha, T.; Gautam, A.; Mukherjee, A.; Lahiri, M.; Talukdar, P. J. J. o. t. A. C. S. Chloride transport through supramolecular barrel-rosette ion channels: lipophilic control and apoptosis-inducing activity. *J. Am. Chem. Soc.* **2016**, *138* (50), 16443-16451.

(11) Busschaert, N.; Park, S.-H.; Baek, K.-H.; Choi, Y. P.; Park, J.; Howe, E. N.; Hiscock, J. R.; Karagiannidis, L. E.; Marques, I.; Félix, V. J. N. c. A synthetic ion transporter that disrupts autophagy and induces apoptosis by perturbing cellular chloride concentrations. *Nat. Chem.* **2017**, *9* (7), 667-675.

(12) Melvin, M. S.; Tomlinson, J. T.; Saluta, G. R.; Kucera, G. L.; Lindquist, N.; Manderville, R. A. J. J. o. t. A. C. S. Double-strand DNA cleavage by copper⊙ prodigiosin. *J. Am. Chem. Soc.* **2000**, *122* (26), 6333-6334.

(13) Haynes, C. J.; Busschaert, N.; Kirby, I. L.; Herniman, J.; Light, M. E.; Wells, N. J.; Marques, I.; Félix, V.; Gale, P. A. J. O.; chemistry, b. Acylthioureas as anion transporters: the effect of intramolecular hydrogen bonding. *Org. Biomol. Chem.* **2014**, *12* (1), 62-72.

(14) Solinas, A.; Faure, H. l. n.; Roudaut, H.; Traiffort, E.; Schoenfelder, A. l.; Mann, A.; Manetti, F.; Taddei, M.; Ruat, M. J. J. o. m. c. Acylthiourea, acylurea, and acylguanidine derivatives with potent hedgehog inhibiting activity. *J. Med. Chem.* **2012**, *55* (4), 1559-1571.

(15) Burgeson, J. R.; Moore, A. L.; Boutilier, J. K.; Cerruti, N. R.; Gharaibeh, D. N.; Lovejoy, C. E.; Amberg, S. M.; Hruby, D. E.; Tyavanagimatt, S. R.; Allen III, R. D. J. B.; et al. SAR analysis of a series of acylthiourea derivatives possessing broad-spectrum antiviral activity. *Bioorg. Med. Chem. Lett.* **2012**, *22* (13), 4263-4272.

(16) Wang, G.; Chen, X.; Deng, Y.; Li, Z.; Xu, X. J. J. o. a.; chemistry, f. Synthesis and nematicidal activities of 1, 2, 3-benzotriazin-4-one derivatives against Meloidogyne incognita. *J. Agric. Food Chem.* **2015**, *63* (31), 6883-6889.

(17) Miao, B.; Skidan, I.; Yang, J.; Lugovskoy, A.; Reibarkh, M.; Long, K.; Brazell, T.; Durugkar, K. A.; Maki, J.; Ramana, C. J. P. o. t. N. A. o. S. Small molecule inhibition of phosphatidylinositol-3, 4, 5-triphosphate (PIP3) binding to pleckstrin homology domains. *Proc. Natl. Acad. Sci. U.S.A.* **2010**, *107* (46), 20126-20131.

(18) Cantley, L. C. J. S. The phosphoinositide 3-kinase pathway. *Science* **2002**, *296* (5573), 1655-1657.

(19) Vivanco, I.; Sawyers, C. L. J. N. R. C. The phosphatidylinositol 3-kinase–AKT pathway in human cancer. *Nat. Rev. Cancer* **2002**, *2* (7), 489-501.

(20) Miao, B.; Skidan, I.; Yang, J.; You, Z.; Fu, X.; Famulok, M.; Schaffhausen, B.; Torchilin, V.; Yuan, J.; Degterev, A. J. O. Inhibition of cell migration by PITENINs: the role of ARF6. *Oncogene* **2012**, *31* (39), 4317-4332.

(21) Manna, D.; Albanese, A.; Park, W. S.; Cho, W. J. J. o. B. C. Mechanistic basis of differential cellular responses of phosphatidylinositol 3, 4-bisphosphate-and phosphatidylinositol 3, 4, 5-trisphosphate-binding pleckstrin homology domains. *J. Biol. Chem.* **2007**, *282* (44), 32093-32105.

(22) Yamamoto, E.; Kalli, A. C.; Yasuoka, K.; Sansom, M. S. J. S. Interactions of pleckstrin homology domains with membranes: adding back the bilayer via high-throughput molecular dynamics. *Structure* **2016**, *24* (8), 1421-1431.

(23) Lee, E.-B.; Ryu, H.; Lee, I.; Choi, S.; Hong, J.-H.; Kim, S. M.; Jeon, T.-J.; Cho, D.-G. J. C. C. Synthetic anion transporters that bear a terminal ethynyl group. *Chem. Commun.* **2015**, *51* (45), 9339-9342.

(24) Skidan, I.; Miao, B.; Thekkedath, R. V.; Dholakia, P.; Degterev, A.; Torchilin, V. J. D. d. In vitro cytotoxicity of novel pro-apoptotic agent DM-PIT-1 in PEG-PE-based micelles alone and in combination with TRAIL. *Drug Deliv.* **2009**, *16* (1), 45-51.

(25) Hibbert, D. B.; Thordarson, P. J. C. C. The death of the Job plot, transparency, open science and online tools, uncertainty estimation methods and other developments in supramolecular chemistry data analysis. *Chem. Commun.* **2016**, *52* (87), 12792-12805.

(26) Thordarson, P. J. C. S. R. Determining association constants from titration experiments in supramolecular chemistry. *Chem. Soc. Rev.* **2011**, *40* (3), 1305-1323.

(27) Howe, E. N.; Busschaert, N.; Wu, X.; Berry, S. N.; Ho, J.; Light, M. E.; Czech, D. D.; Klein, H. A.; Kitchen, J. A.; Gale, P. A. J. J. o. t. A. C. S. pH-regulated nonelectrogenic anion transport by phenylthiosemicarbazones. *J. Am. Chem. Soc.* **2016**, *138* (26), 8301-8308.

(28) Valkenier, H.; López Mora, N.; Kros, A.; Davis, A. P. J. A. C. I. E. Visualization and quantification of transmembrane ion transport into giant unilamellar vesicles. *Angew. Chem.* **2015**, *54* (7), 2137-2141.

(29) Wu, X.; Small, J. R.; Cataldo, A.; Withecombe, A. M.; Turner, P.; Gale, P. A. J. A. C. I. E. Voltage-switchable HCl transport enabled by lipid headgroup–transporter interactions. *Angew. Chem.* **2019**, *58* (42), 15142-15147.

(30) Busschaert, N.; Elmes, R. B.; Czech, D. D.; Wu, X.; Kirby, I. L.; Peck, E. M.; Hendzel, K. D.; Shaw, S. K.; Chan, B.; Smith, B. D. J. C. s. Thiosquaramides: pH switchable anion transporters. *Chem. Sci.* **2014**, *5* (9), 3617-3626.

(31) Jowett, L. A.; Howe, E. N.; Soto-Cerrato, V.; Van Rossom, W.; Pérez-Tomás, R.; Gale, P. A. J. S. r. Indole-based perenosins as highly potent HCl transporters and potential anti-cancer agents. *Sci. Rep.* **2017**, *7* (1), 1-11.

(32) Busschaert, N.; Wenzel, M.; Light, M. E.; Iglesias-Hernández, P.; Pérez-Tomás, R.; Gale, P. A. J. J. o. t. A. C. S. Structure–activity relationships in tripodal transmembrane anion transporters: the effect of fluorination. *J. Am. Chem. Soc.* **2011**, *133* (35), 14136-14148.

(33) Lisbjerg, M.; Valkenier, H.; Jessen, B. M.; Al-Kerdi, H.; Davis, A. P.; Pittelkow, M. J. J. o. t. A. C. S. Biotin [6] uril Esters: Chloride-Selective Transmembrane Anion Carriers Employing C□H··· Anion Interactions. *J. Am. Chem. Soc.* **2015**, *137* (15), 4948-4951.

(34) Gorai, S.; Paul, D.; Borah, R.; Haloi, N.; Santra, M. K.; Manna, D. J. C. Role of Cationic Groove and Hydrophobic Residues in Phosphatidylinositol-Dependent Membrane-Binding Properties of Tks5-Phox Homology Domain. *ChemistrySelect* **2018**, *3* (4), 1205-1214.

(35) Gorai, S.; Paul, D.; Haloi, N.; Borah, R.; Santra, M. K.; Manna, D. J. M. B. Mechanistic insights into the phosphatidylinositol binding properties of the pleckstrin homology domain of lamellipodin. *Mol. Biosyst.* **2016**, *12* (3), 747-757.

(36) Gorai, S.; Paul, S.; Sankaran, G.; Borah, R.; Santra, M. K.; Manna, D. J. M. Inhibition of phosphatidylinositol-3, 4, 5-trisphosphate binding to the AKT pleckstrin homology domain by 4-amino-1, 2, 5-oxadiazole derivatives. *MedChemComm* **2015**, *6* (10), 1798-1808.

(37) Naredla, R. R.; Klumpp, D. A. J. T. l. Benzamide synthesis by direct electrophilic aromatic substitution with cyanoguanidine. *Tetrahedron Lett.* **2012**, *53* (35), 4779-4781.

(38) Sun, N.; Li, B.; Shao, J.; Mo, W.; Hu, B.; Shen, Z.; Hu, X. J. B. j. o. o. c. A general and facile one-pot process of isothiocyanates from amines under aqueous conditions. *Beilstein J. Org. Chem.* **2012**, *8* (1), 61-70.

(39) Valkenier, H.; Dias, C. M.; Goff, K. L. P.; Jurček, O.; Puttreddy, R.; Rissanen, K.; Davis, A. P. J. C. c. Sterically geared tris-thioureas; transmembrane chloride transporters with unusual activity and accessibility. *Chem. Commun.* **2015**, *51* (75), 14235-14238.

Chapter 3

Photoinduced Generation of the Active Chloride/Phosphate Anionophore from its Inactive Proanionophore

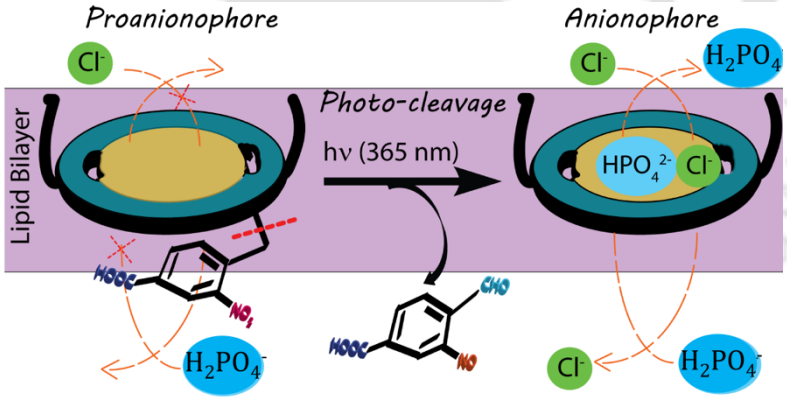

3.1. Background and objective of present work

Phosphate serves as an important unit in our body and is also involved with many important functions in the body. In the human body mainly sodium dependent NaP_i-I, NaP_i-II and NaP_i-III phosphate transporters are involved in maintaining the optimum concentration of P_i in the body with the help of P_i transport across the cells [1]. However due to stunted transport of P_i through the natural transporters, imbalance of P_i concentration occurs resulting in hypophosphatemia and hyperphosphatemia conditions. Tumor cells maintain a high concentration of phosphate ions inside and the concentration of Cl^- is higher outside the cancer cells. Hence designing synthetic ion transporter capable of mediating Cl^-/phosphate transport can disrupt the ionic gradient in tumor cells and also can initiate apoptosis. Using the 'ion therapy' unwanted cell cytotoxicity has been observed in the normal cells. Hence to increase the selectivity of the synthetic ion transporters towards the normal cells w.r.t the stimuli triggered ion transporters have been used by researchers. The stimuli concerned can be either naturally present like enzymes, GSH, pH or can be externally applied like thermal energy, mechanical pressure, light, etc. Among the various stimuli, employment of light is very beneficial as precise site selectivity and optical control can be achieved [2]. Hence deliberately putting a photocleavable appendage in the synthetic transporter which will cleave only in the presence of light stimulus in the cancer cells would be very advantageous.

In this regard C2 symmentric class of guanidium-based macrocyclic synthetic anionophores were developed in the current work. The presence of guadinium moiety ensures higher selectivity towards phosphate ion and the needed H-bond for stabilising the ions. To impart correct lipophilicity the macrocycles were endowed with alkyl chains of varying chain length (n=4, 8, 10). Thorough experiments were done to check the selectivity of the synthetic anionophores and the mechanism of ion transport across the vesicles. The studies revealed the successful mediation of Cl^- and phosphate across the vesicles.

To further investigate the effect of having a photocleavable group connected to the anionophore, *o*-nitrobenzyl (ONB) group was attached to the most potent anionophore. The ONB group has been utilised in various other applications as a photocleavable scaffold however its use in ion transport field has been very limited

[3, 4]. The phenomenon of photoinduced generation of the active synthetic transporter were observed fluorometrically and in *in-vitro* condition in the HeLa cell lines.

3.2. Results and discussions

3.2.1. Design and synthesis of the guanidine macrocycles

The guanidium macrocycles were easily synthesised in two steps (Scheme 3.1). Initially the thiourea containing macrocycle was constructed and then the thiourea group was converted to the guanidium groups with the help of desulfurization reaction in presence of alkyl amines of varying chain lengths (n = 4, 8, and 10) [5, 6]. The logp values of the resulting guanidium macrocycles were calculated using Marvin ketch program and they range within 6.0-12.4 values which ensures their membrane locating propensity.

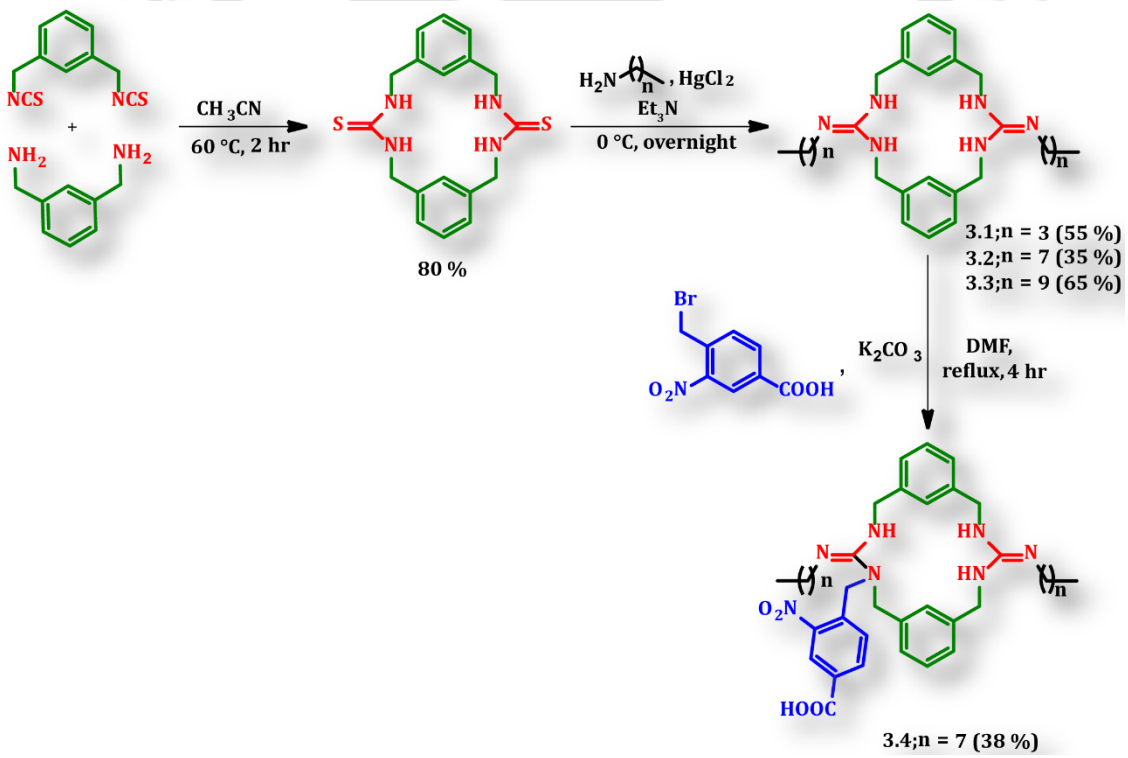

Scheme 3.1. Synthetic routes to the modular anion transporters.

3.2.2. Anion binding studies of the guanidine-based macrocycle

With the help of UV-based titration studies of **3.2** with phosphate, Cl^- and NO_3^-, it was found that the transporter **3.2** was able to bind phosphate and Cl^- ion

successfully but the binding with NO_3^- was weak enough to be calculated (unsubstantial spectral change) (Table 3.1). Better binding with Cl^- and phosphate ion could be due to the presence of the cyclic guanidium moieties (Fig. S3.1-S3.3).

3.2.3. Ion transport activities of the guanidine-based macrocyclic derivatives

Next the ion transport properties of the guanidium macrocycles were investigated using EYPC/CHOL-LUV⊃lucigenin. The fluorescence intensity of bis-*N*-methylacridinium nitrate (lucigenin) is sensitive w.r.t the concentration of biologically important ions like Cl^- and phosphate [7,8] (Fig. S3.4). Here LUVs were used as model membranes to investigate the ion transport properties of the guanidium-based macrocycles. EYPC (egg-yolk phosphatidylcholine) and CHOL (cholesterol) were used in 8:2 molar ratio to prepare the liposomes. Initially LUVs were prepared entrapping 20 mM HEPES buffer containing 225 mM $NaNO_3$ and 1 mM lucigenin, pH 7.2. and the liposomes were dispersed in 20 mM HEPES buffer containing isotonic NaCl or NaH_2PO_4, pH 7.2. However, on addition of the transporter no significant changes in the lucigenin fluorescence intensity was seen in any of the cases which indicates inability of the transporter to transfer NO_3^- across the vesicles. These results are in conformity with the UV-titration results where transporter **3.2** showed inconsequential binding with NO_3^-. Next the inside buffer was changed to 20 mM HEPES buffer containing 225 mM NaCl and 1 mM lucigenin, pH 7.2 and the LUVs were dispersed in a 20 mM HEPES buffer containing isotonic NaH_2PO_4, pH 7.2. This time for anionophore **3.2** significant increase in lucigenin fluorescence intensity was seen. When buffers were reversed, i.e., the LUVs were prepared using 20 mM HEPES buffer containing 225 mM NaH_2PO_4, pH 7.2 and they were dispersed in 20 mM HEPES buffer containing isotonic NaCl, pH 7.2, the lucigenin fluorescence increases, signifying anionophore **3.2** mediated Cl^-/phosphate transport from the results. Hence, the latter assay was used to check the transport activities of all anionophores (Fig. 3.1).

The ion transport activity of all the transporters (**3.1**-**3.4**) were checked using the lucigenin-based fluorescence experiment by suspending the vesicles in 20 mM HEPES buffer containing 225 mM NaCl, pH 7.2. Compound pulse was added at t = 50 s to initiate the kinetics of the fluorescent experiment. Among the four anionophores being tested, anionophore **3.2** was found to be the most proficient one showing

highest transport efficiency. This can be due to its optimum lipophilicity. Transporter **3.4** shows very low phosphate-mediated Cl^- ion transport ability which could be justified due to the strong binding of the phosphate ion with the nitro group present in the photocleavable part of transporter **3.4**. Due to the strong binding, release of the ion on the other side of the vesicles becomes very difficult. Accordingly, transporter **3.4** was chosen for selectivity and mechanism investigation using the fluorescent-based assays.

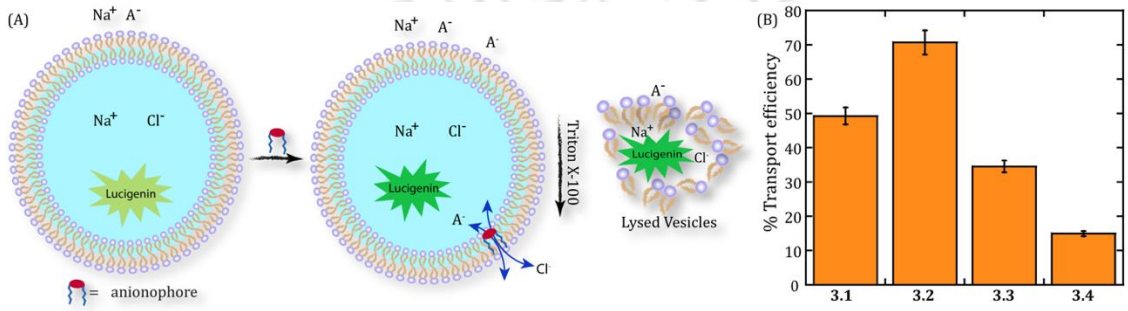

Figure 3.1. Schematic representation of lucigenin assay (A). The anion transport properties of the compounds (7 μM or 18.48 mol% with respect to lipids) across the EYPC/CHOL-LUVs⊃lucigenin (prepared in 20 mM HEPES buffer containing 225 mM NaCl, pH 7.2) suspended in 20 mM HEPES buffer containing 225 mM NaH_2PO_4, pH 7.2. At t = 50 s, the kinetics was started by adding a pulse of compounds (B)

3.2.4. Mechanism of chloride ion transport activities of the guanidine-based macrocyclic derivatives

For checking the anion selectivity, the LUVs entrapping lucigenin were suspended in 20 mM HEPES buffer containing 225 Na_xA_y, pH 7.2 (where Na_xA_y = NaH_2PO_4, Na_2SO_4, $NaClO_4$, NaOAc, and $NaNO_3$). In this experiment, the kinetics was initiated at t = 50 s with the addition of the anionophore after which gradual increment in the fluorescence intensity was observed. Higher fluorescent intensity increment in presence of phosphate ions, establishing higher selectivity for the ion (Fig. 3.2A). With the help of the dose-dependent lucigenin-based fluorescent experiment, the phosphate mediated Cl^- transport of the anionophores (**3.1**-**3.3**) were determined and the half-maximal transport efficiency was determined for the transporters (Table 3.2, Fig. S3.5-S3.7). Besides to further confirm the phosphate mediated Cl^- transport, Cl^- efflux was monitored through ion selective electrode (ISE)

(Fig. 3.2C). Different concentrations of anionophore **3.2** were added at t = 50 s and the Cl^- efflux was found to increase with increase in concentration of the anionophore clearly depicting phosphate mediated Cl^- transport across the lipid bilayers.

By varying the cations (Li^+, Na^+, K^+, Rb^+ and Cs^+), no significant change was observed in the Cl^- transport efficiency in each case, indicating that the cations (M^+) are not involved in the mechanistic pathway (Fig. 3.2B). To know whether the phosphate mediated Cl^- transport by anionophore **3.2** is through carrier pathway or the anionophore forms channels, the Cl^- transport efficiency at 25 °C and 45 °C were checked using DPPC LUVs. The transition temperature (T_m) of DPPC is around 41 °C, hence at a temperature higher than the transition temperature the viscosity of the liposomes will decrease which will escalate the ion transport efficiency of carrier like transporters. However, for the channel forming transporters increasing the temperature won't create any difference in the transport efficiency. In this case a significant boost in the phosphate-mediated Cl^- transport efficiency of transporter **3.2** was observed hinting at the carrier mediated pathway followed by it (Fig. 3.3B).

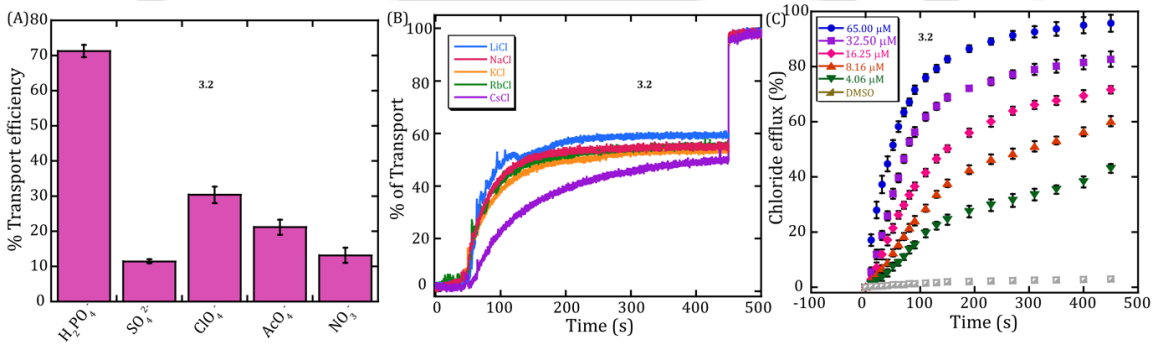

Figure 3.2. Anion (A) and Cation selectivity (B) of transporter **3.2** across the EYPC/CHOL-LUVs⊃lucigenin. Ion selective electrode-based chloride efflux studies using transporter **3.2** (C).

The other probable mechanisms of transport include involvement of H^+ or OH^-. To check their involvement, the FCCP experiment was done. Phosphate mediated Cl^- transport efficiency of anionophore **3.2** was checked once in presence and absence of anionophore **3.2**. Significant difference in the transport efficiency was found in both the cases suggesting H^+ is not involved in the mechanistic process. Hence the

only conceivable mechanistic possibility is Cl^-/phosphate antiport (Fig. 3.3A). To check this likelihood, a set of U-Tube experiment was done in which 225 mM NaH_2PO_4 solution was taken in the source end and in the receiver end 225 mM NaCl was taken. In the middle in the organic phase, transporter **3.2** was kept to mimic the bilayer entrapped with the transporter **3.2**. With progress in time, it was found that the concentration of NaH_2PO_4 and NaCl increased on the opposite side of the U-tube (Fig. 3.3D, S3.8). The increase in Cl^- concentration in the source tube-

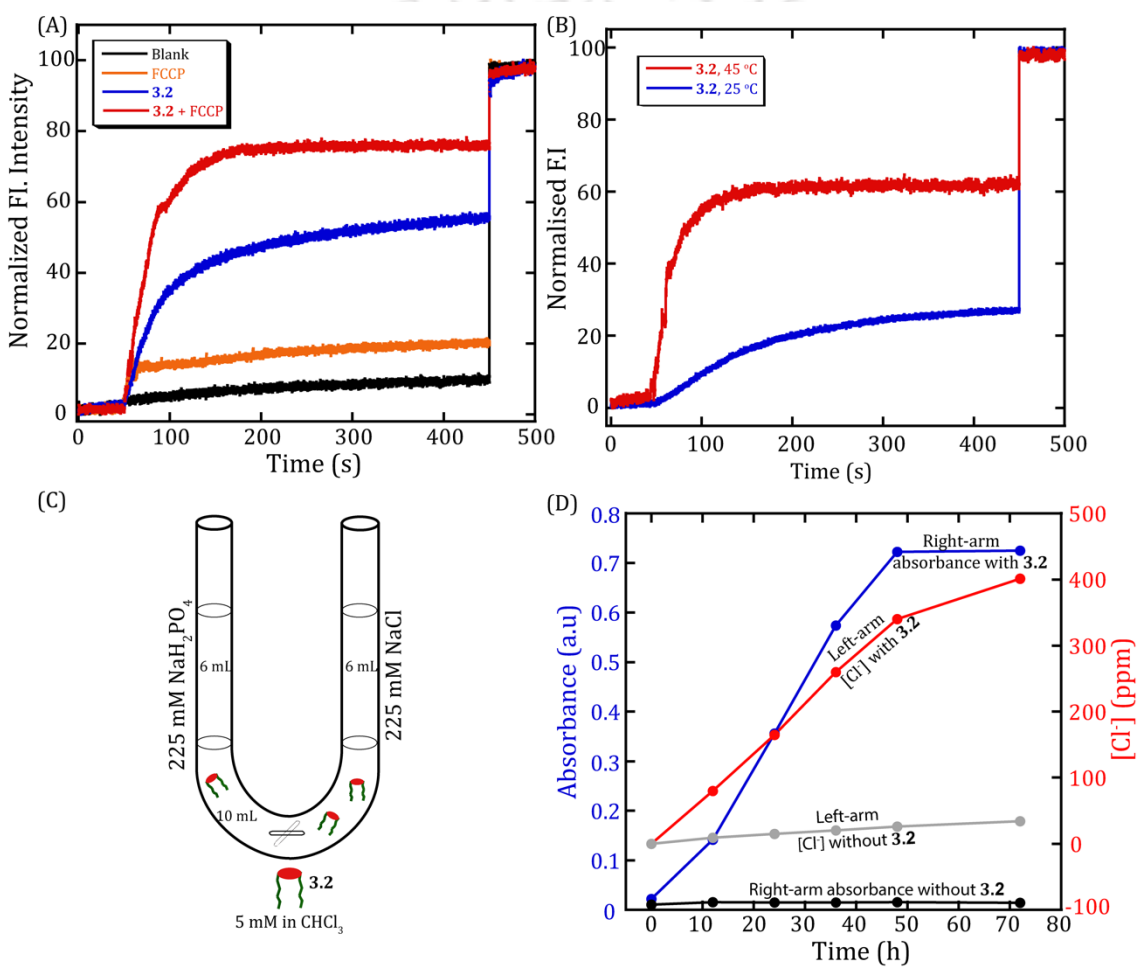

Figure 3.3. Assessment of Cl^- ion transport of **3.2** (1.75 μM) in presence and absence of FCCP (1.5 μM) (A). Temperature-dependent DPPC assay using transporter **3.2** across the DPPC⊃lucigenin (B). Schematic representation of the U-Tube experiment (C). Change of concentration of $H_2PO_4^-$ and Cl^- ions with time both in the presence and absence of compound **3.2** (5 mM) using spectrophotometer and ISE, respectively (D).

was monitored through ISE and the concentration of NaH_2PO_4 in the receiver end was monitored with the help of a spectrophotometric and colorimetric method. A continuous increment in the blue color of the ammonium phosphomolybdate due to addition of solution from the receiver end clearly depicted increase in phosphate concentration in the receiver end of the U-Tube mediated by transporter **3.2**. This experiment really exhibited phosphate mediated Cl^- transport ability of anionophore **3.2**. The transport moderated by anionophore **3.2** in the U-Tube experiment also proves that the anionophore follows carrier mediated pathway. To more evidently show phosphate ion transport, LUVs were prepared using a fluorescent phosphate chemosensor, a Tb(III)-complex. Due to phosphate ion influx selectively, the fluorescence of the H_3Tb complex (initially high) decreases on addition of anionophore **3.2** to initiate the kinetics (Fig. S3.9). This result corroborates the phosphate transport ability of the transporter **3.2** across the vesicles.

3.2.5. Chloride-mediated phosphate transport by the guanidine macrocyclic anionophore across GUVs

Next the transport behaviour of the anionophore **3.2** were also scrutinized with the help of the experiment involving GUVs. In the first set of experiments the GUVs were prepared in 100 mM HEPES buffer containing 200 mM sucrose, 225 mM NaH_2PO_4, and 1 mM lucigenin, pH 7.2 and they were dispersed in 100 mM HEPES buffer containing 200 mM glucose containing 225 mM NaH_2PO_4, pH 7.2. The transporter **3.2** (final concentration 45 μM) was added in the microscope chamber to the solution of the GUVs and instantly it was observed that the lucigenin fluorescence intensity of the GUVs as observed under the microscope, quenches. The reverse concentration gradient was employed to see the fluorescent intensity behaviour in the microscope and immediately after addition of the transporter **3.2** (45 μM) and NaH_2PO_4, it was found the quenched lucigenin fluorescence intensity increased. Hence with the help of GUV imaging experiment, the influx of $H_2PO_4^-$ and Cl^- respectively can be concluded (Fig. 3.4).

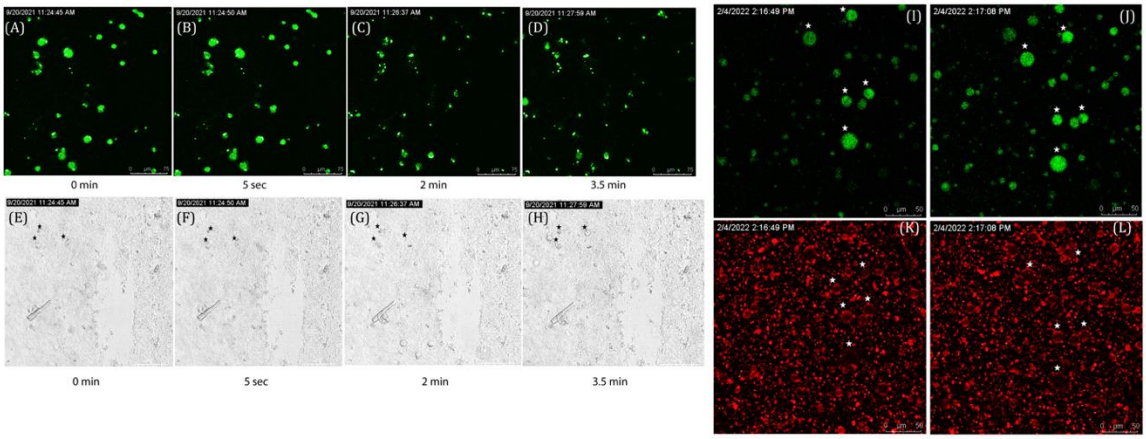

Figure 3.4. Fluorescence microscopic images of the lucigenin-encapsulated GUVs were recorded at different time intervals after the addition of compound **3.2** (45 μM). GUVs were prepared in 100 mM HEPES buffer containing 200 mM glucose, 225 mM NaH_2PO_4, and 1 mM lucigenin and dispersed in 100 mM HEPES buffer containing 200 mM sucrose and 225 mM NaCl. The change in the integrity of the GUVs and encapsulated lucigenin fluorescence intensity were monitored using bright-field and green channels, respectively (A-H). Confocal fluorescence microscopic images of the lucigenin and Texas Red and compound **3.2** (45 μM) -encapsulated GUVs after the addition of compound **3.2** (45 μM). GUVs were prepared in 100 mM HEPES buffer containing 200 mM glucose, 225 mM NaCl, and 1 mM lucigenin and dispersed in 100 mM HEPES buffer containing 200 mM sucrose and 225 NaH_2PO_4. The change in the integrity of the GUVs and encapsulated lucigenin fluorescence intensity were monitored using red-field and green channels, respectively.

3.2.6. Cl^-/NaH_2PO_4 antiport transportation of guanidine-based macrocyclic compound across the vesicles using ^{31}P NMR experiment

To invariably prove phosphate mediated Cl^- transport, ^{31}P NMR was used to monitor the phosphate efflux. On addition of anionophore **3.2**, due to phosphate efflux and its interaction with the paramagnetic Mn^{+2}, the ^{31}P peak in the NMR decreases. After complete lysis with Triton X-100, the ^{31}P peak entirely vanishes (Fig. 3.5 & S3.10).

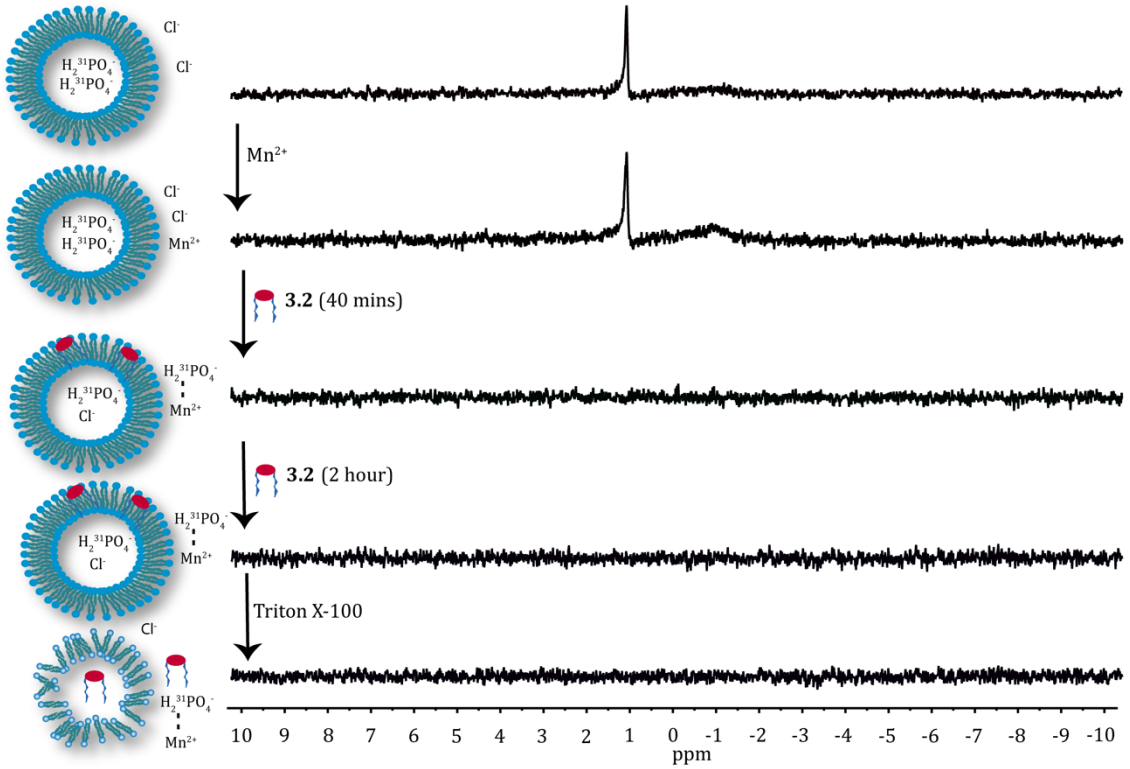

Figure 3.5. ^{31}P NMR experiment showed that compound **3.2** (8 μM) is capable of phosphate transport via the $Cl^-/H_2PO_4^-$ antiport pathway.

3.2.7. Molecular dynamics (MD) simulation studies of guanidine-based macrocyclic compound with a model membrane

Embedding anionophore **3.2** and Cl^- inside a pre-equilibrated dipalmitoyl phosphocholine (DPPC)/water lipid bilayer system, molecular dynamics (MD) simulation studies were done (Figure 3.6). These studies reveal that the anionophore **3.2** stays within the bilayer and the phosphate ion is expelled from the complex indicating successful transport of the phosphate ion mediated by **3.2** [9]. Moreover, the interaction of phosphate ion with that of guanidinium moiety of anionophore **3.2** is shown by the gas-phase optimized structure.

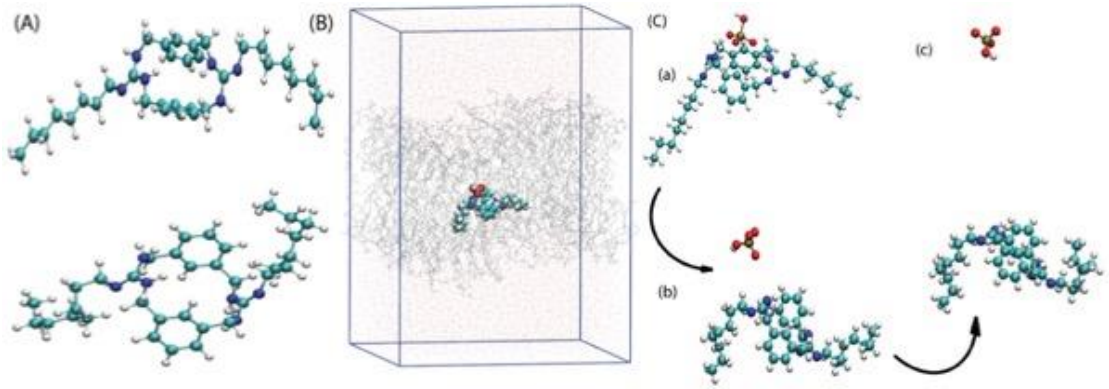

Figure 3.6. Optimized gas-phase structure of compound **3.2** (A). The simulated system with compound **3.2** bound to phosphate ion inserted in DPPC lipid layer (B). Time-dependent expulsion of phosphate ion from the DPPC lipid bilayers. Water and membrane were removed for clarity (C).

3.2.8. Regeneration of the active guanidine-based macrocyclic anionophore from proanionophore

Now to probe into the regeneration of the proanionophore **3.4**, NMR-based studies were performed in DMSO-d_6 solution [2, 10]. The proanionophore was subjected to 5 minutes and 15 minutes of UV irradiation and their NMR spectra was analysed to check the regeneration process. Clearly the benzylic proton H_e was found to decrease under UV irradiation and also the emergence of the aldehyde peak H_a clearly depicted cleavage of the photolabile part (Fig. 3.7A). The efficiency of the photocleavage was also studied with the help of fluorescence-based experiment where EYPC/CHOL-LUV⊃lucigenin was prepared enclosing 20 mM HEPES buffer containing 225 mM NaCl, pH 7.2 and they were dispersed in 20 mM HEPES buffer containing isotonic NaH_2PO_4, pH 7.2. Initially at t = 50 s, the transporter was added and the kinetics was initiated recording the phosphate mediated Cl^- transport efficacy of the proanionophore **3.2**. At t = 200 s the sample was irradiated with light (365 nm) for 5 mins and 15 minutes respectively. Immediately after irradiation the fluorescence intensity was seen increasing depicting photocleavage of the anionophore to yield the active anionophore **3.2**, which is responsible for the transport phenomenon taking place. After 15 minutes of light irradiation, the transport efficiency increased by almost 60% which is phenomenal. But when DMSO

was added at t = 50 s and after light irradiation for 5 minutes and 15 minutes at t = 200 s, no change in lucigenin

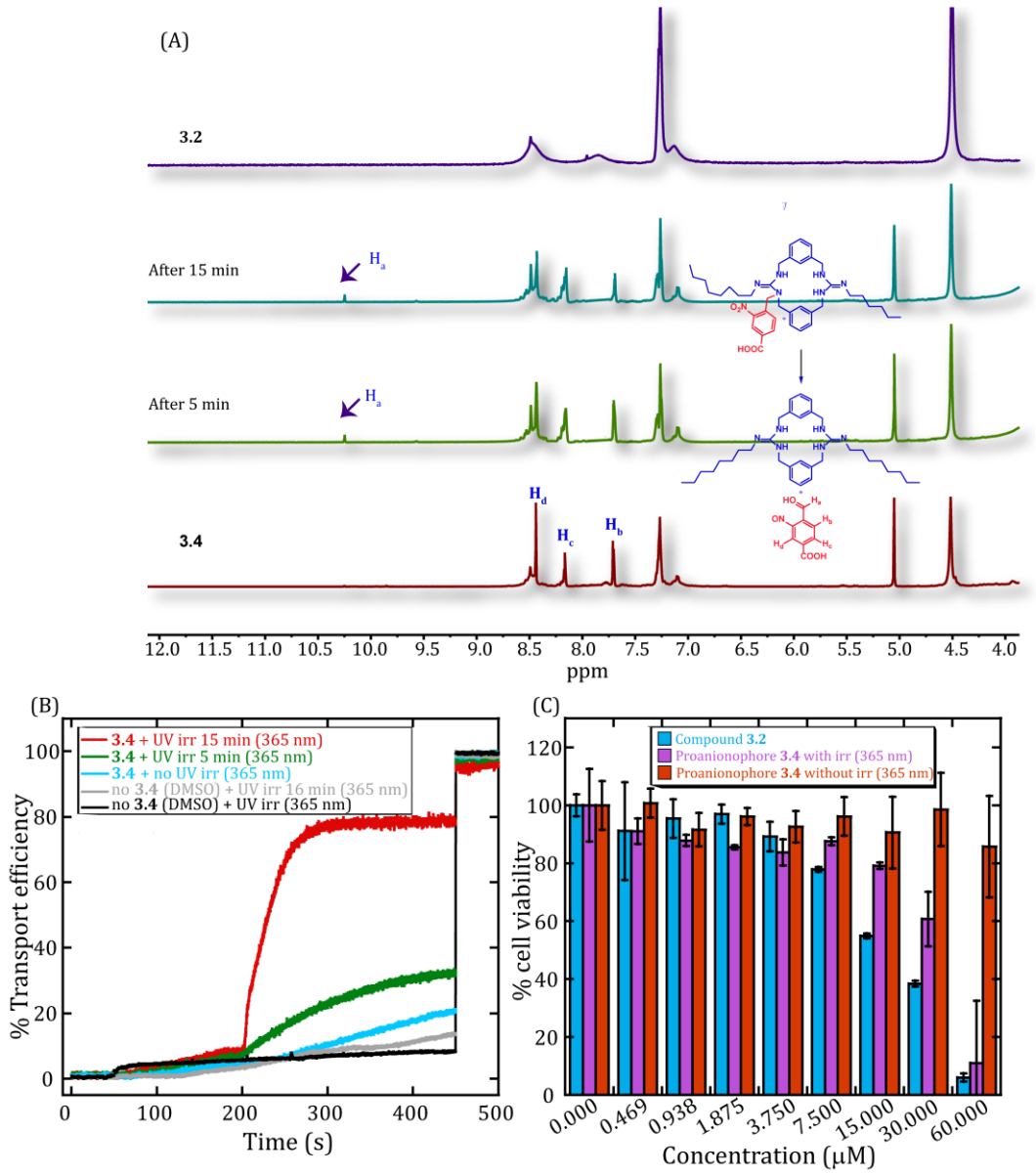

Figure 3.7. Photo induced release of anionophore **3.2** from proanionophore **3.4** was monitored by ^{1}H NMR titration experiment in DMSO-d_6 solvent (A). Measurement of Cl^- ion transport efficiency of proanionophore **3.4** before and after photo-irradiation (B). Viability of compound treated (48 h) HeLa cells before and after photo-irradiation.

fluorescence intensity was seen conforming that the sudden jump in lucigenin fluorescence intensity was surely not only due to UV irradiation but it was due to regeneration of the active anionophore **3.2** from the inactive proanionophore **3.4** (Fig. 3.7B).

3.2.9. Biological activity studies of guanidine-based macrocyclic compound

It is known that cancer cells require a high concentration of P_i ions inside them due to their high energy requirement needed for their high proliferation rate. The Cl^- ion concentration is also higher outside the cancer cells. Hence disruption of this Cl^-/phosphate ionic homeostasis of the cancer cells can possibly trigger apoptosis in the cancer cells. Hence to check the hypothesis, the cell viability of the HeLa cells were checked in presence of the anionophore **3.2** and proanionophore **3.4** under UV irradiation conditions. In presence of the active anionophore **3.2**, the toxicity started showing after 7.5 μM, however for the proanionophore **3.4** under normal conditions, the HeLa cells showed insignificant signs of toxicity upto 60 μM of concentrations. Proanionophore **3.4** under just 5 minutes of UV irradiation started showing HeLa cell death above 15 μM of concentration thus implying partial generation of anionophore **3.2** in-situ under light treatment (Fig. 3.7C).

3.3. Summary

Thus, in this work guanidium-based macrocycles and a proanionophore were developed and their ion transport properties were checked across EYPC/CHOL-LUV⊃lucigenin. Macrocycles have a fixed sized core. Therefore, they are excellent candidate for binding hydrophilic ions like phosphate which gets shielded within the hydrophobic core of the macrocycle. Anionophore **3.2** was found to be the most potent and the anion selectivity studies with the help of the anionophore **3.2** revealed that it has the highest selectivity for the phosphate ion. Bis-guanidium groups present in the macrocycle moiety may be responsible for this selectivity. Additionally, to explore the stimuli responsive behaviour of a proanionophore, photocleavable *o*-nitrobenzyl (ONB) group was tethered to the most potent anionophore **3.2**. The feasibility of the regeneration process was examined with the

help of NMR-based and fluorescence-based assay after irradiation with light (365 nm) and also through in-vitro studies carried out in HeLa cell line.

3.4. Experiential section

3.4.1. Synthesis of guanidine-based macrocyclic compounds

3.4.1.1. General information

The information of reagents, solvents and data accruing instrumentation were similar as mentioned in section 2.4.1.1.

3.4.1.2. Synthetic Procedure of the guanidine-based macrocyclic Compounds

3.4.1.2.1. Synthesis of 1,3-bis(isothiocyanatomethyl)benzene[11]

To a gently stirring THF solution of *m*-xylenediamine, CS_2 (100 mg, 7.34 mmol) was carefully added to the solution dropwise in an inert condition. To the resulting cloudy solution *N*,*N*-dicyclohexylcardiimide (100 mg, 11.01 mmol) in THF was added. The solution was then stirred for 2 hours and the completion of the reaction was checked with the help of TLC. After maximum consumption of the starting material, the suspension was filtered off and the filtrate was collected and concentrated under reduced pressure to obtain a yellow-coloured oil as the crude product. The crude product was further purified with column chromatography using silica gel with ethyl acetate/hexane (0-10%) and the pure product was obtained as a yellow oil. All the characterization data were matched with the known literature data for the compound.[11]

3.4.1.2.2. Synthesis of 3,5,9,11-tetraaza-1,7(1,3)-dibenzenacyclododecaphane-4,10-dithione[12]

To a stirring solution of 1,3-bis(isothiocyanatomethyl)benzene (100 mg, 1 equiv.) in 100 mL of acetonitrile was added an acetonitrile solution of 1,3-phenylenedimethanamine (61 mg, 1 equiv.) dropwise over 30 minutes. White precipitate was observed after 15 minutes of completion of addition. After stirring for 1.5 hr, the solution was filtered and the precipitate was collected and washed with CH_2Cl_2 and diethyl ether to remove the excess impurities. The resulting white product was further purified by column chromatography using silica gel with ethyl acetate/hexane (0-10%) as the eluting solvent: The pure product was obtained in

pale yellow colour. All the characterization data were matched with the literature data to confirm the product.

3.4.1.2.3. Synthesis of guanidine derivatives [6]

To a gently stirring solution of the thiourea macrocycle (1 equiv.) in anhydrous DMF, the respective amine (5 equiv.) and triethylamine (10 equiv.) were added sequentially in an inert atmosphere and the corresponding temperature was lowered to 0-5 °C. After 15 minutes of stirring $HgCl_2$ (5 equiv.) was added into the solution. After 15 minutes of stirring at 0-5 °C, a black coloured ppt was obtained. The temperature was increased to rt and the mixture was stirred overnight. The black ppt (HgS) was removed through filtration and the filtrate was collected and concentrated in reduced pressure. The crude product was then purified through column chromatography using methanol/CH_2Cl_2 as the eluting solvent.

3.4.1.2.4. Synthesis of (4*E*, 10*E*)-*N*,*N*-dibutyl-3,5,9,11-tetraaza-1,7(1,3)-dibenzeneacyclododecaphane-4,10-diimine (3.1)

The above procedure was followed to synthesis **3.1** [6]. The white coloured product was purified in 55% yield with the help of column chromatography using methanol/CH_2Cl_2 (0-14%) as the eluting solvent. The compound was characterised by ^{1}H NMR, $^{13C\{1H\}}$ NMR and HRMS analyses. ^{1}H NMR (600 MHz, DMSO-d_6) δ_{ppm} 8.72 – 8.25 (brs, 3H), 8.09 – 7.59 (brs, 1H), 7.29 – 7.09 (brs, 8H), 4.60 - 4.42 (s, 8H), 1.54 - 1.49 (m, 2H), 1.47 – 1.42 (m, 4H), 1.35 -1.28 (m, 2H), 1.23 – 1.16 (m, 4H), 0.83 – 0.81 (t, J = 12 Hz, 6H). ^{13} C{1H} NMR (150 MHz, DMSO-d_6) δ_{ppm} 154.2, 138.5, 128.6, 127.2, 43.8, 41.5, 31.0, 30.4, 19.7, 14.1. HRMS (ESI) calcd. for $C_{26}H_{38}N_6$ $(M+H)^+$: 435.3231, found: 435.3250.

3.4.1.2.5. Synthesis of (4*E*, 10*E*)-*N*,*N*-dioctyl-3,5,9,11-tetraaza-1,7(1,3)-dibenzeneacyclododecaphane-4,10-diimine (3.2)

The above procedure was followed to synthesis **3.2** [6]. The white coloured product was purified in 35% yield with the help of column chromatography using methanol/CH_2Cl_2 (0-12%) as the eluting solvent. The compound was characterised by ^{1}H NMR, $^{13C\{1H\}}$ NMR and HRMS analyses. ^{1}H NMR (600 MHz, DMSO-d_6) δ_{ppm} 8.49 – 8.45 (brs, 3H), 7.87 – 7.85 (brs, 1H), 7.30 – 7.14 (m, 8H), 4.50 (s, 8H), 1.48 - 1.44 (m, 4H), 1.28 – 1.18 (m, 24H), 0.87 -0.85 (m, 6H). $^{13C\{1H\}}$ NMR (150 MHz, DMSO-d_6) δ_{ppm}

154.2, 138.5, 128.6, 127.2, 43.8, 41.5, 31.0, 30.4, 19.7, 14.1. HRMS (ESI) calcd. for $C_{34}H_{54}N_6$ $(M+H)^+$: 547.4483, found: 547.4496.

3.4.1.2.6. Synthesis of (4*E*, 10*E*)-*N*,*N*-didecyl-3,5,9,11-tetraaza-1,7(1,3)-dibenzeneacyclododecaphane-4,10-diimine (3.3)

The above procedure was followed to synthesis **3.3** [6]. The white coloured product was purified in 65% yield with the help of column chromatography using methanol/CH_2Cl_2 (0-8%) as the eluting solvent. The compound was characterised by ^{1}H NMR, $^{13C\{1H\}}$ NMR and HRMS analyses. ^{1}H NMR (600 MHz, DMSO-d_6) δ_{ppm} 8.57 – 8.30 (brs, 3H), 7.82 – 7.72 (brs, 1H), 7.29 – 7.09 (m, 8H), 4.50 (s, 8H), 1.47 - 1.42 (m, 4H), 1.28 – 1.15 (m, 32H), 0.85 -0.78 (m, 6H). ^{13}C{1H} NMR (150 MHz, DMSO-d_6) δ_{ppm} 154.3, 138.4, 128.7, 127.0, 43.8, 41.8, 31.8, 29.6, 29.5, 29.2, 29.2, 26.5, 25.3, 22.6, 14.5. HRMS (ESI) calcd. for $C_{34}H_{62}N_6$ $(M+H)^+$: 603.5109, found: 603.5122.

3.4.1.2.7. Synthesis of 4-(((4*E*,10*E*)-4,10-bis(octylimino)-3,5,9,11-tetraaza-1,7(1,3)-dibenzenacyclododecaphane-3-yl)methyl)-3-nitrobenzoic acid (3.4)[13]

To a constant stirring of **3.2** (1 equiv.) in anhydrous DMF, KOH (1.2 equiv.) was added and the solution was stirred under inert condition for 15 minutes. To the stirring solution was added a DMF solution of 4-(bromomethyl)-3-nitrobenzoic acid (1 equiv.). The resulting solution was heated at 50 °C overnight. After maximum consumption of the starting material, the solution was filtered and the filtrate was collected and concentrated under reduced pressure. The crude product was purified through column chromatography using (methanol/CH_2Cl_2 (0-20%) as the solvent gradient system. The compound was characterised by ^{1}H NMR, ^{13}C NMR and HRMS analyses. . ^{1}H NMR (600 MHz, DMSO-d_6) δ_{ppm} 8.44 (brs, 1H), 8.17 – 8.16 (m, 1H), 7.71 – 7.70 (m, 1H), 7.33 – 7.11 (s, 6H), 7.09 – 7.06 (m, 2H), 5.05 (s, 2H), 4.52 (s, 8H), 1.50 – 1.42 (m, 6H), 1.29 – 1.15 (m, 24H), 0.86 – 0.84 (m, 6H). ^{13}C NMR (150 MHz, DMSO-d_6) δ_{ppm} 175.5, 170.5, 154.4, 147.4, 147.3, 138.4, 134.5, 132.0, 129.1, 128.7, 127.1, 125.7, 125.4, 62.8, 43.9, 43.1, 41.9, 31.7, 29.11, 26.5, 22.6, 21.0, 14.4. HRMS (ESI) calcd. for $C_{34}H_{62}N_6$ $(M+H)^+$: 764.462, found: 764.4635.

3.4.2. Binding studies of guanidine-based macrocyclic compounds

3.4.2.1 Spectrophotometric titration studies

The DMSO aliquot of the anionophores **3.1**, **3.2** and **3.3** were taken in the clean quartz cuvettes each time and different equivalent of salts (TBACl, $TBAH_2PO_4$ or $TBANO_3$) were added sequentially and the corresponding UV absorption was recorded between 200 nm and 900 nm (at 298 K). the corresponding binding constant was obtained using BindFit v0.5 (1:1 UV binding model).

Table 3.1. Anion binding efficacy of the compounds measured by UV-Vis spectroscopic method.

Salt	Binding affinities (K_a); (M^{-1})		
	Compound **3.1**	Compound **3.2**	Compound **3.3**
$TBAH_2PO_4$	167.27 (± 5.27%)	1265.24 (± 8.49%)	256.79 (± 12.50%)
TBACl	—	1209.26 (± 11.21%)	—
$TBANO_3$	—	NM	—

NM- Nonmeasurable

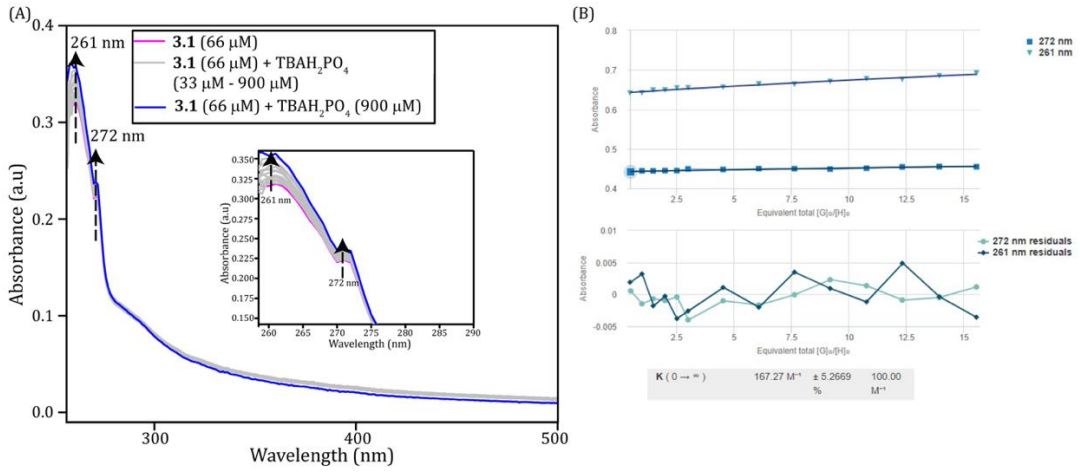

Figure S3.1. UV-vis absorption spectrophotometric titration of compound **3.1** (66 µM) with increasing amounts of $TBAH_2PO_4$ (A) and the plot of absorbance vs. equivalent total ($[G_0]/[H_0]$), fitted to a 1:1 binding model (B)

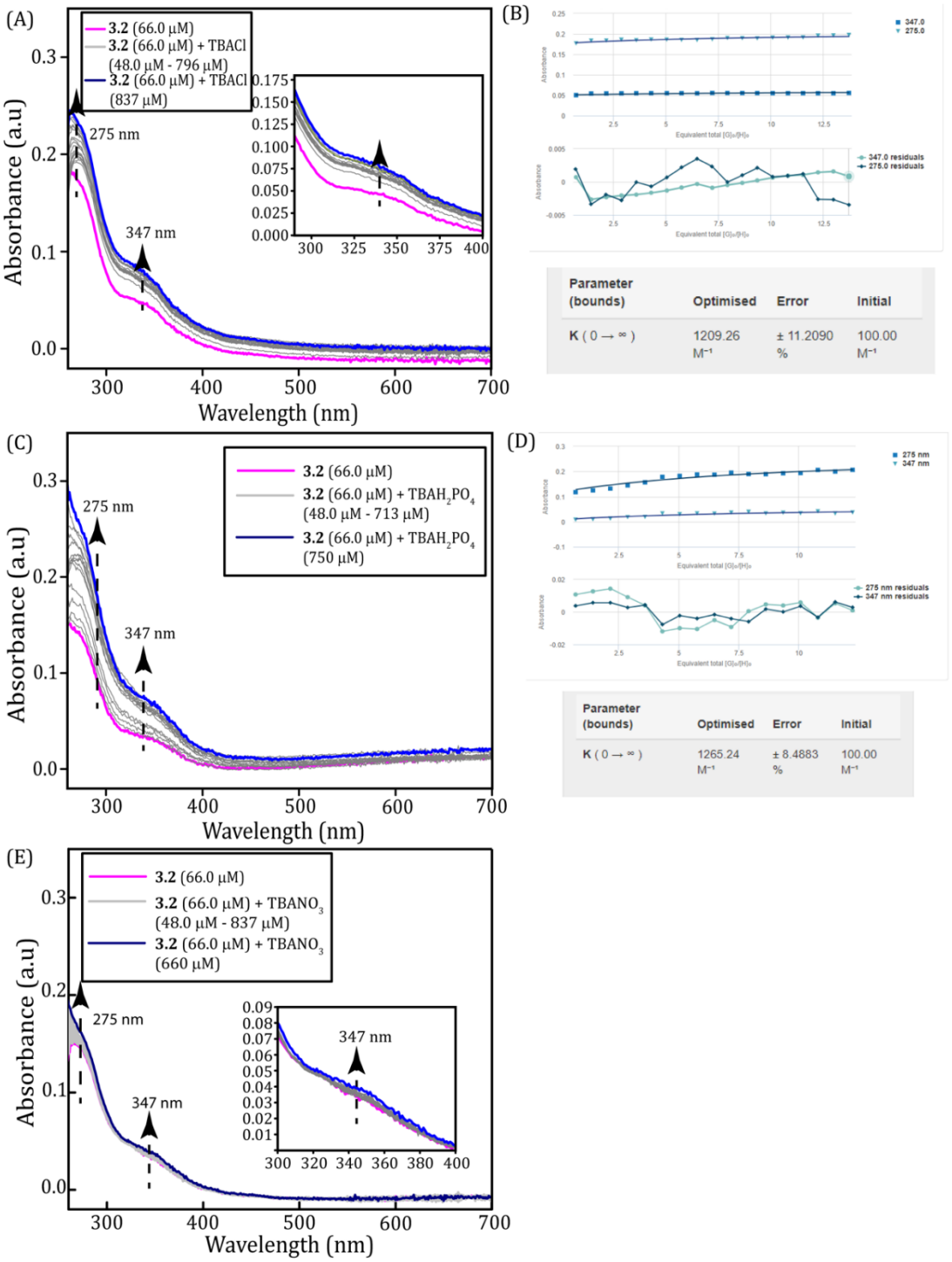

Figure S3.2. UV-vis absorption spectrophotometric titration of compound **3.2** (66 µM) with increasing amounts of TBACl (A) and the plot of absorbance vs. equivalent total ($[G_0]/[H_0]$), fitted to a 1:1 binding model (B), $TBAH_2PO_4$–(C) and the plot of absorbance vs. equivalent total ($[G_0]/[H_0]$), fitted to a 1:1 binding model (D) and $TBANO_3$, in DMSO (E).

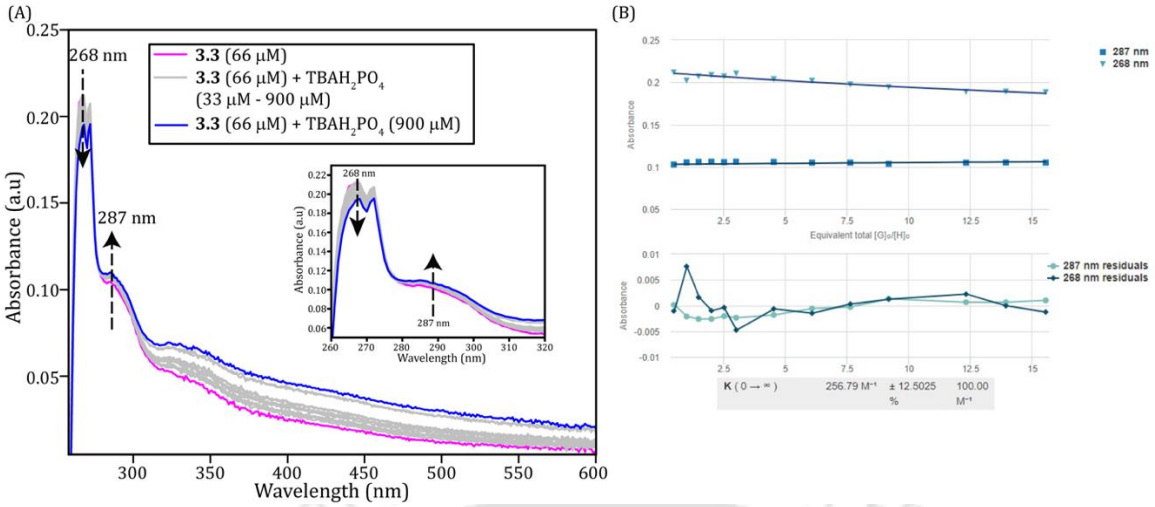

Figure S3.3. UV-vis absorption spectrophotometric titration of compound **3.3** (66 μM) with increasing amounts of $TBAH_2PO_4$ (A) and the plot of absorbance vs. equivalent total ($[G_0]/[H_0]$), fitted to a 1:1 binding model (B)

3.4.3. Lucigenin fluorescence quenching measurements of guanidine-based macrocyclic compounds in the presence of different anions

Initially, 120 μM of lucigenin was taken in a clean fluorescence cuvette, and the emission spectra were recorded at λ_{ex} = 455 nm. After sequential addition of the anions, the intensity decreases sharply. Hence lucigenin can be used to monitor different oxoanions.

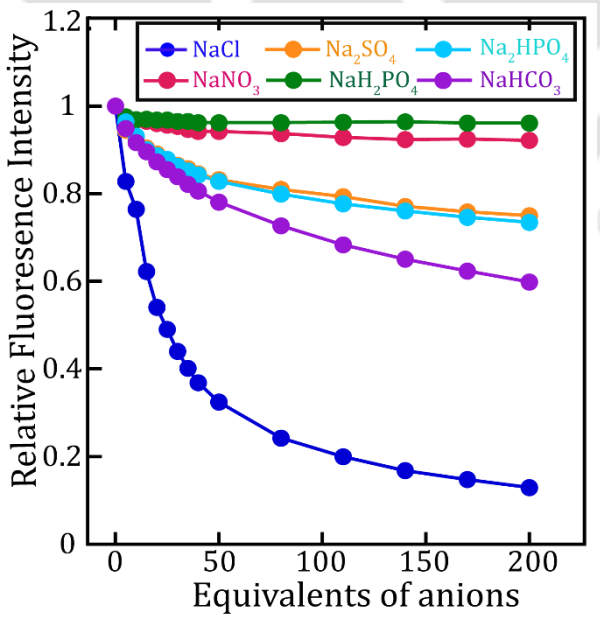

Figure S3.4. Fluorescence titration curve of lucigenin (120 μM in aqueous solution) with different anions. Excitation 455 nm, emission 505 nm.

3.4.4. Ion transport activity studies of guanidine-based macrocyclic compounds

3.4.4.1. Ion transport activity studies using the fluorescence-based assay

3.4.4.1.1. Lucigenin-based ion transport studies

3.4.4.1.1.1. Preparation of EYPC-LUVs lucigenin using $NaNO_3$ as the intravesicular solution

For the fluorescent-based transport studies, EYPC (50 mg/mL in deacidified $CHCl_3$) and CHOL (25 mg/mL in deacidified $CHCl_3$) were taken in a clean and dry sample vial in the molar ratio of 8:2. A thin lipid film was formed by evaporating the chloroform solution of EYPC and CHOL under reduced pressure. The sample was dried for 6 hours and rehydrated with 225 mM $NaNO_3$ solution (4 mM lucigenin). The suspension was consequently vortexed 6-7 times in the next 1 hour. The suspension was subjected to 17-19 times freeze-thaw cycles followed by 15 minutes of vortexing. To achieve a liposome size of 200 nm, the lipid suspension was extruded using a mini extruder (a polycarbonate membrane from Avanti Polar Lipids having 200 nm pore size) for 19-21 times (must be an odd number). Finally, to remove the unencapsulated lucigenin dye from the extravesicular solution, the gel filtration technique was used (Sephadex G-50) using 225 mM of $NaNO_3$ solution. The final lipid concentration obtained was 25 mM (assuming 100 % lipid regeneration).

$$Transport\ activity\ (T_{Lucigenin}) = \frac{F_t - F_0}{(F_\infty - F_0)} \times 100\ \% \ldots\ldots\ldots Eq - 3.1$$

3.4.4.1.1.3. Lucigenin-based ion transport studies using NaCl as the intravesicular solution [14]

The LUVs were prepared as mentioned in section 3.4.4.1.1.1 with 225 mM NaCl solution as the intra-vesicular buffer.

3.4.4.1.1.4. Ion transport activity across EYPC/CHOL-LUV⊃lucigenin

The ion transport studies were performed according to the procedure mentioned in 3.4.4.1.1.2.

3.4.4.2. Measurement of half-maximal effective concentrations (EC_{50}) of the compounds for different anions

The half-maximal effective concentrations (EC_{50}) of the anionophores **3.1**, **3.2** and **3.3** were mentioned using intravascular NaCl containing liposome. The anion efflux efficiency (Y-axis) obtained from the lucigenin fluorescence assay were normalized [t = 0 to t = 500 s (X-axis)]. The normalized efflux efficiency (EE) values at t = 450 s (just before the addition of Triton X-100) were considered as the transport activity of the compound at that particular concentration. The efflux efficiency (EE) of a compound at a particular concentration was determined by using the equation Eq.-3.1. Effective concentrations (EC_{50} values) of the compounds were calculated by plotting the respective anion efflux efficiency values against concentration (μM) and fitted with the modified Hill equation Eq-3.2.

Table 3.2 Anion transport efficacy of the selected compounds.

Salt	EC_{50} (μM); (n^a)		
	3.1	**3.2**	**3.3**
NaH_2PO_4	14.00; (0.81)	4.10; (0.78)	21.52; (1.04)

n^a is the Hill coefficient.

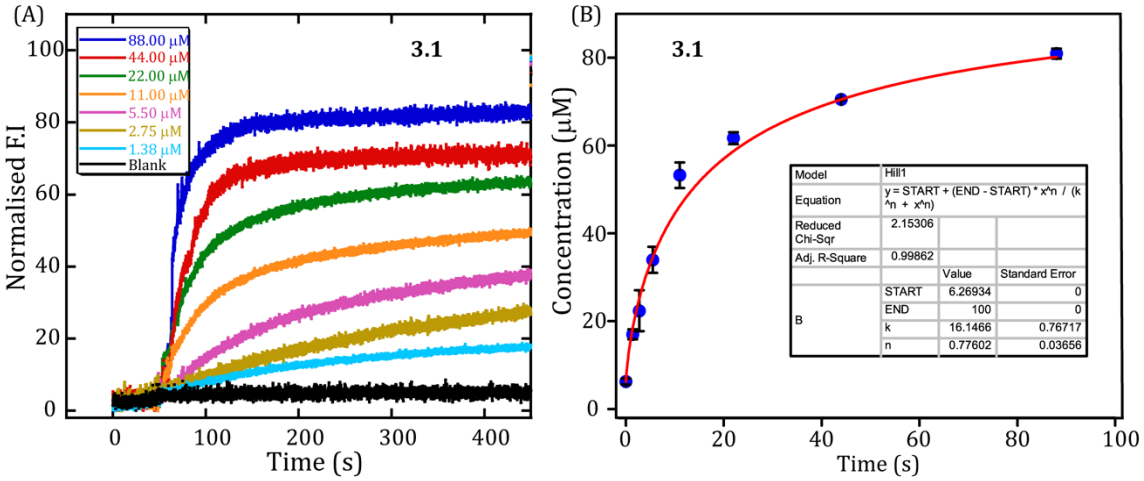

Figure S3.5. Concentration-dependent transmembrane transport of phosphate-mediated Cl^- ion transport in the presence of compound **3.1** across the EYPC/CHOL-LUV⊃Lucigenin. The ion transport activity was measured by lucigenin fluorescence assay (A). The EC_{50} value was calculated using the modified Hill equation (B).

$$y = a + (b - a) * \left(\frac{x^n}{k^n + x^n}\right) = Vmax\frac{x^n}{k^n + x^n} = 100 * \left(\frac{x^n}{EC50^n + x^n}\right) \ldots\ldots Eq - 3.2$$

Where, a = 0 and b = 100, y is the anion efflux at 450 s (%), x is the carrier concentration (μM), V_{max}, k, and n are the fitted parameters. V_{max} is the maximum efflux of anion possible (usually fixed to 100 % as this is the maximum chloride efflux possible), n is the Hill coefficient, and k is the carrier concentration required to reach $V_{max}/2$ (when V_{max} is fixed to 100% then k is the EC_{50}). EC_{50} values at 450 s were obtained directly from the Hill plot. The normalized % transport efficiency (%EE) at t = 500 s was considered for the particular anion transport efficiency of the compounds.

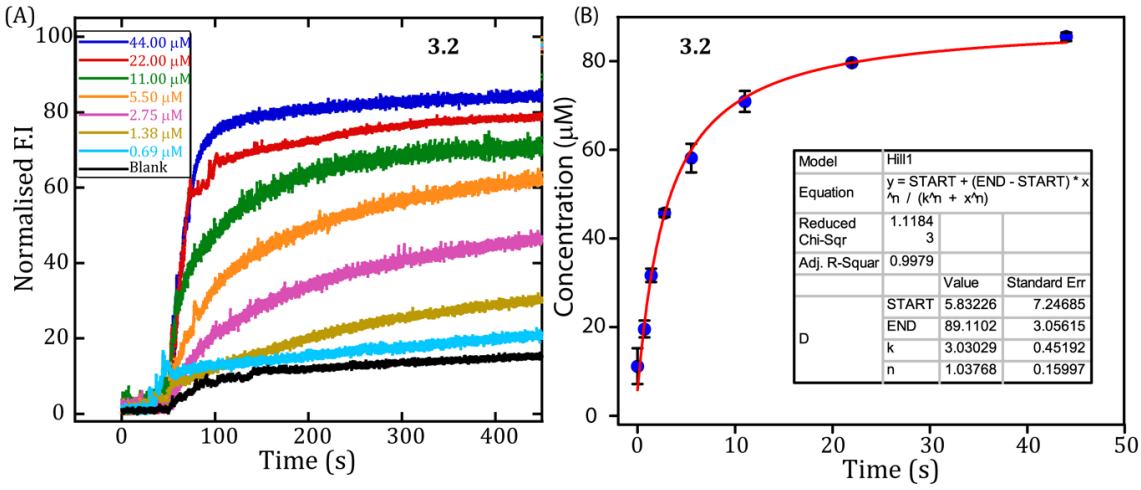

Figure S3.6. Concentration-dependent transmembrane transport of phosphate-mediated Cl^- ion transport in the presence of compound **3.2** across the EYPC/CHOL-LUV⊃Lucigenin. The ion transport activity was measured by lucigenin fluorescence assay (A). The EC_{50} value was calculated using the modified Hill equation (B).

3.4.4.3. Lucigenin-based selectivity studies

3.4.4.3.1. Anion transport activity across EYPC/CHOL-LUVs lucigenin

For the fluorescence-based anion selectivity assay, in a clean fluorescence cuvette (3 mL), 2940 μL of 225 mM of Na_xA_y solution (where Na_xA_y = NaH_2PO_4, Na_2SO_4, $NaHCO_3$, NaOAc, $NaClO_4$, and $NaNO_3$) and EYPC/CHOL-LUVs lucigenin (50 μL) was taken, and it was placed in the fluorescence spectrophotometer under slow stirring condition for 3 minutes. The fluorescence was evaluated as a function of time (λ_{em} = 505 nm, λ_{ex} = 455 nm). At 50 s, the kinetics was initiated by the addition of 10 μL of the

compound from the DMSO stock solution. The vesicles were completely lysed by adding 20 µL of 20% Triton X-100 at 450 s, and the fluorescence intensity measurement was continued for a further 50 s.

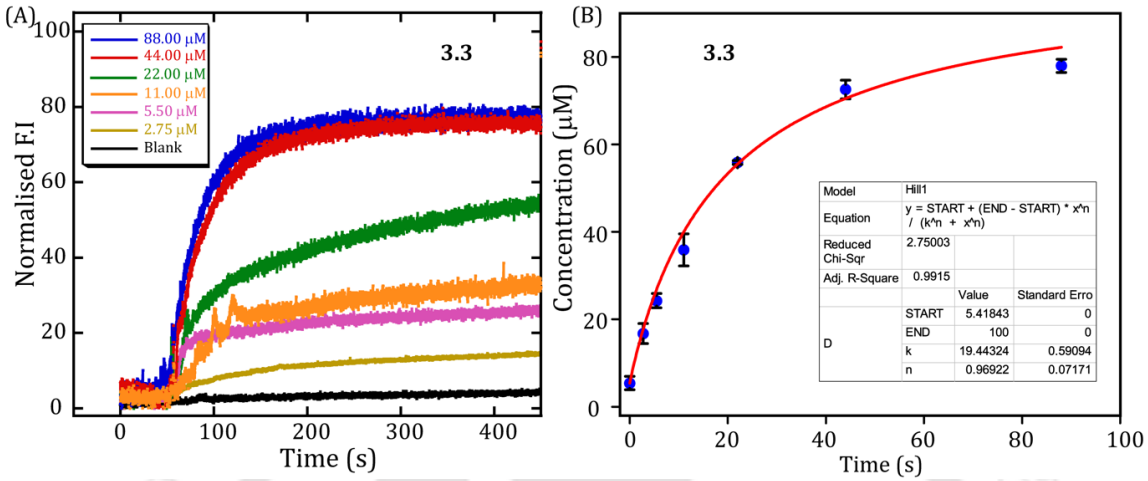

Figure S3.7. Concentration-dependent transmembrane transport of phosphate-mediated Cl^- ion transport in the presence of compound **3.3** across the EYPC/CHOL-LUV⊃Lucigenin. The ion transport activity was measured by lucigenin fluorescence assay (A). The EC_{50} value was calculated using the modified Hill equation (B).

3.4.4.3.2. Cation transport activity across EYPC/CHOL-LUV⊃lucigenin

The LUVs were prepared as mentioned in section 4.4.4.1.2. In this case the LUVs were prepared incorporating 20 mM HEPES buffer containing 225 mM MCl, pH 7.2 (where M = Li^+, Na^+, K^+, Rb^+ and Cs^+). The LUVs were suspended in 20 mM HEPES buffer containing 225 mM NaH_2PO_4, pH 7.2 solution.

3.4.4.4. Ion transport activity studies using the ion-selective electrode-based assay

3.4.4.4.1. Chloride ion efflux studies using chloride-ion-selective electrode (chloride-ISE)

Phosphate/Cl^-antiport was measured indirectly by monitoring the Cl^- concentration outside the liposomes using a Cl-ISE (Thermo Scientific™ Orion™). Before each set of the experiment, the chloride ISE was calibrated using 1 ppm, 10 ppm, and 100 ppm standard aqueous solution of NaCl.

3.4.4.4.2. Preparation of EYPC/CHOL-LUV

For the ISE-based ion transport studies, the LUVs were prepared as mentioned in the earlier section. The thin film was rehydrated with an aqueous solution of 20 mM HEPES buffer containing 225 mM of NaCl, pH 7.2. The LUVs were finally dialyzed using a buffer solution of 20 mM HEPES buffer containing 225 mM of NaH_2PO_4, pH 7.2, to remove unwanted adhered NaCl on the liposomes.

3.4.4.4.3. Chloride efflux study across EYPC/CHOL-LUV

In a dry and clean glass vial, 3940 µL of buffer solution (20 mM of HEPES buffer containing 225 mM NaH_2PO_4, pH 7.2) and 50 µL of the EYPC/CHOL-LUV were taken, and the glass electrode was immersed into the solution under mild stirring condition. The phosphate/Cl^- antiport process was tracked by monitoring Cl^- concentration using a Cl-ISE (t = 0 s). After 50 s, 10 µL of the respective transporter (from their respective DMSO stock solution) was added to initiate the Cl^- transport kinetics. Consequently, at t = 500 s, the vesicles were lysed using 50 µL of 20% of the Triton X-100 solution. Total Cl^- ion efflux reading was taken at t = 500 s.

3.4.4.4.4. Quantitative measurement of transport activity from chloride ISE assay

The Cl^- ion efflux for anionophore **3.2** was normalized and the respective values at t = 0 and t = 700 s were considered as 0 and 100 units, respectively.

$$Chloride\ efflux\ efficiency,\ \ EE_{Chloride} = \frac{EE_t - EE_0}{(EE_\infty - EE_0)} \times 100\ \% \ldots\ldots Eq.-3.3$$

Here (EE) stands for the normalized Cl^- ion efflux efficiency at t = 500 s, just before addition of Triton X-100. EE_t stands for the Cl^- ion efflux efficiency at t = 500 s (just before the addition of Triton X-100 solution), EE_0 stands for the Cl^- ion efflux efficiency immediately before the addition of the compound (at t = 0 s) and EE_∞ stands for the Cl^- ion efflux efficiency after addition of Triton X-100 solution.

3.4.4.5. U-tube assay

For the U-Tube experiment, DMSO solution of anionophore **3.2** was taken in 8 mL $CHCl_3$ which is taken in the organic phase in the middle of U-Tube. In the left arm

of the U-Tube 225 mM aqueous of NaH_2PO_4 solution was taken and in the right arm isotonic solution of NaCl was taken. The organic phase was gently stirred using an external magnetic stirrer. At regular intervals, the transported Cl^- concentration in the left arm was monitored with the help of ISE. For determining phosphate transport in the right arm, 200 µL of solution from the left arm was taken and added to a clean sample vial containing 250 µL of 0.5 M hydrazine hydrate, ammonium molybdate solution (500 µL of 2.5%) and 125 µL of 20 N H_2SO_4. After 1 minute a blue-coloured was observed and the UV spectra was recorded (50 µL of the blue-coloured solution from the cuvette and diluted to 1 mL volume). This blue-coloured solution was due to formation of ammoniumphosphomolybdate. The formation of the blue-coloured solution shows the phosphate transport from the right arm to the left arm. The experiment also exhibits carrier-mediated pathway taken by anionophore **3.2** to transport the ions.

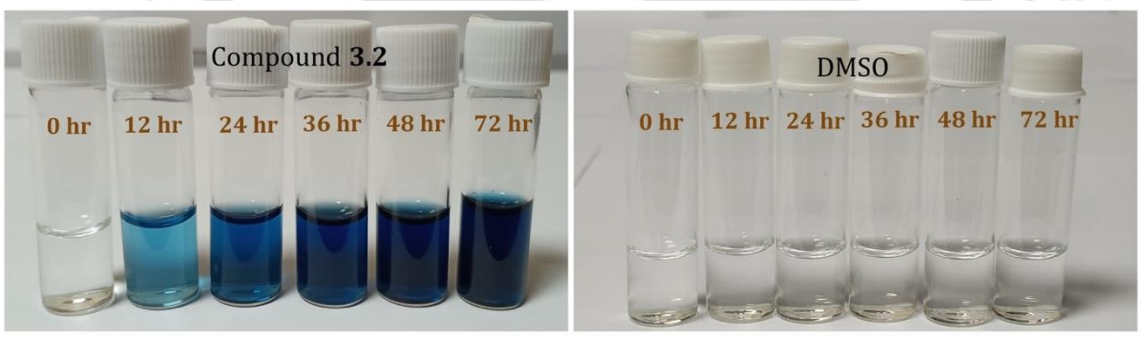

Figure S3.8. Representative images of the colorimetric U-tube assay using ammonium molybdate in the presence and absence of **3.2** (1 mM) to detect the transport of phosphate ion. The phosphate ion reacts with ammonium molybdate in the presence of hydrazine in an acidic medium to generate blue-colored ammonium phosphomolybdate.

3.4.4.6. Evidence of mechanistic pathway of transport of the anionophore

3.4.4.6.1. Temperature-dependent DPPC assay

3.4.4.6.1.1. Preparation of DPPC/CHOL-LUVs⊃Lucigenin[15]

1,2-Dipalmitoylphosphatidylcholine (DPPC, in deacidified $CHCl_3$) was taken in a clean and dry sample vial in the molar ratio 8:2 to probe into the fact whether the transporters are following carrier mechanism for transport or they are forming

channels. The latter procedure of liposome formation in 225 mM NaCl has been followed the same as in the earlier section.

3.4.4.6.1.2. Ion transport activity across DPPC/CHOL-LUV⊃Lucigenin

The fluorescence assay was performed according to the reported procedure using a spectrofluorometer connected with a refrigerated system for temperature control (where the temperature was regulated using a Peltier temperature controller). Briefly, in a clean and dry fluorescence cuvette (3 mL), buffer solution (2940 µL of an aqueous solution containing 225 mM of NaH2PO4 or Na2SO4) and DPPC/CHOL-LUVs Lucigenin (50 µL of 25 mM) were taken, and the cuvette was placed in the fluorescence spectrophotometer under the slow stirring condition for approximately 3 minutes at 25 ºC. The lucigenin fluorescence intensity was monitored (at t = 0 s) at λem = 505 nm (λex = 455 nm). The kinetics was initiated by adding 10 µL of the respective compound in the DMSO solution to the cuvette at t = 50 s. The vesicles were completely lysed by adding 20 µL of 20% Triton X-100 after 450 s, and the fluorescence intensity measurement was continued for a further 50 s. A similar experiment was performed for the measurement of the transport efficiency of compound **3.2** at 45 ºC and at 25 ºC. The temperature-dependent DPPC assay was conducted to show the carrier pathway of oxyanion transportation of compounds **3.2**. The phase transition temperature (T_m) of DPPC lipid is 41 °C, beyond which the randomness of the lipid bilayer increases. Hence, the experiment was performed at 25 °C and 45 °C (temperature below and above phase transition, respectively), and compound **3.2** showed marked differences in the ion transport efficiencies at the two temperatures, clearly stating the carrier pathway of transport.

3.4.4.7. Ion transport activity studies using HPTS-based fluorescence assay

3.4.4.7.1. Preparation of EYPC/CHOL-LUV⊃HPTS

The LUVs were prepared according to the procedure mentioned in 3.4.4.6.1.1 using 20 mM HEPES buffer containing 225 mM NaH_2PO_4 and 1 mM HPTS, pH 7.2.

3.4.4.7.2. Ion transport activity across EYPC/CHOL-LUV⊃HPTS in presence of FCCP

In a clean and dry fluorescence cuvette, 2940 µL of 20 mM HEPES buffer containing 225 mM NaH_2PO_4, pH 7.8 and 50 µL of EYPC/CHOL-LUV⊃HPTS were taken and placed in the fluorescence spectrophotometer under gently stirring condition. The HPTS fluorescence intensity was monitored at t = 0 s, λ_{em} = 510 nm, λ_{ex} = 450 nm. After 3 minutes of stirring, the kinetics was initiated at t = 50 s, by addition of the anionophore and FCCP (1.5 µM). At t = 450 s, the vesicles were finally lysed by addition of 20 µL 20 % Triton X-100. The HPTS fluorescent measurement was carried for a further 50 s (total t = 500 s).

3.4.4.8. Evaluation of transport of phosphate using Tb(III) fluorescent chemosensor[16]

3.4.4.8.1. Preparation of liposomes encapsulating Tb(III) fluorescent chemosensor

For this experiment the LUVs were prepared encapsulating the Tb(III) complex. Briefly in a clean and dry sample vial, EYPC (in deacidified $CHCl_3$) and cholesterol (in deacidified $CHCl_3$) was taken in 8:2 molar ratio and a thin lipid film was formed by evaporating the solvent under reduced pressure. The lipid film was then rehydrated using 20 mM HEPES buffer containing 225 mM NaCl and 4 mM Tb (III), pH 7.2. The resulting suspension was vortexed for atleast 6-7 times. After 1 hour, the suspension was subjected to 17 to 19 freeze-thaw cycles, which was followed by immediate vortexing for minimum 15 minutes. Next the liposomes was extruded using a mini extruder (a polycarbonate membrane from Avanti Polar Lipids) to obtain a uniform liposome size of 200 nm. Finally, the liposome suspension was dialyzed using 20 mM HEPES buffer containing 225 mM NaCl, pH 7.2.

3.4.4.8.2. Ion transport activity across the Tb(III) complex entrapped LUVs through fluorescence

For the fluorescence-based experiment, 2940 µL of 20 mM HEPES buffer containing 225 mM NaH_2PO_4, pH 7.2 and 50 µL of LUVs were taken in a clean and dry fluorescence cuvette and the cuvette was placed in a gentle stirring condition in the fluorescence spectrophotometer. After 3 minutes of stirring, fluorescence of the Tb(III) was monitored at t = 0 s, λ_{em} = 550 nm, λ_{ex} = 293 nm. At t = 50 s, the kinetics was initiated by addition of the anionophore **3.2**. At t = 450 s, the vesicles were finally

lysed by addition of 20 µL 20 % Triton X-100. The Tb(III) fluorescent measurement was carried for a further 50 s (total t = 500 s).

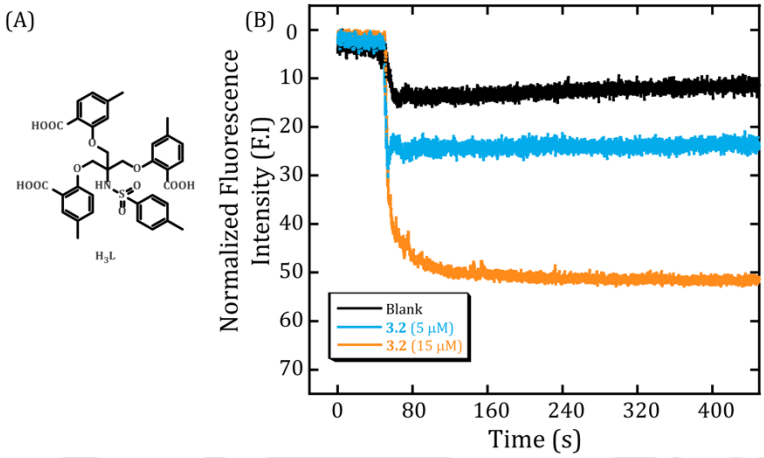

Figure S3.9. Structure of $H_3L.Tb$ (A). Assessment of phosphate ion transport of **3.2** in the presence of $H_3L.Tb$ (1 mM) (B).

3.4.4.9. Transport of phosphate ion through GUVs (Giant Unilamellar Vesicles)

3.4.4.9.1. Preparation of GUVs encapsulating 100 mM HEPES, 200 mM sucrose, and 225 mM NaH_2PO_4

The GUVs were prepared similarly according to a previously reported procedure [17]. Concisely, EYPC, CHOL, and DPPS were taken respectively in the molar ratio 8:1.5:0.5 in a dry and clean glass vial. The resulting solution was dried for 4 hours under reduced pressure to form a thin lipid film. To the lipid film, 200 µL of liquid paraffin oil was added and sonicated until the film dissolved completely, followed by the addition of 20 µL of the upper buffer (100 mM HEPES containing 200 mM sucrose. 100 mM NaH_2PO_4, and 1 mM bis-N-methylacridinium nitrate (Lucigenin) in H_2O, pH 7.2) and the solution was mixed nicely to form a white-colored emulsion. The emulsion was then slowly added to 500 µL of lower buffer (100 mM HEPES containing 200 mM glucose and 1 mM bis-N-methylacridinium nitrate (Lucigenin) in H_2O, pH 7.2) and pipetted up and down thoroughly in a centrifuge tube to mix everything. The emulsion was centrifuged for 15 minutes at 10000 to remove the excess unencapsulated dye and the oil. The precipitate of liposomes was washed 3 times with 200 µL of lower buffer to eliminate excess oil and the unencapsulated lucigenin dye. After the final washing, the precipitate of GUVs was mixed with 200 µL

of lower buffer, 10 µL of 100 µM Texas Red DHPE (Invitrogen, CA) solution in MeOH was added for membrane labeling, following which the solution was kept undisturbed for 1 hour. After that, the excess Texas Red dye was washed with the lower buffer solution. The final precipitate of liposomes was mixed with 100 µL of lower buffer (final vesicle concentration of 15 mM). The microscopic images were collected using these GUVs.

3.4.4.9.2. Ion transport measurements using GUVs coated on the glass surface

The coating on the glass surface was done according to the procedure as mentioned in 3.4.4.11.2. The freshly prepared GUVs (30 µL) were kept undisturbed for 5-6 minutes on the coated glass surface. After 5-6 minutes, a solution of NaCl and transporter **3.2** (45 µM) were added carefully to the solution of the GUVs and the decrease in the lucigenin fluorescence intensity was recorded with time with the help of images both in the bright field and in the green field (λ_{ex} = 458 nm).

3.4.4.9.3. Preparation of GUVs encapsulating 100 mM HEPES, 200 mM sucrose, and 225 mM NaCl

The GUVs were prepared according to the procedure mentioned in section 3.4.4.11.1. The GUVs were prepared using 100 mM HEPES, 200 mM sucrose, 225 mM NaCl, 1 mM bis-N-methylacridinium nitrate (Lucigenin) in H_2O and the GUVs were dispersed in 100 mM HEPES buffer containing 200 mM glucose and 225 mM NaCl.

3.4.4.9.4. Ion transport measurements using GUVs coated on the glass surface

The GUVs were prepared according to the procedure mentioned 3.4.4.11.1. To 100 µL of the GUV solution, 10 µL of Texas Red-PE was added and the solution was mixed thoroughly. After 15 minutes, the GUV suspension was centrifuged 2-3 times with the upper buffer to remove the excess Texas Red-PE dye. The freshly centrifuged GUVs (30 µL) were kept undisturbed for 5-6 minutes on the coated glass surface. After 5-6 minutes, a solution of Na_2HPO_4 and transporter **3.2** (45 µM) were added carefully to the solution of the GUVs and the increase in the lucigenin fluorescence intensity was recorded with time with the help of images both in the red field and in the green field (λ_{ex} = 458 nm). The increase in lucigenin fluorescence intensity

signifies transport phosphate ion from the extravesicular solution to the intravesicular solution.

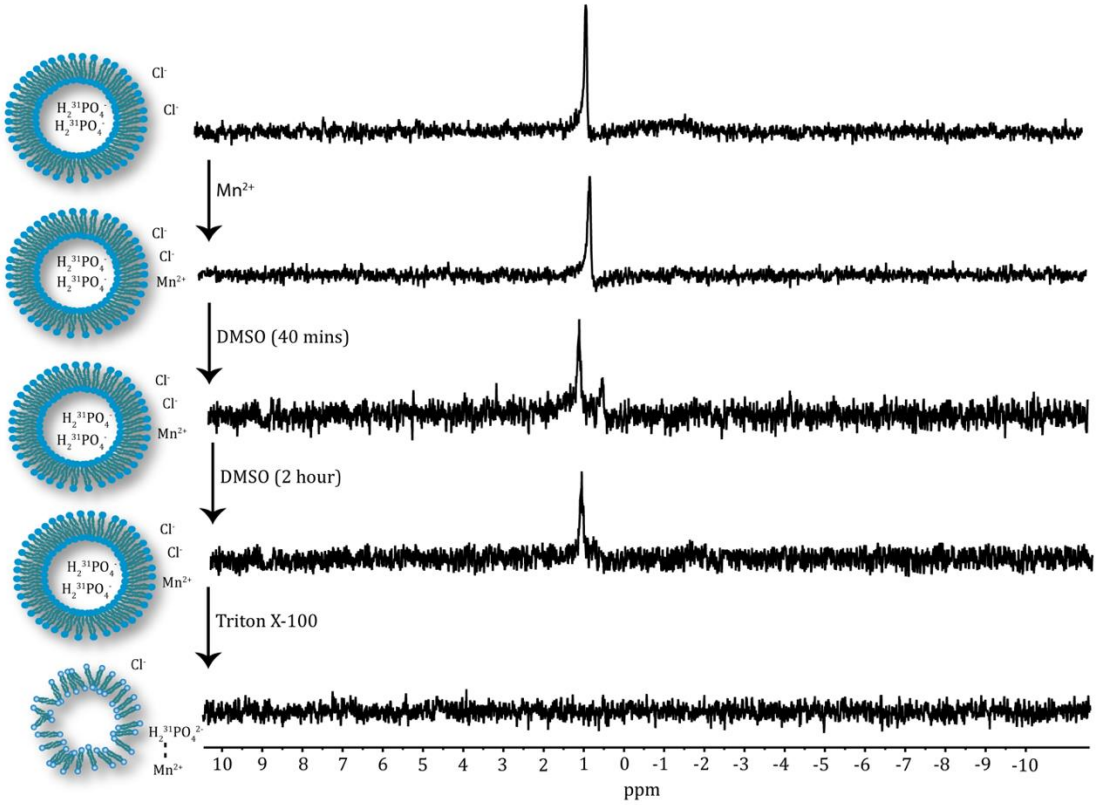

Figure S3.10. ^{31}P NMR experiment showed that DMSO is not capable of phosphate transport via the $Cl^{-}/H_2PO_4^{-}$ antiport pathway.

3.4.4.10. Direct evidence for phosphate transport by ^{31}P NMR measurements

The EYPC/CHOL-LUVs were prepared according to the method described in the earlier section. The dry film was rehydrated with HEPES buffer (500 µL of 20 mM HEPES containing 50 mM NaH_2PO_4, pH 7.2). Finally, the LUVs were dialyzed using 20 mM HEPES containing isoosmotic NaCl, pH 7.2 overnight. The ^{31}P NMR studies were done using a 600 MHz Brucker NMR instrument (ASCEND 600) with a heteronuclear probe. The ^{31}P NMR shifts were referenced with 80% H_3PO_4 (δ 0.0 ppm). The higher ^{31}P isotopic abundance (around 100%) and a relatively higher gyromagnetic ratio allowed us to perform a ^{31}P NMR study. The vesicle solution (450 µL) was taken in an NMR tube, and D_2O (50 µL) was added to it (final H_2O: D_2O mixture of 9:1), and the first spectra were taken (clearly showing the ^{31}P NMR peak). Then 10 µL of Mn^{2+}

from its stock solution of 115 mM was added to the vesicle solution (5 mol % Mn^{2+}: $H_2PO_4^-$) was added to the vesicle solution, and the solution was shaken for 2-3 minutes, followed by recording the NMR spectra. Then the solution was incubated for 3 hours with 30 μM of the transporter **3.2** (8 μM)or DMSO, and another spectrum was recorded showing the disappearance of the ^{31}P NMR signal indicating phosphate transport. Finally, the vesicles were lysed by adding 20 μL of 20% Triton X-100 (prepared in 9:1 mole ratio of H_2O: D_2O mixture), leading to all phosphate ions coming outside and getting quenched due to the presence of Mn^{2+} (in the NMR spectra no ^{31}P NMR signal can be seen).

3.4.4.11. Molecular dynamics (MD) simulation studies

The cartesian coordinates of anionophore **3.2** and the phosphate ion was obtained using AVOGADRO software [18]. The geometry optimization of the gas-phase of the anionophore and phosphate was carried out B3LYP/6-311g* label using TeraChem software [19]. The optimized structures of one molecule of anionophore **3.2** and one phosphate ion was used in classical molecular dynamics CHARMM-GUI [20]. The transit of the ions by all-atom molecular dynamics (MD) simulations were modelled as implemented in the NAMD package [21]. The anionophore molecule and the phosphate were modelled using the Generalized Amber Force Field (gaff), the bilayer has been modelled using Particle-mesh Ewald (PME) method while the water molecules have modelled using TIP3P. the cut-off for Van der Waals was set at 10 Å [22, 23]. Periodic boundary conditions were used and to constrain the covalent hydrogen atoms the SHAKE algorithm was used [24]. The time step used was 1fs and the systems were modelled in NPT ensembles at T = 300 K. To thermalize the systems the Langevin damping was used and the damping coefficient γ is 1 ps^{-1}. All the systems were minimized by 100,000 steps initially. Next the system was equilibrated for 10 ns at 300 K and the ions were held fixed. Following the systems were equilibrated for 20 ns at 300 K. The simulated system consists of one compound **3.2**, one phosphate ion and 180 DPPC molecules. To conserve the charge neutrality sodium ions were added. The simulated box has dimensions of 84 × 88 × 130 $Å^3$. The first bilayer membrane was solvated into a water box to acquire the structure of the molecule and phosphate ion in the bilayer membrane. Subsequently the gas-phase optimized one compound **3.2** and the phosphate was placed inside the membrane layer. The water

molecules can also be added to bind the phosphate, to maintain simplicity all the $H_2PO_4^-$ bound water was removed. The ion and the anionophore **3.2** was held fixed, however the system was minimized. The whole system was equilibrated for 10 ns and the anionophore **3.2** and ion were kept fixed. After equilibrating the membrane, the molecule was relaxed and equilibrated again for 10 ns. The interaction between the ion and the anionophore diminished due to the reason that now the anionophore interacts more with the lipid. After around 15 ns, the anionophore **3.2** unfolded more, hence the ion became free to abandon the molecular enclosure. After around 10 ns, the phosphate ion was removed from the membrane while anionophore **3.2** remained inside. This was highly expected as phosphate is a hydrophilic ion and hence wouldn't want to stay for longer period in the hydrophobic membrane. The ion can go out from the membrane from either of the sides, when the ion goes out from the other side then the transportation of the ion takes place.

3.4.4.12. Regeneration of the active anionophore from proanionophore

3.4.4.12.1. Light-mediated regeneration of active anionophore using NMR spectroscopy

A 2 mM DMSO-d_6 solution of proanionophore **4** was taken in an NMR tube and the NMR tube was light-irradiated (365 nm LED light) for 5 minutes, the solution was vortexed so as to result in a homogeneous solution in the tube and the corresponding ^{1}H NMR spectra was recorded. The same sample was light irradiated for 15 minutes this time and the corresponding ^{1}H NMR spectra was recorded.

3.4.4.12.2. Light-mediated regeneration of active anionophore fluorescent-based experiment

3.4.4.12.2.1. Preparation of EYPC/CHOL-LUV⊃lucigenin

TheLUVs were prepared according to the procedure mentioned in 3.4.4.1.1.1 using 20 mM HEPES buffer containing 225 mM NaCl and 1 mM lucigenin, pH 7.2**.**

3.4.4.12.2.2. Ion transport activities of the EYPC/CHOL-LUV⊃lucigenin under light irradiation condition

The fluorescence-based experiment was done by taking 2940 μL of 20 mM HEPES buffer containing 225 mM NaH_2PO_4 and 50 μL of LUVs in a clean and dry

fluorescence cuvette. The cuvette was placed in the fluorescence spectrophotometer under gently stirring condition for 3 minutes. The lucigenin fluorescence intensity was monitored at t = 0 s, λ_{em} = 505 nm, λ_{ex} = 455 nm. After 3 minutes of stirring, the kinetics was initiated at t = 50 s, by addition of the proanionophore **3.4**. At t = 450 s, the vesicles were finally lysed by addition of 20 µL 20 % Triton X-100. The HPTS fluorescent measurement was carried for a further 50 s (total t = 500 s). At t = 200 s, the kinetics was paused and the fluorescent cuvette was irradiated with light (365 nm) for 5 minutes and the kinetics was reinitiated to monitor the ion transport property. The experiment was repeated by irradiating the sample for 15 minutes this time. Control experiments were repeated without addition of proanionophore **3.4** (DMSO was added in place of **3.4**), and corresponding light irradiaion at t = 200 s for 5 minutes and 15 minutes correspondingly.

3.4.4.13. Biological activity studies of guanidine-based macrocyclic compounds

3.4.4.13.1. MTT-based cytotoxicity assay

The cellular cytotoxicity of the transporters was assessed by the standard 3-[4,5-dimethylthiazol-2-yl]-2,5-diphenyl tetrazolium bromide (MTT) assay on the model cancer cell line, (human cervical cancer) HeLa and normal cell line (human immortalized non-tumorigenic keratinocyte) HaCaT.[25] Approximately, 10^5 cells/well (per 100 µL) were seeded in a 96-well flat-bottom tissue culture plates and grown in media containing 10% fetal bovine serum (FBS) in Dulbecco's Modified Eagle Medium (DMEM) and incubated at 37°C in 5% CO_2 pressure. After 12-16 h, the media was discarded, and each well was washed with phosphate-buffered saline (PBS) followed by the addition of the serially diluted compounds in plain DMEM media without FBS to each well and incubated for 48 h at 37°C in 5% CO_2 pressure. Following, 100 µL of fresh plain DMEM medium with MTT (5mg/mL) were added to wells and incubated for another 3 h at 37°C. MTT containing medium was removed from each well, and the formazan crystal formed was solubilized at 100 µL, and absorbance was recorded on a microplate reader (Multiskan™ GO) at the wavelength of 570 nm. All experiments were performed in triplicate, and the relative cell viability (%) was expressed as a percentage relative to the untreated cells.

3.4.4.13.2. MTT-based cytotoxicity assay using photo-trigger

According to the procedure mentioned in the above section, MTT-based cytotoxicity experiment under light treatment was performed. The media was taken out after 12-16 h of cell culture and subsequently each of the wells were washed with PBS following the addition of different concentrations of the transporters in serial dilution method in plain DMEM media without using FBS in each well and the resulting culture was incubated for 48 h at 37°C in 5% CO_2 pressure. With the help of the glass lid the plate was covered followed by light irradiation for 5 minutes with a LED light (365 nm). Once again, the plates were incubated for 10-12 h. The media was taken out and subsequently each of the wells were washed with PBS following the addition of different concentrations of the transporters in serial dilution method in plain DMEM media without using FBS in each well and the resulting culture was incubated for 48 h at 37°C in 5% CO_2 pressure. In all the wells, MTT reagent (5 mg/mL) was added and the solution was further incubated for another 3 h at 37°C. from each of the well the medium containing MTT was removed. The formazan crystals which were formed was solubilized in 100 µL of SDS-HCl solution. The corresponding absorbance was recorded with the help of microplate reader (Multiskan™ GO) at 570 nm wavelength. The experiments were performed in triplicates and the cell viability (%) was expressed as a percentage relative to the untreated cells.

3.5. ^{1}H and ^{13}C NMR spectra of synthesised guanidine-based macrocyclic molecules

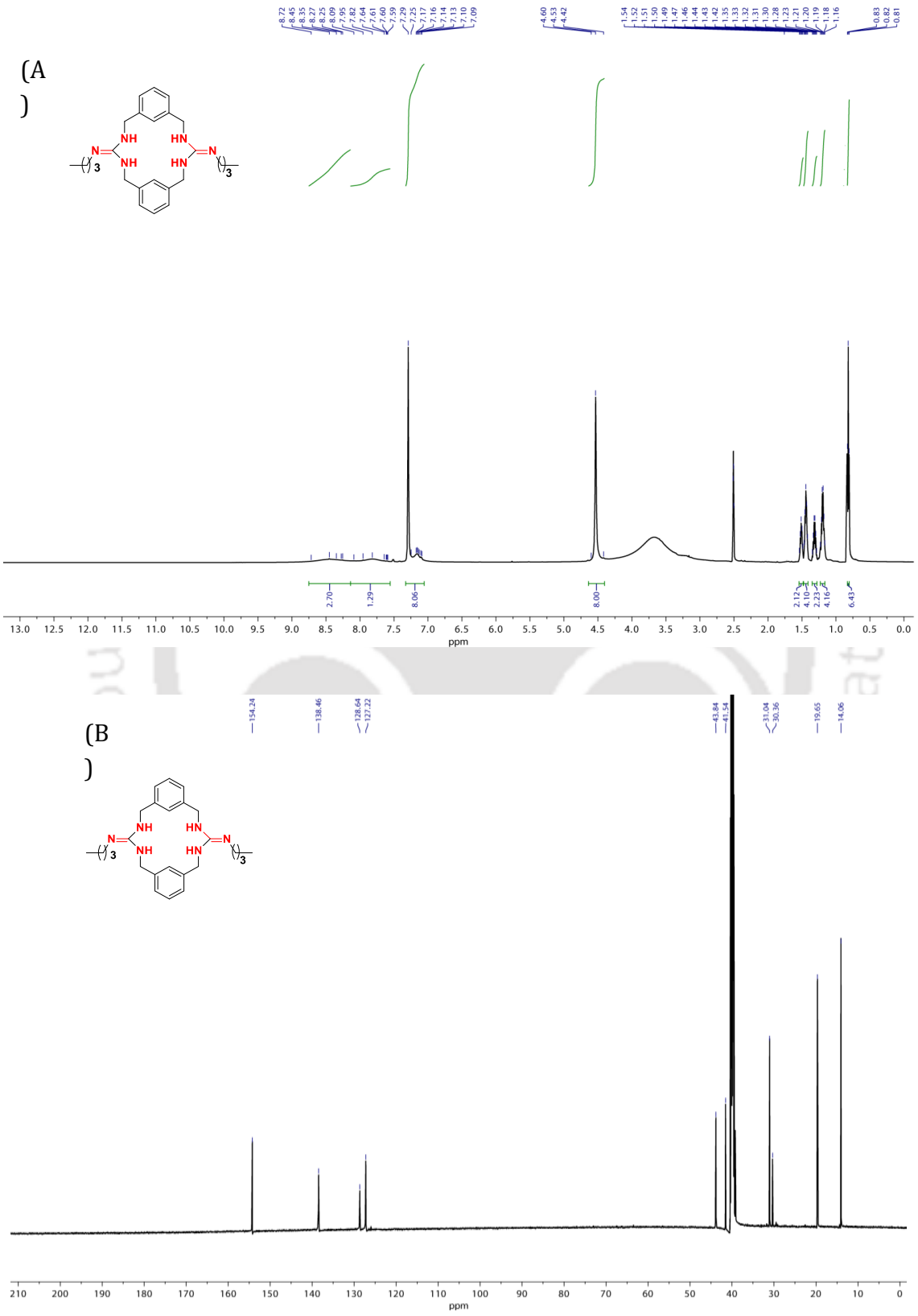

Figure S3.11. ^{1}H NMR and ^{13}C NMR spectra of compound **3.1.**

(A)

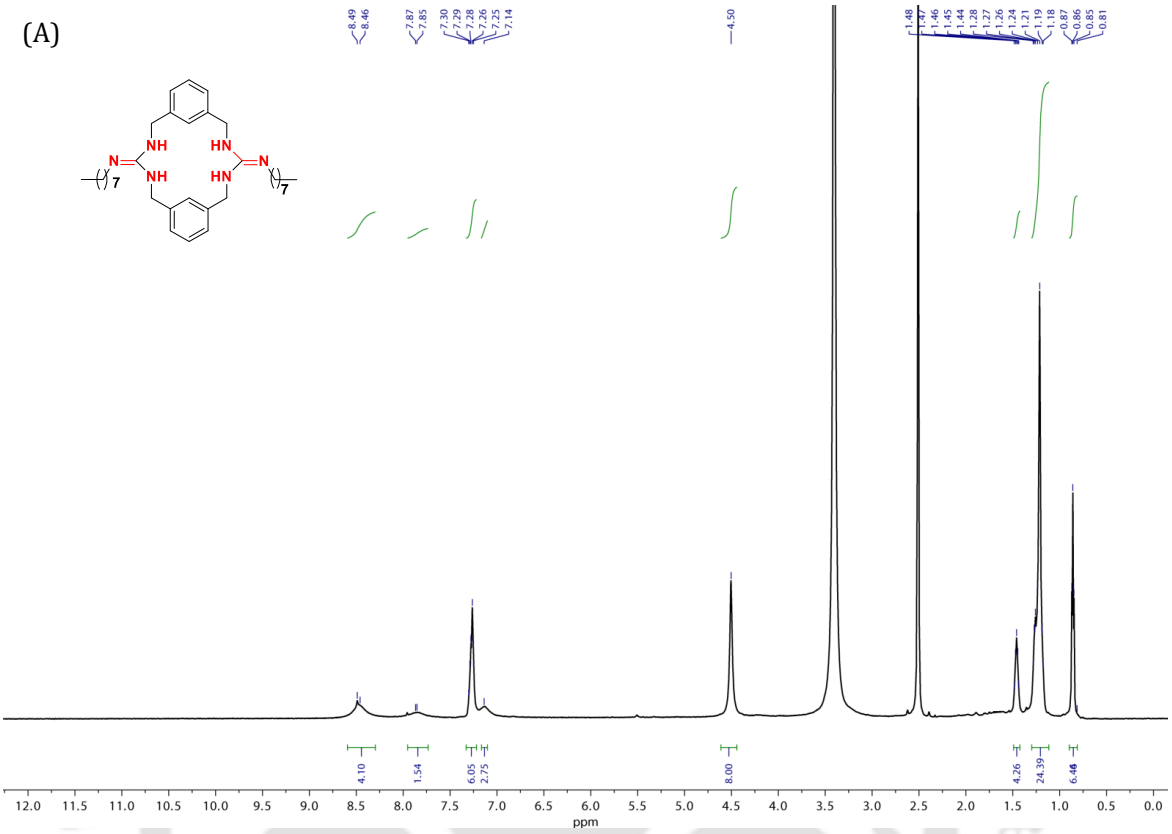

(B)

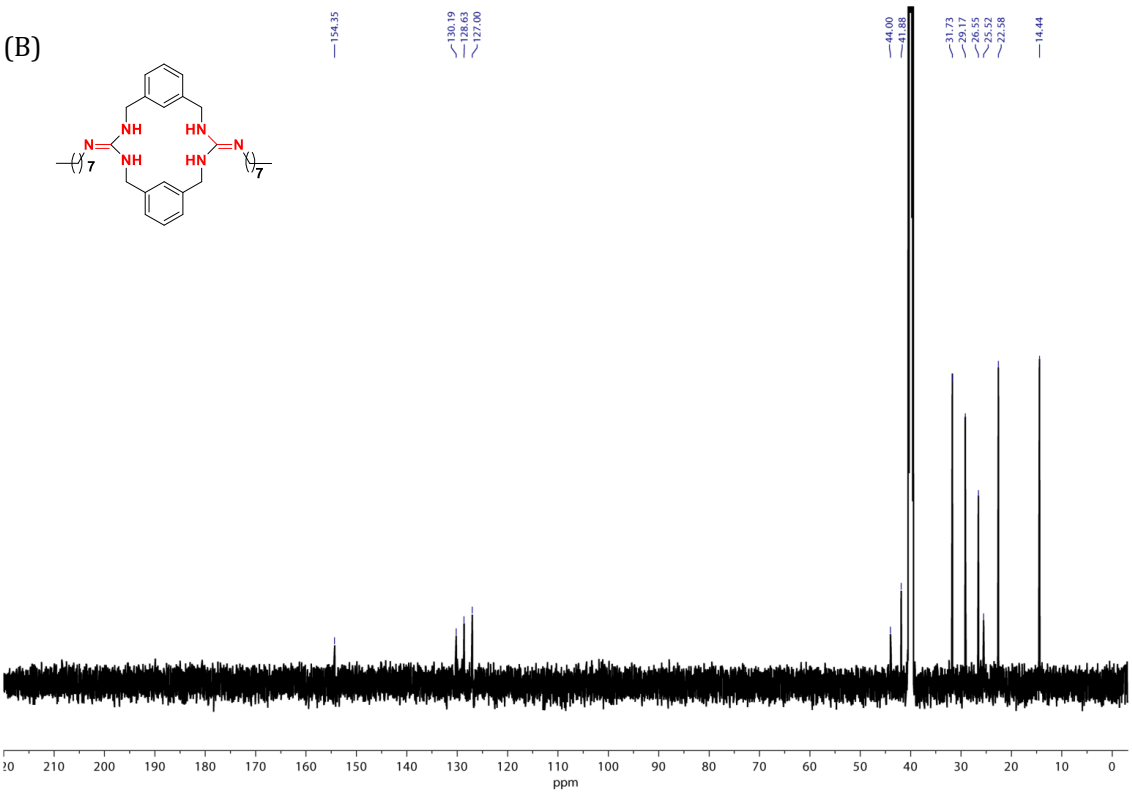

Figure S3.12. ^{1}H NMR and ^{13}C NMR spectra of compound **3.2.**

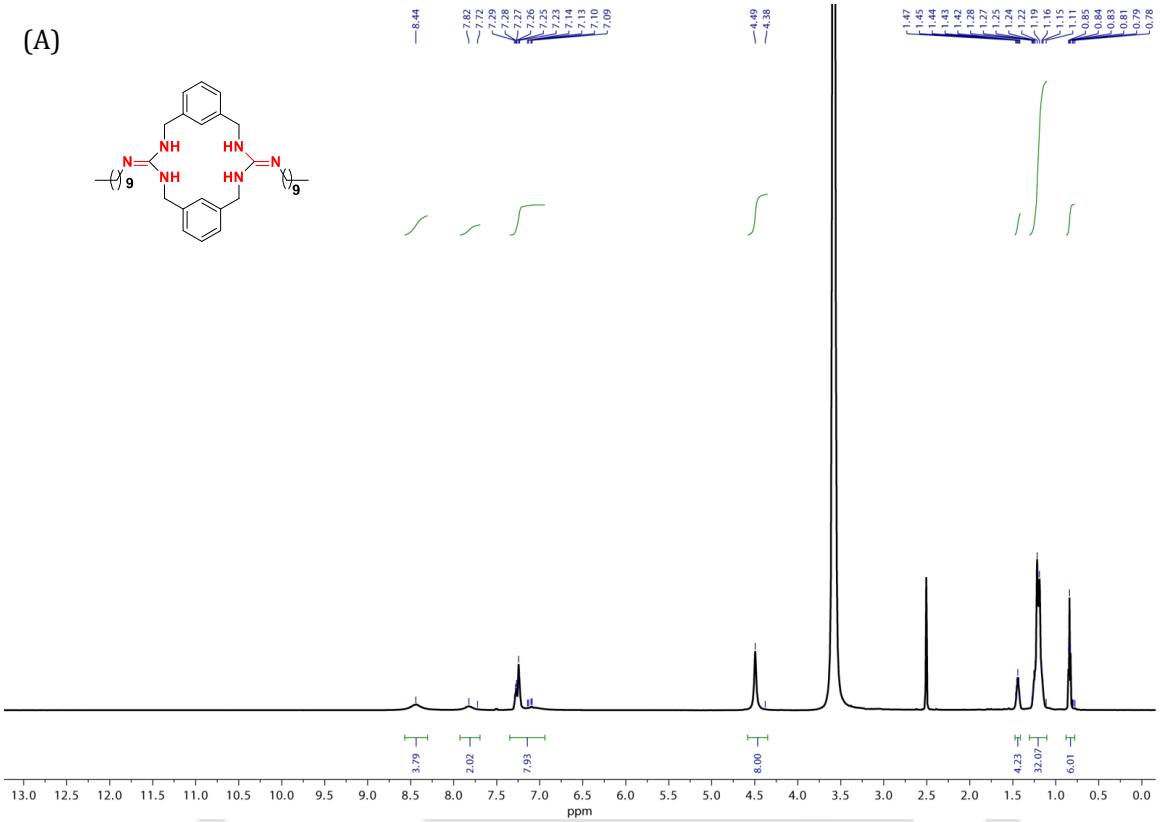

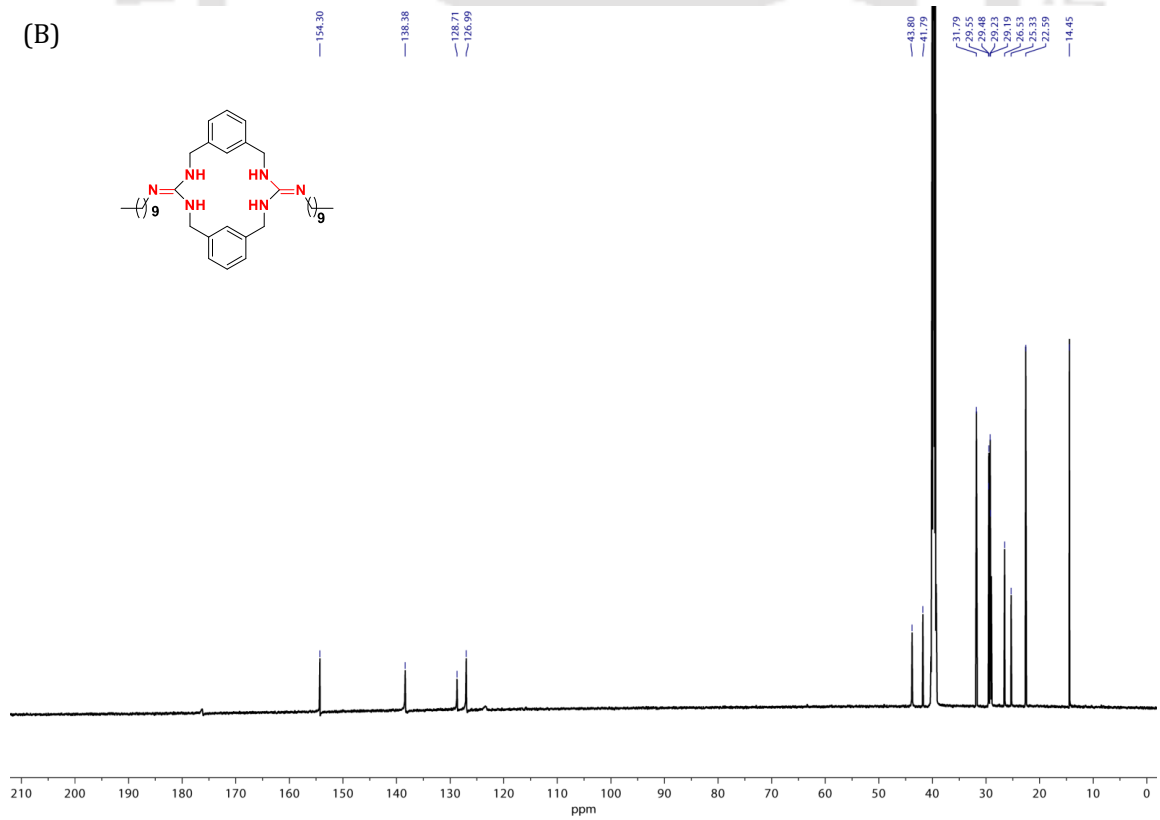

Figure S3.13. ^{1}H NMR and ^{13}C NMR spectra of compound **3.3.**

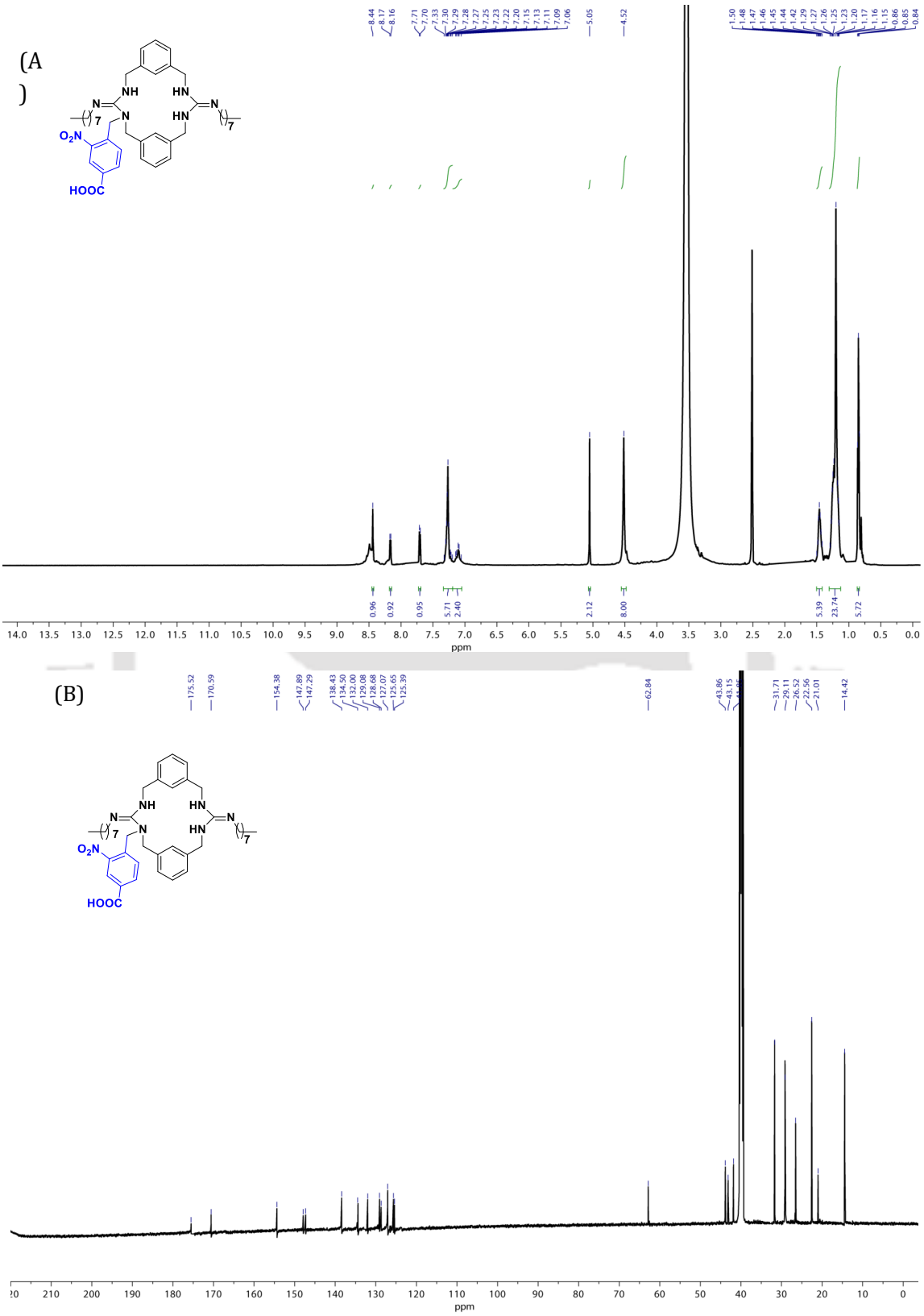

Figure S3.14. ^{1}H NMR and ^{13}C NMR spectra of compound **3.4.**

3.6. References

(1) Levi, M.; Gratton, E.; Forster, I. C.; Hernando, N.; Wagner, C. A.; Biber, J.; Sorribas, V.; Murer, H. J. N. R. N. Mechanisms of phosphate transport. *Nat Rev Nephrol.* **2019**, *15* (8), 482-500.

(2) Salunke, S. B.; Malla, J. A.; Talukdar, P. J. A. C. I. E. Phototriggered Release of a Transmembrane Chloride Carrier from an o-Nitrobenzyl-Linked Procarrier. *Angew. Chem.* **2019**, *58* (16), 5354-5358.

(3) Bao, C.; Ma, M.; Meng, F.; Lin, Q.; Zhu, L. J. N. J. o. C. Efficient synthetic supramolecular channels and their light-deactivated ion transport in bilayer lipid membranes. *New J. Chem.* **2015**, *39* (8), 6297-6302.

(4) Das, S.; Biswas, O.; Akhtar, N.; Patel, A.; Manna, D. J. O.; Chemistry, B. Multi-stimuli controlled release of a transmembrane chloride ion carrier from a sulfonium-linked procarrier. *Org. Biomol. Chem.* **2020**, *18* (45), 9246-9252.

(5) Saha, A.; Akhtar, N.; Kumar, V.; Kumar, S.; Srivastava, H. K.; Kumar, S.; Manna, D. J. O.; Chemistry, B. pH-Regulated anion transport activities of bis (iminourea) derivatives across the cell and vesicle membrane. *Org. Biomol. Chem.* **2019**, *17* (23), 5779-5788.

(6) Cunha, S.; Costa, M. s. B.; Napolitano, H. B.; Lariucci, C.; Vencato, I. J. T. Study of N-benzoyl-activation in the HgCl2-promoted guanylation reaction of thioureas. Synthesis and structural analysis of N-benzoyl-guanidines. *Tetrahedron* **2001**, *57* (9), 1671-1675.

(7) Wu, X.; Gale, P. A. J. C. C. Measuring anion transport selectivity: a cautionary tale. *Chem. Commun.* **2021**, *57* (33), 3979-3982.

(8) Bąk, K. M.; van Kolck, B.; Maslowska-Jarzyna, K.; Papadopoulou, P.; Kros, A.; Chmielewski, M. J. J. C. C. Oxyanion transport across lipid bilayers: direct measurements in large and giant unilamellar vesicles. *Chem. Commun.* **2020**, *56* (36), 4910-4913.

(9) Roy, A.; Saha, D.; Mandal, P. S.; Mukherjee, A.; Talukdar, P. J. C. A. E. J. pH-Gated Chloride Transport by a Triazine-Based Tripodal Semicage. *Chem. Eur. J.* **2017**, *23* (6), 1241-1247.

(10) Malla, J. A.; Sharma, V. K.; Lahiri, M.; Talukdar, P. J. C. A. E. J. Esterase-Activatable Synthetic M+/Cl− Channel Induces Apoptosis and Disrupts Autophagy in Cancer Cells. *Chem. Eur. J.* **2020**, *26* (52), 11946-11949.

(11) Zepik, H. H.; Benner, S. A. Catalysts, anticatalysts, and receptors for unactivated phosphate diesters in water. *J Org Chem* **1999**, *64* (22), 8080-8083. DOI: DOI 10.1021/jo982418+.

(12) Akhtar, N.; Pradhan, N.; Saha, A.; Kumar, V.; Biswas, O.; Dey, S.; Shah, M.; Kumar, S.; Manna, D. Tuning the solubility of ionophores: glutathione-mediated transport of chloride ions across hydrophobic membranes. *Chem Commun* **2019**, *55* (58), 8482-8485. DOI: 10.1039/c9cc04518j.

(13) Das, S.; Biswas, O.; Akhtar, N.; Patel, A.; Manna, D. Multi-stimuli controlled release of a transmembrane chloride ion carrier from a sulfonium-linked procarrier. *Organic & biomolecular chemistry* **2020**, *18* (45), 9246-9252. DOI: 10.1039/d0ob00938e.

(14) Malla, J. A.; Roy, A.; Talukdar, P. J. O. l. Anion selective ion channel constructed from a self-assembly of bis (cholate)-substituted fumaramide. *Org. Lett.* **2018**, *20* (19), 5991-5994.

(15) Akhtar, N.; Saha, A.; Kumar, V.; Pradhan, N.; Panda, S.; Morla, S.; Kumar, S.; Manna, D. J. A. a. m.; interfaces. Diphenylethylenediamine-based potent anionophores: Transmembrane chloride ion transport and apoptosis inducing activities. *ACS Appl. Mater. Interfaces* **2018**, *10* (40), 33803-33813.

(16) Wang, Y. W.; Liu, S. B.; Yang, Y. L.; Wang, P. Z.; Zhang, A. J.; Peng, Y. A Terbium(III)-Complex-Based On-Off Fluorescent Chemosensor for Phosphate Anions in Aqueous Solution and Its Application in Molecular Logic Gates. *Acs Appl Mater Inter* **2015**, *7* (7), 4415-4422.

(17) Akhtar, N.; Biswas, O.; Manna, D. J. O.; Chemistry, B. Stimuli-responsive transmembrane anion transport by AIE-active fluorescent probes. *Org. Biomol. Chem.* **2021**, *19* (34), 7446-7459.

(18) Hanwell, M. D.; Curtis, D. E.; Lonie, D. C.; Vandermeersch, T.; Zurek, E.; Hutchison, G. R. J. J. o. c. Avogadro: an advanced semantic chemical editor, visualization, and analysis platform. *J. Cheminform.* **2012**, *4* (1), 1-17.

(19) Titov, A. V.; Ufimtsev, I. S.; Luehr, N.; Martinez, T. J. J. J. o. c. t.; computation. Generating efficient quantum chemistry codes for novel architectures. *J. Chem. Theory Comput.* **2013**, *9* (1), 213-221.

(20) Jo, S.; Kim, T.; Iyer, V. G.; Im, W. J. J. o. c. c. CHARMM-GUI: a web-based graphical user interface for CHARMM. *J. Comput. Chem.* **2008**, *29* (11), 1859-1865.

(21) Phillips, J. C.; Braun, R.; Wang, W.; Gumbart, J.; Tajkhorshid, E.; Villa, E.; Chipot, C.; Skeel, R. D.; Kale, L.; Schulten, K. J. J. o. c. c. Scalable molecular dynamics with NAMD. *J. Comput. Chem.* **2005**, *26* (16), 1781-1802.

(22) Wang, J.; Wolf, R. M.; Caldwell, J. W.; Kollman, P. A.; Case, D. A. J. J. o. c. c. Development and testing of a general amber force field. *J. Comput. Chem.* **2004**, *25* (9), 1157-1174.

(23) Darden, T.; York, D.; Pedersen, L. J. T. J. o. c. p. Particle mesh Ewald: An N· log (N) method for Ewald sums in large systems. *J. Chem. Phys.* **1993**, *98* (12), 10089-10092.

(24) Miyamoto, S.; Kollman, P. A. J. J. o. c. c. Settle: An analytical version of the SHAKE and RATTLE algorithm for rigid water models. *J. Comput. Chem.* **1992**, *13* (8), 952-962.

(25) Akhtar, N.; Pradhan, N.; Barik, G. K.; Chatterjee, S.; Ghosh, S.; Saha, A.; Satpati, P.; Bhattacharyya, A.; Santra, M. K.; Manna, D. J. A. a. m.; et al. Quinine-based semisynthetic ion transporters with potential antiproliferative activities. *ACS Appl. Mater. Interfaces* **2020**, *12* (23), 25521-25533.

Chapter 4

Targeted Delivery of Pro-anionophore: Photo-induced transport of Cl^- ion Across the Lipid Bilayer

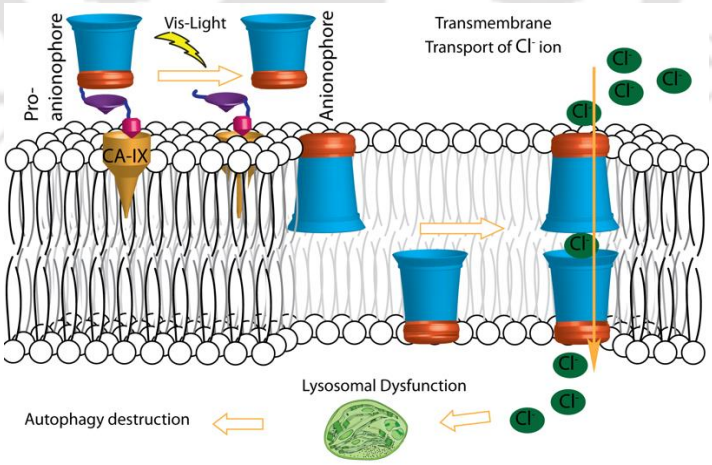

4.1. Background and objective of present work

Maintaining a harmony of the ions across the cells is vital in maintaining very important cellular processes. This osmolality is maintained with the help of intricately designed transmembrane proteins spanning across the lipid bilayer and 'ferrying' charged ions. Many of these transmembrane proteins depict gated behaviour like voltage-gating, ligand-gating, mechanical gating, etc.[1, 2] Regardless of the smooth functioning of the natural ion channels many a times due to mutation, disruption in the normal transport of the ions take place giving rise to many disease conditions known as channelopathies. Over the last two decades several attempts have been made by supramolecular chemists around the world to replicate the ion transport properties of the natural ion transporters with the assistance of small organic molecules capable of carrying ions across the vesicles. This ion transport property of the synthetic ion transporters has triggered apoptosis in the cancer cells, but along the cancer cells cytotoxicity have also been somewhat observed in the normal cells which is detrimental. To reduce the toxicity towards the normal cells several approaches were taken including mimicking the gating behaviour of the natural gated ion channels. For the last few years pH, mechanical stress, presence of a chemical in high concentration in the cancer cells, light has been successfully used to discriminate the cancer cells from the normal cells.[1-3] Light as a stimulus is very appealing due to the high spatio-temporal control it provides and its good bio-orthogonality. If the active anionophore is installed with a photo-separable, then the active anionophore will be judiciously generated in the cancer cells. This will result in the anionophore differentiating the healthy cells from the diseased cells. Here in this work, we have adopted a "photocleavable targeted-proanionophore" strategy designing a cancer cell targeted proanionophore intended to alleviate the toxic effects of anionophores on the normal cells. Previously *o*-nitrobenzyl (ONB) group has been used in few cases to produce the active anionophore. Simultaneously many light-triggered prodrugs were utilised in drug delivery and these candidates exhibited excellent photodynamic therapy (PDT). So encouraged from these reports the photo activated proanionophore was designed incorporating three salient fusings. Firstly, the macrocycle which serves as the principal ion recognition unit. It has been instilled with three hydrophobic cholic amine groups which is responsible for the membrane insertion property. The photolabile moiety has been implanted

with the cancer cell directing acetazolamide moiety that will help the proanionophore in targeting the cancer cells selectively and ensure that the anionophore is generated in the cancer cells selectively. Acetazolamide is a known carbonic anhydrase-IX (CA-IX) inhibitor which is over-expressed in some cancer cells. It has been reported that CA-IX assists the cancer cells in adapting to the microenvironmental conditions like hypoxia, deprived nutrient condition, slight acidity among others.[4] Hence using the inhibition capacity of acetazolamide in addition to that of the anionophoric capability of the anionophore can be utilised to effectively achieve cancer cell death.[5]

The concept of photocaging was already explored by few other groups. However, in their case and also in the previous chapter of this thesis, it has been observed that the photocleavage event occurs at 365 nm. In some cases, the duration of UV irradiation is higher (45 minutes) which may prove damaging to the normal cells. A proanionophore was designed by grafting the photoresponsive *o*-nitrobenzyl group with the crown ether moiety bestowing photosensitivity to the ion channels. However, in this case light irradiation disrupts channels formation and therefore ion transport giving control over the turn off of the ion transport property while the opposite would have been more beneficial.

Consequently, in this work the conjugation in the photolabile moiety has been augmented to be able to cleave the photo group at a higher wavelength (> 400 nm). It has been done by using 7- aminocoumarin group in the photolabile group which exhibits long wavelength absorption properties and good photolysis efficiency. 7-aminocoumarin group has intrinsic fluorescent properties and favourable biocompatible results.[6, 7] The active anionophore is linked with the photolabile squaric acid (SA)-coumarin (CM)-acetazolamide (AZ) tether was hypothesised to synergistically cause cancer cell death because of both PDT and the ion transport property.[8, 9]

4.2. Results and discussions

4.2.1. Design and synthesis of the synthetic ionophore derivatives

In this work the design and synthesis of cholic amine instilled guadinium-based macrocycles has been discussed. Cholic acid's hydrophobic β-face may be responsible for the membrane insertion property of the anionophore and the opposite face may be responsible for providing the polar path requisite for ion

recognition. It was envisaged that the guanidine-based macrocycle would help in recognising and binding the Cl^- ion and the hydroxyl groups of the cholic amine moiety would help in facilitation of the transport process across the lipid bilayer. The designed proanionophore facilitates the targeted delivery of the proanionophore specifically to the cancer cells and subsequently photo-triggered discharge of the anionophore. The designed photo-responsive targeted proanionophore has several benefits-(I) presence of a cancer cell targeting group, (II) photo-induced discharge of the active anionophore under light irradiation at slightly higher wavelength (>400 nm), (III) highly selective Cl^- ion transport behaviour, (IV) anticancer activities due to the synergistic effect of the ionophoric activities and PDT effect of the photocleavable moiety photoproduct (AZ-SA-CM-OH).

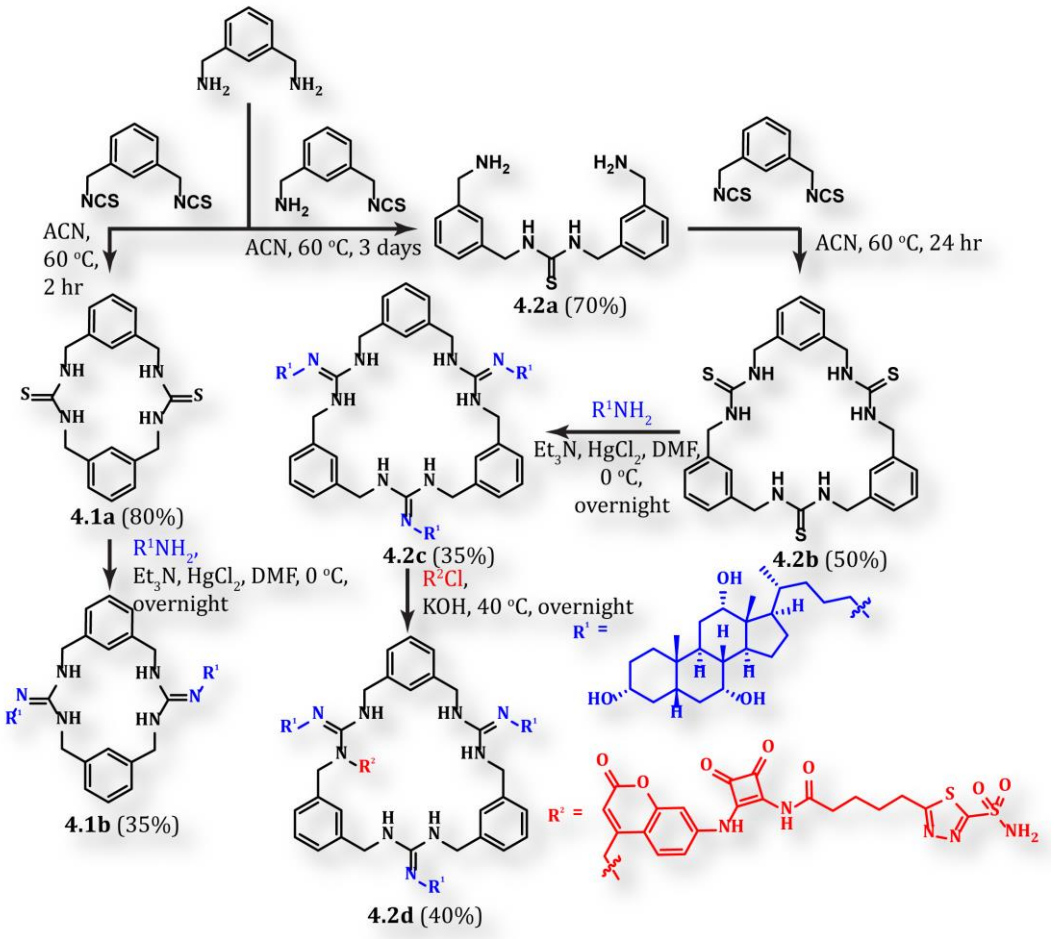

Scheme 4.1. Synthetic route to the macrocyclic anion transporters.

The thiourea-based macrocycle was prepared according to the reported protocol using 1,3-phenylenedimethanamine, (3-(isothiocyanatomethyl)phenyl)methanamine, and 1,3-

bis(isothiocyanatomethyl)benzene in two steps. Then guanidium group was introduced by installing cholic amine groups in the macrocycle.[10] A smaller 16-membered guanidium-based macrocycle was also synthesized using 1,3-phenylenedimethanamine and 1,3-bis(isothiocyanatomethyl)benzene. Cholic amine was then appended to the macrocycle in presence of $HgCl_2$ and Et_3N to introduce the guanidium groups in the macrocycle. The smaller macrocycle was synthesised to check its Cl^- transport property and compare it with **4.2c**. Eventually the cancer-cell directing photo-labile group AZ-SA-CM-Br (**4.7**) was connected with the macrocycle to attain the proanionophore **4.2d**. The proanionophore can be visualized as barrel-shaped transporter which can shelter the hydrophilic ion in the cavity and shield the charge of the ion from the hydrophobic environment of the lipid bilayer (Scheme 4.1 ans 4.2).

4.2.2. Anion binding studies of the synthetic ionophore derivatives

Initially with the help of UV-based titration of **4.2c** with Cl^- ions, the binding stoichiometry of **4.2c** with Cl^- was evaluated. Here interestingly it was found that **4.2c** the binds with Cl^- in a 2:1 host/guest stoichiometry, calculated from BindFit analysis. From the corresponding studies it can be concluded that **4.2c** recognises the ions in a moderately good manner.

4.2.3. Chloride ion transport activities of the synthetic ionophore derivatives

Nextly the ion transport properties of the anionophores were tested initially in EYPC/CHOL-LUV⊃lucigenin. bis-*N*-methylacridinium nitrate (lucigenin) is very much sensitive to the concentration of Cl^- ions. Hence lucigenin has been used in this case. The LUVs were prepared by taking EYPC and CHOL in 8:2 ratio encapsulating 20 mM HEPES buffer containing 225 mM $NaNO_3$ and 1 mM lucigenin and were suspended in 20 mM HEPES containing 225 mM NaCl, pH 7.2. Initially the transport activities of **4.1a**, **4.1b**, **4.2b**, **4.2c** and **4.2d** were checked in this system. After transporter addition at t = 50 s, the lucigenin intensity was observed to decrease signifying Cl^- transport. Transporter **4.2c** has shown highest Cl^- transport in the system. Compound **4.2d** has showed unsubstantial Cl^- transport ability which could be due to its photo-labile appendage which shields the ion recognizing frame from the ion. The lower brim contains the cholic amine groups which help in ion passage

through them but can't trap them from the aqueous milieu consequently showing very less Cl^- transport (Fig. 4.1).

The dose-dependent experiment using different concentrations of the ion transporter, **4.2c** was done to determine the transport efficiency of the transporters. This experiment also demonstrated that **4.2c** (EC_{50} = 3.30 μM) is proficient in transporting Cl^- across the vesicles. Another interesting feature was noted while calculating the EC_{50} values, the hill coefficient value (n) of **4.2c**, which denotes the number of species participating to transport Cl^- ion, was found to be close to 2.0. It denotes two **4.2c** molecules are required to carry the transport process. [11] The involvement of two transporters in case of **4.2c** may be the reason for its better transport activity.

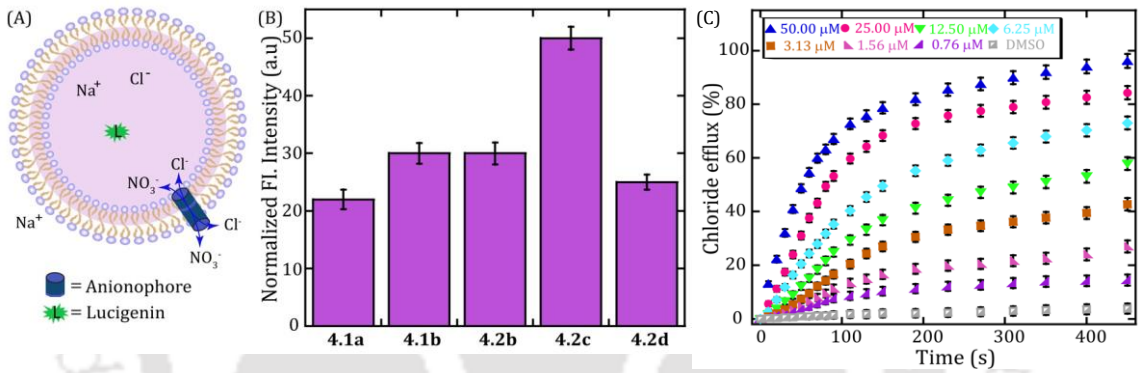

Figure 4.1. Representative scheme of chloride transport across the EYPC/CHOL-LUV⊃Lucigenin (A), the ion transport activity of different ionophores (3.3 μM) across the EYPC/CHOL-LUV⊃Lucigenin (B). Cl^- ion transport activity of **4.2c** across EYPC/CHOL-LUV was measured by chloride ion-selective electrode at pH 7.2 (C).

4.2.4. Relative cation and anion selectivity studies of the synthetic ionophore derivatives

Next the ion selectivity of the transporters was investigated using EYPC/CHOL-LUV⊃HPTS. The corresponding LUVs were prepared using 8:2 EYPC:CHOL in molar ratio. The LUVs were prepared using 20 mM HEPES buffer containing 225 mM NaCl and 1 mM HPTS dye. NaOH was added in the extravesicular buffer to create a pH gradient (ΔpH = 0.8) across the vesicles. [13, 14] The LUVs were dispersed in 20 mM HEPES buffer containing 225 mM Na_xA_y (where A = Cl^-, Br^-, I^-, ClO_4^-, and NO_3^-). The kinetics was initiated at t = 50 s after addition of the transporter. Among the ions

tested, **4.2c** showed highest selectivity for Cl^- (Fig. 4.2A). However, on repeating the experiment by varying the cations (Li^+, Na^+, K^+, Rb^+ and Cs^+) insignificant difference in pH dissipation by the transporter was observed stating the fact that Cl^- transport efficiency is almost similar in all the cases. Thus, from the result it can be derived that the cations don't participate in the mechanistic pathway (Fig. 4.2B).

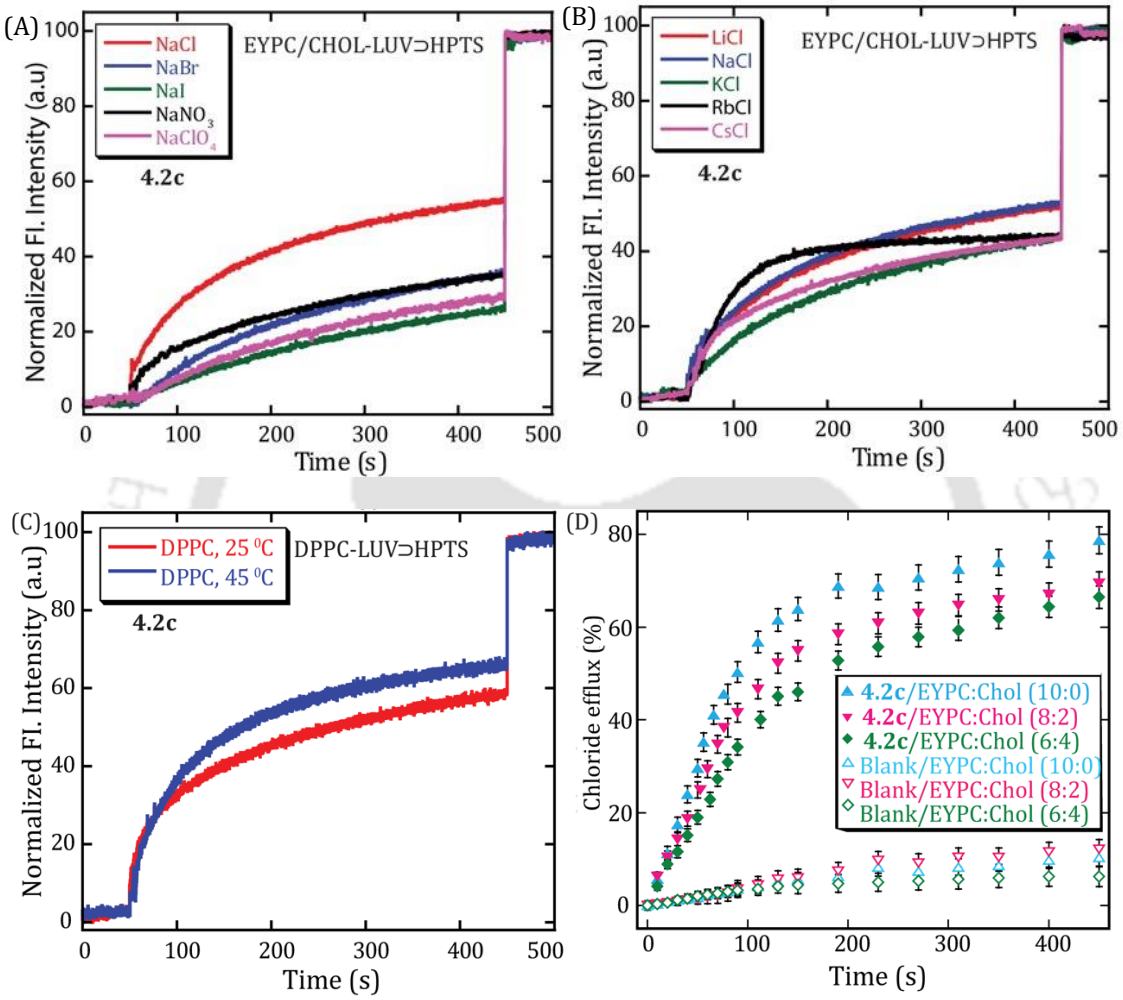

Figure 4.2. Anion selectivity of compound **4.2c** (3.3 μM) using the HPTS assay across EYPC/CHOL-LUVs⊃HPTS (A). Cation selectivity of compound **4.2c** (3.3 μM) using the HPTS assay across EYPC/CHOL-LUVs⊃HPTS (B). Temperature-dependent HPTS assay with aninophore **4.2c** (C). Effect of the concentration of cholesterol in the EYPC/CHOL membrane on Cl^- ion transport properties of aninophore **4.2c** (D).

4.2.5. Mechanism of chloride ion transport activities of the synthetic ionophore derivatives

Beside the Cl^-/NO_3^- pathway, the other possible pathways are M^+/Cl^-, M^+/OH^-. The initial two prospects can be negated from the result obtained from the metal ion selectivity experiment. To delve into the transport mode of transporter **4.2c**, the Cl^- ion transport activity of **4.2c** was checked across DPPC-LUV⊃HPTS at 25 °C and 45 °C. The Cl^- ion transport activity of **4.2c** was found to be the same in both the temperatures which suggests the transporter is not following carrier pathway to transport ions across the vesicles (Fig. 4.2C). It is highly possible that the two molecules of transporter **4.2c** are responsible for creating pores across the lipid bilayer through which the transport takes place. To substantiate this hypothesis, additionally the cholesterol dependency experiment was done. In this experiment, the cholesterol concentration in preparation of the vesicles were varied and the resulting effect in the chloride ion transport activity was observed. It was noticed that the chloride efflux changed insignificantly upon increasing the cholesterol concentration in the vesicles (Fig. 4.2D). This result also corroborated the fact that bi-molecular pore formation may be the dominant operative pathway. [15, 12]

4.2.6. Regeneration of the active anionophore from proanionophore

Now, to check the regeneration of the active anionophore fluorescent-based experiment was performed. The photo-product is fluorescent in nature due to the extended conjugation present in the molecule. With the cleavage happening under light irradiation (405 nm), the concentration of the photo product increases upon increase in light exposure time of the targeted proanionophore. Initially in absence of light irradiation (405 nm) upon excitation of the proanionophore **4.2d** at 410 nm. no significant peak was observed. Upon light irradiation (405 nm) for different time periods (10 secs, 1 minute, 2 minutes, 3 minutes, 5 minutes, 10 minutes, 20 minutes, and 30 minutes), a sharp peak centered at 513 nm was noticed, the fluorescence intensity of which went on increasing with increase in light exposure time. This happens due to increase in the fluorescent photo-product. The regeneration studies were studied with the help fluorescent-based kinetics studies and ion selective electrode (ISE)-based kinetic studies. In case of fluorescent-based regeneration studies, the initial kinetics was initiated with the addition of the anionophore at t =

50 s. At t = 100 s, the fluorescence cuvette was irradiated with light (405 nm) for 5 minutes, 10 minutes and 20 minutes respectively for different

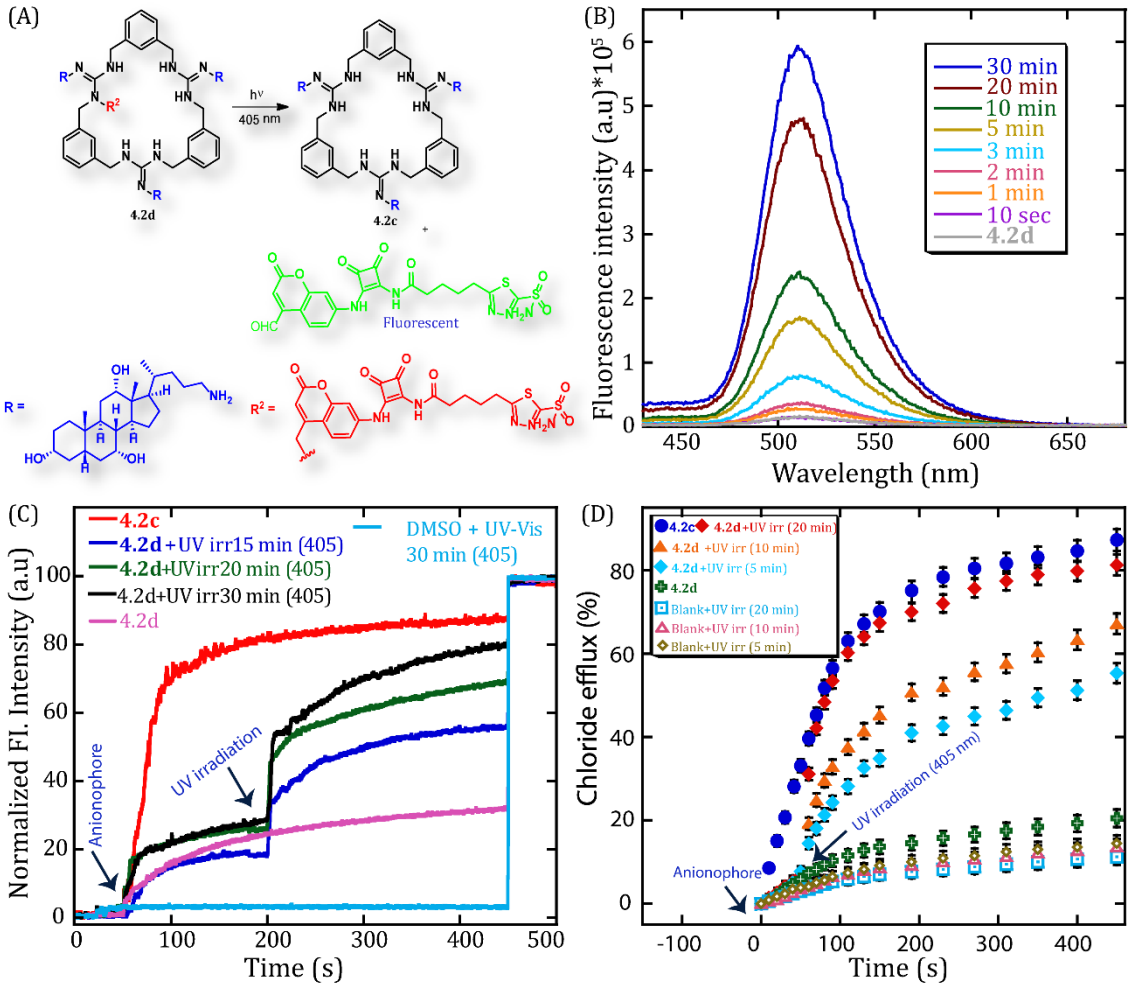

Figure 4.3. The proposed regeneration pathway of the active anionophore (**4.2c**) from the proanionophore (**4.2c**) (A). Measurement of active anionophore regeneration in the fluorescence cuvette upon UV irradiation (B). The Cl^- ion transport property of **4.2d** upon UV irradiation was studied through the HPTS-based fluorescence method (C). The Cl^- ion transport property of **4.2d** upon UV irradiation was studied through the ISE-based method (D) [13].

experiment sets and the kinetics was again started and correspondingly recorded. It was discerned that after light irradiation, the pH dissipation mediated by proanionophore increases proving the fact that due to light irradiation the anionophore is regenerated which leads to increase in the Cl^- ion transport. With the help of ISE also it was observed that after light irradiation (405 nm), the chloride

efflux from the LUVs has increased. From these experiments the regeneration of the active anionophore and the photo product could be discerned (Fig. 4.3).

4.2.7. Activities of the synthetic ionophore under Cellular Environment

Studies on the cancer cells reveals that the extracellular concentration of Cl^- ions are higher (110 mM) than the intracellular concentrations (40 mM-80mM), i.e., an ion gradient is maintained across the tumour cells. Hence it was hypothesised that

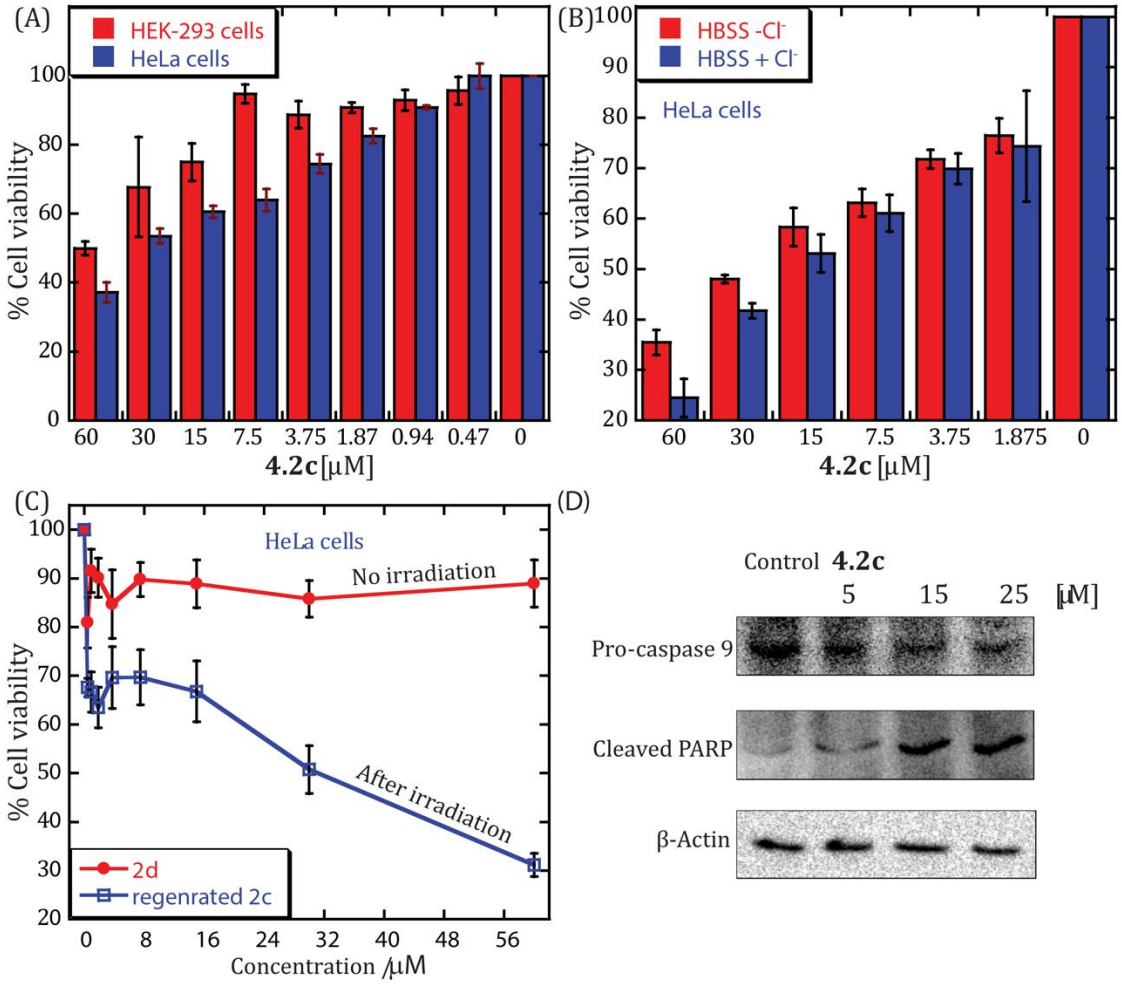

Figure 4.4. Viability of HeLa and HEK-293 cells in the presence of different concentrations of anionophore **4.2c** (A). Viability of HeLa cells in the absence and presence of Cl^- ions in the HBSS buffer in the presence of different concentrations of anionophore **4.2c** (B). Viability of HeLa cells without or with light irradiation (405 nm, 5 min) (C). Western blot analysis of HeLa cells in the presence of anionophore **4.2c** (D). The pro-casepase 9, PARP and β-actin antibodies were used to develop the Western blot. All measurements were performed in triplicates.

the active anionophore also will be capable of disrupting the Cl^- ion gradient across the tumour cells and hence may be able to trigger apoptosis in the disease cells. Initially the cell viability was checked in HeLa cells (cervical cancer cell line), T47D (breast cancer cell line) and HEK-293 (normal embryonic kidney) in presence of proanionophore **4.2d** under 5 minutes of light irradiation (405 nm). In the normal cell line (HEK 293), the cells did not show significant cytotoxicity up to 60 μM of concentration under 5 minutes of light irradiation of the proanionophore. This shows that the active anionophore which was regenerated due to light irradiation didn't show that much toxicity to the normal cell line. In the HeLa cell line however under similar conditions, the toxicity was seen from 15 μM of concentration of the proanionophore **4.2d**. In HeLa cell lines carbonic anhydrase IX is present in high concentration, hence it can be derived that the toxicity which was seen was not only because of the anionophoric activity of the active anionophore but also due to the inhibition of CA-IX with the acetazolamide moiety present in the photo-product and the PDT (photodynamic therapy) effect due to the photo-product. In T47D cell lines however, CA-IX is absent due to which the toxicity was somewhat less, just because of the disruption of the ion gradient created because of the active anionophore present. The toxicity of the proanionophore in absence of UV irradiation was also checked and the results confirm that the toxicity obtained was much less than that under the influence of UV irradiation which signifies that the proanionophore itself is not toxic to the cancer cells unless the active anionophore is released under light irradiation (405 nm) conditions. To confirm that the toxicity seen under light irradiation condition was not because of light irradiation induced toxicity a control experiment was done in absence of any transporter only applying light irradiation for 5 minutes. The insignificant toxicity results obtained manifest that the toxicity obtained before was not because of 5 minutes light treatment of the proanionophore. Following this to know whether the Cl^- concentration is responsible for the toxicity of the cancer cells or not, the cell viability of the HeLa cells in the cancer cells were checked in HBSS buffer in presence and absence of Cl^- ion. In presence of Cl^- ion, the cell viability of the HeLa cells obtained was much less than in absence of Cl^- ion. In case of intrinsic pathway of apoptosis activation, apoptosome forms due to binding of the released cytochrome c with Apaf-1. This in turn activates the caspase 9 pathway (procaspase 9 gets converted to caspase 9) which subsequently triggers the

caspase 3 pathway. Hence, to check whether the mode of cell death was by apoptosis or any other event, the concentration of the procaspase-9 was investigated with the help of immunoblot experiment I HeLa cells on addition of proanionophore **4.2d** and subsequent light irradiation for 5 minutes thereafter. The blot showed an inverse relation of the concentration of the proanionopore with the procaspase 9 concentration. Alternatively, poly(ADP-ribose) polymerase (parp-1) has also been known to promote apoptotic pathway by prohibiting DNA repair. Increase in concentration of cleaved parp was observed in the experiment with increase in concentration of proanionophore. These results suggest apoptosis triggered cell death.

Cleavage of the photoproduct upon light irradiation can lead to ROS production. To test this hypothesis a ROS probe, 2', 7'-dichlorodihydrofluorescein (H_2DCFDA) was used to detect the ROS generation in cells. In the diacetate state the probe is in its non-fluorescent state. Due to hydrolysis of the ester groups due to esterases followed by oxidation in presence of ROS results in a green fluorescent 2',7'-dichlorofluorescein (DCF). The HeLa cells were stained with proanionophore in a time dependent manner, light irradiated for 5 minutes and then the cells were stained with H_2DCFDA dye. Upon analyses under a confocal microscope a time-dependent increase in green fluorescence of the dye indicates time dependent increase in ROS-generation.

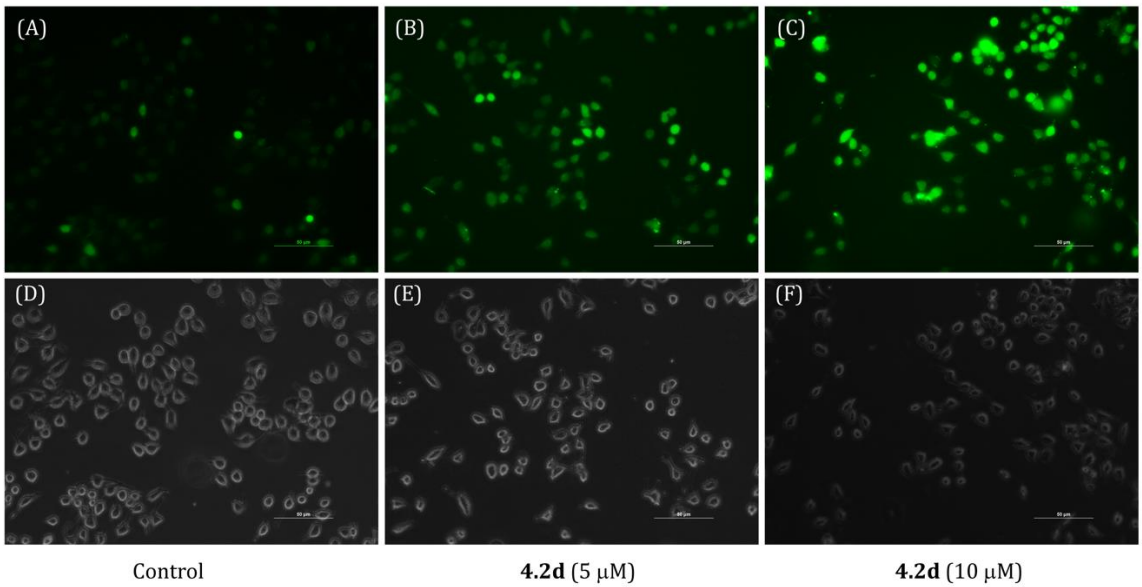

Figure 4.5. Live cell images of HeLa cells incubated with compound **4.2d**, and H_2DCFDA as ROS probe in a concentration dependent manner

4.3. Summary

Briefly, in this work the cholic acid-functionalized guanidine-based macrocyclic derivatives were discussed. The macrocyclic moiety was mainly chosen to efficiently bind the Cl^- ions. The cholic functionality imparted hydrophobicity to overall structure. The most potent guanidine-based macrocyclic derivative **4.2c** forms a bi-molecular pore across the lipid bilayer to transport Cl^- ion. The attached photolabile tether to the anionophore containing acetazolamide derivative and the photosensitive coumarin group helped to effectively target the cancer cells without showing much toxicity to the normal cells. Irradiation with visible light (405 nm) helped to achieve a controlled way of regenerating the active anionophore **4.2c** from its proanionophore both under in vitro and cellular conditions as indicated by the experiments conducted, promising real-life applications of the anionophores. To the best of our knowledge, the current study reveals the first example of an inherently fluorescent photocleavable targeted-proanionophore, which has the potential to function as a gated ion transport system.

4.4. Experimental Procedures

4.4.1. General information

The information of reagents, solvents and data accruing instrumentation were similar as mentioned in section 2.4.1.1.

4.4.2. Synthesis and characterization of compounds

4.4.2.1. Synthesis of 3,5,9,11-tetraaza-1,7(1,3)-dibenzenacyclododecaphane-4,10-dithione (4.1a)

To a gently stirring solution of 100 mg 1,3-bis(isothiocyanatomethyl)benzene in acetonitrile (100 mL), was dropwise added a 30 mL acetonitrile solution of 1,3-phenylenedimethanamine (61 mg) over 30 minutes time. After 15 minutes of stirring white precipitation occurs. After I hour of stirring and maximum consumption of the starting material as monitored by TLC, the precipitate was filtered and the white precipitate was used for the next step as such without further purification. All the characterization data have been compared with the literature data.

4.4.2.2. Synthesis of compound 4.1b

To a gently stirring DMF solution of **4.1a** (300 mg, 1 equiv.), NEt_3 (0.59 mL, 10 equiv.), cholic acid (1658 mg, 5 equiv) was added sequentially under ice condition (5

°C). The resulting solution was stirred for 40 minutes after which $HgCl_2$ (2287 mg, 10 equiv) was added. The entire solution turned black after stirring due to formation of HgS and the solution was stirred overnight. After maximum consumption of the starting material, HgS was filtered using celite bed. The resulting solution was concentrated in-vacuo under reduced pressure to obtain a solid product. The crude product was purified with column chromatography using silica gel with MeOH/DCM (0-30%): as the solvent gradient system to obtain the white-coloured pure product. The compound was characterized by ^{1}H NMR, ^{13}C NMR and HRMS analyses.

^{1}H NMR (500 MHz, DMSO-d_6) δ_{ppm} 8.2 (brs, 1H), 8.03 – 7.94 (m, 2H), 7.30 – 7.06 (m, 8H), 4.67 - 4.66 (s, 8H), 4.13 - 3.99 (m, 6H), 3.79 (s, 3H), 3.61 (s, 3H), 3.22 -3.16 (m, 3H), 2.26 – 1.96 (m, 14H), 1.82 – 1.61 (m, 14H), 1.48 – 1.10 (m, 22H), 1.01 – 0.81 (m, 12H), 0.59 (s, 6H). ^{13}C NMR (125 MHz, DMSO-d_6) δ_{ppm} 140.7, 128.1, 125.3, 123.2, 71.5, 70.9, 66.8, 47.6, 46.9, 46.6, 46.3, 42.0, 41.9, 35.8, 35.6, 35.4, 34.9, 32.8, 31.5, 31.4, 30.9, 29.0, 27.8, 26.7, 23.3, 23.1, 17.4, 12.8. HRMS (ESI) calcd. for $C_{99}H_{153}N_9O_9$ $(M+H)^+$: 435.3231, found: 435.3250.

4.4.2.3. Synthesis of 3,5,9,11,15,17-hexaaza-1,7,13(1,3)-tribenzenacyclooctadecaphane-4,10,16-trithione

The synthesis was carried out in accordance with a reported protocol in literature.

4.4.2.4. Synthesis of compound 4.2b

The macrocycle was prepared in accordance with a reported protocol in the literature. All the characterization data have been matched with the literature data for the compound.

4.4.2.5. Synthesis of compound 4.2c

To a gently stirring DMF solution of **4.2b**, NEt_3 (1.17 mL, 15 equiv.) and cholic amine (1656 mg, 7.5 equiv.) were added sequentially under ice condition (5 ^{0}C). After stirring the solution for around 40 minutes, $HgCl_2$ (2284 mg, 15 equiv.) was added to the solution. After 15 minutes of stirring, the solution turned black due to the formation of black coloured HgS. The reaction was stirred overnight. After maximum consumption of the starting materials, the solution was filtered using celite bed and the filtrate was collected and concentrated under reduced pressure to obtain the

crude product. The crude product was then purified with column chromatography using silica gel with MeOH/DCM (0-30%): as the solvent gradient system to obtain the white-coloured pure product.

^{1}H NMR (600 MHz, DMSO-d_6) δ_{ppm} 8.11 – 7.80 (brs, 4H), 7.38 – 7.16 (m, 12H), 4.66 (s, 12H), 4.48 - 4.44 (m, 3H), 4.19 (s, 3H), 4.08 (s, 3H), 3.78 (s, 4H), 3.21 - 3.16 (m, 3H), 2.25 - 2.07 (m, 13H), 1.99 - 1.91 (m, 3H), 1.80 – 1.62 (m, 20H), 1.45 -1.11 (m, 38H), 0.99 – 0.80 (m, 24H), 0.58 (s, 10H). ^{13}C NMR (150 MHz, DMSO-d_6) δ_{ppm} 151.6, 140.6, 128.6, 126.8, 123.9, 71.5, 71.4, 66.7, 46.6, 46.5, 46.2, 46.1, 41.9, 41.8, 35.7, 35.5, 35.4, 35.3, 34.9, 31.3, 31.2, 30.8, 28.9, 27.8, 26.6, 23.3, 23.1, 17.4, 12.8. HRMS (ESI) calcd. for $C_{99}H_{153}N_9O_9$ $(M+H)^+$: 435.3231, found: 435.3250.

4.4.2.6. Synthesis of 5-amino-N-(5-sulfamoyl-1,3,4-thiadiazol-2-yl)pentanamide (4.5)

To a gently stirring DMF solution of compound **4.4** (1 equiv,100 mg), 5-aminopentanoic acid (1 equiv, 65 mg), HBTU (2 equiv., 420.92 mg), DIPEA (1.5 equiv, 0.15 mL) and HOBt (2 equiv, 150 mg) was added sequentially. The solution was stirred overnight at room temperature. After maximum consumption of the starting materials, the solution was concentrated under reduced pressure. Saturated solution of NH_4Cl (10 mL) was poured in the mixture and the compound was extracted 3 times using EtOAc (30*3 mL). The crude product was purified with column chromatography using silica gel with MeOH/DCM (0-20%): as the solvent gradient system to obtain the white-coloured pure product. The compound was characterized by ^{1}H NMR, ^{13}C NMR and HRMS analyses. ^{1}H NMR (600 MHz, DMSO-d_6) δ_{ppm} 8.72 – 8.25 (brs, 3H), 8.09 – 7.59 (brs, 1H), 7.29 – 7.09 (brs, 8H), 4.60 - 4.42 (s, 8H), 1.54 - 1.49 (m, 2H), 1.47 – 1.42 (m, 4H), 1.35 -1.28 (m, 2H), 1.23 – 1.16 (m, 4H), 0.83 – 0.81 (t, J = 12 Hz, 6H). ^{13}C NMR (150 MHz, DMSO-d_6) δ_{ppm} 154.2, 138.5, 128.6, 127.2, 43.8, 41.5, 31.0, 30.4, 19.7, 14.1. HRMS (ESI) calcd. for $C_7H_{13}N_5O_3S_2$ $(M+H)^+$: 435.3231, found: 435.3250.

4.4.2.7. Synthesis of 6-((2-ethoxy-3,4-dioxocyclobut-1-en-1-yl)amino)-N-(5-sulfamoyl-1,3,4-thiadiazol-2-yl)hexanamide (4.6)

To the gently stirring ethanol solution of 3,4-diethoxycyclobut-3-ene-1,2-dione (1 equiv, 300 mg), compound **5.5** (1.2 equiv,474 mg) and 10 mol % zinc triflate (64 mg) was added under inert atmosphere. The reaction mixture was stirred for 12

hours under room temperature. After maximum consumption of the starting materials as monitored by TLC, the solution was concentrated under reduced pressure. The crude product was purified with column chromatography using silica gel with MeOH/DCM (0-20%): as the solvent gradient system to obtain the white-coloured pure product. The compound was characterized by ^{1}H NMR, ^{13}C NMR and HRMS analyses.

^{1}H NMR (600 MHz, DMSO-d_6) δ_{ppm} 8.72 – 8.25 (brs, 3H), 8.09 – 7.59 (brs, 1H), 7.29 – 7.09 (brs, 8H), 4.60 - 4.42 (s, 8H), 1.54 - 1.49 (m, 2H), 1.47 – 1.42 (m, 4H), 1.35 -1.28 (m, 2H), 1.23 – 1.16 (m, 4H), 0.83 – 0.81 (t, J = 12 Hz, 6H). ^{13}C NMR (150 MHz, DMSO-d_6) δ_{ppm} 154.2, 138.5, 128.6, 127.2, 43.8, 41.5, 31.0, 30.4, 19.7, 14.1. HRMS (ESI) calcd. for $C_{13}H_{17}N_5O_6S_2$ $(M+H)^+$: 435.3231, found: 435.3250.

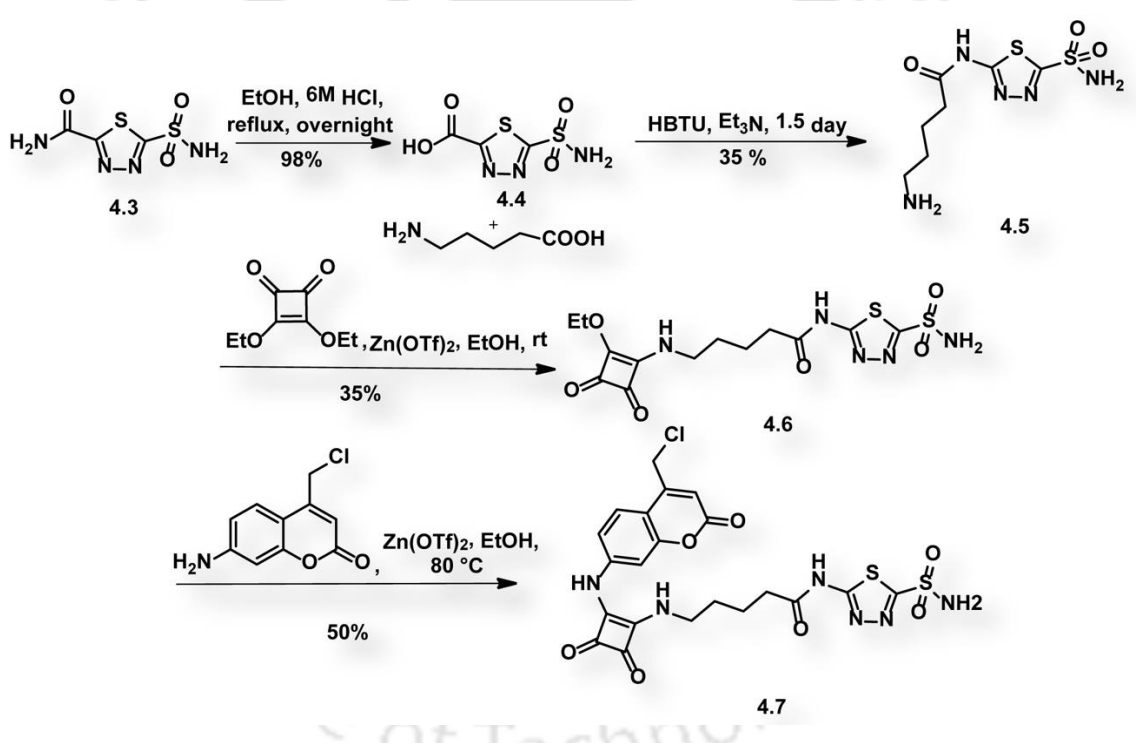

Scheme 4.2. Synthetic routes of the photo-linker of **4.7**.

4.4.2.8. Synthesis of 6-((2-((4-(chloromethyl)-2-oxochroman-6-yl)amino)-3,4-dioxocyclobut-1-en-1-yl)amino)-N-(5-sulfamoyl-1,3,4-thiadiazol-2-yl)hexanamide (4.7)

To a gently ethanol solution of 7-amino,4-chloromethyl coumarin (1 equiv,100 mg), **4.6** and 10 mol% zinc triflate was added to the solution under inert condition. The solution was stirred overnight under reflux condition. The progress of the reaction was monitored with the help TLC and after maximum consumption of the

starting materials the solvent was evaporated under reduced pressure to get the crude product. Reddish-brown coloured pure product was obtained through column chromatography using silica gel with MeOH/DCM (0-20%): as the solvent gradient system. The compound was characterized by ^{1}H NMR, ^{13}C NMR and HRMS analyses.

^{1}H NMR (600 MHz, DMSO-d_6) δ_{ppm} 8.72 – 8.25 (brs, 3H), 8.09 – 7.59 (brs, 1H), 7.29 – 7.09 (brs, 8H), 4.60 - 4.42 (s, 8H), 1.54 - 1.49 (m, 2H), 1.47 – 1.42 (m, 4H), 1.35 -1.28 (m, 2H), 1.23 – 1.16 (m, 4H), 0.83 – 0.81 (t, J = 12 Hz, 6H). ^{13}C NMR (150 MHz, DMSO-d_6) δ_{ppm} 154.2, 138.5, 128.6, 127.2, 43.8, 41.5, 31.0, 30.4, 19.7, 14.1. HRMS (ESI) calcd. for $C_{28}H_{32}ClN_{11}O_{10}S_4$ $(M+H)^+$: 435.3231, found: 435.3250.

4.4.2.9. Synthesis of compound 4.2d

To the gently stirring solution of **4.2c** (100 mg, 1 equiv.) and KOH (1.5 equiv.) in DMF, was added a DMF solution of **4.7** to the reaction mixture. After maximum consumption of **5.7**, the solvent was evaporated under reduced pressure. A 5 mL 3M HCl solution was added to the mixture and the product was extracted three times using EtOAc (3*20 mL) solution. The combined EtOAc extracts were dried over $MgSO_4$ and concentrated under reduced pressure. Brown-coloured pure product was purified through column chromatography using MeOH/DCM (0-30%) as the eluent system. The compound was characterized by ^{1}H NMR, ^{13}C NMR and HRMS analyses.

^{1}H NMR (600 MHz, DMSO-d_6) δ_{ppm} 8.72 – 8.25 (brs, 3H), 8.09 – 7.59 (brs, 1H), 7.29 – 7.09 (brs, 8H), 4.60 - 4.42 (s, 8H), 1.54 - 1.49 (m, 2H), 1.47 – 1.42 (m, 4H), 1.35 -1.28 (m, 2H), 1.23 – 1.16 (m, 4H), 0.83 – 0.81 (t, J = 12 Hz, 6H). ^{13}C NMR (150 MHz, DMSO-d_6) δ_{ppm} 154.2, 138.5, 128.6, 127.2, 43.8, 41.5, 31.0, 30.4, 19.7, 14.1. HRMS (ESI) calcd. for $C_{120}H_{170}N_{14}O_{16}S_2$ $(M+H)^+$: 435.3231, found: 435.3250.

4.4.3. UV-Vis Titrations

A 50 μM stock solution of **4.2c** was taken in DMSO in a quartz cuvette, and the UV-Vis absorbance spectrum at 298 K was recorded between 250 nm and 550 nm. Aliquots of the DMSO stock solution of 12.5 mM TBACl were sequentially added to the receptor solution, and the UV-Vis spectra was documented each time. By fitting the obtained values in the bindfit 1:2 model.

4.4.4. Ion transport activity studies

4.4.4.1. Ion transport activity studies using the fluorescence-based assay

4.4.4.1.1. Lucigenin-based ion transport studies

EYPC-LUVs lucigenin using $NaNO_3$ as the intravesicular solution was prepared according to earlier mentioned protocol in section 3.4.4.1.

4.4.4.1.2. Ion transport activity across EYPC/CHOL-LUVs lucigenin

Ion transport activity of synthesized macrocyclic compounds across EYPC/CHOL-LUV⊃lucigenin was performed by following protocol in section 3.4.4.1.

4.4.4.2. HPTS-based selectivity studies

4.4.4.2.1. Anion selectivity studies

4.4.4.2.1.1. Preparation of EYPC-LUVs⊃HPTS

The liposomes were prepared for conducting the HPTS-based anion selectivity experiments as mentioned according to the procedure in section 3.4.4.1 incorporating HPTS dye.

4.4.4.2.1.2. Ion transport activity across EYPC/CHOL-LUV⊃HPTS

The anion transport selectivity for the fluorescence assay, in a clean and dry 3 mL fluorescence cuvette, 2940 µL of 20 mM HEPES buffer containing 225 mM of Na_xA_y, pH 7.2 (where Na_xA_y = NaCl, NaBr, NaI, $NaClO_4$ and $NaNO_3$), pH 7.2, 50 µL of the EYPC/CHOL-LUV⊃HPTS and 50 µL of 0.75 M NaOH was added in the cuvette. The cuvette was placed under gently stirring condition for 3 minutes in the fluorescence spectrophotometer (Fluoromax-4 spectrofluorometer, Horiba Scientific, Singapore) which was equipped with an external magnetic stirrer. In this 3 minute approximately 0.6 pH gradient was developed between the intravesicular and the extravesicular solution. The HPTS fluorescence was evaluated as a function of time (λ_{em} = 510 nm, λ_{ex} = 450 nm). At t = 50 s, 10 µL of the anionophore solution was added to initiate the kinetics. The vesicles were completely lysed by adding 20 µL of 20% Triton X-100 at 450 s, and the fluorescence intensity measurement was continued for a further 50 s.

4.4.4.2.1.3. Quantitative measurement of transport activity from HPTS assay

The HPTS fluorescence emission intensity was normalized as 0 and 100 unit for the intensities appearing at t = 0 s and t = 500 s respectively. The ion transport efficiency at t = 450 s (before addition of Triton X-100)

$$Transport\ activity, T_{HPTS} = \frac{F_t - F_0}{F_\infty - F_0} \times 100\% \ldots\ldots Eq.-4.3$$

F_t is the fluorescence intensity measured at t = 450 s (before addition of Triton X-100 solution), F_0 is the fluorescence intensity recorded immediately before addition of anionophore (t = 0 s) and F_∞ is the fluorescence intensity after addition of Triton X-100 solution after final vesicle lysis at t = 500 s.

4.4.4.2.2. Cation selectivity studies

4.4.4.2.2.1. Preparation of EYPC-LUVs⊃HPTS

The liposomes were prepared for conducting the HPTS-based cation selectivity experiments as mentioned according to the procedure in section 3.4.4.1. incorporating HPTS dye.

4.4.4.2.2.2. Ion transport activity across EYPC/CHOL-LUV⊃HPTS

The anion transport selectivity for the fluorescence assay were performed according to section 4.4.4.4.1.2.

4.4.4.3. Ion transport activity studies using the ion-selective electrode-based assay

4.4.4.3.1. Chloride ion efflux studies using chloride-ion-selective electrode (chloride-ISE)

The Cl^- ion efflux from the LUVs were measured with the help of ISE. Before starting each set of experiments, the ISE was calibrated using solutions of 1 ppm, 10 ppm and 100 ppm.

4.4.4.3.2. Preparation of EYPC/CHOL-LUV

The LUVs were prepared accordingly as mentioned in section 2.4.4.4.2.

4.4.4.3.3. Chloride efflux study across EYPC/CHOL-LUV

The Cl^- efflux studies were studied according to the procedure mentioned in section 2.4.4.4.3.

4.4.4.3.4. Quantitative measurement of transport activity from chloride ISE assay

The Cl^- ion efflux efficiency of the compounds was evaluated according to the procedure mentioned in 2.4.4.4.4.

4.4.4.4. Evidence for mobile carrier mechanism

4.4.4.4.1. CHOL dependency assay

The EYPC/CHOL-LUVs for the cholesterol dependency experiment with ISE were prepared according to the procedure mentioned in section 2.4.4.4.2. Three liposomes were prepared with varying cholesterol concentrations (10:0, 8:2, and 6:4) and the chloride efflux was determined with these three lipisomes. The ion transport with these LUVs were carried out according to the procedure mentioned in section 2.4.4.4.3. The chloride ion efflux mediated by anionophore **4.2c** from the three types of liposomes were found comparable which indicates the anionophore **4.2c** doesn't form channels across the lipid bilayer.

4.4.4.4.2. Temperature-dependent DPPC assay

For preparing the liposomes 1,2-dipalmitoylphosphatidylcholine (DPPC, in deacidified $CHCl_3$) was taken in a clean and dry sample vial. The rest of the procedure was followed as mentioned in section 3.4.4.1.

4.4.4.5. Regeneration studies using proanionophore

4.4.4.5.1. Fluorescent experiment to study the regeneration of anionophore from proanionophore

For the experiment, in a completely clean fluorescence cuvette, 800 µL of phosphate saline buffer (PBS) was added along with the proanionophore **4.2d** (1 mM). The fluorescent spectra of proanionophore was recorded (λ_{ex} = 410 nm). No prominent fluorescent peak was observed at this time. However, after UV irradiation for 10 secs, 2 minutes, 3 minutes, 5 minutes, 10 minutes, 20 minutes and 30 minutes, a fluorescent peak centered at 513 nm was observed which gradually increased. The peak observed at 513 nm corresponded to the photolabile fluorescent aldehyde formed due to photocleavage of the proanionophore to the photo-moiety and the active anionophore.

4.4.4.5.2. Ion transport studies under photomodulation

4.4.4.5.2.1. Ion transport studies after UV irradiation (405 nm) by the fluorescence-based method

The EYPC/CHOL-LUV⊃HPTS were prepared in accordance with the procedure mentioned in 5.1.1. For the ion transport measurement in a clean and dry 3 mL fluorescence cuvette, 2940 µL of 20 mM HEPES buffer containing 225 mM of NaCl, pH 7.2, 50 µL of the EYPC/CHOL-LUV⊃HPTS and 50 µL of 0.75 M NaOH was added in

the cuvette. The cuvette was placed under gently stirring condition for 3 minutes in the fluorescence spectrophotometer (Fluoromax-4 spectrofluorometer, Horiba Scientific, Singapore) which was equipped with an external magnetic stirrer. In this 3 minute approximately 0.6 pH gradient was developed between the intravesicular and the extravesicular solution. The HPTS fluorescence was evaluated as a function of time (λ_{em} = 510 nm, λ_{ex} = 450 nm). At t = 50 s, 10 µL of the proanionophore **4.2d** solution was added to initiate the kinetics. At t = 80 s, the kinetics was paused and the sample was light irradiated for 5 minutes and the kinetics was restarted. The vesicles were completely lysed by adding 20 µL of 20% Triton X-100 at 450 s, and the fluorescence intensity measurement was continued for a further 50 s. Same experiments were repeated by irradiating the samples for 10 minutes and 20 minutes correspondingly. Control experiments were repeated in absence of proanionophore **4.2d** with same light exposure time. The increase in pH dissipation mediated by proanionophore **4.2d** upon light irradiation suggests regeneration of the active anionophore **4.2c** which is responsible for the result.

4.4.4.5.2.2. Ion transport studies after UV irradiation (405 nm) by ISE-based method

The Cl^- ion efflux was evaluated with the help of ISE. The LUVs for the experiment were prepared as mentioned according to the section 2.4.4.4.2. For the Cl^- ion efflux studies under UV irradiation in a clean and dry glass vial 3940 µL of buffer solution (5 mM phosphate and 100 mM $NaNO_3$, pH 7.2) and 50 µL of the EYPC/CHOL-LUV were taken, and the glass electrode was immersed into the solution under mild stirring condition. The efflux of Cl^- was monitored using a chloride ion-sensitive electrode (t = 0 s). After 50 s, 10 µL of the respective transporter (from their respective DMSO stock solution) was added to initiate the Cl^- transport kinetics. At t = 100 s, the kinetics was paused and the sample vial was light irradiated (410 nm) for 5 minutes. After 5 minutes of light irradiation, the kinetics was restarted Consequently, at t = 500 s the vesicles were lysed using 50 µL of 20% of Triton X-100 solution. Total Cl^- ion efflux reading was taken at t = 700 s. The initial reading was considered as 0% Cl^- efflux, and the final reading at t = 700 s was considered as 100% Cl^- efflux. The same experiment was repeated with light irradiation 10 minutes and 20 minutes respectively. Three control experiments were repeated in absence of

proanionophore **4.2d** under irradiation of 5 minutes, 10 minutes and 20 minutes respectively.

4.4.5. Biological Activity Studies

4.4.5.1. MTT-based cytotoxicity assay

Similar procedure was followed as mentioned in section 3.4.4.13.

4.4.5.2. MTT-based cytotoxicity assay using photo-trigger

Similar procedure was followed as mentioned in section 3.4.4.13.2. However, the light irradiation used was 405 nm of wavelength for 5 minutes.

4.4.5.3. Chloride mediated cell death

4.4.5.3.1. HBSS assay

Similar procedure was followed as mentioned in section 2.4.4.12.3.1.

4.4.5.3.2. Immunoblot analysis

Similar procedure was followed as mentioned in section 2.4.4.12.3. Similar procedure was followed as mentioned in section 2.4.4.12.3.

4.4.5.3.3. ROS generation studies

The HeLa cells were seeded in 35 mm dishes at 5×10^5 cells per plate. The HeLa cells were incubated with proanionophore **4.2d** (5 µM and 10 µM) for 24 hrs. After 24 hrs, the HeLa cells were incubated with ROS sensitive DCFDA (1 µM) dye for 20 minutes time. Finally, after 20 minutes, the external DCFDA dye was washed with PBS dye and the HeLa cell images were acquired using green channel with Nikon Eclipse TS 100 fluorescence microscope.

4.5. ^{1}H and ^{13}C NMR spectra of synthesized compounds

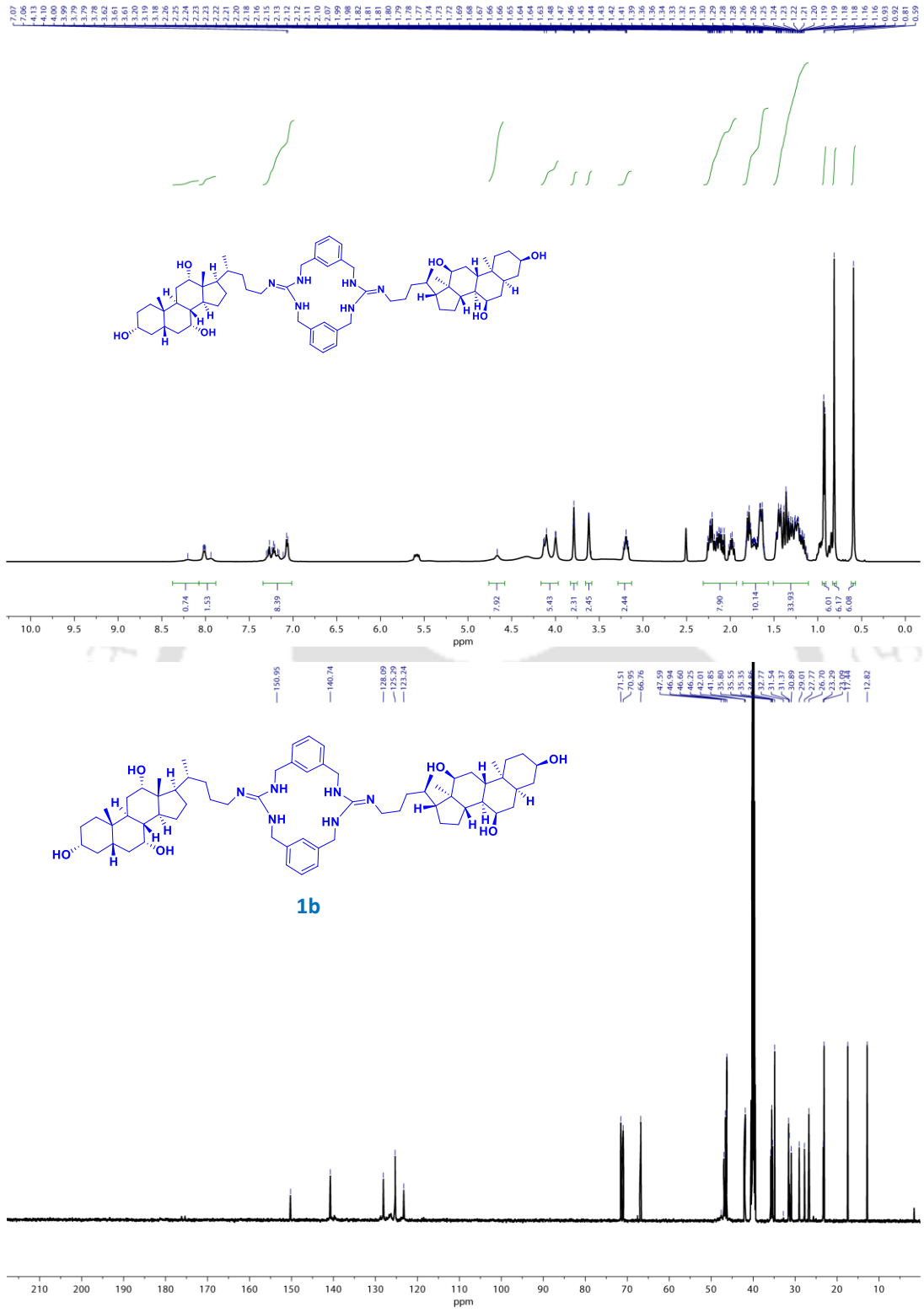

Figure S4.1. ^{1}H NMR (A) and ^{13}C NMR (B) spectra of compound **4.1b**.

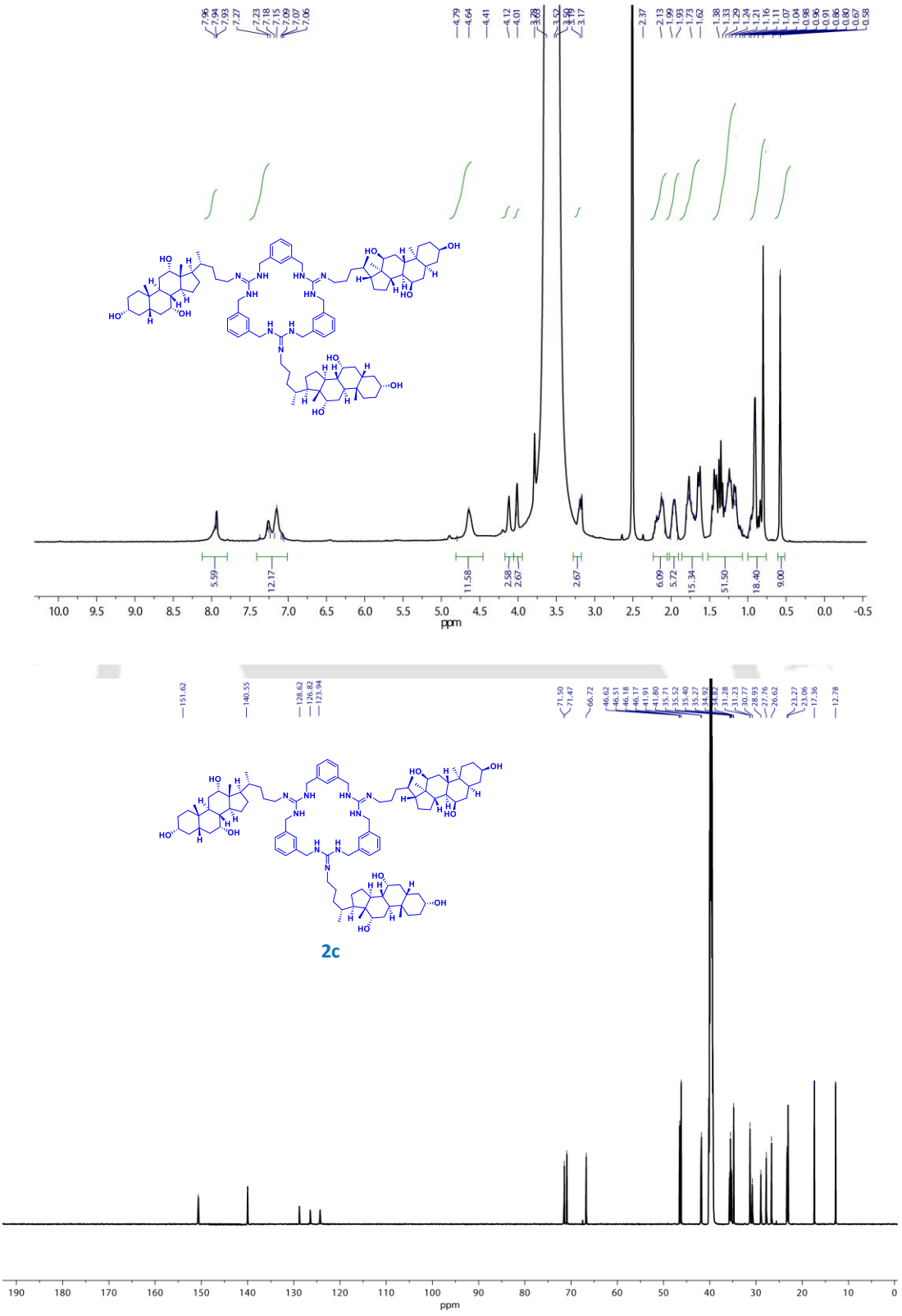

Figure S4.2. ^{1}H NMR (A) and ^{13}C NMR (B) spectra of compound **4.2c**.

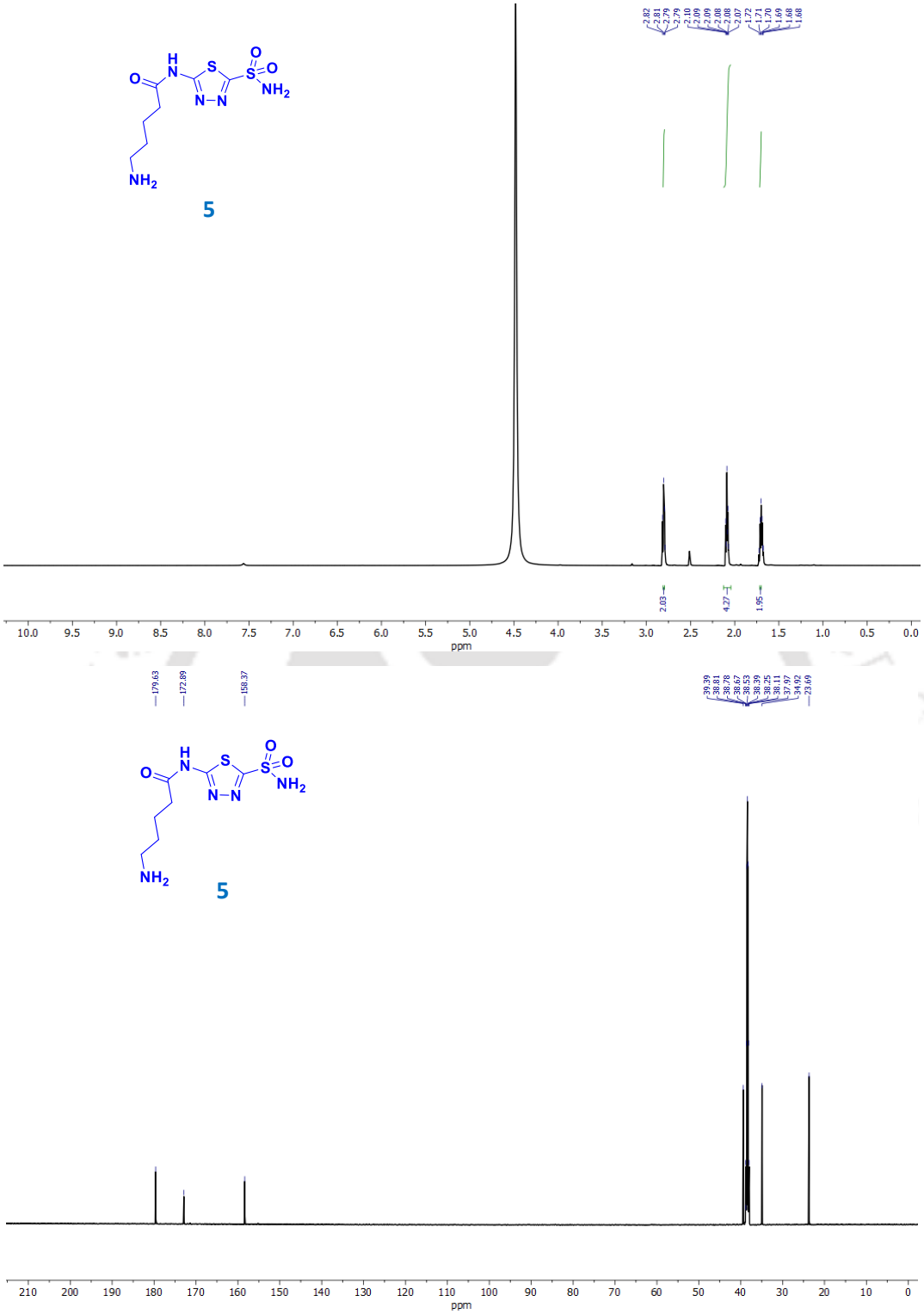

Figure S4.3. ^{1}H NMR (A) and ^{13}C NMR (B) spectra of compound **4.5**.

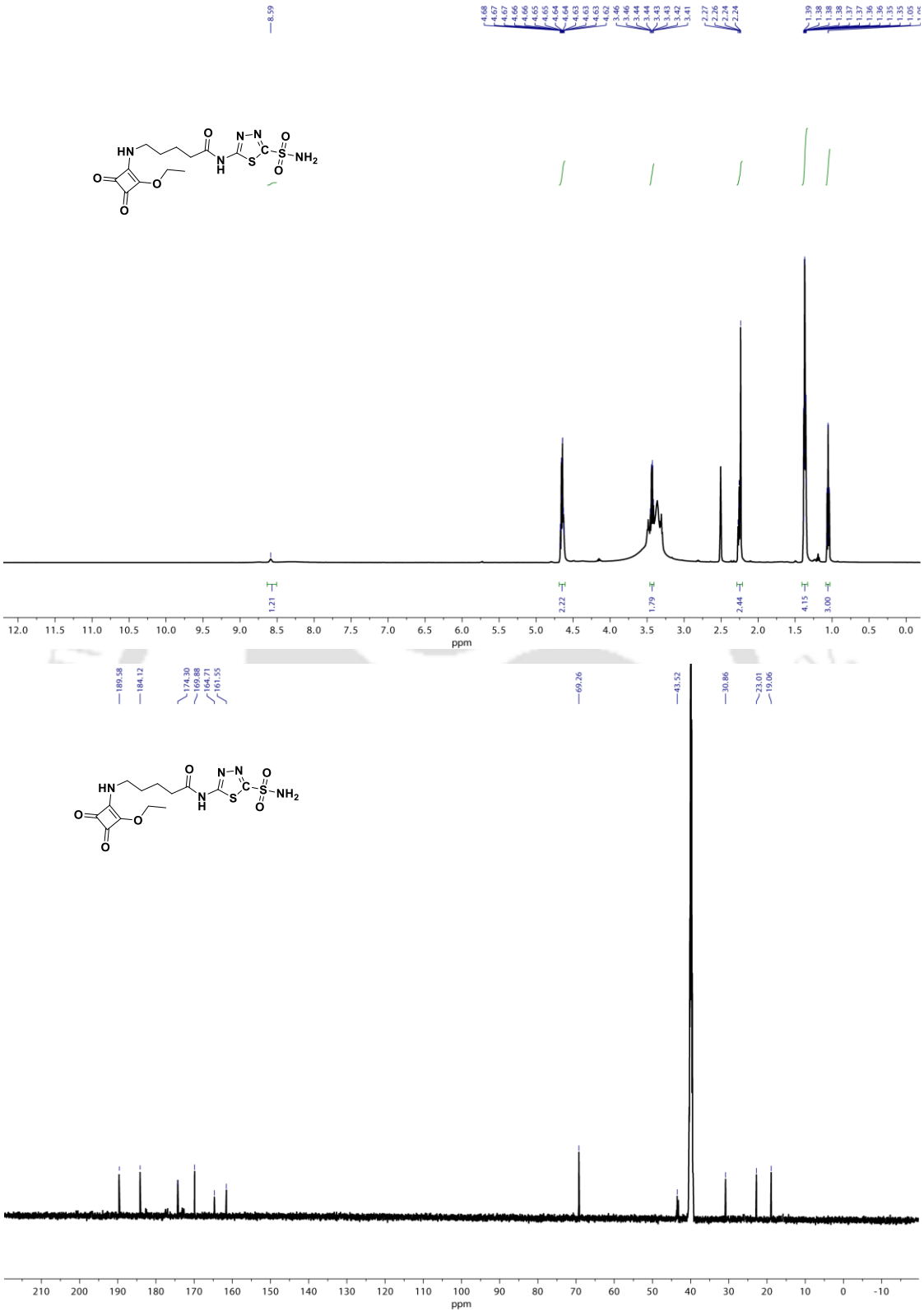

Figure S4.4. ^{1}H NMR (A) and ^{13}C NMR (B) spectra of compound **4.6**.

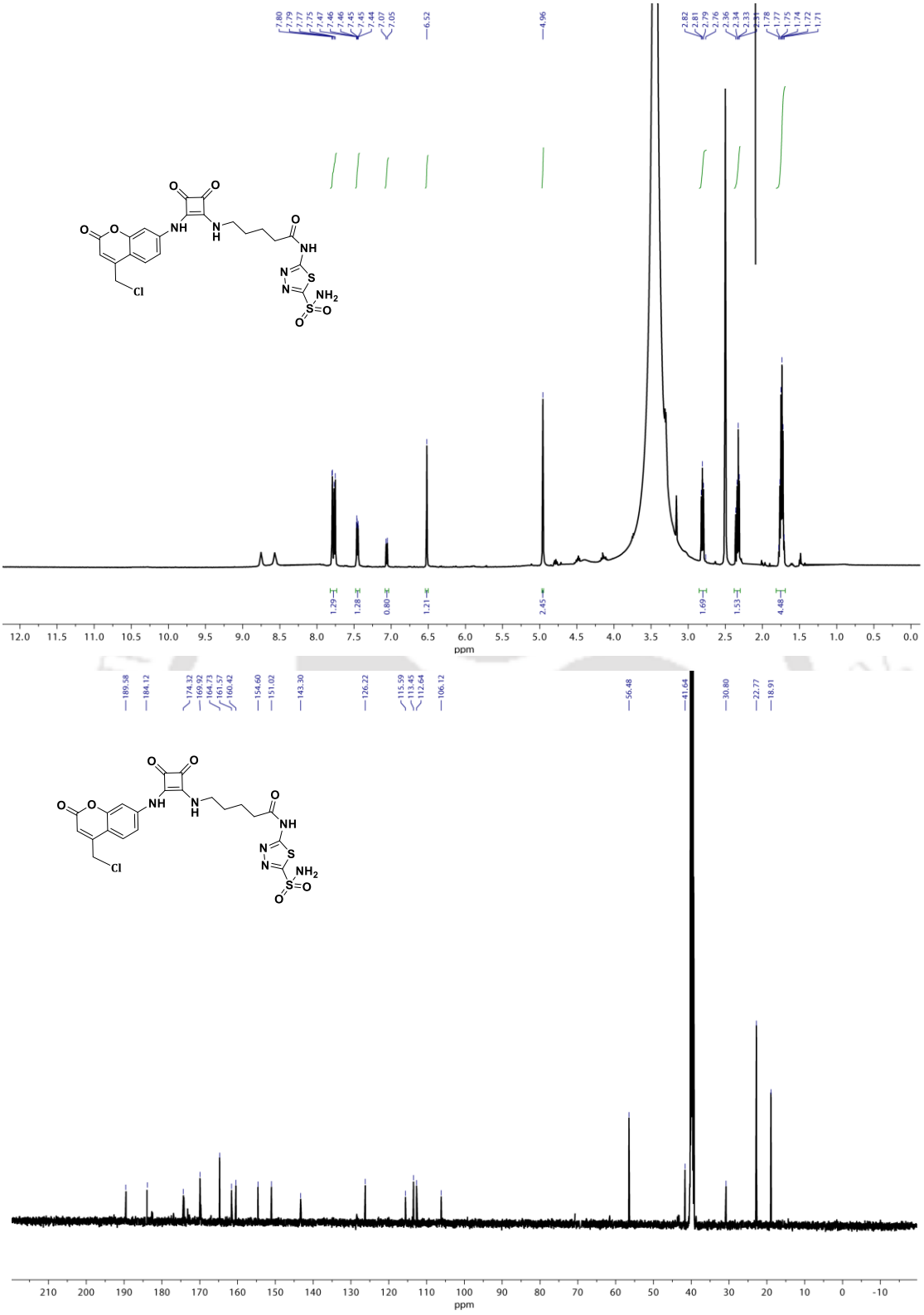

Figure S4.5. ^{1}H NMR (A) and ^{13}C NMR (B) spectra of compound **4.7**.

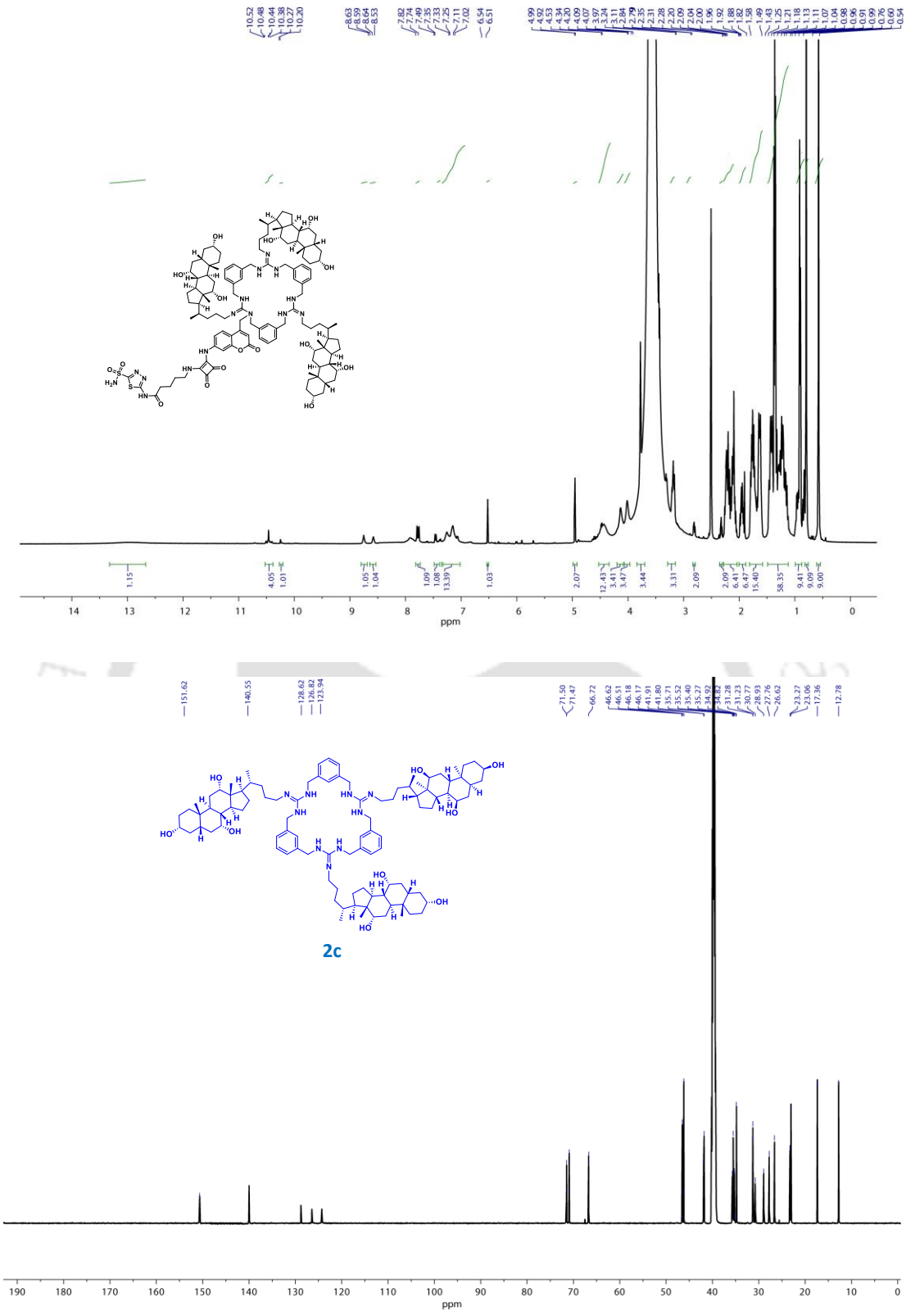

Figure S4.6. ^{1}H NMR (A) and ^{13}C NMR (B) spectra of compound **4.2d**

4.6. References

(1) Davis, J. T.; Gale, P. A.; Quesada, R. J. C. S. R. Advances in anion transport and supramolecular medicinal chemistry. *Chem. Soc. Rev.* **2020**, *49* (16), 6056-6086.

(2) Akhtar, N.; Biswas, O.; Manna, D. J. C. C. Biological applications of synthetic anion transporters. *Chem. Commun.* **2020**, *56* (91), 14137-14153.

(3) Salunke, S. B.; Malla, J. A.; Talukdar, P. J. A. C. I. E. Phototriggered Release of a Transmembrane Chloride Carrier from an o-Nitrobenzyl-Linked Procarrier. *Angew. Chem.* **2019**, *58* (16), 5354-5358.

(4) Kalinin, S.; Malkova, A.; Sharonova, T.; Sharoyko, V.; Bunev, A.; Supuran, C. T.; Krasavin, M. J. I. J. o. M. S. Carbonic anhydrase IX inhibitors as candidates for combination therapy of solid tumors. *Int. J. Mol. Sci.* **2021**, *22* (24), 13405.

(5) Supuran, C. T. J. W. j. o. c. o. Inhibition of carbonic anhydrase IX as a novel anticancer mechanism. *World J. Clin. Oncol.* **2012**, *3* (7), 98.

(6) Lin, Q.; Bao, C.; Fan, G.; Cheng, S.; Liu, H.; Liu, Z.; Zhu, L. J. J. o. M. C. 7-Amino coumarin based fluorescent phototriggers coupled with nano/bio-conjugated bonds: Synthesis, labeling and photorelease. *J. Mater. Chem.* **2012**, *22* (14), 6680-6688.

(7) Weinstain, R.; Slanina, T.; Kand, D.; Klan, P. J. C. r. Visible-to-NIR-light activated release: from small molecules to nanomaterials. *Chem. Soc. Rev.* **2020**, *120* (24), 13135-13272.

(8) Beverina, L.; Crippa, M.; Landenna, M.; Ruffo, R.; Salice, P.; Silvestri, F.; Versari, S.; Villa, A.; Ciaffoni, L.; Collini, E. J. J. o. t. A. C. S. Assessment of water-soluble π-extended squaraines as one-and two-photon singlet oxygen photosensitizers: design, synthesis, and characterization. *J. Am. Chem. Soc.* **2008**, *130* (6), 1894-1902.

(9) Xia, G.; Wang, H. J. J. o. P.; Reviews, P. C. P. Squaraine dyes: The hierarchical synthesis and its application in optical detection. *J. Photochem. Photobiol.* **2017**, *31*, 84-113.

(10) Berlinck, R. G.; Burtoloso, A. C. B.; Kossuga, M. H. J. N. P. R. The chemistry and biology of organic guanidine derivatives. *Nat. Prod. Rep.* **2008**, *25* (5), 919-954.

(11) Wu, X.; Judd, L. W.; Howe, E. N.; Withecombe, A. M.; Soto-Cerrato, V.; Li, H.; Busschaert, N.; Valkenier, H.; Pérez-Tomás, R.; Sheppard, D. N. J. C. Nonprotonophoric electrogenic Cl− transport mediated by valinomycin-like carriers. *Chem* **2016**, *1* (1), 127-146.

(12) Basak, D.; Sridhar, S.; Bera, A. K.; Madhavan, N. J. B.; Letters, M. C. A minimalistic tetrapeptide amphiphile scaffold for transmembrane pores with a preference for sodium. *Bioorg. Med. Chem. Lett.* **2017**, *27* (13), 2886-2889.

(13) Malla, J. A.; Umesh, R. M.; Vijay, A.; Mukherjee, A.; Lahiri, M.; Talukdar, P. J. C. s. Apoptosis-inducing activity of a fluorescent barrel-rosette M+/Cl− channel. *Chem. Sci.* **2020**, *11* (9), 2420-2428.

(14) Howe, E. N.; Gale, P. A. J. J. o. t. A. C. S. Fatty acid fueled transmembrane chloride transport. *J. Am. Chem. Soc.* **2019**, *141* (27), 10654-10660.

(15) Zeng, F.; Liu, F.; Yuan, L.; Zhou, S.; Shen, J.; Li, N.; Ren, H.; Zeng, H. J. O. l. A Pore-Forming Tripeptide as an Extraordinarily Active Anion Channel. *Org. Lett.* **2019**, *21* (12), 4826-4830.

(13) Akhtar, N.; Biswas, O.; Manna, D. Stimuli-responsive transmembrane anion transport by AIE-active fluorescent probes. *Org. Biomol. Chem.*, **2021**,19, 7446-7459

5. Thesis Conclusion

Accordingly in this thesis four different scaffolds were designed and synthesised and their curative properties were investigated thoroughly. In **Chapter 1** the importance of several anionophores and their several therapeutic applications were discussed in detail. Subsequently in **Chapter 2** a new class of anionophore was developed, their Cl^- ion ability was studied and their anticancer properties were investigated. To further achieve selectivity over the cancer cells, light as a stimulus was used in **Chapter 3** and the generation of the active anionophore from the inactive anionophore was studied along with the Cl^- ion arbitrated phosphate ion transport ability of the anionophore. **Chapter 4** demonstrated the construction of photocleavable targeted proanionophore to better target the cancer cells and induce cancer cell death due to enhanced production of ROS upon UV irradiation on the proanionophores. Overall, in the thesis anionophoric properties of a number of synthetic transporters were investigated with the help of well-known experiments and their biological applications were examined.

6. Future Prospects

The anion transport-related research works are gaining momentum over the last 15 years because of their therapeutic potential against cancer, cystic fibrosis, and other channelopathies. Although the development of classical anionophores has a considerable prospect in therapeutics, but still this field is associated with a number of hurdles such as poor deliverability due to lipophilic nature, cellular uptake, and selectivity between the cancer cells and normal cells. To overcome these hurdles, supramolecular chemists have come up with numerous new concepts like stimuli-responsive proanionophore where using this concept one may overcome all these hurdles associated with anionophore development. But this concept still needs to be explored more from the detailed biological point of view.

Mainly chloride anion transporting molecules are extensively explored for several therapeutic prospects. So, the importance of designing and exploring the other ion transporting molecules specially the really important oxoanions and amino acids, needs to be investigated. Also, their thorough mechanistic pathway needs to be scrutinized. Besides, the anion transport facilitated by those molecules and their biological activities should be thoroughly investigated to open up numerous other therapeutic prospects from the conventional ones. Additionally tagging the

anionophores with a targeting group can also prove to be a good approach to reduce toxicity towards the normal cell lines. It is also well documented that various monovalent anions have potential activity against multiple viruses. The antiviral property of the anionophores can have considerable potential, which can also be explored. Anomalous functions of the chloride channel can lead to several pathological conditions like arrhythmogenesis in myocardial injury, cardiac ischemic preconditioning, and the adaptive remodeling of the heart during myocardial hypertrophy and heart failure. So, in this scenario, the artificial chloride ion transporter molecules can have an immense perspective against these pathological conditions. Unregulated anion transport also plays an essential role in kidney diseases, and the implications of the artificial anion transporter molecules can have an enormous role to control this anionic imbalance and can prevent this chronic kidney disease. Hence, a search for the applications of anionophores against these unexplored areas is also required.time.

Table: XYZ Cartesian coordinates for **2.2** (**PIT-1**).

	B3LYP/6-31+G(d)				B3LYP/6-31++G(d,p)		
	TE = -2323.3775	#IF = 0.00			TE = -2323.3778	#IF = 0.00	
A	x	y	z	A	x	y	z
C	1.306148	2.511638	1.34135	C	1.306385	2.512535	1.340669
C	2.054454	1.648021	0.544232	C	2.054001	1.647508	0.54445
C	1.555501	1.221784	-0.71991	C	1.553785	1.218868	-0.71838
C	0.271047	1.677594	-1.10953	C	0.269306	1.674622	-1.10806
C	-0.48758	2.514706	-0.31187	C	-0.48833	2.513574	-0.31137
C	0.047577	2.931039	0.910413	C	0.047876	2.932053	0.909722
H	1.694964	2.847455	2.291231	H	1.695756	2.849578	2.289881
H	-1.46686	2.851239	-0.62407	H	-1.46756	2.850217	-0.62353
N	3.324836	1.190928	0.954056	N	3.324696	1.191032	0.954189
C	3.632122	0.543474	2.127219	C	3.632373	0.544108	2.127559
N	4.911465	-0.01433	2.029933	N	4.911737	-0.0137	2.029976

S	2.616035	0.382083	3.435425	S	2.616747	0.383553	3.436206
C	5.774237	-0.37352	3.061379	C	5.774922	-0.37277	3.061102
O	5.600116	-0.07473	4.232597	O	5.600788	-0.0743	4.232399
C	6.993255	-1.15995	2.636344	C	6.994078	-1.15911	2.635943
C	7.176293	-1.71708	1.360773	C	7.179993	-1.71119	1.358615
C	7.983948	-1.35032	3.613568	C	7.981948	-1.35466	3.615028
C	8.334223	-2.44572	1.074179	C	8.337641	-2.44038	1.072278
H	6.440634	-1.58945	0.572545	H	6.446857	-1.57955	0.568687
C	9.137281	-2.07671	3.324163	C	9.135013	-2.08157	3.325885
H	7.821454	-0.92019	4.596061	H	7.817357	-0.92815	4.598738
C	9.31587	-2.62813	2.050384	C	9.316323	-2.62816	2.050417
H	8.463329	-2.86666	0.081292	H	8.468829	-2.8573	0.077976
H	9.896291	-2.21354	4.089868	H	9.891712	-2.22258	4.093091
H	5.25838	-0.1164	1.07005	H	5.257687	-0.11661	1.069875
H	4.02403	1.091161	0.204768	H	4.023585	1.090783	0.20464

O	2.194608	0.405808	-1.55522	O	2.191883	0.40072	-1.55238
Cl	-0.37894	1.150397	-2.65124	Cl	-0.3819	1.145202	-2.64849
O	-1.85353	4.175889	1.346811	O	-1.85253	4.178353	1.345551
O	-0.22589	4.241768	2.797281	O	-0.22351	4.24653	2.79433
N	-0.72638	3.840505	1.740819	N	-0.7251	3.84336	1.739115
H	3.165935	0.24227	-1.37339	H	3.163822	0.239104	-1.37207
H	10.21471	-3.1948	1.821254	H	10.21495	-3.19525	1.821561
Cl	5.20098	0.03892	-1.26182	Cl	5.199421	0.03872	-1.26267

Table: XYZ Cartesian coordinates for **2.5 (DM-PIT-1).**

	B3LYP/6-31+G(d)				B3LYP/6-31++G(d,p)		
	TE = -1942.4282		#IF = 0.00		TE = -1942.4287		#IF = 0.00
A	x	y	z	A	x	y	z
C	1.105181	2.205543	1.160018	C	1.103714	2.203077	1.159885
C	1.986792	1.476333	0.362712	C	1.987523	1.47724	0.361928
C	1.769807	1.412862	-1.04157	C	1.772723	1.417564	-1.04286

C	0.685365	2.122072	-1.59952	C	0.687857	2.126459	-1.60045
C	-0.1727	2.866441	-0.81047	C	-0.17256	2.867128	-0.81049
C	0.040643	2.894265	0.573569	C	0.038607	2.891314	0.573942
H	1.249795	2.244875	2.229778	H	1.246828	2.239939	2.229918
H	-1.00236	3.414967	-1.23798	H	-1.00268	3.415334	-1.23752
N	3.078621	0.77551	0.920426	N	3.079334	0.776139	0.919477
C	4.066464	1.281731	1.729286	C	4.065517	1.281366	1.731036
N	5.116657	0.361531	1.81544	N	5.116285	0.361731	1.816565
S	4.056617	2.787646	2.440548	S	4.053058	2.78554	2.445908
C	6.091365	0.25044	2.803835	C	6.091217	0.250293	2.804732
O	6.056434	0.844675	3.87038	O	6.056399	0.844121	3.871498
C	7.217007	-0.70395	2.481203	C	7.217253	-0.70358	2.4815
C	7.479401	-1.19884	1.198803	C	7.477082	-1.20186	1.199677
C	8.045625	-1.08299	3.550015	C	8.047965	-1.08009	3.549379
C	8.553144	-2.07458	0.975517	C	8.550504	-2.07766	0.976245

H	6.854958	-0.92964	0.352314	H	6.850635	-0.93553	0.353787
C	9.116422	-1.95515	3.355202	C	9.118681	-1.95263	3.354439
H	7.82838	-0.67698	4.532893	H	7.832502	-0.67223	4.531851
C	9.355356	-2.443	2.059426	C	9.355535	-2.44312	2.059431
H	5.120917	-0.35012	1.076793	H	5.121476	-0.34846	1.076594
H	3.303545	-0.12125	0.468708	H	3.305971	-0.11909	0.465516
O	2.53913	0.738906	-1.90676	O	2.544554	0.747451	-1.90888
O	-1.79586	4.268946	0.870755	O	-1.80068	4.262143	0.872568
O	-0.70435	3.617519	2.642857	O	-0.71061	3.607319	2.644287
N	-0.87466	3.641051	1.417843	N	-0.87919	3.634161	1.419089
H	3.192165	0.091287	-1.51791	H	3.196852	0.098546	-1.52096
H	10.18608	-3.12837	1.894905	H	10.18596	-3.12862	1.894827
H	0.552095	2.066164	-2.67458	H	0.556037	2.073211	-2.67579
C	9.99618	-2.38226	4.509766	C	9.999938	-2.3775	4.508691

H	9.745534	-1.83234	5.421506	H	9.75923	-1.81645	5.416343
H	9.881971	-3.45248	4.723844	H	9.875923	-3.44439	4.733866
H	11.05657	-2.20722	4.291678	H	11.06088	-2.21536	4.283689
C	8.830008	-2.58816	-0.41966	C	8.825937	-2.59385	-0.41829
H	7.897283	-2.80752	-0.94828	H	7.892634	-2.77659	-0.9594
H	9.372054	-1.8417	-1.01444	H	9.403107	-1.86496	-1.00191
H	9.438778	-3.498	-0.39642	H	9.401026	-3.52535	-0.39256
Cl	4.385579	-1.4646	-0.85393	Cl	4.389168	-1.45914	-0.85906

A=Atoms; TE = Total Energy in Hartree; #IF = Imaginary Frequency.

Biological applications of synthetic anion transporters

N. Akhtar, O. Biswas and D. Manna, *Chem. Commun.*, 2020, **56**, 14137 **DOI:** 10.1039/D0CC05489E

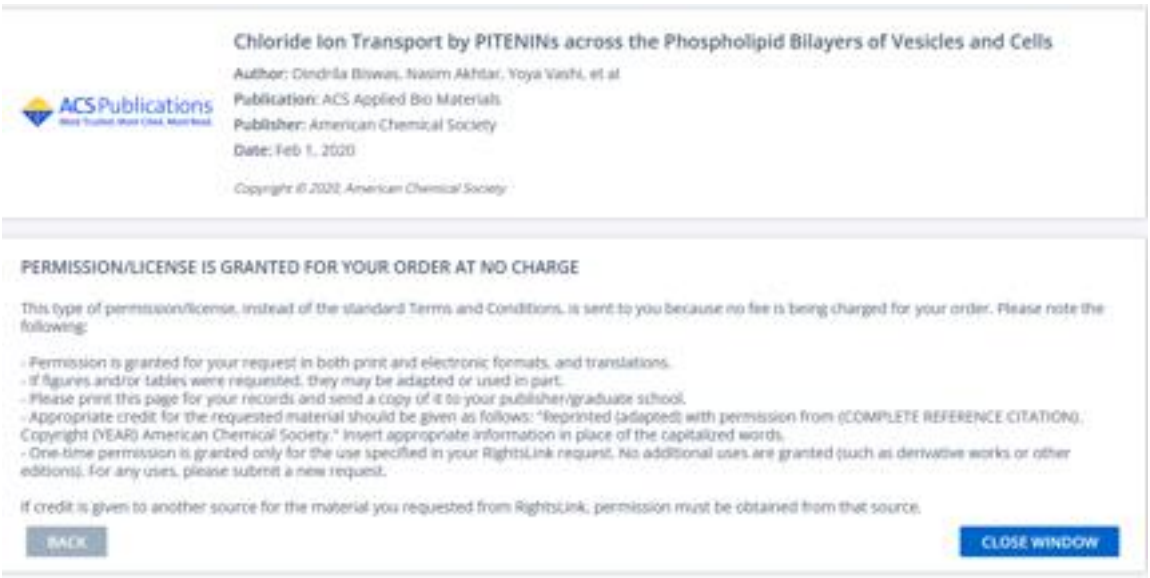

Chloride Ion Transport by PITENINs across the Phospholipid Bilayers of Vesicles and Cells

Author: Dindrila Biswas, Nasim Akhtar, Yoya Vashi, et al

Publication: ACS Applied Bio Materials

Publisher: American Chemical Society

Date: Feb 1, 2020

PERMISSION/LICENSE IS GRANTED FOR YOUR ORDER AT NO CHARGE

This type of permission/license, instead of the standard Terms and Conditions, is sent to you because no fee is being charged for your order. Please note the following:

- Permission is granted for your request in both print and electronic formats, and translations.
- If figures and/or tables were requested, they may be adapted or used in part.
- Please print this page for your records and send a copy of it to your publisher/graduate school.
- Appropriate credit for the requested material should be given as follows: "Reprinted (adapted) with permission from (COMPLETE REFERENCE CITATION). Copyright (YEAR) American Chemical Society." Insert appropriate information in place of the capitalized words.
- One-time permission is granted only for the use specified in your RightsLink request. No additional uses are granted (such as derivative works or other editions). For any uses, please submit a new request.

If credit is given to another source for the material you requested from RightsLink, permission must be obtained from that source.

BACK CLOSE WINDOW

Publications

1. **Biswas, O.**; Mazumder, P.; Naskar, A.; Srimayee, S.; Patra, N.; Kumar, S.; Manna, D.*, "Photoinduced generation of the active chloride-phosphate anionophore from its inactive proanionophore". (Manuscript submitted).

2. Akhtar, N.; **Biswas, O.**; Manna, D.*, "Transmembrane Anion Transport by Stimuli-responsive AIE-active Fluorescent Probe" *Org. Biomol. Chem.*, **2021**, 19, 7446-7459.

3. Das, S. [+]; **Biswas, O.**[+]; Akhtar, N.; Patel, A.; Manna, D.*, "Multi-stimuli Controlled release of Transmembrane Chloride ion Carrier from Sulfonium-linked Procarrier" *Org. Biomol. Chem.,* **2020**, 18, 9246-9252. (+ = Equal contribution)

4. Akhtar, N.; **Biswas, O.**; Manna, D.*, "Biological Applications of Synthetic Anion Transporters" *Chem. Commun.,* **2020**, 56, 14137-14153.

5. **Biswas, O.**; Akhtar, N.; Vashi, Y.; Saha, A.; Kumar, V.; Pal.; S.; Kumar, S.; Manna, D.*, "Chloride Ion Transport by PITENINs across the Phospholipid Bilayers of Vesicles and Cells" *ACS Appl. Bio Mater*., **2020**, 3(2), 935–944.

6. Dey, S.; Patel, A.; Raina, K.; Pradhan, N.; **Biswas, O.**; Rajkumar P. Thummer, P. R.*; Manna, D.*, "Stimuli-Responsive Anticancer Drug Delivery System with Inherent Antibacterial Activities" *Chem. Commun.,* **2020,** 56, 1661-1664.

7. 6. Akhtar, N.; Pradhan, N.; Saha, A.; Vishnu Kumar, V.; **Biswas, O**.; Dey, S.; Shah, M.; Kumar, S.; Manna. D.*, "Tuning the Solubility of the Ionophores: Glutathione-Mediated Transport of Chloride Ion across the Membranes" *Chem. Commun.,* **2019**, 55, 8482-8485.

8. Roy, A.; **Biswas, O.**; Talukdar. P.*, "Bis(sulfonamide) Transmembrane Carrier Allows pH-Gated Inversion of Ion Selectivity" *Chem. Commun.,* **2017**, 53, 3122-3125.